Coordination Chemistry of High Oxidation Nitrogen containing Amides and Heterocycles

By

Zhijie Chua

A thesis submitted to McGill University in partial fulfilment of the requirements in the degree of:

DOCTORATE OF PHILOSOPHY

Department of Chemistry, Faculty of Science

McGill University

Montreal, Quebec, Canada

© Zhijie Chua. 2013

Abstract

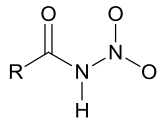
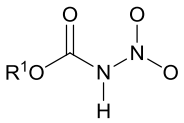
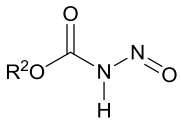
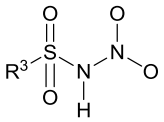

N-nitroamide		N-nitrocarbamate		N-nitrosocarbamate		N-nitrosulfonamide	
R	Label	R^1	Label	R^2	Label	R^3	Label
CH_3	**2-2**	CH_3	**2-4**	CH_3	**2-6**	*p*-tolyl	**2-8**
C_2H_5	**2-3**	C_2H_5	**2-5**	C_2H_5	**2-7**		
$Ir^{(I)}$-CH_3	**3-3**	$Ir^{(I)}$-CH_3	**3-4**	$Ir^{(I)}$-CH_3	**3-6**	$Ir^{(I)}$-*p*-tolyl	**3-7**
		$Ir^{(I)}$-C_2H_5	**3-5**				
$Ir^{(III)}$-CH_3	**3-11**	$Ir^{(III)}$-CH_3	**3-13**				
$Ir^{(III)}$-C_2H_5	**3-12**	$Ir^{(III)}$-C_2H_5	**3-14**				
$Re^{(I)}$-CH_3	**4-8**	$Re^{(I)}$-CH_3	**4-9**	$Re^{(I)}$-CH_3	**4-10**, **4-11A**	$Re^{(I)}$-*p*-tolyl	**4-12**

The catalytic reduction of nitrous oxide (N_2O) to dinitrogen (N_2) by nitrous oxide reductase (N_2OR) is poorly understood. The N_2O molecule is a poor ligand with relatively sparse coordination chemistry. We proposed the synthesis of probable nitrous oxide precursors which can be coordinated to transition metals prior to conversion to nitrous oxide.

Nitramide, H_2NNO_2, **2-1**, and the related nitrogen amide acids N-nitroamide **2-2**, **2-3**; N-nitrocarbamate **2-4**, **2-5**, N-nitrosocarbamate **2-6**, **2-7**; N-nitrosulfonamide **2-8** have been synthesized as possible nitrous oxide precursors for coordination studies with transition metals. The silver salts of the conjugate base of the nitrogen acids N-nitroamide **2-2Ag**; N-nitrocarbamate **2-4Ag**, **2-5Ag**; N-nitrosocarbamate **2-6Ag**; N-nitrosulfonamide **2-8Ag** are synthesized from the reaction of the acids with Ag_2CO_3. Similarly the potassium salts of the nitrogen acids N-nitroamide **2-2K**; N-nitrocarbamate **2-4K**; N-nitrosocarbamate **2-6K**; N-nitrosulfonamide **2-8K** are synthesized from the reaction of the nitrogen acids with K_2CO_3 or CH_3OK.

To investigate the π-acidity of the nitrogen acids, a series of Ir(I) complexes of the nitrogen acids, *trans*-$Ir^{(I)}(\eta^1\text{-X})(CO)(PPh_3)_2$, (X = nitrogen acid) N-nitroamide **3-3**; N-nitrocarbamate **3-4**, **3-5**; N-nitrosocarbamate **3-6**; N-nitrosulfonamide **3-7** are synthesized from the reaction of Vaska's complex, *trans*-$Ir^{(I)}(Cl)(CO)(PPh_3)_2$

(**3-1**) with the silver salts of the conjugate base of the nitrogen acids (N-nitroamide **2-2Ag**; N-nitrocarbamate **2-4Ag**, **2-5Ag**; N-nitrosocarbamate **2-6Ag**; N-nitrosulfonamide **2-8Ag**). Comparative studies with the related amides, dinitramide and bistriflimide, have also been done.

The oxidative addition of the nitrogen acids (N-nitroamide **2-2**, **2-3**; N-nitrocarbamate **2-4**, **2-5**) to *trans*-$Ir^{(I)}(Cl)(N_2)(PPh_3)_2$ (**3-2**) afford the Ir(III) complexes of the nitrogen acids, $Ir^{(III)}(\eta^2\text{-}X)(H)(Cl)(PPh_3)_2$, (X = nitrogen acid) N-nitroamide **3-11**, **3-12**; N-nitrocarbamate **3-13**, **3-14**. The ^{31}P, ^{1}H NMR and IR spectroscopic reaction monitoring profiles of the oxidative addition reactions give evidence of reaction intermediates that eventually convert to the final product. The reaction of **3-11** with CO and $P(CH_3)_2Ph$ result in the formation of multiple isomers of the addition products and also phosphine substitution. Addition of methyl triflate to **3-11** in CH_3CN is found to result in the substitution and loss of the nitrogen acid.

The Re(I) complexes of the nitrogen acids , *trans*-$Re^{(I)}(\eta^2\text{-}X)(CO)_2(PPh_3)_2$, (X = nitrogen acid) N-nitroamide **4-8**; N-nitrocarbamate **4-9**; N-nitrosulfonamide **4-12** are synthesized from the reaction of *trans*-$[Re^{(I)}(CH_3CN)_2(CO)_2(PPh_3)_2](Y)$, (Y = ClO_4: **4-3**, BF_4: **4-7**) with the potassium salts of the conjugate base of the nitrogen acids **2-2K**, **2-4K** and **2-8K** respectively. The reaction of **4-7** with N-nitrosocarbamate **2-6K** at room temperature gives mostly the kinetic isomer *trans*-$Re^{(I)}(\eta^2\text{-}X)(CO)_2(PPh_3)_2$ (**4-10**). The same reaction at reflux conditions gives mostly a thermodynamic isomer $Re^{(I)}(\eta^2\text{-}X)(CO)_2(PPh_3)_2$ (**4-11A**). Complex **4-9** and **4-10** are found to crystallize in an unusual space group R-3 that gives a large unit cell with huge solvent channels between the Re complexes and CH_2Cl_2 solvate molecules.

The Dimroth/amidine rearrangement of benzotriazoles has been shown to exist in solution for **5-1** by variable temperature ^{19}F NMR. The reaction of **3-2** with the benzotriazoles **5-1** and **5-2** gives the new Ir(I) complex, *trans*-$Ir^{(I)}(Cl)(\eta^1\text{-}$**5-1**$)(PPh_3)_2$ (**5-7**) and Ir(III) complex, *trans*-$Ir^{(III)}(Cl)(\eta^3\text{-}$**5-2**$)(PPh_3)_2$ (**5-8**) respectively. Complex **5-7** undergoes addition and substitution reactions readily to give multiple isomers while **5-8** is inert towards nucleophiles.

Abstrait

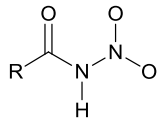
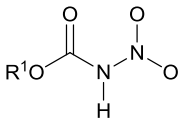
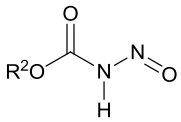
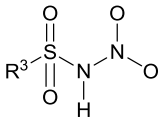

N-nitroamide		N-nitrocarbamate		N-nitrosocarbamate		N-nitrosulfonamide	
R	Label	R^1	Label	R^2	Label	R^3	Label
CH_3	**2-2**	CH_3	**2-4**	CH_3	**2-6**	*p*-tolyl	**2-8**
C_2H_5	**2-3**	C_2H_5	**2-5**	C_2H_5	**2-7**		
$Ir^{(I)}$-CH_3	**3-3**	$Ir^{(I)}$-CH_3	**3-4**	$Ir^{(I)}$-CH_3	**3-6**	$Ir^{(I)}$-*p*-tolyl	**3-7**
		$Ir^{(I)}$-C_2H_5	**3-5**				
$Ir^{(III)}$-CH_3	**3-11**	$Ir^{(III)}$-CH_3	**3-13**				
$Ir^{(III)}$-C_2H_5	**3-12**	$Ir^{(III)}$-C_2H_5	**3-14**				
$Re^{(I)}$-CH_3	**4-8**	$Re^{(I)}$-CH_3	**4-9**	$Re^{(I)}$-CH_3	**4-10**, **4-11A**	$Re^{(I)}$-*p*-tolyl	**4-12**

La réduction de l'oxyde nitreux (N_2O) en diazote (N_2) par le réductase de l'oxyde nitreux (N_2OR) est très peu comprise. La molécule N_2O n'est pas un très bon ligand et à une coordination chimique limité. Nous proposons la synthèse de précurseurs de l'oxyde nitreux qui peuvent se coordonner aux métaux de transitions avant leurs conversions en oxyde nitreux.

Nitramide, H_2NNO_2, **2-1,** et les acides d'azotes amidés N-nitroamide **2-2**, **2-3**; N-nitrocarbamate **2-4**, **2-5**, N-nitrosocarbamate **2-6**, **2-7**; N-nitrosulfonamide **2-8** ont étés synthétisés en tant que de possible précurseurs de l'oxyde nitreux pour des études de coordination avec des métaux de transitions. Les sels d'argents des bases conjugués des acides d'azotes N-nitroamide **2-2Ag**; N-nitrocarbamate **2-4Ag**, **2-5Ag**; N-nitrosocarbamate **2-6Ag**; N-nitrosulfonamide **2-8Ag** ont étés synthétisés par les réactions des ces acides avec Ag_2CO_3. Similairement, les sels de potassium des bases conjugués des acides d'azotes N-nitroamide **2-2K**; N-nitrocarbamate **2-4K**; N-nitrosocarbamate **2-6K**; N-nitrosulfonamide **2-8K** ont étés synthétisés par les réactions des ces acides soit avec K_2CO_3 ou CH_3OK.

Pour examiner l'acidité du système π de ces acides d'azotes, des séries the complexes d'acides d'azotes d'Ir(I) *trans*-$Ir^{(I)}(\eta^1\text{-X})(CO)(PPh_3)_2$, (X = acide d'azote) N-nitroamide **3-3**; N-nitrocarbamate **3-4**, **3-5**; N-nitrosocarbamate **3-6**; N-nitrosulfonamide **3-7** ont étés étés synthétisés par les réactions du complexe de

Vaska, *trans*-$Ir^{(I)}(Cl)(CO)(PPh_3)_2$ (**3-1**), avec les sels d'argents des bases conjugués des acides d'azotes (N-nitroamide **2-2Ag**; N-nitrocarbamate **2-4Ag**, **2-5Ag**; N-nitrosocarbamate **2-6Ag**; N-nitrosulfonamide **2-8Ag**). Des études comparatives avec des amides reliés, dinitramide et bistriflimide, ont aussi étés faites.

Les complexes de Re(I) des acides d'azotes, *trans*-$Re^{(I)}(\eta^2\text{-}X)(CO)_2(PPh_3)_2$, (X = acide d'azote) N-nitroamide **4-8**; N-nitrocarbamate **4-9**; N-nitrosulfonamide **4-12** ont étés synthétisés par les réactions de *trans*-$[Re^{(I)}(CH_3CN)_2(CO)_2(PPh_3)_2](Y)$, (Y = ClO_4: **4-3**, BF_4: **4-7**) aves les sels de potassium des bases conjugués des acides d'azotes **2-2K**, **2-4K** et **2-8K** respectivement. La réaction de **4-7** avec N-nitrosocarbamate **2-6K** à température de la pièce procure principalement l'isomère cinétique *trans*-$Re^{(I)}(\eta^2\text{-}X)(CO)_2(PPh_3)_2$ (**4-10**). La même réaction en condition de reflux procure principalement l'isomère thermodynamique $Re^{(I)}(\eta^2\text{-}X)(CO)_2(PPh_3)_2$ (**4-11A**). Les complexes **4-9** et **4-10** cristallisent dans un groupe d'espace insolite, soit R-3, qui à une grande unité cellulaire avec de larges canaux de solvant entre les complexes de Re et les molécules de solvant de CH_2Cl_2.

Le réarrangement Dimroth/amidine des benzotriazoles ont démontré leur existence en solution pour **5-1** via la RMN ^{19}F en température variable. Les réactions de **3-2** avec les benzotriazoles **5-1** et **5-2** donnent de nouveaux complexes d'Ir(I), *trans*-$Ir^{(I)}(Cl)(\eta^1\text{-}\mathbf{5\text{-}1})(PPh_3)_2$ (**5-7**) et d'Ir(III), *trans*-$Ir^{(III)}(Cl)(\eta^3\text{-}\mathbf{5\text{-}2})(PPh_3)_2$ (**5-8**) respectivement. Le complexe **5-7** subit facilement des réactions de substitution et d'addition pour donner de multiples isomères tandis que le complexe **5-8** est inerte envers les nucléophiles.

Acknowledgements

I would like to thank first and foremost my supervisor Prof D. Scott Bohle, for giving me the opportunity, his patient guidance, never-ending belief and encouragement during the course of my doctorate studies. Great thanks to past and present members of the Bohle research group: Aaron Kosar, Marie-Josée Bellemare, Rae Moore, Carla Spina, Heather Philips, Alex Czerniewski, Erin Dodd, Kristopher Rosadiuk, Wei Gu Yuxuan, Joël Poisson, Ivor Wharf, Mirna Veruca and Laura Brothers who have contributed in one way or another, both to the joys and annoyance of working in a lab which resembles much like a family. Special thanks to Kristopher Rosadiuk who had to endure the proof reading of most of this dissertation. Thanks also to Tina Lam of the Kakkar group for the French translation of the abstract.

I would like to give special thanks and gratitude to Dr Inna Perepichka for the countless discussions regarding anything under the sun which kept my sanity and humorous outlook of life. We have numerous collaborations and our research findings extend beyond the current of contents of this dissertation.

I would like to thank my family ZhiRen, ZhiYuan, ZhiYu and ZhiQian for their support and encouragement. In particular my parents for their utmost patience trust and encouragement in supporting me to pursue my doctorate studies overseas. I hold special gratitude to Aunt Eleanor and Uncle James Kee for giving me kinship support when I first arrive in Canada.

The following staff of the Department of Chemistry, McGill University: Dr Fred Morin, Dr Nadim Saade, Rick Rossi, Weihua Wang, Fred Kluck, Jean-Philippe Guay and Chantal Marotte own my gratitude for providing their expertise and prompt assistance during the course of my studies.

Last but not least I would like to thank Jean-Phillipe Demers, Wayne Mah, Kenward Vong and members of the Asian Dragons dragonboat team for showing me that there is much more to life than just chemical reactions!

To end, thanks to McGill University and the supporting grants for funding my doctoral studies throughout.

Contribution of Authors

This dissertation contains two research papers in sections of Chapter 2, 3 and 5.

Chapters 2 and 3: N-H activation in N-nitropropionamide: Coordination chemistry of a primary nitroamide.
D. Scott Bohle, Z. Chua, *Inorg. Chem.*, **2011**, *50*, 3135.

Chapter 5: Facile N-N Activation in Benzotriazole: Capturing the Dimroth-azo/triazole Intermediate by Complexation to Iridium.

D. Scott Bohle, Z. Chua, I. Perepichka, *ChemPlusChem*, *ASAP*.

The work in this dissertation is carried out solely by the author under the supervision of Prof. D. Scott Bohle except for the following in collaboration:

Chapter 2
Prof. D. Scott Bohle synthesized the N-nitro-*p*-tolylsulfonamide (**2-8**), its ammonium salt (**2-8NH$_4$)** and also carried out the computational calculations.

Chapter 5
Dr Inna Perepichka prepared the following benzotriazoles: 1-[(nonafluorobutane)sulfonyl]-1H-benzotriazole (**5-1**), 1,1′-sulfonylbis(benzotriazole) (**5-2**), 1-nitro-1,2,3-benzotriazole (**5-3**), 1-cyano-benzotriazole (**5-4**), 1-*p*-nitrophenylsulfonyl-1,2,3-benzotriazole (**5-5**) and 1-*p*-tolylsulfonyl-1,2.3-benzotriazole (**5-6**). She also carried out the VT-NMR ^{19}F, ^{1}H NMR experiments and UV-vis studies. She assisted with the synthesis of $Ir^{(III)}(\eta^3$-$NNPhNSO_2Btz)(Cl)(PPh_3)_2$ (**5-8**). Prof D. Scott Bohle carried out the computational calculations for the benzotriazole compounds.

I hereby give copyright clearance for the inclusion of the following papers, of which I am a co-author, in the dissertation of Zhijie Chua.

N-H activation in N-nitropropionamide: Coordination chemistry of a primary nitroamide.
D. Scott Bohle, Z. Chua, *Inorg. Chem.*, **2011**, *50*, 3135.

Facile N-N Activation in Benzotriazole: Capturing the Dimroth-azo/triazole Intermediate by Complexation to Iridium.

D. Scott Bohle, Z. Chua, I. Perepichka, *ChemPlusChem*, *ASAP*.

D. Scott Bohle
Professor and CRC Chair in Chemistry
Department of Chemistry
McGill University
801 Sherbrooke St West
Montreal
QC H3A 2K6

I hereby give copyright clearance for the inclusion of the following papers, of which I am a co-author, in the dissertation of Zhijie Chua.

Facile N-N Activation in Benzotriazole: Capturing the Dimroth-azo/triazole Intermediate by Complexation to Iridium.

D. Scott Bohle, Z. Chua, I. Perepichka, *ChemPlusChem*, *ASAP*.

Inna Perepichka, Phd
Research Associate
Department of Chemistry
McGill University
801 Sherbrooke St West
Montreal
QC H3A 2K6

Table of Contents

Chapter 1

Chapter 2

Chapter 3

Chapter 4

Chapter 5

Chapter 6

Appendix

References

List of Equations

Chapter 1

Chapter 2

Chapter 3

List of Figures

Chapter 1

Chapter 2

Chapter 3

Chapter 4

Chapter 5

Appendix

List of Schemes

Chapter 1

Chapter 2

Chapter 3

Chapter 4

Chapter 5

Chapter 6

Appendix

List of Tables

Chapter 1

Chapter 2

Chapter 3

Chapter 4

Chapter 5

Appendix

List of complexes with labels.

Chapter 2

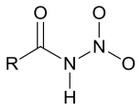

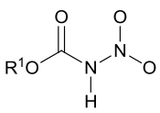

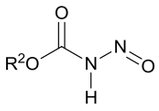

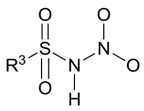

N-nitroamide		N-nitrocarbamate		N-nitrosocarbamate		N-nitrosulfonamide	
R	Label	R^1	Label	R^2	Label	R^3	Label
CH_3	**2-2**	CH_3	**2-4**	CH_3	**2-6**	*p*-tolyl	**2-8**
C_2H_5	**2-3**	C_2H_5	**2-5**	C_2H_5	**2-7**		

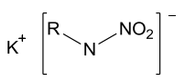

R	Compound
$CH_3C(O)$	**2-2K**
p-tolylSO_2	**2-8K**

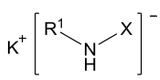

R^1	X	Compound
CH_3O	NO_2	**2-4K**
CH_3O	NO	**2-6K**

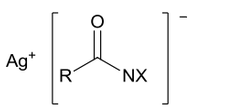

R	X	Compound
CH_3	NO_2	**2-2Ag**
CH_3O	NO_2	**2-4Ag**
C_2H_5O	NO_2	**2-5Ag**
CH_3O	NO	**2-6Ag**

Chapter 3

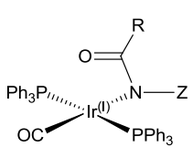

R	Z	Complex
CH_3	NO_2	**3-3**
CH_3O	NO_2	**3-4**
C_2H_5O	NO_2	**3-5**
CH_3O	NO	**3-6**

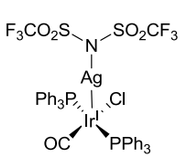

3-9

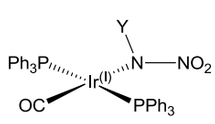

Y	Complex
p-tolylSO_2	**3-7**
NO_2	**3-8**

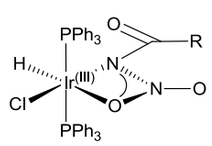

R	Complex
CH_3	**3-11**
C_2H_5	**3-12**
CH_3O	**3-13**
C_2H_5O	**3-14**

Chapter 4

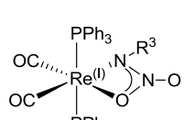

R^3	Complex
$CH_3C(O)$	**4-8**
$CH_3OC(O)$	**4-9**
p-tolylSO_2	**4-12**

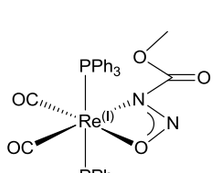

4-10

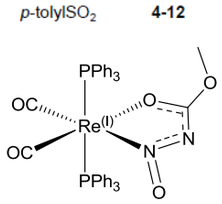

4-11A

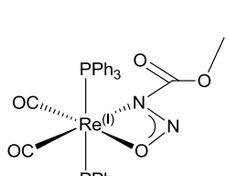

4-11B

Chapter 5

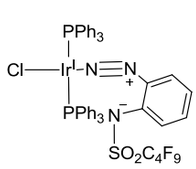

5-7

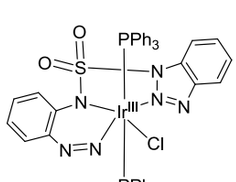

5-8

Chapter 1: Introduction

1.1 Nitrogen cycle and various nitrogen oxidation states

Inorganic nitrogen containing compounds are metabolised by enzymes in the bacteria domain to its various oxidation states that play out in the biogeochemical nitrogen cycle (Figure 1-1). The oxidation states of nitrogen that is present in the natural environment range between +5 in NO_3^- to -3 in NH_4^+. Almost all of these enzymes contain transition metal complexes or clusters that catalyse the redox reactions to convert the different nitrogen species in the nitrogen cycle.

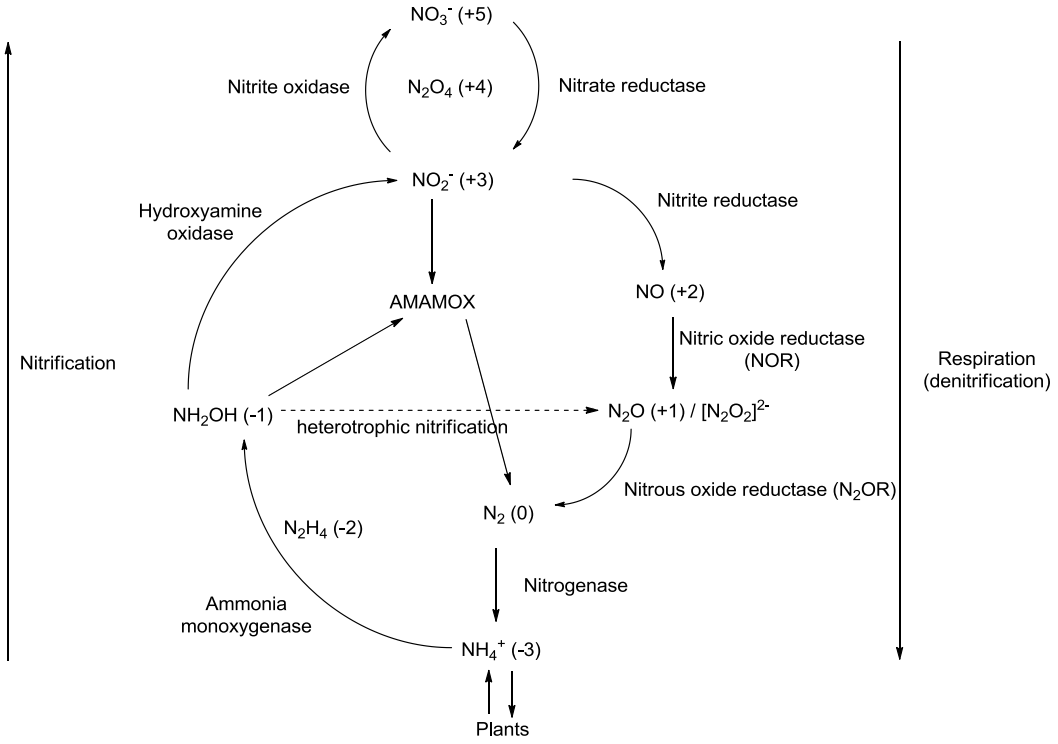

Figure 1-1. The nitrogen cycle in the natural environment.[1]

In many cases, these enzymes are located in environments that have limited access to oxygen such as deep ocean or soil which give rise to a need for an alternative source of electron carrier for respiration. The dinitrogen composition of air is approximately 78 % but in its elemental form is not useful with regards to both flora and fauna uptake. Therefore these enzymes play a very important role

in converting the different forms of nitrogen to allow the uptake and conversion of nitrogen into the ecosystem.

In particular, the nitrogenase enzyme has been the main focus of research as it plays an unique and essential role in 'fixing' dinitrogen in the atmosphere for uptake by plants in the form of ammonium salts. The reduction of dinitrogen to ammonia is a thermodynamically favourable process (-45.9 kJ mol^{-1}) but has a high activation energy (420 kJ mol^{-1}) thus requiring a catalyst for the reaction to be favourable.[2] Most nitrogenase contains a unique and unusual $MoFe_7S_9C$ metal cluster that is the site of the catalytic reduction of N_2 to ammonia. Modern methods of nitrogen fixation since the agricultural revolution include cultivation nitrogen fixation from fodder legumes, fossil fuel combustion and the Haber-Bosch process.[3]

1.1.1 Nitrous oxide reductase (N_2OR)

The focus on nitrogen fixation, with regards to reduction of N_2, for mainly agricultural uses has however overlooked the important role that the enzyme nitrous oxide reductase (N_2OR) plays. N_2OR catalyses the reduction of N_2O to N_2 (Equation 1-1).[4]

$$N_2O + 2H^+ + 2e^- \longrightarrow N_2 + H_2O \quad \Delta G = -339.5 \text{ kJ mol}^{-1}$$
$$E_{red} \text{ (pH 7.0)} = +1.35 \text{ V}$$

Equation 1-1. Reduction of N_2O.

Even though the reduction is highly exogenic at standard conditions, the reaction does not proceed at an appreciable rate without any catalyst. Nitrous oxide is a very stable molecule such that minimal thermal decomposition occurs even at temperatures between 400-530 ^oC.[5] This phenomenon is attributed to the spin-forbidden decomposition[6] deriving an activation energy of around 250 kJ mol^{-1} (Equation 1-2).[7]

$$2N_2O \longrightarrow 2N_2 + O_2 \qquad E_a = +250 \text{ kJ mol}^{-1}$$

Equation 1-2. Decomposition of N_2O.

Nitrous oxide is often perceived as environmentally benign and has a more commonly known moniker as laughing gas. It is not an environmentally neutral species formed during the denitrification process of the nitrogen cycle because it is both a greenhouse gas and ozone depleting substance. Nitrous oxide's ozone depleting ability derives from its reaction with excited oxygen atoms in the stratosphere which in turn generates various nitrogen oxides that contribute to the destruction of ozone.[8] It is also a much more potent greenhouse gas than carbon dioxide.[9] With a long half-life of around 120 years, coupled with its increased emissions from both natural sources[10] and anthropogenic process such as combustion, agriculture use[11] and waste water treatment,[12] nitrous oxide, with its persistency, will become one of the main factors affecting climate change and ozone depletion.[3, 8, 13]

The implications are that there is urgent need to better understand the functioning of the enzyme N_2OR. To this end, significant progress has been made in understanding the biogenesis/gene-sequencing and structure of N_2OR in recent years.[14] N_2OR is a homodimer that consists of two metal sites that contains solely Cu. Both the copper sites within N_2OR do not conform to the standard three types of Cu proteins from spectroscopic analysis.[15]

1.1.2 N_2OR Cu_A site

The two sites of N_2OR have been designated Cu_A and Cu_Z.[1a] The Cu_A site has been identified as a dinuclear Cu complex that bears great similarity to the mitochondrial-type cytochrome *c* oxidase (Figure 1-2).[16]

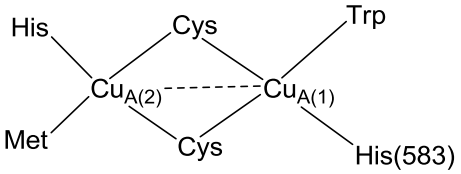

Figure 1-2. Cu_A site of N_2OR.

Cu_A has been identified as a cupredoxin which makes it a redox active site with low reorganisation energy and therefore recognised as the electron transfer site in N_2OR and cytochrome oxidase.[4, 17]

1.1.3 N_2OR Cu_Z site

The Cu_Z site, which is now identified as the catalytic site, is unique as it was found to be the only tetranuclear Cu cluster with a sulfur atom bridging the four Cu atoms. Although originally assigned as being an oxygen bridged cluster,[16a] the bridging atom was subsequently corrected to a sulfur atom based on more precise sulfur determination and also better resolution crystal structures (Figure 1-3).[18]

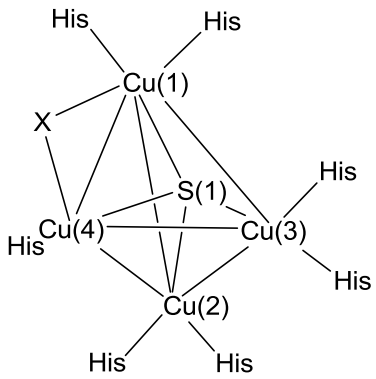

Figure 1-3. Cu_4S core of N_2OR Cu_Z site. X = H_2O/OH^-,[16b, 18] $H_2O + OH^-$,[19] I^- inhibited form,[19] $S(2)^{2-}$.[20]

This is the first kind of Cu_4S cluster found in enzymes which is as unique as the MoFe cofactor in nitrogenase[21] or Mn_xCa_y cluster in the oxygen-evolving complex (OEC) of photosystem II.[22] With limited precedence of such a Cu cluster motif in enzymes, great interest was generated in deriving the machinery of the catalytic reduction of N_2O. Before such an endeavour could be attempted, there was a need to resolve the different forms of the N_2OR enzymes that have been isolated this far.

Before structural determination of N_2OR was achieved, different coloured forms of the enzyme were reported. The different coloured forms of N_2OR were due to the protocols of isolation of N_2OR, either aerobically or anaerobically and also the

state of isolation, either as isolated or in the presence of reducing agents (Table 1-1).

Table 1-1. Different assignments of multiple redox states of N_2OR (Cu_Z is the active state; Cu_Z^* the inactive state).

	Cu_A state	Cu_Z[a] state	
Anaerobic (Cu_Z)		Type[14b]	Form[23]
As isolated (fully oxidised) – purple	$[Cu^{1.5+} - Cu^{1.5+}]$	(**A**): $[2Cu^{2+} - 2Cu^{+}]$	**I:** $[3Cu^{2+} - Cu^{+}{:}2S]$
Ascorbate reduced	$[Cu^{1+} - Cu^{1+}]$	(**B**): $[2Cu^{2+} - 2Cu^{+}]$	**III**: $[3Cu^{2+} - Cu^{+}{:}2S]$
Dithionite reduced	$[Cu^{1+} - Cu^{1+}]$	(**C**): $[Cu^{2+} - 3Cu^{+}]$	
	Cu_A state	Cu_Z^*[a] state	
Dithionite reduced	$[Cu^{1+} - Cu^{1+}]$		**III***: $[Cu^{2+} - 3Cu^{+}{:}S]$
Aerobic (Cu_Z^*)		Type	Form
As isolated (fully oxidised) – pink	$[Cu^{1.5+} - Cu^{1.5+}]$	(**D**): $[Cu^{2+} - 3Cu^{+}]$	**II**: $[3Cu^{2+} - Cu^{+}{:}S]$
Dithionite/ascorbate reduced - blue	$[Cu^{1+} - Cu^{1+}]$	(**E**): $[Cu^{2+} - 3Cu^{+}]$	**III***: $[Cu^{2+} - 3Cu^{+}{:}S]$
Fully reduced (activated form)[b]	$[Cu^{1+} - Cu^{1+}]$	(**F**): $[4Cu^{+}]$	

a: There is still a debate as to the true redox state of Cu_Z/Cu_Z^*.

b: Form F has only been isolated under aerobic conditions (methyl viologen reduced).[24]

The difference between the anaerobic and aerobic isolation of N_2OR is that only under anoxic conditions, can the Cu_Z state can be obtained. However even anaerobic isolation of N_2OR, using the strongly reducing dithionite[25] will result in the formation of the Cu_Z^* state. All oxic protocols give only Cu_Z^* state. It is also shown in Table 1-1 that mild reducing agents such as ascorbate will selectively reduce only the Cu_A site. This selectivity has been used to determine the different 'redox forms' of the N_2OR as will be explained next. For all the crystal structures of N_2OR obtained (Figure 1-3), the edge along the Cu(1)-Cu(4) in the Cu_Z site has some residual electron density. Furthermore, all the Cu centers except Cu(4) have at least two His ligands binding to it. In structures determined prior to 2011, this residual electron density has been assigned either as water

and/or hydroxyl ions.[16b, 18-19] An inhibited form of the N_2OR enzyme using sodium iodide was also shown to have an iodide ion bonded to the Cu(1) and Cu(4) centers.[19] Only recently in 2011, Einsle and co-workers[20], using anaerobic methods of isolating N_2OR, have determined that the residual electron density along the Cu(1)-Cu(4) edge is actually a second sulfur atom, S(2). This has been confirmed using modern techniques of sulfur determination and more importantly by explaining the observed UV-visible spectrums of the different forms of N_2OR. The purple form of N_2OR (**form I**) (Table 1-1) is usually obtained only under anaerobic conditions. **Form I** N_2OR has a distinct absorption maximum at 538 nm which can be deconvoluted into separate absorption bands due to the Cu_A and Cu_Z centers. By using ascorbate to selectively reduce Cu_A to the [Cu^+ - Cu^+] colourless state, **B** or **form III** (Cu^+ - d^{10} complexes are usually colourless due to absence of d-d transitions) (Table 1-1), the absorption contribution of the Cu_A can be removed to allow only the absorption spectrum of the Cu_Z site to be observed.[20, 26] This subspectrum of Cu_Z site has been modeled to show absorption bands at 552 and 650 nm[20, 23] and is designated as the Cu_Z state. It is further suggested that the two transitions arise from the charge transfers of the two sulfur atoms to the Cu atoms. Under oxic conditions, a pink form of N_2OR (**form II**) (Table 1-1) was isolated which shows a different absorption maximum due to the missing absorption contribution at 552 nm[20] and this has been attributed to the loss of S(2) under such conditions. **Form II** N_2OR has been described as the Cu_Z^* state in literature.[27] Prior to the work by Einsle *et al*., the Cu_Z and Cu_Z^* state of the Cu_Z site has been attributed to the oxidation states of the Cu atoms which is believed to derive from the active/inactive state (Table 1-1). The difference in the classification: oxidation states of the Cu atoms versus the presence of S(2) of the CuZ centers from their UV-visible spectrums is still a subject of debate. This is complicated by recent findings of a new Cu_Z^o state[28] and a purple form of N_2OR[29] isolated under aerobic conditions.[14b, 23] An extension of the controversy is that for **form I** N_2OR, the first reduction by ascorbate is quick but a second much slower reduction[23] by sodium dithionite is required before the enzyme is catalytically active (induction period). Compared

with the newly discovered Cu_Z^o state, which does not need an induction period to be active, it is a puzzle as to what is the main determinant to represent the true form of N_2OR. Electron paramagnetic resonance (EPR) measurements of the catalytically active state of **form I** will have been useful in allowing a better comparison with this new Cu_Z^o state. Currently the two groups of researchers involved in this debate are also using different species of the N_2OR enzyme.

1.1.4 Nitrous oxide binding location in N_2OR

The next topic of debate relates to the electron transfer pathway and N_2O binding site in N_2OR. Solomon *et al.*[24] had proposed a possible N_2O binding site along the Cu(1) and Cu(4) edge, through actual N_2O reduction by N_2OR of a fully reduced Cu_Z state **F** (Table 1-1) together with Density functional theory (DFT) optimised models (Figure 1-4) prior to the work of Einsle *et al.*[20]

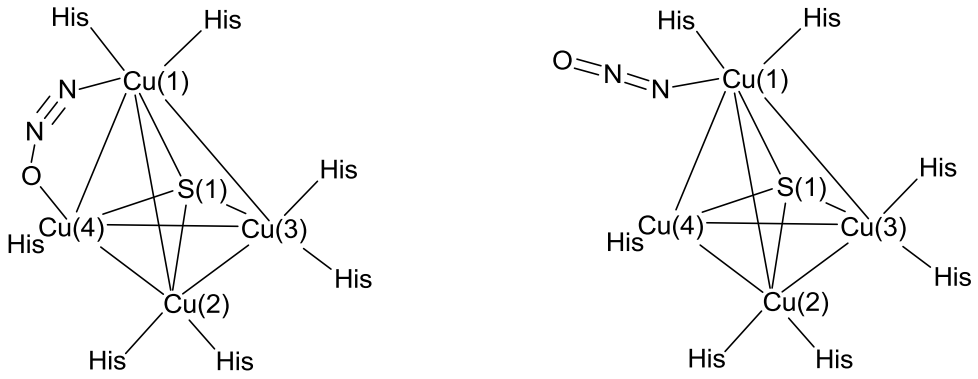

Figure 1-4. DFT calculated geometries of N_2O complexes of Cu_Z site. **1-1A** is fully reduced [$4Cu^+$] and **1-1B** is [Cu^{2+} - $3Cu^+$].

Model **1-1A** shows nitrous oxide bound in a side-on fashion compared to **1-1B** which is in a linear form through the terminal nitrogen. The N_2O binding energy of **1-1A** is larger compared to **1-1B** and together with then-current experimental results, EPR, UV-vis spectroscopy, magnetic circular dichroism (MCD) and X-ray absorption spectroscopy (XAS) studies, the authors proposed **1-1A** to be a very likely model for N_2O binding and reduction. The N_2OR dimer is also bound

in a head to tail orientation of the monomers with the Cu_A site of subunit 1 about 10 Å from the Cu_Z site of subunit 2 (Figure 1-5). The authors also proposed suitable electron-transfer pathways between Cu_A subunit 1 and Cu_Z subunit 2.[30]

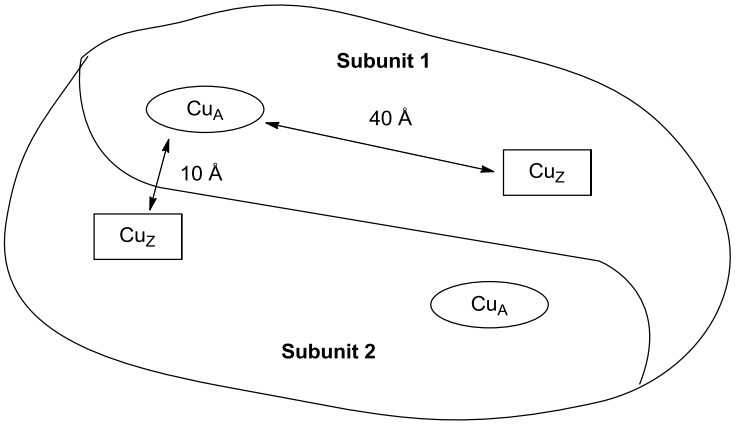

Figure 1-5. Orientation of subunits in N_2OR.

The above model **1-1A** is now put into question with the most recent crystallographic structure of N_2OR. With S(2) located in the proposed bound position of N_2O (Figure 1-3), a new binding site for nitrous oxide has been proposed. Nitrous oxide was pressurized with the crystals of **form I** N_2OR and was located at a hydrophobic channel near the interface of subunit 1 and 2 between Cu_A and Cu_Z site (Figure 1-6).[20] Of particular note is that His(583) in Cu_A site is now coordinated to $Cu_{A(1)}$; N_2O-free N_2OR has His(583) un-coordinated to $Cu_{A(1)}$. The nitrous oxide molecule is not found to be coordinated to either Cu_A or Cu_Z sites with the closest Cu-N_2O distance at least 3.1 Å. The nitrous oxide molecule is positioned in a side-on manner to the (3Cu-2S) surface formed by Cu(1), Cu(2), Cu(4), S(1) and S(2) atoms at the Cu_Z site. Based on the observed substrate induced His(583) coordination, together with the substrate location between the two metal sites, the authors proposed that Cu_Z is not the actual catalytic site but a metal cluster that is able to 'prime' N_2O for direct reduction by the Cu_A site.[23] This proposition is highly unlikely due to the need for two simultaneous single electron transfers to reduce N_2O to N_2 during which highly reactive oxygen radicals may form.[31].

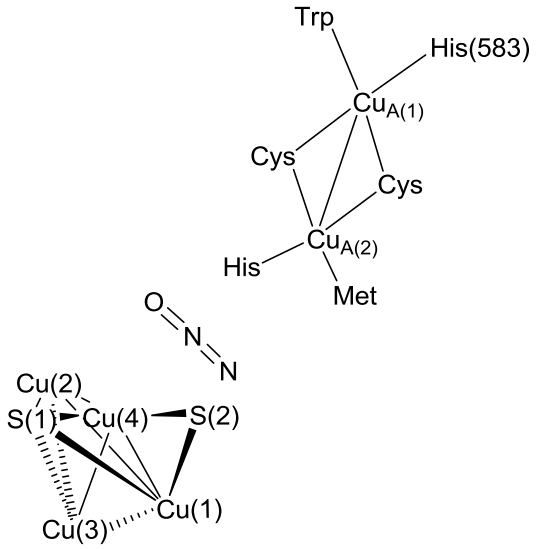

Figure 1-6. Form I N_2OR with N_2O bound. His ligands for Cu_Z site are not shown.

The kinetic inertness (Equation 1-2) of nitrous oxide hinders its potential as a green oxidant (Equation 1-1) for industrial processes as the only waste product from this process is N_2.[32] Nevertheless some applications of nitrous oxide as an oxidant have been developed e.g. oxidation of benzene to phenol.[33] However extending the scope of such oxidation reactions have been limited even with extensive research.[5, 34] We believe that a better understanding of N_2O reduction to N_2 through coordination chemistry will allow further development in this area. A particularly interesting example to highlight is the dicopper-disulfido cluster complex reduction of N_2O which bears much similarity with the N_2OR Cu_Z cluster in the UV-vis absorbance changes (Scheme 1-1).[35]

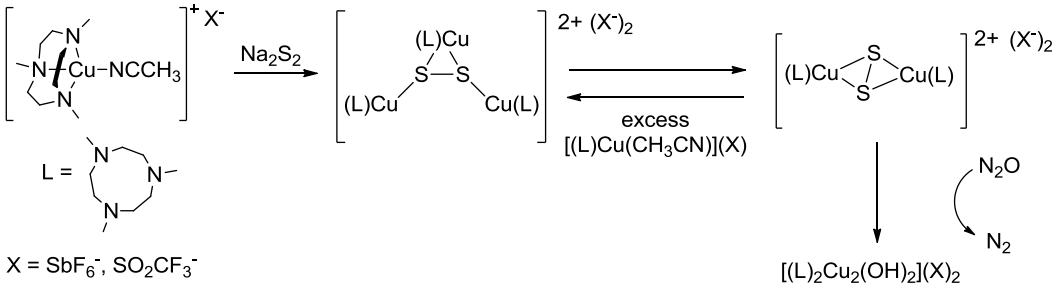

Scheme 1-1. Reduction of N_2O by Cu_2S_2 cluster to N_2.

1.2 Coordination chemistry of nitrous oxide, N_2O

1.2.1 First transition metal N_2O complex

The first N_2O complex was prepared by both Diamantis[36] and Taube[37] in their investigations of $[Ru(NH_3)_5(H_2O)]^{2+}$ salts with N_2O to give a compound identified as $[Ru(NH_3)_5(N_2O)](X_2)$ (X = BF_4, Br), (**1-2**) from IR spectroscopy, decomposition gas evolution and elemental analyse (Equation 1-3).

$$[Ru(NH_3)_5(OH_2)]^{2+} + N_2O \rightleftharpoons [Ru(NH_3)_5(N_2O)]^{2+} + H_2O$$

1-2

$$\textbf{1-2} + 2H^+ + 2e \longrightarrow [Ru(NH_3)_5(N_2)]^{2+} + H_2O$$

Equation 1-3. N_2O reaction with Ru complex.

This compound is unstable and depending on the reaction conditions[38] (e.g. N_2O pressure, use of additional external reducing agents as $[Ru(NH_3)_2(OH_2)]^{2+}$ is a strong reductant) tends to give variable yields and product mixtures raising doubts on the purity of the samples due to the differences in the IR spectroscopy reported.

Bottomley *et al.*[39] established an alternative method to $[Ru(NH_3)_5(N_2O)](Y)_2$ (Y = Cl, Br, I) (**1-2**) by the reaction of $[Ru(NH_3)_5(NO)](Y)_3$ with hydroxylamine hydrogen chloride, $NH_2OH.HY$ which gave a reasonable and good purity of the product (Equation 1-4).

$$[Ru(NH_3)_5(NO)]^{3+} + NH_2OH + OH^- \longrightarrow [Ru(NH_3)_5(N_2O)]^{2+} + 2H_2O$$

1-2

Equation 1-4. Synthesis of Ru N_2O complex.

The IR characteristics for this compound are a strong band in the 1160 cm^{-1} region and a weak band in the 2250 cm^{-1} assigned to the υ_1 and υ_3 mode of the coordinated N_2O respectively (gaseous N_2O has bands at 1286 and 2224 cm^{-1}).[39b] Unfortunately no suitable single crystals for the compound (**1-2**) could be obtained due to the rapid dissociation of N_2O in **1-2** in solutions. The lack of definitive structural connectivity gave rise to debates on whether the N_2O ligand

binds to the Ru metal through the N or O terminus atom.[40] This debate has since been put to rest with a thorough and careful analysis of IR, Raman and electronic structure with comparison to DFT calculated values using isotopic ^{15}N substitution of the N_2O ligand of the Ru complex.[41] The results are best described as N_2O bound to Ru through the N-terminus atom in a linear geometry. Since the discovery of **1-2**, no complexes of N_2O as a ligand have been isolated till 2009. However multiple reports on attempts at N_2O complex formation have resulted in mostly metal oxide complexes[42] (mostly from O-atom abstraction), metal nitride with metal nitrosyls[43] formation and oxidised side products such as phosphine oxide.[44] Other instances of N_2O reduction to form N_2 complexes have also been reported.[35, 45] The rarity and difficulty of forming such N_2O complexes also gave rise to a series of articles using computational methods to account for N_2O and complexation reactivity.[46]

1.2.2 Frustrated Lewis Pairs N_2O complex

The start of the renaissance of N_2O complexation began with the first example of a frustrated Lewis pair (FLP) complex containing N_2O by Stephan *et al*. (Scheme 1-2).[47]

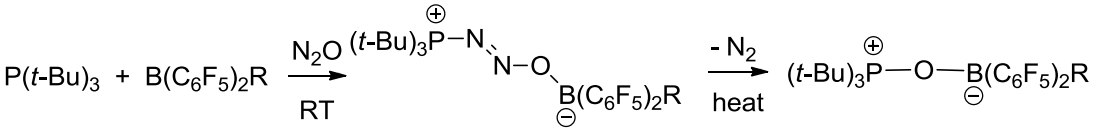

1-3a: R = C_6F_5
1-3b: R = Ph

Scheme 1-2. Formation of N_2O FLPs.

Subsequently articles featuring such modular assembly of nitrous oxide with other FLP components such as Zn, Zr and Ti Lewis acidic complexes have been reported.[48] The crux of the formation of nitrous oxide FLPs has been attributed to the strength of the Lewis basicity of the nucleophile as facile Lewis acid substitution can still occur once the FLP complex is formed.[48b] Nucleophiles which are less basic e.g, nitrogen bases or P(*o*-tolyl)$_3$, do not result in the

precipitations (essential step) of the FLP complex formation. Further investigations of the N_2O FLPs reveal that heating or prolonged exposure of the non-precipitated phosphines to N_2O result eventually in the formation of phosphine oxides.[48b]

1.2.3 First structurally characterised transition metal N_2O complex

The real breakthrough of an actual N_2O complex fully characterised was obtained by Chang *et al*.[49] in 2011 (Scheme 1-3).

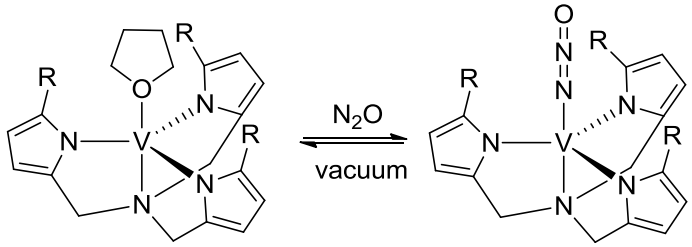

Scheme 1-3. Synthesis of vanadium N_2O complex.

In the single crystal structural determination of **1-4**, the N_2O ligand was found to bind through the terminal N atom in a linear arrangement which is similar to **1-2** proposed by both Bottomley and Taube. The atomic assignment of N_2O in **1-4** was confirmed with $^{15}N^{15}NO$ substitution in IR spectroscopy and also DFT calculations using a basis set derived from crystallography determined structures followed by geometry optimisation. The binding of N_2O to the vanadium metal was also found to be labile in solution such that application of a reduced atmosphere results in the loss of N_2O and the formation of the starting complex. Since the announcement of this remarkable complex, no further news regarding **1-4** for catalysis or mechanism of activation for N_2O has been reported.

1.2.4 N-heterocyclic carbene activation of N_2O

More recent advances in N_2O coordination/activation has been reported when N-heterocyclic carbenes are shown to react with nitrous oxide to generate a previously unknown N_2O adduct (Scheme 1-4).[50]

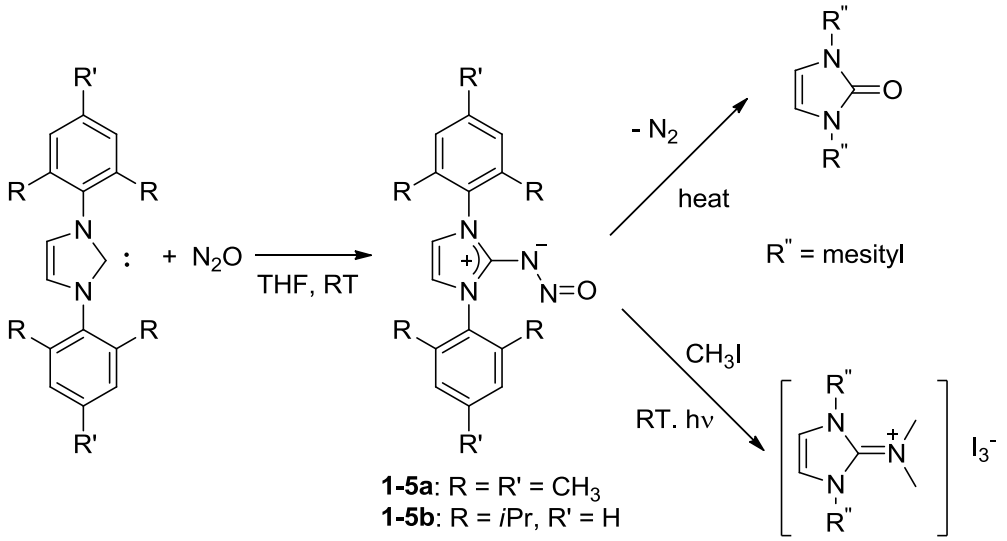

Scheme 1-4. Synthesis of N-heterocyclic N_2O adduct and reactivities.

N-heterocyclic carbenes are strong Lewis bases and have found been found to activate other small molecules such as carbon dioxide.[51] Compounds **1-5** are similar to N_2O FLPs such as **1-3** except that no Lewis acid pairing is required for the formation of the addition adduct. Compounds **1-5** are also stable to both water and air, however heating **1-5** results in a facile loss of N_2 to generate a urea product (Scheme 1-4) and reaction with CH_3I with UV radiation give a guanidinium salt product from N-N scission.

Compound **1-5a** has been further reacted with a vanadium complex to generate a vanadium oxo complex coupled with an insertion into one of the V-C bonds to give a hydrazine-like complex (Scheme 1-5).[52]

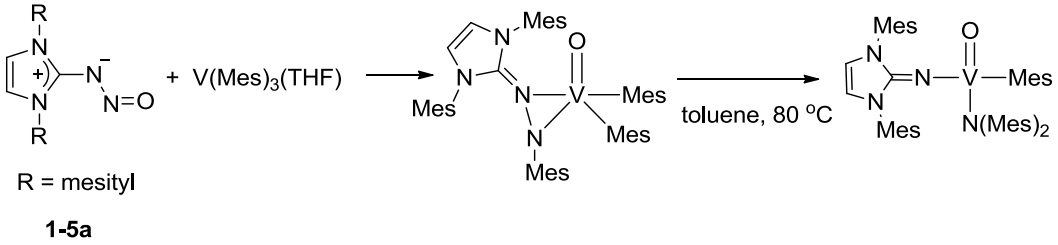

Scheme 1-5. O-abstraction of N_2O carbene adduct.

The O-abstraction reaction product is often encountered in early transition metals due to their oxophilic nature. Subsequent heating of the complex ruptures the long N-N bond of the hydrazine-like ligand.

The above examples of N_2O complexes and activation so far have provided some possible details into the mechanistic activation of N_2O by N_2OR. The vanadium N_2O complex characterised by Chang *et al*. has proven yet again that N_2O is a poor ligand shown by the lability of the N_2O molecule even on coordination. No further reports of **1-4** with regards to N_2O activation or reactivity are known. The successful activation of N_2O towards decomposition to N_2 and O atom by N-heterocyclic carbenes is a clue that such activation requires a strong nucleophile/Lewis base attack on the terminal N atom of nitrous oxide. This is further supported by nucleophilic addition to the terminal nitrogen of N_2O in the synthesis sodium *cis*-hyponitrite from the reaction of sodium oxide and N_2O gas (Scheme 1-10).[53]

This is in agreement with our hypothesis that the sulfur atoms in the N_2OR are probable nucleophiles which attack the terminal nitrogen of nitrous oxide in the first stage of the activation before protons are transferred to effect N-O cleavage and water formation. Therefore the Cu_z site in N_2OR may not be a site for N_2O coordination but is instead a strong nucleophilic reagent that attacks N_2O to form an intermediate which is more reactive towards decomposition to release N_2 and water. Such chemical reactivity is actually very relevant in biological process with regards to Zn enzymes such as carbonic anhydrase (Scheme 1-6).

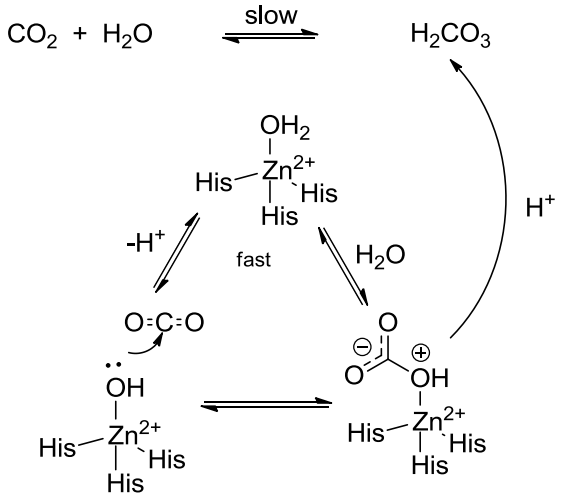

Scheme 1-6. Formation of carbonic acid catalyse by carbonic anhydrase.

Based upon this concept, we proposed to synthesize N_2O-precursor adduct complexes that may mimic the N_2O reduction process in N_2OR (Scheme 1-7).

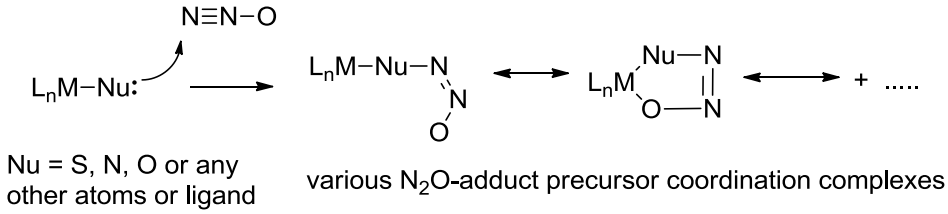

Scheme 1-7. Proposed N_2O-adduct precursor coordination complexes.

The complexes synthesized will be studied for their reactivity which may provide additional information for understanding N_2OR functionality.

1.3 Nitrous oxide adduct precursors

In the natural environment, N_2O is formed from the reduction of nitric oxide (NO) by the heme-based nitric oxide reductase (NOR)[1] (Figure 1-1). Thus NO itself could be a potential precursor to N_2O, through the reductive coupling of NO to give N_2O is very uncommon.[54] The chemistry of nitric oxide is known to give rise to 1) a kinetically important dimerization to give $[NO]_2$ and 2) facile disproportionation by both NO and $[NO]_2$ (Equation 1-5).

$$3NO \longrightarrow NO_2 + N_2O$$

Equation 1-5. Disproportionation of NO and $[NO]_2$.

It is however not a suitable precursor to N_2O as the reactions are complex and difficult to control. Other possible precursors of N_2O are the hyponitrites, nitroxyl and nitramide. An alternative pathway to N_2O is by heterotrophic nitrification from hydroxylamine which is still poorly understood.

1.3.1 Hyponitrites $[N_2O_2]^{2-}$

Hyponitrites as salts of the corresponding hyponitrous acid have been since the first discovery of hyponitrites by Divers in 1870.[55] There are several ways of making hyponitrites of which two of these are the more commonly used method. The first method was developed by Divers through the reduction of sodium nitrite with sodium amalgam and modified by Addision and co-workers (Scheme 1-8).[56]

$$NaNO_2 + Na/Hg \longrightarrow Na_2N_2O_2 + N_2O + ...$$

Scheme 1-8. Reduction of sodium nitrite with sodium amalgam.

This preparation gave poor yields and is often contaminated with unreacted sodium nitrite, sodium hydroxide (from sodium) and sodium carbonate (CO_2 in the atmosphere). Subsequent attempts at improving the synthesis was reported by Polydoropoulos through purification by formation of the silver hyponitrite and reconverting back to the sodium salt with sodium iodide.[57] An overall improvement using this reduction method was reported by Hughes.[58] The

alternative method involves the reaction of nitrous acid with hydroxylamine and its derivatives.[59] The yield from this method varies depending on the source of the actual nitrosating reagent.

There are three possible structural isomers of hyponitrite as shown in Figure 1-7. In all the discussion above, no mention of which form of hyponitrite has been isolated.

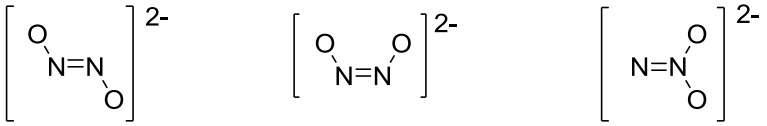

trans-hyponitrite *cis*-hyponitrite nitridonitrate

Figure 1-7. Possible isomeric forms of $[N_2O_2]^{2-}$.

Electronic excitation studies of the hyponitrites have only been able to identify the presence of the N=N bond which tends to give an absorbance around 248 nm (ε = 6900),[58] therefore vibrational spectrum is required to differentiate the isomers. The molecular point group symmetries of *trans*-hyponitrite, *cis*-hyponitrite and nitridonitrate are C_{2h}, C_{2v} and C_{2v} respectively. Based on the mutually exclusive rules of the IR and Raman bands for C_{2h} symmetry, experimental evidence assigns the hyponitrites obtained from the above methods as *trans*-hyponitrite.[60] These assignments were confirmed with the structural determination of *trans*-hyponitrous acid and its various anions by X-ray diffraction.[61] The mechanistic study of sodium *trans*-hyponitrite is well covered.[62] There has been much speculation that the synthesis of sodium hyponitrite from the reduction of sodium nitrite or nitrosation of hydroylamine involves the formation of both *cis* and *trans* hyponitrites. However as the *cis* is believed to be kinetically unstable to its products, it rapidly decomposes to give nitrous oxide leaving only the sodium *trans*-hyponitrite upon isolation. This preposition lends itself some weight due to the fact that vigorous evolution of nitrous oxide is always observed during the synthesis of sodium *trans*-hyponitrite which accompanies its low yield. These outcomes are in contrast with high level computational studies of the isomeric forms of hyponitrous acid which predicts that *cis*-hyponitrous acid is more stable than *trans*-hyponitrous acid.[63]

Since then multiple attempts to synthesize *cis*-hyponitrites have been met with the first successful synthesis of a Pt *cis*-hyponitrite complex which was obtained with low yields from the reaction of $Pt(PPh_3)_4$ with nitric oxide by reductive NO coupling (Scheme 1-9).[64]

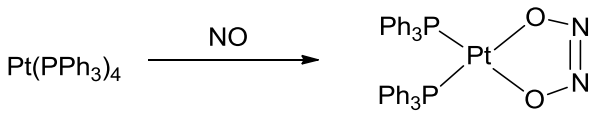

Scheme 1-9. Synthesis of *cis* $Pt(\eta^2\text{-}N_2O_2)(PPh_3)_2$.

The first successful synthesis of sodium *cis*-hyponitrite was isolated from a high pressure and temperature gas-solid reaction of nitrous oxide with sodium oxide (Scheme 1-10).[53, 65]

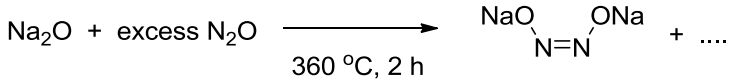

Scheme 1-10. Synthesis of sodium *cis*-hyponitrite.

The compound was structurally characterised from its powder diffraction pattern with vibrational analysis and conditions had to be optimised to get a decent yield as it decomposes over prolonged reaction times and is sensitive to moisture. In further elaboration, the authors were actually trying to synthesize the third isomeric form of hyponitrite, the nitridonitrate form (Figure 1-7), which by serendipity was isolated as a *cis*-hyponitrite.

To date, more examples of *cis*-hyponitrites have been synthesized mostly by the reaction of diazeniumdiolates with transition metal complexes (Scheme 1-11). These diazeniumdiolates are in turn obtained from the reductive dimerization of NO. These *cis*-hyponitrites are always isolated as chelate complexes which tend to decompose on heating releasing nitrous oxide.[66]

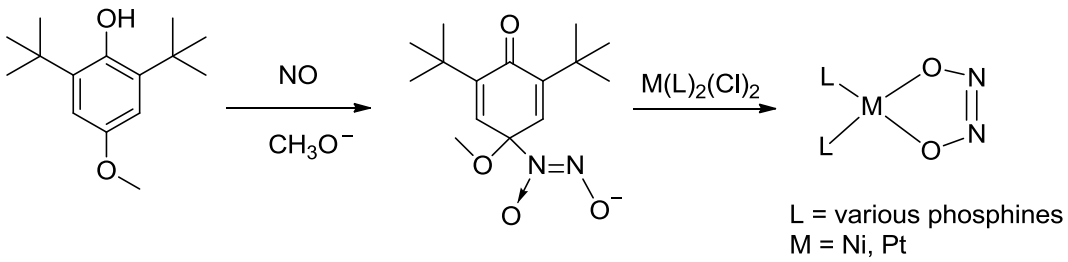

Scheme 1-11. Formation of *cis*-$M(L)_2(\eta^2\text{-}N_2O_2)$.

Hyponitrous acid and the related hyponitrites discussed above produce nitrous oxide on decomposition but are generally made in low yields and their limited reactivity have shown them to readily decomposed to nitrous oxide. Formally, nitrous oxide can be considered the anhydride of hyponitrous acid (Equation 1-6).

$$N_2O + H_2O \Longrightarrow H_2N_2O_2$$

Equation 1-6. Proposed 'Hydration' of N_2O to give hyponitrous acid.

Hyponitrous acid as possible precursor of nitrous oxide, has limited reactivity that can be carried out to better understand nitrous oxide reduction. The related nitridonitrate isoform (Figure 1-7) will be discussed in section 1.3.3. The hyponitrites with relation to hyponitrous acid display marked differences in stability with regards to pH of the solutions. As hyponitrous acid is a weak diacid with estimated pKa_1 = 7 and pKa_2 = 11[67], different dominant species are present in solution depending on pH which contributes to differences in decomposition pathways. At pH < 4, the dominant species is the protonated form of hyponitrous acid which slowly decomposes to give N_2, NO and N_2O.[68] Between pH 4 – 11, the dianion $[N_2O_2]^{2-}$ is stable, with the free acid relatively stable too. However the monoanion $[HN_2O_2]^-$ is very unstable and rapidly decomposes to give N_2O and hydroxide (Equation 1-7) which attacks the free acid resulting in a chain decomposition.

$$[HN_2O_2]^- \longrightarrow N_2O + OH^-$$

Equation 1-7. Decomposition of $[HN_2O_2]^-$.

1.3.2 Nitroxyl (HNO)

A possible alternative for the nitrous oxide precursor comes in the form of the nitroxyl (HNO) molecule. The existence of nitroxyl was first described in separate reports by Angeli[69] and Piloty[70] towards the end of the 19th century. The reagents from these reports that generate nitroxyl were henceforth named Angeli's salt ($Na_2N_2O_3$) and Piloty's acid ($PhSO_2NHNOH$). Nitroxyl in both the reports is said to be an intermediate that arise from the decomposition of the reagents and much work has been done to better understand its chemistry, particularly its biological chemistry.

The main obstacle in understanding nitroxyl chemistry is due to its rapid dimerization to give nitrous oxide and water which is proposed to proceed through the transient *cis*-hyponitrous acid as mentioned in the above section (Equation 1-8)[71] which may be exploited as a source of N_2O.

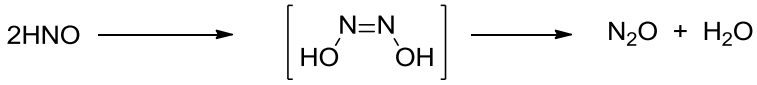

Equation 1-8. Dimerisation of nitroxyl to give N_2O and water.

There are various HNO sources in literature,[72] but Angeli's salt and Piloty's acid or its derivatives (some synthesized readily from hydroxylamine and sulfonyl chlorides)[73] are usually the common reagents used to generate HNO.[72b, 74]

There have been various studies carried out on the decomposition of Angeli's salt and it is generally accepted to undergo a pH independent decomposition between pH 4 - 8 (Scheme 1-12) by the initial protonation of the nitroso oxygen, rearrangement and finally N-N bond scission.[58, 69, 75]

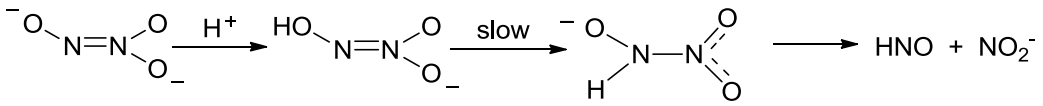

Scheme 1-12. Decomposition of Angeli's salt.

As nitrite is released with the formation of HNO, the presence of excess nitrite in solution has been found to suppress the decomposition of Angeli's salt which demonstrates some extent of reversibility of the decomposition.[58] At pH < 3,

Angeli's salt will decompose to give solely NO from a different decomposition mechanism that has yet to be elucidated. It is stable at pH > 9.

In contrast, Piloty's acid however undergoes base catalysed decomposition to give HNO (Scheme 1-13) through the initial deprotonation of the sulfoxamic proton and S-N bond cleavage.[70, 72a]

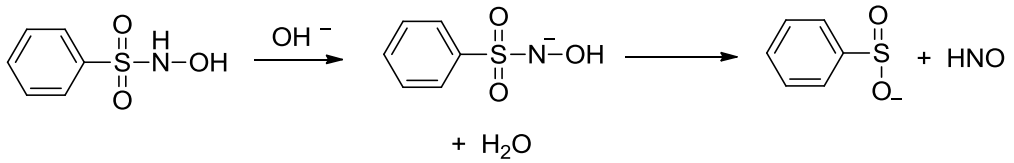

Scheme 1-13. Decomposition of Piloty's acid.

At pH > 13, the rates of decomposition of Piloty's acid is similar to Angeli's salt between pH 4 – 8 allowing the opportunity to utilise the reagents according to the required conditions to generate HNO. Extra precautions (under an anaerobic atmosphere) must however be taken when using Piloty's acid in alkaline conditions as it readily undergoes oxidation to form nitroxide radicals which decomposes to give NO.[76]

Nitroxyl and its related anion, NO^-, are of significant interest with relation to physiological studies stemming from their close relation to the nitric oxide radical which plays a major role in cellular metabolism. HNO and NO^- may be related by simple acid-base relationship however fundamentally may exhibit very different reactivity due to the difference in their ground state spin states. NO^- is isoelectronic to O_2 which derives a triplet ground state while HNO is known to have a singlet ground state. The kinetics of transformation between HNO and NO^- have been a topic of some debate with results reported by flash photolysis concurrent with DFT calculations by Shafirovich *et al*. to be generally accepted.[77]

HNO coordination chemistry is relatively sparse in comparison to the huge number of metal nitrosyl (M-NO) complexes that are available. There are limited methods of synthesizing HNO complexes: 1) protonation of nitrosyl ligands through HCl addition[78] or C-H activation;[79] 2) hydride addition to nitrosyl

ligand;[80] 3) Oxidation of hydroxylamine ligand[81] and 4) NO^+ insertion into a metal hydride bond (Scheme 1-14).[82]

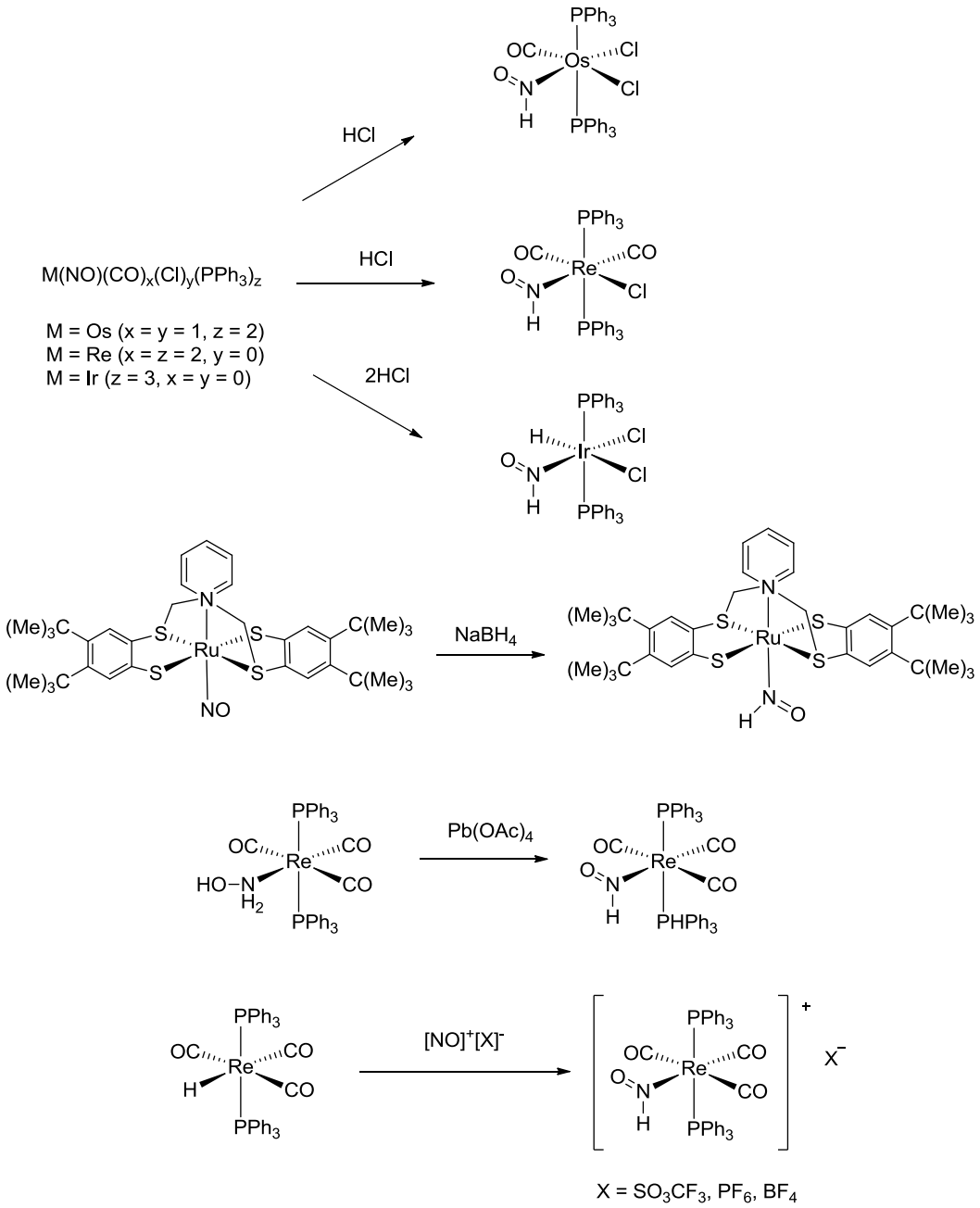

Scheme 1-14. Synthetic methods to HNO complexes.

In all the above examples, there is a distinct resonance between δ = 19 – 23 ppm in the ^{1}H NMR spectrum which is assigned to the proton of the HNO ligand. The recent discovery of HNO-bound myoglobin has important biological implications. Much effort into understanding the chemical and biological properties of this

HNO-myoglobin has been made.[83] Recently an article regarding the synthesis of LiNO[84] was reported which could potentially be used to access HNO complexes, however the findings from the report are not convincing in confirming either the purity or identity of the putative LiNO salt.

HNO is therefore a possible molecule that could be used as a precursor for N_2O, however the pH dependency and facile redox behaviour of the HNO sources such as Angeli's salt and Piloty's acid makes it a difficult reagent to work with. Furthermore, the nitroxyl complexes obtained so far are mostly through nitrosyl ligand reactivity, which makes accessibility of the possible HNO complexes less likely.

1.3.3 Nitramide (H_2NNO_2)

Nitramide, **2-1**, is the simplest nitroamide where one of the hydrogen of ammonia is substituted for a nitro group. Compound **2-1** was first synthesized by Thiele and Lachman from the acid hydrolysis of dipotassium nitrocarbamate[85] (Equation 1-9).

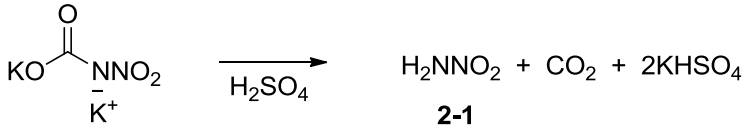

Equation 1-9. Synthesis of nitramide by Thiele and Lachman.

A modified three-step synthesis using the above preparation was reported by Marlies *et al*.[86] starting from the nitration of ethyl carbamate using ethyl nitrate and has been the method of choice even though this multi-step synthesis is tedious and gives a low yield.

There are several possible isomers of **2-1** (Figure 1-8) and the assignment of the correct isomer was a point of contention during the initial discovery during the period in the early 19th century.[87]

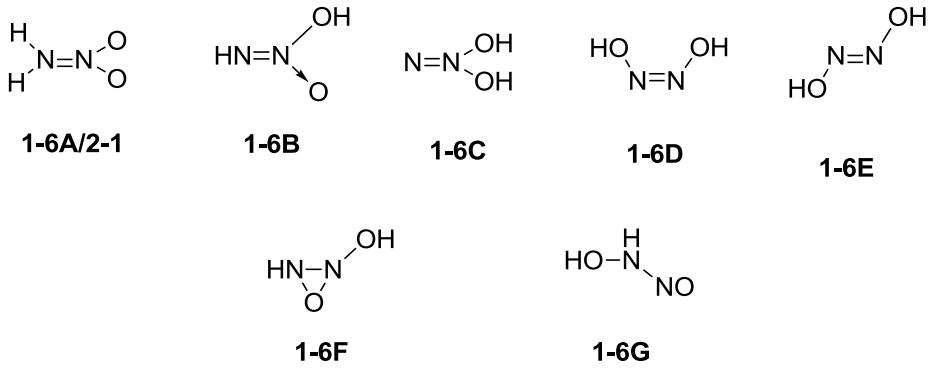

Figure 1-8. Possible isomers of nitramide.

Based on the method of synthesis and reactivity, Thiele had suggested isomer **1-6A** to be the correct isomer. Hanztsch differed and proposed isomers **1-6D** and eventually **1-6B** due to the high acidity of the protons in nitramide with he believed to be due to the presence of the OH groups.[88] Isomers **1-6C**, **1-6D** and **1-6E** were mentioned in the hyponitrite section and correspond to the possible free acid form of hyponitrous acid (Figure 1-7). As mentioned above, the structure of hyponitrous acid was eventually assigned as *trans*-hyponitrous acid, **1-6E**, with mentioned that *cis*-hyponitrite, **1-6D**, as kinetically unstable. Subsequent preparation of N-nitrosohydroxylamine also ruled out the possibility of isomer **1-6G** as the isomeric form of nitramide.[89]

The structure of **2-1** was confirmed as that of isomer **1-6A** by Raman,[90] IR[91] and single crystal diffraction studies.[92] UV-vis absorbance[93] (H_2O, λ_{max} = 207 (6300)) and ^{1}H and ^{15}N NMR[92b, 94] parameters were also obtained in later studies. The N-*H* protons of nitramide do not fall in the usual range for common amides and amines (δ = 4 – 6 ppm) but are located between 8 – 10 ppm increasing with increasing polarity of the solvent. An interesting structural aspect of nitramide relates to the planarity of the nitramide molecule. Microwave measurement carried out in gas-phase[95] indicate the molecule to be non-planar between the NH_2 and the NNO_2 plane and gas phase calculations indicate an inversion rotation barrier of about 6.3 kJ mol^{-1}.[96] In contrast, X-ray single crystal diffraction studies at room to various low temperatures[92b] show an increasing planarity of the molecule as temperature decreases. The N-N bond lengths in **2-1**

and *trans*-hyponitrous acid are 1.322(2) Å and 1.226(4)[61] respectively which represents the N-N bond order in nitramide is less that of hyponitrous acid.

Nitramide is known to decompose to give nitrous oxide and water (Equation 1-10).

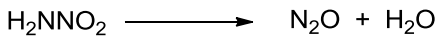

Equation 1-10. Decomposition of nitramide.

This decomposition is usually catalysed by the presence of base. It should be mentioned that after Brønsted proposed[97] the well-known theory of Brønsted-Lowry acids and bases, Brønsted studies on acid-base catalysis[98] was derived from catalytic decomposition of nitramide.[99]

There are two possible pathways of decomposition by **2-1**. The conventional pathway was first proposed by Brønsted to involve the tautomerization of nitramide to the aci-isomer **1-6B** before deprotonation and formation of nitrous oxide and hydroxide (Equation 1-11).[99a, 100]

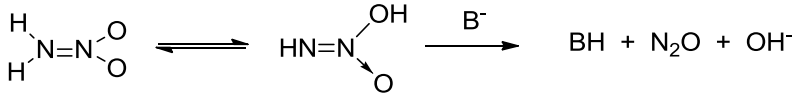

Equation 1-11. Conventional base-catalysed decomposition of nitramide.

This first pathway was found to be applicable mostly to bases with a conjugate acid of $pK_a \leq 8$. When the conjugate acids of stronger bases are used as catalysts, $pK_a > 10$, such as hydroxide, nitramide decomposition was found to follow general base-catalysed decomposition where isomerisation is not involved in the decomposition (Equation 1-12).[101]

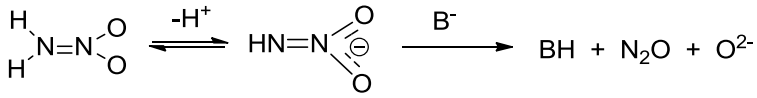

Equation 1-12. Second pathyway of base-catalysed decomposition of nitramide.

In general both pathways can exist simultaneously when the values of pK_a of conjugate acid of the bases fall between the limits described above. The kinetics of the decomposition has also been examined by theoretical *ab initio* methods.[102]

Nitramide can also undergo acid-catalysed decomposition. In dilute acid solutions, the behaviour is similar to neutral solutions, where water acts as the

base for **2-1** decomposition.[99a] A proposed mechanism involving two water molecules in cyclic arrangement is proposed (Scheme 1-15).[103]

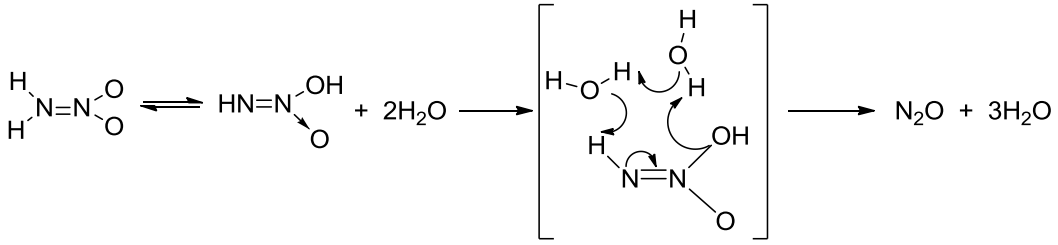

Scheme 1-15. Proposed decomposition mechanism of **2-1** by water.

In stronger acid solutions, an alternative mechanism of decomposition is proposed that is through the *O*-protonation of the aci-form **1-6B** followed by nucleophilic attack of a water molecule to generate nitrous oxide and water (Scheme 1-16).[103]

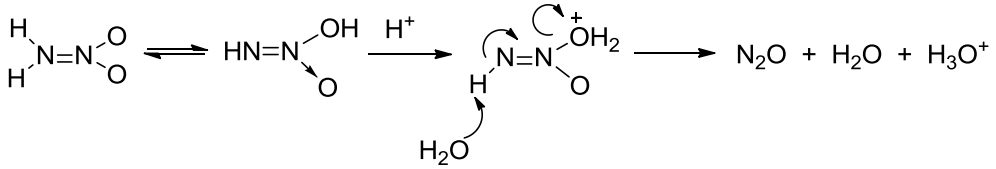

Scheme 1-16. Proposed mechanism of acid-catalysed decomposition of **2-1**.

In spite of numerous reports on the properties of **2-1**, there is only a single report of a nitramide complex (Scheme 1-17).

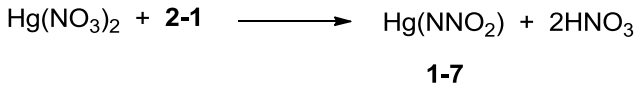

1-7

Scheme 1-17. Synthesis of $Hg(NNO_2)$.

Complex **1-7** is formed from the reaction of $Hg(NO_3)_2$ with **2-1** which precipitates out of solution as white solids. The IR spectrum of **1-7** shows a medium intensity band at 1053 cm^{-1} which is assigned to the N=N stretch in $Hg(NNO_2)$.[104] The white **1-7** solids are friction and heat sensitive, decomposing explosively to evolve N_2 and yellow HgO. The formation of **1-7** is attributed to the increase covalency of mercury compounds. Complex **1-7** is stable in the mother liquor and acid media for days, but decompose at a faster rate in other solutions. Attempts at using **1-7** as '$[NNO_2]^{2-}$' transfer fragments were unsuccessful. Bubbling H_2S into a suspension of **1-7** regenerates **2-1** with the formation of HgS.[104] The protons on

2-1 are acidic as indicated by the reaction with $Hg(NO_3)_2$. Even though **2-1** is a diprotic acid, experimentally, only one pK_a value of 6.6 has been obtained. This is because both the monoanion $[HNNO_2]^-$ as shown above and the dianion, nitridonitate $[NNO_2]^{2-}$, are very unstable and acts as its own base generating the following chain reaction (Scheme 1-18).[104]

$$[NNO_2]^{2-} \longrightarrow N_2O + O^{2-}$$

$$O^{2-} + H_2O \longrightarrow 2OH^-$$

$$H_2NNO_2 + 2OH^- \longrightarrow 2H_2O + [NNO_2]^{2-}$$

Scheme 1-18. $[NNO_2]^{2-}$ self-catalysed decomposition.

The decomposition pathway is both similar and in contrast to hyponitrous acid as shown in section 1.3.1 where both the monoanions $[HON{=}NO]^-$ and $[HNNO_2]^-$ are unstable while the *trans* and *cis* hyponitrite salts $[ON{=}NO]^{2-}$ are relatively more stable than the nitridonitrate dianion of **2-1** (Figure 1-7).

1.4 Conclusion

The N_2OR enzyme plays an important and significant role in converting nitrous oxide into N_2 for fixation and current information on the active form of the enzyme is still under debate. With increasing N_2O emissions from man-made processes which contributes to climate and environment changes, a greater understanding of N_2OR operations is essential that may contribute eventually to its potential use as a mild oxidant. The current knowledge about N_2O with regards to coordination chemistry is that N_2O is a very poor ligand which contributes to the limited reactivity associated with the gas. The complexes or adducts of N_2O for a long time have been poorly characterised with significant improvement only in recent times.

To contribute to this emerging field of study, we propose the synthesis of precursor adducts of N_2O possibly from nitramide or related nitro compounds for reaction with transition metal complexes to give new coordination complexes. The new N_2O-precursor adduct complexes will be investigated for reactivity studies which may provide new insight into N_2OR functions.

Chapter 2: Synthesis of Nitrogen Acids

2.0 Introduction

To pursue the synthesis of N_2O precursor complexes, nitramide (**2-1**) was chosen as a suitable candidate. The related compounds: N-nitroamides, N-nitrocarbamates, N-nitrosocarbamates and N-nitrosulfonamides were also considered (Figure 2-1).

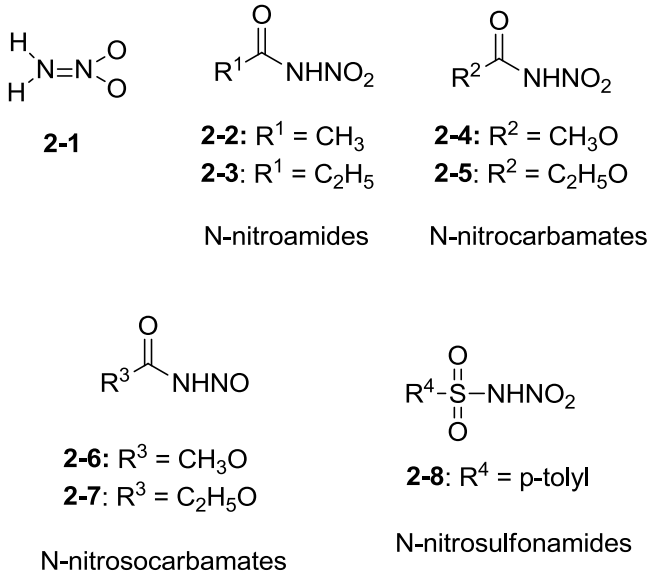

Figure 2-1. Compounds of interest.

Due to the sensitivity of **2-1** to rapid decomposition to give nitrous oxide and water, the carboxy groups such as acyl and ester functional groups for **2-2** to **2-7** were considered as protecting groups for the 'NNO_2' fragment. The 'NNO_2' fragment is a proposed synthon for nitrous oxide. The sulfonyl group in **2-8** was also considered as an alternative to the 'protecting' carboxy groups. Upon successfully coordination of the ligands to transition metals forming coordination complexes, attempts can be made to remove the protecting groups.

During the course of our studies, we discovered that the primary N-nitroamides, N-nitrocarbamates, N-nitrosocarbamates and the N-nitrosulfonamide have acidic properties which will be discussed below. This acidic property allows access to

the anions of the above class of compounds which widens the scope of potential reaction pathways.

The primary N-nitroamides (**2-2** and **2-3**), N-nitrocarbamates (**2-4** and **2-5**), N-nitrosocarbamates (**2-6** and **2-7**) and N-nitrosulfonamide, **2-8**, termed as nitrogen acids and nitramide (**2-1**) have been synthesized before. However some of the described preparations were vague and irreproducible in particular the N-nitrosocarbamate, **2-7**. Coupled with mostly skeletal characterizations in the form of melting points and elemental determinations, the spectroscopic and structural information of this class of compounds were almost non-existent. This chapter aims to improve and better describe the synthetic procedures for these compounds as well as provide additional spectroscopic and if possible structural characterizations of the nitrogen acids.

2.1 General Experimental

General: Except noted all reagents and solvents are used as supplied commercially. Dry CH_3OH is distilled from freshly generated magnesium methoxide and dry hexane is distilled from sodium benzophenone ketyl. ^1H spectra are recorded on Varian Mercury 200, 400 or 500 MHz spectrometers and ^{13}C spectra on a Varian Mercury 300 MHz spectrometer. All chemical shifts are recorded in δ (ppm) relative to residual solvent signals for ^1H and ^{13}C spectra. Melting/decomposition points are measured by using a TA-Q2000 differential scanning calorimeter calibrated against an internal standarad. The IR spectra are recorded in KBr disks or a gas-tight cell for gas-phase spectra by using ABB Bomem MB Series IR spectrometer with spectral resolution of 4 cm^{-1}. UV/visible spectra were measured using a HP 8453 Diode Array spectrophotometer from HP. Elemental analyses are performed in the Elemental Analyses Laboratory at University of Montreal. Sublimation purifications are carried out under vacuum with cold fingers inserts containing dry-ice acetone mixtures or ice-water and heated to the required temperatures.

X-ray crystallography: Crystals are mounted on glass fibre with epoxy resin or Mitegen mounts using Paratone-N from Hampton Research and X-ray diffraction experiments are carried out with a BRUKER SMART CCD or BRUKER APEX-II CCD diffractometer by using graphite-monochromated MoK_α radiation (λ = 0.71073 Å) and KRYOFLEX for low temperature experiments. SAINT[105] is used for integration of the intensity reflections and scaling and SADABS[106] for absorption correction. Direct methods are used to generate the initial solution for all structural solution that do not contain heavy atom e.g. potassium and Patterson methods are used to generate the initial solution for all potassium containing structures. Location of non-hydrogen atoms are carried out using Fourier difference maps with the refinements solved by full-matrix least-squares method on F^2 of all data using SHELXTL[105] software. The hydrogen atoms positions are placed in calculated positions.

Crystals of the neutral N-nitroamides and N-nitrocarbamates suitable for X-ray crystal diffraction are grown from slow evaporation of CH_2Cl_2. Crystals suitable for single crystal diffraction of the N-nitrosocarbamates are obtained from slow sublimation under vacuum with an ice-water cold finger. N-nitro-*p*-tolylsulfonamide crystals are obtained from recrystallization in toluene. The N-nitroamides, N-nitrocarbamates and N-nitrosocarbamates are all low melting solids with the N-nitrosocarbamates having significantly vapour pressure even at room temperature. Low temperature diffraction data collection is therefore required to prevent vapourisation of the crystals due to high energy X-ray bombardment during collection. Crystallographic data and data collection parameters of the neutral compounds are shown in Table 2-1.

Crystals of the potassium salt of the N-nitroamide are obtained from layered C_2H_5OH/hexanes solutions, N-nitrocarbamate from C_2H_5OH/H_2O/hexanes and N-nitrosocarbamate from C_2H_5OH/hexanes at -21 ^oC. Crystals of the ammonium salt of N-nitro-*p*-tolylsulfonamide is obtained from the aqueous media. Crystal and data collection of the salts are shown in Table 2-2.

Theoretical methods:

Gaussian03 was used for all calculations with B3LYP density functional theory and the triple zeta basis set 6-311++g**.

Precaution!

The nitro and nitroso compounds synthesized may be explosive. For dinitrourea (**2-1A**) and the N-nitrosocarbamates, **2-4** and **2-5**, special precautions must be taken as they are known to spontaneously decompose!

Table 2-1: Crystallographic data of N-nitroamides, N-nitrocarbamates, N-nitrosocarbamates and N-nitro-*p*-tolylsulfonamide.

Compound	**2-2**	**2-3**	**2-4**	**2-5**	**2-6**	**2-7**	**2-8**
empirical formula	$C_2H_4N_2O_3$	$C_3H_6N_2O_3$	$C_2H_4N_2O_4$	$C_3H_6N_2O_4$	$C_2H_4N_2O_3$	$C_3H_6N_2O_3$	$C_7H_8N_2O_4S$
T (K)	100(2)	100(2)	100(2)	100(2)	100(2)	100(2)	298(2)
fw (g mol^{-1})	104.07	118.10	120.07	134.10	104.07	118.10	216.21
cryst sys	orthorhombic	monoclinic	triclinic	monoclinic	Monoclinic	monoclinic	monoclinic
space group	Pnma	$P2_1/m$	P-1	$P2_1/c$	$P2_1/m$	$P2_1/m$	$P2_1/c$
a (Å)	9.509(3)	4.897(2)	7.6247(17)	9.909(4)	4.8755(14)	4.7863(15)	7.1784(9)
b (Å)	5.849(2)	5.952(3)	7.8003(17)	6.084(2)	5.9345(18)	6.0338(19)	17.799(2)
c (Å)	7.453(3)	8.852(4)	8.3539(18)	9.487(4)	7.808(2)	9.375(3)	9.1462(8)
α (deg)	90	90	80.955(2)	90	90	90	90
β (deg)	90	100.975(5)	89.992(2)	103.643(4)	99.205(3)	90.945(3)	127.869(6)
γ (deg)	90	90	76.536(2)	90	90	90	90
V ($Å^3$)	414.5(3)	253.3(2)	476.84(18)	555.7(4)	223.01(11)	266.67(15)	922.51(18)
Z	4	2	4	4	2	2	4
density (g cm^{-3})	1.668	1.549	1.673	1.603	1.550	1.471	1.557
abs coeff (mm^{-1})	0.157	0.138	0.163	0.149	0.145	0.131	0.341
No. of reflns collected	3249	2199	5451	1824	2534	1715	8059
No. of indep reflns	531	636	2154	924	569	316	2140

Data/restraints/parameters	531/0/43	636/0/49	2154/0/145	924/0/90	569/0/43	316/0/49	2140/0/128
Final R indices [$I > 2s(I)$] R1	0.0334	0.0306	0.0539	0.0364	0.0471	0.0380	0.0371
*w*R2	0.0880	0.0827	0.1643	0.0843	0.1220	0.0963	0.1051
R indices (all data) R1	0.0347	0.0331	0.0622	0.0494	0.0589	0.0426	0.0471
*w*R2	0.0894	0.0851	0.1688	0.0892	0.1302	0.0990	0.1128
Goodness-of-fit on F^2	1.118	1.092	1.125	1.128	1.147	1.103	1.080

Table 2-2: Crystallographic data of potassium and ammonium salts of N-nitroamides, N-nitrocarbamates, N-nitrosocarbamates and N-nitro-*p*-tolylsulfonamide.

Compound	**2-2K**	**2-4K**	**2-6K**	**2-8K**	**2-8NH$_4$**
empirical formula	$C_2H_3KN_2O_3$	$C_2H_3KN_2O_4.H_2O$	$C_2H_3KN_2O_3$	$C_7H_7KN_2O_4S$	$NH_2C_7H_7N_2O_4S$
T (K)	100(2)	100(2)	100(2)	100(2)	298(2)
fw (g mol^{-1})	142.16	176.18	142.16	254.31	231.23
cryst sys	triclinic	triclinic	orthorhombic	orthorhombic	orthorhombic
	P-1	P-1	$P2_12_12_1$	Pbcn	Pbcn
	6.147(3)	7.060(3)	5.8792(7)	7.4440(6)	7.661(2)
b (Å)	6.801(3)	7.506(3)	6.8542(8)	10.7526(9)	11.011(3)
c (Å)	7.518(3)	7.648(3)	12.8207(14)	24.996(2)	25.156(7)
α (deg)	63.809(4)	63.478(3)	90	90	90
β (deg)	66.994(4)	65.572(3)	90	90	90
γ (deg)	68.221(4)	62.565(3)	90	90	90
V (Å^3)	252.0(2)	310.64(19)	516.64(10)	2000.7(3)	2122.1(10)
Z	2	2	4	8	8
density (g cm^{-3})	1.874	1.884	1.828	1.689	1.448
abs coeff (mm^{-1})	0.962	0.823	0.938	0.734	0.304
No. of reflns collected	2804	3444	5630	10156	17195
No. of indep reflns	1140	1400	1201	2325	2514

Data/restraints/parameters	1140/0/73	1400/0/99	1201/0/74	2325/0/137	2514/0/149
Final R indices [$I > 2s(I)$] R1	0.0361	0.0309	0.0262	0.0310	0.0567
*w*R2	0.0816	0.1090	0.0714	0.0859	0.1334
R indices (all data) R1	0.0498	0.0403	0.0268	0.0361	0.0732
*w*R2	0.1145	0.1693	0.0718	0.0896	0.1423
Goodness-of-fit on F^2	1.229	1.172	1.121	1.063	1.193

2.2 N-Nitroamides and their salts

Experimental

Nitramide and N-nitroacetamide (**2-2**) is synthesized using a modified method of Lobonova *et al*. outline below.[107] Ag_2CO_3 is synthesized from the reaction of silver nitrate and sodium carbonate.

2.2.1 Synthesis of nitramide, H_2NNO_2 (2-1)

Oleum (20 g) is added to conc. nitric acid (20 g, d = 1.5 g mL^{-1}) in an ice bath (T < 5 ^oC). Urea (5.720 g, 95.3 mmol) is added in portions between -5 ^oC and 0 ^oC. The reaction mixture is allowed to stir for 40 min between 0 ^oC and 5 ^oC during which a white precipitate is formed. Some foaming may be observed. The reaction mixture is cooled to -15 ^oC and filtered, washed with cold trifluoroacetic acid (TFA) (3 x 5 mL) and squeezed. The white precipitate is dinitrourea, $(O_2NNH)_2CO$ (**2-1A**).

Dinitrourea, **2-1A**, (14.3 g, 95.3 mmol) is dissolved in a urea solution (5.75 g, 95.8 mmol in 10 mL deionised H_2O) at T < 20 ^oC. The mixture is stirred for 15 min and cooled to 5 ^oC. The white precipitate is collected by filtration, washed with minimum cold deionised H_2O and dried in air. The white precipitate is dinitrourea-urea salt, $(O_2NNH)_2CO.(H_2N)_2CO$ (**2-1B**) (crude, 20.02 g).

Compound **2-1B** (20.02 g, 95.3 mmol) is dissolved in portions in H_2SO_4 (20.02 g in 50 mL deionised H_2O) at T < 20 ^oC. The reaction is stirred till homogenous and subjected to ether extractions (3 x 80 mL). The ether extracts are combined and allowed to stand for 4 h at room temperature. The ether is removed by rotary evaporation to give white solids which are further purified by vacuum sublimation (dry ice-acetone) at 70 ^oC to give nitramide (**2-1**) (3.339 g, 53.9 mmol, 28.3 % yield).

IR (cm^{-1}): 3363s, 3261s, 3200s, 3170s, 3046vs, 1583m, 1567w, 1534vs, 1516vs, 1414vs, 1403vs, 1205s, 1189s, 1049w, 783w, 708w, 590w.[91a, 108]

Raman (cm^{-1}): 1051vs, 711w, 576w.[90]

^{1}H NMR (200 MHz, $CDCl_3$) ppm: δ = 8.05 (NH_2, broad).

UV: (H_2O λ_{max}, nm (ε, M cm^{-1})): 206 nm, ε = 7675[93a]

$H_2{}^{15}NNO_2$

IR (cm^{-1}): 3356s, 3251s, 3189s, 3160s, 3045vs, 2747m, 2552w, 1580s, 1533vs, 1514vs, 1399vs, 1201s, 1184s, 1039m, 782m, 703m, 587m.

Raman (cm^{-1}): 1042vs, 706w, 573w.

2.2.2 Synthesis of N-nitroacetamide, $CH_3C(O)NHNO_2$ (2-2)

Compound **2-1** (0.500 g, 8.06 mmol) is dissolved in ether (5 mL). The ether solution is cooled to 0 ^{o}C in an ice-bath and acetic anhydride (10 mL, 105.8 mmol) is added. LiCl (0.4 mg, 9.41 μmol) is added and the reaction mixture is allowed to warm to room temperature. The reaction mixture is stirred for 24 h and subjected to vacuum evaporation at T < 40 ^{o}C to give white solids. The white solids are purified by vacuum sublimation (dry ice-acetone) at 70 ^{o}C to give N-nitroacetamide (**2-2**) (0.350 g, 3.37 mmol, 42 % yield).

IR (cm^{-1}): 3433w, 3252m, 3156s, 3018s, 2856m, 2811m, 2735w, 2570w, 1962w, 1728vs, 1623vs, 1443s, 1309vs, 1196vs, 1016vs, 1007vs, 952m, 764m, 723m, 605s, 569m, 454w.

Gas phase IR (cm^{-1}): 1747s, 1738s, 1732s, 1623vs, 1430m, 1371s, 1316s, 1230s, 1185s, 1011m.

Raman (cm^{-1}): 2952vw, 1718m, 1638w, 1307m, 1194m, 1005m, 954m, 763m, 608vs, 454m, 389m, 246w.

^{1}H NMR (200 MHz, $CDCl_3$) ppm: δ = 2.52 (s, 3H), 10.52 (N*H*, broad).

^{13}C NMR (75 MHz, $CDCl_3$) ppm: δ = 24.13 (s), 168.08 (s)

2.2.3 Synthesis of N-nitropropionamide, $C_2H_5C(O)NHNO_2$ (2-3)

Compound **2-1** (0.500 g, 8.06 mmol) is dissolved in ether (5 mL). The ether solution is cooled to 0 ^oC in an ice-bath and propionic anhydride (11 mL, 85.4 mmol) is added. LiCl (0.4 mg, 9.41 μmol) is added and the reaction mixture is allowed to warm to room temperature. The reaction mixture is stirred for 24 h. The product is purified by column chromatography using initially CH_2Cl_2 to remove propionic acid and anhydride followed by ethyl acetate/CH_3OH as eluant to give white solids. The white solids are further purified by vacuum sublimation (dry ice-acetone) at approx. 70 ^oC to give N-nitropropionamide (**2-3**) (0.172 g, 1.46 mmol, 18.1 % yield).

Melting point: 83.5 ^oC (16.97 kJ mol^{-1})

IR (cm^{-1}): 3443w, 3238s, 3206s, 2994w, 2983m, 2948w, 1729vs, 1610vs, 1469m, 1436s, 1412s, 1325s, 1140s, 1064s, 1025m, 976m, 802m, 770w, 745m, 648m, 537m.

Raman (cm^{-1}): 2952w, 2932w, 1727m, 1437w, 1435m, 1406m, 1317m, 1301m, 1116m, 1055w, 1027w, 974s, 745m, 445m, 364vs, 317w.

^1H NMR (200 MHz, $CDCl_3$) : δ = 1.23 (t, 3H, *J*, = 7.3 Hz), 2.77 (q, 2H, *J* = 7.3 Hz), 10.35 (N*H*, broad)

2.2.4 Synthesis of N-nitroacetamide salts:

Potassium N-nitroacetamide, $K[CH_3C(O)NNO_2]$ (**2-2K**)

Compound **2-2** (46 mg, 0.0442 mmol) is dissolved in CH_2Cl_2 (4 mL) and ground K_2CO_3 (30 mg, 0.0217 mmol) is added and stirred overnight at room temperature. The white suspension is collected by filtration washed with minimum CH_2Cl_2 and dried to give white solids of K[N-nitroacetamide] (**2-2K**) (52 mg, 0.0363 mmol, 84 % yield)

IR (cm^{-1}): 1978w, 1641vs, 1427m, 1364w, 1304w, 1220vs, 1096w, 1040w, 991m, 934w, 798m, 766w, 690w, 623m, 477w.

^{1}H NMR (200 MHz, CD_3OD) ppm: δ = 1.90 (s, 3H).

Elemental analysis calcd. for $C_2H_3N_2O_3K$ (142.16 g mol^{-1}) % C, 16.88; H, 2.11; N, 19.69. Found % C, 16.94; H, 2.01; N, 19.31.

Silver N-nitroacetamide, Ag[$CH_3C(O)NNO_2$] (**2-2Ag**)

Compound **2-2** (0.108 g, 1.04 mmol) is dissolved in CH_2Cl_2 (6 mL) and Ag_2CO_3 (0.143 g, 0.518 mmol) added and stirred overnight at room temperature. The white suspension is filtered, washed with minimum CH_2Cl_2 and dried to give white solids of Ag[N-nitroacetamide] (**2-2Ag**) (0.210 g, 0.996 mmol, 96 % yield)

IR (cm^{-1}): 1977vw, 1642vs, 1504w, 1427s, 1364s, 1304s, 1222vs, 1048m, 1037m, 992s, 934m, 797m, 766m, 623m, 477w.

2.3 N-Nitrocarbamates and their salts

Experimental

N-nitrocarbamates are synthesized using modified procedures of Luk'yanov *et al*.[109] Methylcarbamate and ethylcarbamate are used as purchased.

2.3.1 Synthesis of N-nitromethylcarbamate $CH_3OC(O)NHNO_2$ (2-4)

Methyl carbamate (1.000 g, 13.3 mmol) is gradually added at 25 ^oC to a mixture of conc. H_2SO_4 (15 mL) and KNO_3 (2.03 g, 20.01 mmol). The mixture is stirred for 15 min at 25 ^oC and poured onto crushed ice (14.2 g) with stirring and extracted with ether (7 x 6 mL). The ether extracts are dried with anhydrous $MgSO_4$ and the solvent removed in *vacuo* till dryness. The white solids are redissolved in ether (20 mL) and NH_3 is bubbled into the mixture in an ice-water bath to give a white precipitate. The white precipitate is filtered dried and collected to give ammonium N-nitromethylcarbamate (**2-4NH$_4$**) (1.682 g, 12.3 mmol, 92 % yield).

Compound **2-4NH$_4$** (1.682 g, 12.3 mmol) is gradually dissolved in H_2SO_4 (1 mL conc. H_2SO_4, 3.0 g of ice and 10 mL deionised H_2O) and stirred until homogeneous. The solution is extracted with ethyl acetate (7 x 10 mL) and the extracts are dried over anhydrous $MgSO_4$. The solvent is removed in *vacuo* and the white residue is purified by vacuum sublimation (dry ice-acetone) at 65 - 70 ^oC to give N-nitromethylcarbamate (**2-4**) (1.230 g, 10.3 mmol, 77 % yield).

IR (cm^{-1}): 3245s, 3206s, 3060w, 3024w, 2972w, 2850vw, 1748vs, 1615vs, 1549w, 1458s, 1414m, 1325m, 1244s, 1092w, 1003m, 947m, 771m, 736,w, 625m, 456w.

^1H NMR (200 MHz, $CDCl_3$) ppm: δ = 3.91 (s, 3H), 10.12 (N*H*, broad).

2.3.2 Synthesis of N-nitroethylcarbamate, $C_2H_5OC(O)NHNO_2$ (2-5)

Ethyl carbamate (1.000 g, 11.2 mmol) is gradually added at temperature less than 25 ^oC to a mixture of conc. H_2SO_4 (15 mL) and KNO_3 (2.03 g, 20.01 mmol). The mixture is stirred for 15 min at 25 ^oC and poured onto crushed ice (12 g) with stirring and extracted with CH_2Cl_2 (7 x 45 mL). The CH_2Cl_2 extracts are dried with anhydrous $MgSO_4$ and the solvent removed in *vacuo* till dryness. The white solids are redissolved in ether (20 mL) and NH_3 is bubbled into the mixture for 2 min in an ice-water bath to give a white precipitate. The white precipitate is filtered dried and collected to give ammonium N-nitroethylcarbamate (**2-5NH$_4$**) (1.607 g, 10.64 mmol, 95 % yield).

Compound **2-5NH$_4$** (1.607 g, 10.64 mmol) is gradually dissolved in H_2SO_4 (1 mL conc. H_2SO_4, 3.0 g of ice and 10 mL deionised H_2O) and stirred until homogeneous. The solution is extracted with ethyl acetate (7 x 10 mL) and the extracts are dried over anhydrous $MgSO_4$. The solvent is removed in *vacuo* and the white residue is purified by vacuum sublimation (dry ice-acetone) at 65 - 70 ^oC to give N-nitroethylcarbamate (**2-5**) (1.244 g, 9.21 mmol, 87 % yield).

Melting point: 67.7 ^oC (14.5 kJ mol^{-1})

IR (cm^{-1}): 3235s, 3007m, 2988m, 2947w, 2880w, 2810w, 1741vs, 1605vs, 1548m, 1518m, 1453s, 1391s, 1368m, 1329s, 1227s, 1116m, 1017m, 997m, 878m, 798m, 768m, 731w, 603m, 458w.

^1H NMR (200 MHz, $CDCl_3$) ppm: δ = 1.36 (t, 3H, *J* = 7.1 Hz), 4.36 (q, 2H, *J*, = 7.1 Hz), 9.90 (N*H*, broad)[110]

2.3.3 Synthesis of N-nitromethylcarbamate salts

Potassium N-nitromethylcarbamate, $K[CH_3OC(O)NNO_2]$ (**2-4K**)

Compound **2-4** (0.100 g, 0.833 mmol) is dissolved in dry CH_2Cl_2 (5 mL) and anhydrous $KOCH_3$ (0.055 g, 0.786 mmol) is added and stirred overnight at room temperature. The white suspension is filtered and the residue washed with CH_2Cl_2

and dried to give white solids of $K[CH_3OC(O)NNO_2]$ (**2-4K**) (0.087 g, 0.552 mmol, 70 % yield)

IR (cm^{-1}): 2967w, 1682s, 1633m, 1567m, 1453m, 1405s, 1318m, 1234vs, 1192s, 1104s, 963w, 807w, 783m, 739w, 433w.
^1H NMR (400 MHz, CD_3OD) ppm: $\delta = 3.62$ (s, 3H)
Elemental analysis calcd. for $C_2H_3N_2O_4K.0.15H_2O$ (160.85 g mol^{-1}) % C, 14.93; H, 2.07; N, 17.42. Found % C, 15.03; H, 1.86; N, 17.18.

Silver N-nitromethylcarbamate, $Ag[CH_3OC(O)NNO_2]$ (**2-4Ag**)

N-Nitromethylcarbamate (0.045 g, 0.375 mmol) is dissolved in CH_2Cl_2 (5 mL) and Ag_2CO_3 (0.050 g, 0.181 mmol) is added and stirred overnight at room temperature. The white suspension is filtered and the residue washed with CH_2Cl_2 and dried to give white solids of $Ag[CH_3OC(O)NNO_2]$ (**2-4Ag**) (0.060 g, 0.265 mmol, 73 % yield).

IR (cm^{-1}): 3020vw, 2965w, 1683vs, 1453m, 1405s, 1312m, 1236,s, 1191s, 1106s, 963w, 806w, 783m, 739w, 430w.[110]

2.3.4 Synthesis of N-nitroethylcarbamate salt

Silver N-nitroethylcarbamate, $Ag[C_2H_5OC(O)NNO_2]$ (**2-5Ag**)

N-Nitroethylcarbamate (0.200 g, 1.49 mmol) is dissolved in CH_2Cl_2 (5 mL) and Ag_2CO_3 (0.200 g, 0.726 mmol) is added and stirred overnight at room temperature. The white suspension is filtered and the residue washed with CH_2Cl_2 and dried to give white solids of $Ag[C_2H_5OC(O)NNO_2]$ (**2-5Ag**) (0.258 g, 1.07 mmol, 74 % yield).

IR (cm^{-1}): 2990w, 1696s, 1668m, 1488w, 1474w, 1405m, 1369w, 1314m, 1241vs, 1127m, 1097s, 1033w, 994w, 886w, 769w, 487w.[110]

Experimental

N-nitrosocarbamates are synthesized using modified procedures of Thiele *et al*.[85] and Benin *et al*.[111] **2-4NH$_4$** and **2-5NH$_4$** are synthesized using the methods of Luk'yanov *et al*.[109]

2.4.1 Synthesis of N-Nitrosomethylcarbamate, $CH_3OC(O)NHNO$ (2-6) as a mixture of isomers

Compound **2-4NH$_4$** (2.00 g, 14.6 mmol) is dissolved in a mixture of acetic acid (1.76 g, 29.3 mmol) and deionised H_2O (16 mL) at temperature less than 25 ^oC. Commercial zinc dust stored under nitrogen (1.332 g, 20.4 mmol) is added in portions to the reaction mixture such that temperature remains below 25 ^oC. Some ice can be added if the reaction temperature gets above 30 ^oC (It is advisable to use an ice-water bath as the reaction is very exothermic). The reaction mixture turns yellow and is allowed to stir for 1 h during which a green-yellow suspension is formed.

Ice (~ 10 g) is added and cold conc. aqueous ammonia (4.1 mL, 59.5 mmol) is added in excess and stirred for 5 min to give a yellow solution (Ensure there are still some ice floating in solution, if not add more ice). The solution is filtered through a plug of Celite to give a yellow filtrate. If the residue is yellow, it is washed with dilute aqueous ammonia (0.5 mL conc. NH_4OH in 2 mL deionised H_2O) and deionised H_2O until the washings are colourless. Ice (~ 50 g) is added into the yellow filtrate followed by a solution of $AgNO_3$ (1.76 g, 10.4 mmol) with rapid stirring. Acetic acid is added slowly, forming initially a white suspension, which dissolves on further addition of acid (if no ice is visible during the addition, add more ice). A yellow suspension slowly forms and acetic acid is added till the solution is acidic to pH paper (Total volume ~ 150 mL). The reaction mixture is left standing between 10 - 15 min during which substantial yellow precipitate appears. The yellow precipitate, $Ag[CH_3OC(O)NNO)]$ (**2-6Ag**) (assumed 2.18 g,

10.3 mmol), is filtered as rapidly as possible and washed consecutively with deionised H_2O, C_2H_5OH and CH_3OH and processed immediately as it rapidly decomposes on prolonged exposure to moisture (The sintered filter may get clogged due to the fine particulate nature of the Ag salt, an alternative would be to centrifuge the suspension and wash with C_2H_5OH). The filtrate is observed to be pale green.

NaCl (0.610 g, 10.4 mmol) is dissolved in an ice-water solution and added to **2-6Ag** (assumed 2.18 g, 10.3 mmol) and stirred/shaken vigourously for 5 min to give a yellow suspension. The yellow suspension is filtered through a pad of Celite and washed successively with cold deionised H_2O till the filtrate is colourless. The filtrate is added into a separatory funnel containing ethyl acetate (20 mL), ice (~ 2 g) and conc. H_2SO_4 (0.500 g, 5.10 mmol). The organic layer is separated, kept and the yellow aqueous layer further extracted with ethyl acetate (3 x 20 mL) or till the aqueous layer is colourless. The organic extracts are combined and dried over anhydrous $CaCl_2$, kept cold and under a N_2 atmosphere for 30 min. The yellow ethyl acetate suspension is filtered and ethyl acetate is removed using a rotary evaporator without heating to give bright yellow solids of **2-6**. **2-6** is further purified by vacuum sublimation (ice-water) at 22 - 23 ^oC to give bright yellow crystals of N-nitrosomethylcarbamate, (**2-6**) (0.163 g, 1.57 mmol, 15 % yield).

(Note: to minimize the loss of **2-6** due to its low melting point, the sublimator is cooled to around 6 - 7 ^oC before the vacuum is applied.)

Decomposition point: 60.53 ^oC (-83.3 kJ mol^{-1})

IR (cm^{-1}): 3427vs, 3199s, 2969m, 1759vs, 1707s, 1619s, 1529s, 1470s, 1459s, 1432m, 1385w, 1330w, 1250vs, 1089vs, 1061s, 929s, 766m, 717m, 560m, 444w.

^1H NMR (200 MHz, $CDCl_3$) ppm: δ = 3.68 (s, 3H, minor), 3.91 (s, 3H, minor), 4.06 (s, 3H, major), 10.65 (N*H*, broad). Ratio of 0.03:0.05:1 respectively

^1H NMR (200 MHz, CD_3OD) ppm: δ = 3.60 (s, 3H, minor), 3.78 (s, 3H, minor), 3.97 (s, 3H, major). Ratio of 0.02:0.04:1 respectively.

UV (CH_3OH λ_{max}, nm (ε, M^{-1} cm^{-1})): 366sh (12.6), 385sh (34.1), 401 (61.6), 417 (88.5), 436 (76.7).

UV ($CHCl_3$ λ_{max}, nm (ε, M^{-1} cm^{-1})): 368sh (21.3), 383sh (43.0), 396 (75.0), 412 (105.0), 430 (88.7).

2.4.2 Synthesis of N-nitrosoethylcarbamate, $C_2H_5OC(O)NHNO$ (2-7) as a micture of isomers

Compound **2-5NH$_4$** (1.00 g, 6.62 mmol) is dissolved in a mixture of acetic acid (0.84 g, 12.6 mmol) and cold deionised H_2O (15 mL) at temperature less than 25 ^oC. Commercial zinc dust stored under nitrogen (0.600 g, 10.2 mmol) is added in portions to the reaction mixture such that temperature remains below 25 ^oC. Some ice can be added if the reaction temperature gets above 30 ^oC. The reaction mixture turns yellow and is allowed to stir for 1 h during which a yellow-green suspension is observed.

Ice (~ 10 g) is added and cold conc. aqueous ammonia (3.9 mL, 56.6 mmol) is added in excess and stirred for 5 min to give a yellow solution which is filtered through a plug of Celite. If the residue is yellow, it is washed with dilute aqueous ammonia (0.5 mL conc. NH_4OH in 2 mL deionised H_2O) and deionised H_2O until the washings are colourless. Ice (~ 50 g) is added into the yellow filtrate followed by a solution of $AgNO_3$ (0.80 g, 4.71 mmol) with rapid stirring. Acetic acid is added slowly, forming initially a white suspension, which dissolves on further addition of acid. A yellow suspension initially forms and acetic acid is added till the solution is acidic to pH paper (Total volume ~ 150 mL). The reaction mixture is left standing between 10 - 15 min during which substantial yellow precipitate appears. The yellow precipitate, $Ag[C_2H_5OC(O)NNO)]$ (**2-7Ag**) (assumed 1.06 g, 4.71 mmol) is filtered and washed consecutively with deionised H_2O, C_2H_5OH and CH_3OH and processed immediately as it rapidly decomposes on prolonged exposure to moisture. The filtrate is observed to be colourless.

NaCl (0.280 g, 4.79 mmol) is dissolved in an ice-water solution and added to $Ag[C_2H_5OC(O)NNO]$ (assumed 1.06 g, 4.71 mmol) and stirred/shaken

vigourously for 5 min to give a yellow suspension. The yellow suspension is filtered through Celite and washed successively with cold deionised H_2O till the filtrate is colourless. The filtrate is transferred into a separatory funnel containing CH_2Cl_2 (20 mL), ice (~ 2 g) and conc. H_2SO_4 (0.231 g, 2.35 mmol). The organic layer is separated, kept and the yellow aqueous layer further extracted with CH_2Cl_2 (5 x 20 mL) or till the aqueous layer is colourless. The organic extracts are combined and dried over anhydrous $CaCl_2$, kept cold and under a N_2 atmosphere for 30 min. The yellow CH_2Cl_2 suspension is filtered and CH_2Cl_2 is removed using a rotary evaporator without heating to give bright yellow solids of **2-7**. **2-7** is further purified by vacuum sublimation (ice-water) at 27- 28 ^oC to give bright yellow crystals of N-nitrosoethylcarbamate (**2-7**) (0.190 g, 1.61 mmol, 34 % yield).

(Note: to minimize the loss of **2-7** due to its low melting point, the sublimator is cooled to around 6-7 ^oC before the vacuum is applied.)

Decomposition point: 57.4 ^oC (-86.1 kJ mol^{-1})

IR (cm^{-1}): 3430vs, 2989w, 2930vw, 2859vw, 1748s, 1615m, 1520m, 1474m, 1447m, 1431m, 1393m, 1376m, 1329s, 1257s, 1233m, 1205m, 1093vs, 1073vs, 999m, 862w, 541w.

^1H NMR (200 MHz, $CDCl_3$) ppm: δ = 1.35 (t, 3H, *J* = 6.8 Hz, minor), 1.44 (t, 3H, *J* = 6.8 Hz, major), 4.35 (q, 2H, *J* = 6.8 Hz, minor), 4.50 (q, 2H, *J* = 6.8 Hz, major), 10.73 (N*H*, broad).

UV: (CH_3OH λ_{max}, nm (ε, M^{-1} cm^{-1})): 366sh (13.8), 385sh (32.2), 401 (63.5), 417 (91.1), 436 (79.1).

2.4.3 Synthesis of N-nitrosomethylcarbamate salt

Potassium N-nitrosomethylcarbamate, K[CH_3OC(O)NNO] (**2-6K**)

Compound **2-6** (0.082 g, 0.788 mmol) is dissolved in dry CH_2Cl_2 (10 mL) and $KOCH_3$ (0.053 g, 0.757 mmol) is added. The white suspension is stirred overnight to give a yellow suspension. The solvent is removed and the yellow

residue dissolved in CH_3OH and filtered to give a yellow filtrate. The solvent is removed and recrystallized from dry CH_3OH/ether to give yellow crystals of $K[CH_3OC(O)NNO]$ (**2-6K**) (0.075 g, 0.528 mmol , 70 % yield). Note: The yellow crystals are hygroscopic, sensitive to friction and can detonate!

IR (cm^{-1}): 3035w, 2974w, 1685vs, 1631s, 1603s, 1474m, 1447m, 1438w, 1422m, 1384s, 1351m, 1246vs, 1214vs, 1110m, 1071s, 961m, 801m, 788m, 601w, 470m.
^1H NMR (400 MHz, CD_3OD) ppm: 3.63 (s, 3H, minor), 3.73 (s, 3H, minor), δ 3.81 (s, 3H, major)
UV: (CH_3OH) λ_{max} = 395 nm, ε = 37.9 L mol^{-1} cm^{-1}

Silver N-nitrosomethylcarbamate, $Ag[CH_3OC(O)NNO]$ (**2-6Ag**)

Compound **2-6** (0.030 g, 0.288 mmol) is dissolved in dry CH_2Cl_2 (4 mL) and Ag_2CO_3 (0.039 g, 0.142 mmol) is added. The suspension is stirred overnight to give a yellow suspension. The suspension is filtered through filter paper/Buchner funnel set-up, washed with CH_2Cl_2 and dried to give yellow solids of $Ag[CH_3OC(O)NNO]$ (**2-6Ag**) (0.037 g, 0.176 mmol, 62 % yield). Note: The yellow solids are sensitive to friction and can detonate!

IR (cm^{-1}): 2958w, 1697s, 1441m, 1211vs, 1072s, 960w, 798m, 465w.

2.5 N-nitro-*p*-tolylsulfonamide and their salts

2.5.1 N-Nitro-*p*-tolylsulfonamide *p*-$C_7H_8SO_2NHNO_2$ (2-8)

N-nitro-*p*-tolylsulfonamide (**2-8**) is synthesized using the method of B. R. Mathews.[112]

IR (cm^{-1}): 3151s, 2992w, 2936w, 1935w, 1608vs, 1594s, 1494w, 1392s, 1320m, 1299m, 1194s, 1170vs, 1125w, 1085m, 1017w, 971w, 871m, 816m, 801w, 757m, 701w, 667m, 634w, 579m, 541m, 486w.
^{1}H NMR (400 MHz, $CDCl_3$) ppm: δ = 2.49 (s, 3H), 7.41 (d, 2H, J = 8 Hz), 7.95 (d, 2H, J = 8.4 Hz), 10.00 ppm (N*H*, broad)

2.5.2 Synthesis of N-nitro-*p*-tolylsulfonamide salts

Ammonium N-nitro-*p*-tolylsulfonamide, NH_4[*p*-$C_7H_8SO_2NNO_2$] (**2-8NH_4**)
The synthesis is carried out using the method of B. R. Mathews.[112]

IR (cm^{-1}): 3259s, 1920vw, 1597vw, 1401vs, 1299vs, 1281vs, 1183w, 1159s, 1143s, 1082s, 1055m, 1017w, 867m, 815m, 787m, 748w, 706w, 671m, 664m, 597s, 551m, 497w.

Potassium N-nitro-*p*-tolylsulfonamide, K[*p*-$C_7H_8SO_2NNO_2$] (**2-8K**)
Compound **2-8** (0.200 g, 0.926 mmol) is dissolved in dry CH_2Cl_2 (10 mL) and $KOCH_3$ (0.060 g, 0.857 mmol) is added and stirred at room temperature overnight. The white suspension is filtered and washed with CH_2Cl_2 to remove any unreacted N-nitro-*p*-tolylsulfonamide to give white solids of K[*p*-$C_7H_8SO_2NNO_2$] (**2-8**) (0.155 g, 0.611 mmol, 71 % yield).

IR (KBr, cm^{-1}): 3065vw, 3054vw, 1598vw, 1426vs, 1380vw, 1309s, 1289s, 1185w, 1148vs, 1085m, 1056m, 887m, 809w, 792w, 753w, 704w, 665m, 601m, 549m, 502w.

^{1}H NMR (200 MHz, CD_3OD) ppm: δ = 2.41 (s, 3H), 7.33 (d, 2H, *J* = 8.1 Hz), 7.80 (d, 2H, *J* = 8.1 Hz)

Elemental analysis calcd. for $C_7H_7N_2SO_4K$ (254.31 g mol^{-1}) % C, 33.03; H, 2.75; N, 11.01; S, 12.58. Found % C, 33.03; H, 2.67; N, 10.92; S, 12.24.

Silver N-nitro-*p*-tolylsulfonamide, Ag[*p*-$C_7H_8SO_2NNO_2$] (**2-8Ag**)

Compound **2-8** (0.315 g, 1.46 mmol) is dissolved in CH_2Cl_2 (5 mL) and Ag_2CO_3 (0.200 g, 0.726 mmol) is added and stirred overnight at room temperature. The white suspension is filtered and the residue washed with CH_2Cl_2 and dried to give white solids of Ag[*p*-$C_7H_8SO_2NNO_2$] (**2-8Ag**) (0.318 g, 0.986 mmol, 68 % yield).

IR (cm^{-1}): 3045vw, 2920vw, 1596w, 1435s, 1382m, 1301vs, 1286vs, 1151s, 1140s, 1078m, 044m, 1018w, 909w, 870w, 815w, 774w, 755w, 666s, 600s, 543m.

2.6 Results and Discussion

2.6.1 Synthesis of ligands

2.6.1.1 N-nitroamides

There are several methods to synthesize nitramide (**2-1**). The most utilised synthesis is the modified preparation of Thiele and Lachman[85] by Marlies[86] which involves three steps staring from ethyl carbamate (Scheme 2-1).

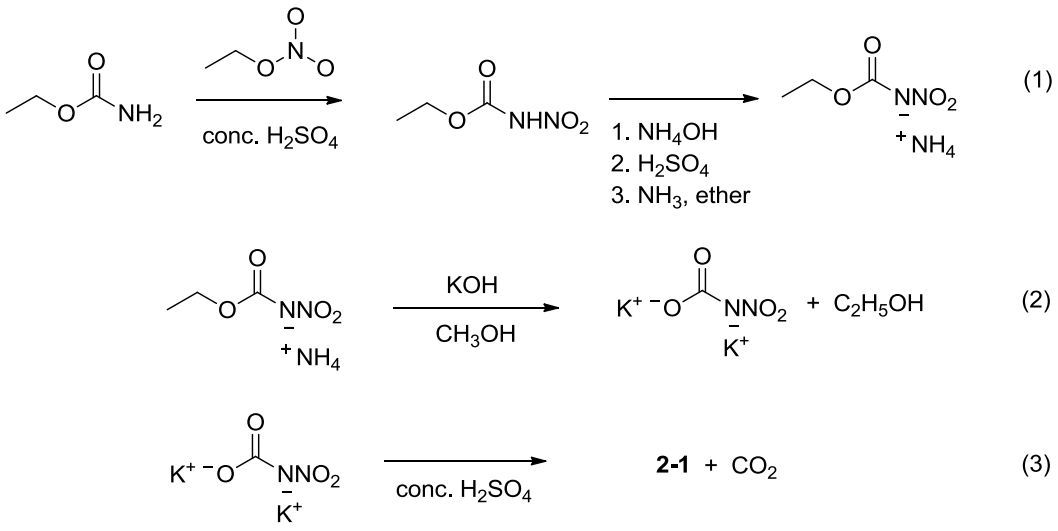

Scheme 2-1. Synthesis of **2-1** from urethane.

This synthesis gives relatively good yields in each step but requires lengthy and tedious work-up. Furthermore during the isolation of dipotassium nitrocarbamate, it must be handled with extreme caution as it can undergo spontaneous decomposition with or without heat, friction or moisture to release CO_2.

The next most commonly used synthesis is the nitration of sodium sulfamate and subsequent hydrolysis (Scheme 2-2).[113]

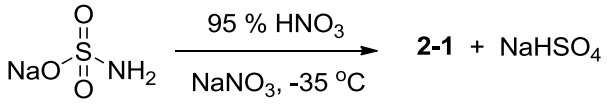

Scheme 2-2. Synthesis of **2-1** from sodium sulfamate.

Sulfamic acid in the presence of nitric acid and sodium nitrate generates **2-1** but only in about 20 % yields.[114] With other alkaline nitrates, a mixture of **2-1**,

which decomposes rapidly to nitrous oxide, ammonium sulfamate, nitric acid and ammonium hydrogen sulfamate is generated.[87] With sodium sulfamate, at low temperatures and sodium nitrate gives **2-1** in yields up to 80 %.

Other methods of synthesizing **2-1** has been explored; from the nitrolysis of ammonia using dinitrogen pentoxide, N_2O_5 (Scheme 2-3) ,[115] to decomposition of nitramines such as 1,3,5-trinitro-1,2,5-triazacyclohexane (RDX) and methylenedinitramine.[87, 116] however in most cases, the yields are low with other side products.

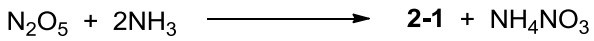

Scheme 2-3. Synthesis of **2-1** from ammonia by dinitrogen pentoxide.

A more recent synthetic pathway involves the nitration of urea followed by hydrolysis to give **2-1** (Scheme 2-4).[107, 117]

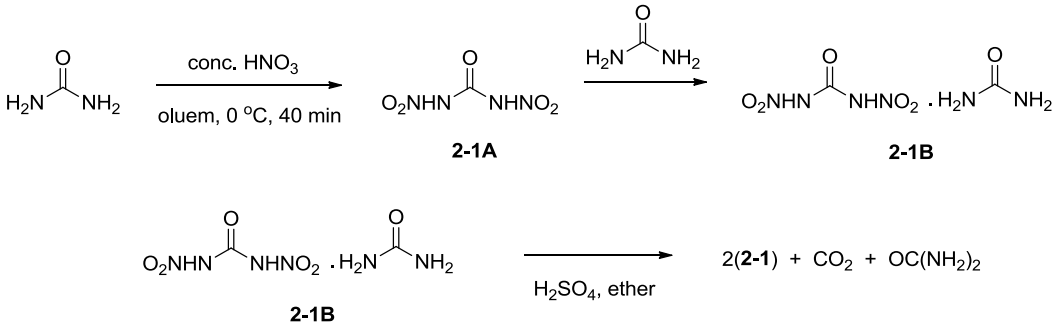

Scheme 2-4. Synthesis of **2-1** from urea

There are several factors to consider in nitration reactions. The most important consideration is the nuclephilicity of the site of nitration. The reason is that all nitration reactions require the electrophilic attack of the NO_2^+ fragment on the nucleophilic site. The weaker the nucleophilicity of the site, the longer the reaction time, or the use of a stronger nitrating reagent (one that is more efficient in generating NO_2^+) is required. In all nitration reactions using nitric acid, the efficiency of the nitration decreases as the reaction progresses due to the dilution effect from the liberation of the proton of the nitrated substrate to give water (Scheme 2-5). Other factors to consider will be the stability of the nitration products and the selectivity of the nitration site.

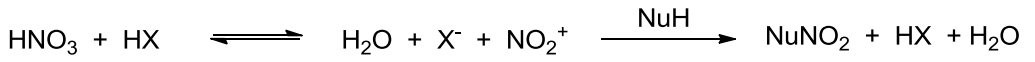

X = conjugate base of mineral acid Nu = nucleophilic site of substrate to be nitrated

Scheme 2-5. General mechanism of nitration using nitric acid.

The nitration of urea requires a strong nitrating agent as the lone pair on the nitrogen of the amide is delocalised over the amide bond. Further complicating this reaction is that dinitrourea, **2-1A**, is unstable in acidic media and decomposes easily to give nitrous oxide, water and carbon dioxide.[118] Therefore a balance in the nitration efficiency and stability/isolation of the nitration product is required. This compromise is achieved with the following reaction conditions proposed by Lobonova *et al.*:[107] first to carry out the reactions at low temperature which helps to reduce the kinetics of decomposition; second by using oleum, which is concentrated sulfuric acid with free sulfur trioxide (SO_3), which reacts with the H_2O side-product to give sulfuric acid, maintaining the nitration efficiency; and finally concentrated nitric acid of at least ρ = 1.5 g mL^{-1} (100 %) which maximises nitration efficiency and minimises the amount of water present which contributes to **2-1A** decomposition. The above conditions also reduces the reaction times, thus minimising decomposition and also results in the precipitation of **2-1A**. The use of a strong acid in the presence of nitric acid supports a strongly oxidising media which in this reaction is not observed to give any over-oxidised nitrogen oxides. The isolation of **2-1A** involves filtration and washing with an acidic miscible solvent. Between dichloromethane and trifluoroacetic acid (TFA), we found that TFA is a better solvent for removing the viscous and dense acidic mixture of oleum and nitric acid as it is more miscible with the nitrating media.

Compound **2-1A** is quite unstable and can spontaneously detonate from heat, shock and friction and therefore has undergone rigorous investigation for its energetic properties for use as propellants and explosives in military research.[117a] Two methods have been developed for storage of **2-1A** through mitigation of its sensitivity to impact and friction. The first method consists of conversion into highly dense salts with nitrogen containing cations such as ammonia, imidazoles and guanadines.[117b] The alternative method which provides subsequent easy

access to **2-1** uses the formation of **2-1B** which is the urea salt of dinitrourea (Scheme 2-4). Compund **2-1B** is relatively stable and can be stored at low temperature over time in absence of moisture with minimum decomposition.

The slow hydrolysis of **2-1B** in acidified ether allows the controlled decomposition of **2-1B** giving **2-1**. We have found that **2-1** isolated from acidic media requires sublimation for purification as there is always some residual acid which recrystallization does not remove.

Compound **2-1** is the simplest nitroamine and gives us access to the acyl substituted N-nitroamides. The N-nitroamides are synthesized from **2-1** by reaction of their corresponding anhydrides (Scheme 2-6).

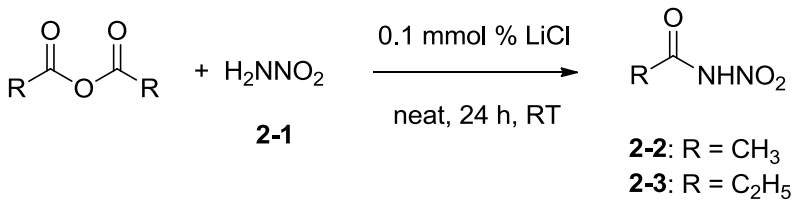

Scheme 2-6. Synthesis of N-nitroamides

The long reaction time and poor yields are the main disadvantage to this procedure. With the addition of catalytic amounts of LiCl, reaction times are halved and the yields are comparable to the literature.[107] N-nitroacetamide is obtained in approximately 40 % yield while N-nitropropionamide is isolated only at about 18 % yield. An alternative more efficient procedure using nitronium tetrafluoroborate, NO_2BF_4, as the nitrating agent for acyl amides such as acetamide or propionamide had been reported.[119] Even though there were two reports using the described procedure,[120] multiple attempts at repeating the synthesis were not successful.

Compounds **2-2** and **2-3** belong to the family of primary N-nitroamides. The proton of the amide is acidic due to the electronegative effect of the nitro group on the amide proton. Numerous studies have been carried out on N-nitroamides, but most of which are done on the secondary N-nitroamides where the proton is substituted with an alkyl group. In particular White and co-workers were concern with the reactivity and decomposition of the secondary N-nitroamides,[121] while

Tselinskii *et al*. were focused on the nitration reactions of various secondary amides and substituted N-nitroamides using NO_2BF_4 in various solvents.[122] In all cases the evolution of gas was observed either during synthesis or decomposition reactions. The gas has been identified as nitrous oxide and is caused by the acid-promoted rearrangement[123] to give the important rate-determining intermediate diazoester, **2-9** confirmed with ^{18}O labeling studies (Scheme 2-7).[121a, 124]

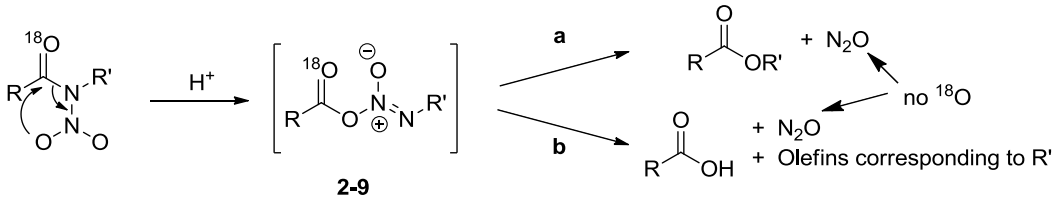

Scheme 2-7. Proposed decomposition mechanisms of secondary N-nitroamides.[121a]

Diazoester **2-9** subsequently decomposes by two possible pathways with pathway **a** usually dominant to give nitrous oxide and the corresponding esters or pathway **b** to give carboxylic acids with olefins. From the proposed reaction mechanism, it can be inferred that the primary N-nitroamides will be more susceptible to decomposition as the resulting extrusion of nitrous oxide generates a carboxylic acid (Scheme 2-8).[121b]

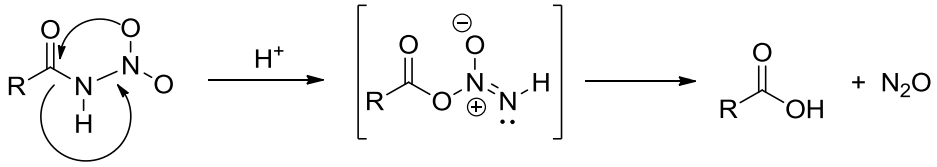

Scheme 2-8. Proposed decomposition mechanism of primary N-nitroamides.

The proton that is present in primary nitroamides also contributes to the decomposition as it is acidic. This coupled with the fact that a strong nitrating media is required for nitration of the less nucleophilic amide which in turn requires a highly acidic media limits the accessibility of primary N-nitroamides. To further elaborate, the nitration of alkyl amides using NO_2BF_4 was unsuccessful in our situation due to the quality of NO_2BF_4; as commercial sources seem to contain residual acid in the form of HBF_4 or HF which affects the reaction.[125] In the two examples where such nitration is successful, the authors synthesized their

own NO_2BF_4 from HNO_3, BF_3 and HF. Without access to the specialty apparatus required for synthesizing NO_2BF_4, the method of using **2-1** as an amine to react with the corresponding anhydrides provides an alternate route to N-nitroamides. The long reaction time is because of the less nucleophilic property of **2-1** due to the presence of the nitro group. The choice of acylation reagent is also limited to anhydrides as the acid chlorides release HCl as the side product. The side product of the anhydride is the weak carboxylic acid which the N-nitroamides are more tolerant of. The additional limitations of this method is that only a large excess of anhydride is required for the reaction to proceed, thus large molecular weight anhydrides will not be feasible. Unsuccessful attempts at using other methods of nitration to obtain the N-nitroamides are discussed in Appendix A.

An important contrast between **2-1** and N-nitroamides **2-2** and **2-3** is that the N-nitroamides are relatively stable to bases but are prone to acid hydrolysis which is the inverse of **2-1**. This significant difference allows us to exploit the use of either class of compounds depending on the reaction conditions.

2.6.1.2 N-nitrocarbamates

The related N-nitrocarbamates are more stable to acid hydrolysis due to resonance effects which lead to a reduction in the electrophilic nature of the carbonyl group[121a] (Scheme 2-9).

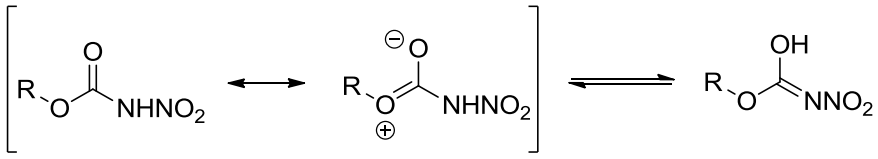

Scheme 2-9. Resonance structures of N-nitrocarbamates.

The greater stability allows the synthesis of N-nitrocarbamates from the nitration of carbamates using nitrate salts in sulfuric acid (Scheme 2-10).[109] Subsequent conversion to the ammonium salt and re-acidification followed by sublimation allows the isolation of high purity N-nitrocarbamates **2-4** and **2-5**.

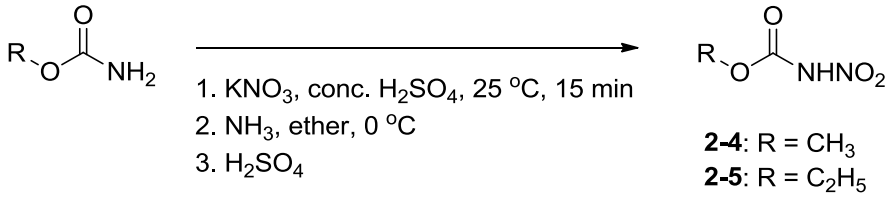

Scheme 2-10. Synthesis of N-nitrocarbamates.

Although the N-nitrocarbamates are more robust to acid hydrolysis, extended durations in acidic media results in the same acid-promoted rearrangement[123] to diazoester intermediate, **2-10**, which rapidly decomposes by two possible pathways to give nitrous oxide and other products (Scheme 2-11).

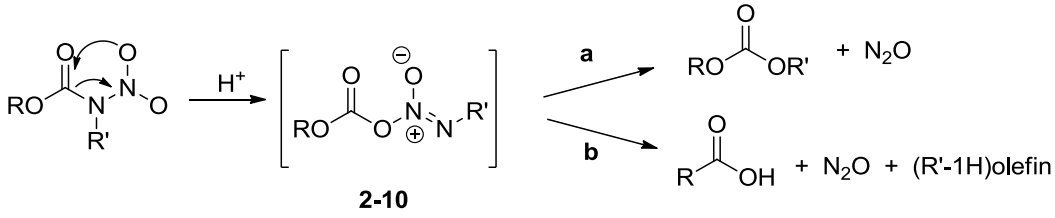

Scheme 2-11. Proposed decomposition of secondary N-nitrocarbamates.[121a]

The decomposition of primary N-nitrocarbamates such as **2-4** and **2-5** follows the same rearrangement mechanism to give nitrous oxide and carbamic acid which further decomposes to CO_2 and alcohol (Scheme 2-12).

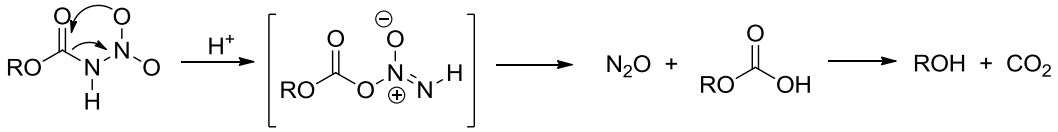

Scheme 2-12. Proposed decomposition of primary N-nitrocarbamates.

Similar to the N-nitroamides, the proton on the amide functional group of N-nitrocarbamates is also acidic due to the presence of the nitro group. The N-nitocarbamates are also relatively stable to base but require stronger bases such as potassium methoxide for complete reaction.

2.6.1.3 N-nitrosocarbamates

The N-nitrosocarbamates are more similar to the N-nitrocarbamates than to the N-nitroamides. N-nitrosation reactions are very well studied and there are several reagents that can be commonly used: nitrogen tetroxide (N_2O_4), nitrosyl halide (NOX), nitrogen trioxide (N_2O_3), alkylnitrite (RONO), nitrosonium salts and acidified nitrite.[126] For the N-nitrosocarbamates, only limited success has been reported for direct nitrosation due to the less nucleophilic amide and nitrosation reactions tending to result in redox reactions. Some examples of N-nitrosocarbamates have been synthesized by White[126a] using sodium nitrite/acetic anhydride mixtures. More studies have been carried out with N-nitrosoamides but it has been established that the N-nitrosocarbamates follow very similar reactivity and decomposition pathways. N-nitrosocarbamates are in general less stable compared to the N-nitrocarbamates and decompose through the same acid-promoted rearrangement[123] to give the essential diazoester intermediate **2-11** (Scheme 2-13).[127]

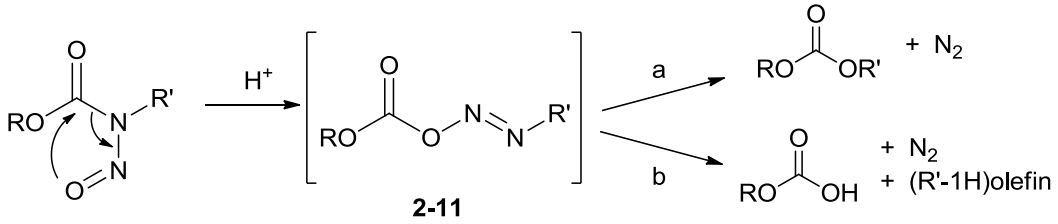

Scheme 2-13. Decomposition of secondary N-nitrosocarbamate.[124]

The diazoester **2-11** subsequently decomposes by two possible pathways to give nitrogen and other organic side products. The size of the R' group has been determined to affect the rate of decomposition with larger R' groups degrading at a faster rate.[121c]

Compounds **2-6** and **2-7** belongs to the class of primary N-nitrosocarbamates and undergoes decomposition to give nitrogen and carbamic acid which further decomposes to release CO_2 and alcohol (Scheme 2-14).

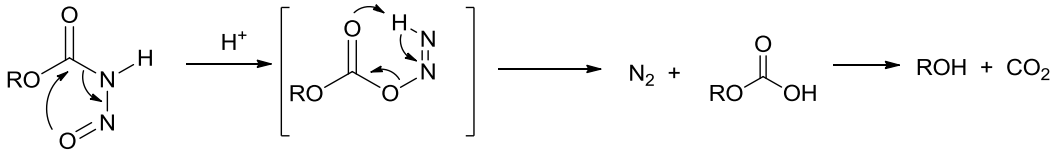

Scheme 2-14. Proposed decomposition of primary N-nitrosocarbamate.

An alternative decomposition pathway is also possible where the elimination of N_2O and results in the formation of aldehyde which is mentioned by Thiele (Scheme 2-15).[85]

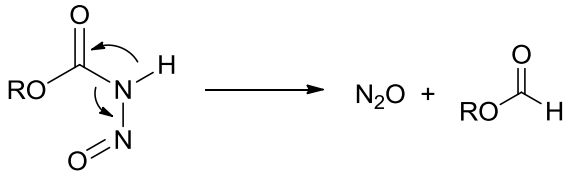

Scheme 2-15. Alternative decomposition pathway of N-nitrosocarbamate.

The amide proton of N-nitrosocarbamates is acidic due to the nitroso group. They are also relatively stable towards bases and are generally much more soluble than the nitro analogs.

Compound **2-7** was first synthesized by Thiele *et al*. from the partial reduction of the **2-5NH$_4$** in 1895 (Scheme 2-16).[85]

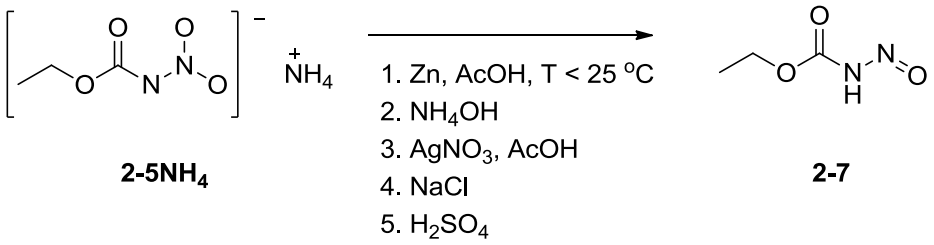

2-5NH$_4$ **2-7**

Scheme 2-16. Synthesis of **2-7**.

The report stated explicitly that the procedure has to be followed exactly and done meticulously for the synthesis to be successful. Since then, only two reports using Thiele's preparation have emerged.[111, 128] In the report by Benin *et al*., the synthesis was completed only to the isolation of the **2-7Ag** with some modification and the reported yield was much lower compared to Thiele. **2-7Ag** was subsequently converted to a tetrabutylammonium salt by cation metathesis to obtain a soluble form for reactivity and stability studies using NMR spectroscopy. In all the above cases, no proper characterisation of the compound was mentioned

other than melting point, combustion data, an inaccurate modern elemental analysis of **2-7Ag** and NMR data of the alkylammonium salt.

We attempted to synthesize **2-7** following Thiele's procedure and were hampered by the low yield and instability of **2-7Ag**. Furthermore some of the described phenomena during the reaction were not observed. The initial yellow precipitate that is formed at the end of the first step of the reaction before the addition of aqueous ammonia was not observed. The quality of the Zn dust was suspected to be an issue as Zn is known to form a $ZnO/ZnCO_3$ layer from prolonged exposure to air. The Zn dust was replaced with freshly purchased reagent grade Zn dust prepared and stored under nitrogen; however there were no changes observed.

The next possible cause was the amount of acetic acid used during the reaction. The original preparation reported a 1:1 stoichiometry of **2-5NH$_4$** to acetic acid with Zn dust in excess. The stoichiometric ratio would be correct based on the balanced equation shown in Scheme 2-17.

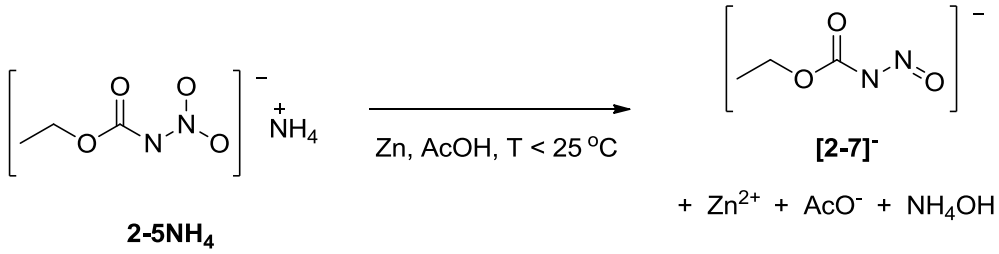

Scheme 2-17. Initial partial reduction of **2-5NH$_4$** to [**2-7**]$^-$ by Zn.

The protons for the reduction would be derived from the acetic acid with the products being a Zn(N-nitrosoethylcarbamate)(acetate) salt and ammonia hydroxide. The equation only applies if the quality of the Zn dust is not compromised. The reaction was repeated with two equivalents of acetic acid giving a yellow precipitate in yellow solution at the end of the reaction. The implications of this would be either that the preparation by Thiele *et al*. was not written in good faith or that the quality of commercial Zn dust in modern times is of inferior quality to that obtained in the 1900s; we believe the latter case is more probable.

The next step of the reaction is the addition of aqueous ammonia. In both the Thiele *et al*. and Benin *et al*. preparations, no specific amounts were given, only

that it was to be used in excess. We believe it is important to use a judicious amount of aqueous ammonia as the isolation of **2-7Ag** requires acidification in subsequent steps. The amount of aqueous ammonia that was initially used was two times the amount of acetic acid that was used. This resulted in a voluminous formation of a yellow-green precipitate in a yellow solution. There were no indications in the reports if this was a normal observation. Filtering of the precipitate gave a yellow filtrate that was further processed. The addition of silver nitrate solution and acidification with acetic acid did generate a yellow precipitate, but the estimated yield was still barely two percent of the starting material. Repeating the experiment multiple times gave consistent results. We decided to analyze the importance of the amount of aqueous ammonia that was added and consider the yellow-green precipitate that formed. We considered all the ions that are present in the reaction mixture before the addition of aqueous ammonia and deduced the possible equilibrium products in the reaction (Scheme 2-18).

Zn^{2+} + NH_4^+ + **[2-7]$^-$** + OAc^- + OH^-

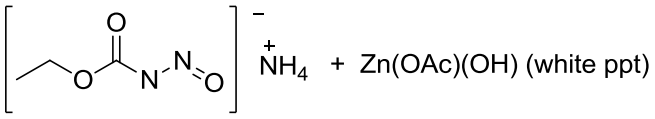

NH_4 + Zn(OAc)(OH) (white ppt)

2-7NH_4

NH_4OH + $Zn(C_2H_5OC(O)NNO)(OH)$ (yellow ppt)

Zn(OH)[2-7]$^-$

$NH_4(OAc)$ + $Zn(C_2H_5OC(O)NNO)(OAc)$ (yellow ppt)

Zn(OAc)[2-7]$^-$

$NH_4(OAc)$ + $NH_4(OH)$ + $Zn(C_2H_5OC(O)NNO)_2$ (yellow ppt)

Zn([2-7]$^-$)$_2$

$(NH_4)_2[Zn(C_2H_5OC(O)NNO)_x(OAc)_y(OH)_z]$

NH_4Zn(OAc)(OH)([2-7]$^-$) $(x + y + z = 4, x > 0)$

Scheme 2-18. Equilibrium mixtures of Zn reduction of **2-5NH_4** reaction.

All Zn^{2+} salts are colourless as the electronic configuration of Zn^{2+} is d^{10} eliminating any visible light absorption due to *d-d* electronic transition. The ammonium, acetate and hydroxyl ions are also colourless which leaves the observe colour of the precipitate derived from the presence of **[2-7]$^-$**. Therefore the possible yellow precipitate that is observe in the reaction mixture are **Zn(OH)[2-7]$^-$**, **Zn(OAc)[2-7]$^-$** and **Zn([2-7]$^-$)$_2$**. The yellow solution that is observed can be **2-7NH_4** and **NH_4Zn(OAc)(OH)([2-7]$^-$)** with its various coordination isomers. The addition of aqueous ammonia in insufficient amounts

will generate more of **Zn(OH)[2-7]$^-$** which is the yellow-green precipitate that was observed. Excess aqueous ammonia will result in the formation of soluble zincate complexes and **NH_4Zn(OAc)(OH)([2-7]$^-$)** therefore allowing the dissolution of all the species in the reaction mixture. In the end the appropriate amount of aqueous ammonia to be added will be three times the amount of **2-5NH_4** (Scheme 2-19).

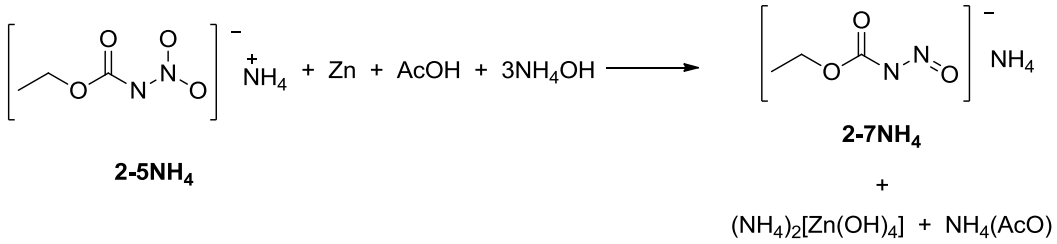

Scheme 2-19. Complete conversion to **2-7NH_4**.

This is still an approximation however, as the amount of Zn and acetic acid used in excess of **2-5NH_4** plays a role in the amount of Zn^{2+} ions present in the solution. Therefore additional amounts of aqueous ammonia are still required. Experimentally, it has been determined that adding four equivalents of aqueous ammonia results in complete dissolution of the yellow-green precipitate to give a yellow filtrate and filtering removes unreacted Zn.

To isolate [**2-7**]$^-$, the soluble **2-7NH_4** is converted to **2-7Ag** using silver nitrate and the solution is subsequently acidified using acetic acid to precipitate the yellow silver salt. It is known that silver nitrate will dissolve in ammoniacal solutions to form silver diammine complexes as shown in Equation 2-1.

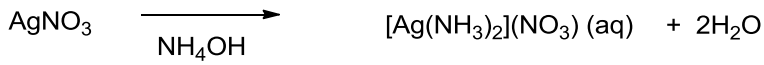

Equation 2-1. Dissolution of $AgNO_3$ in ammoniacal solutions

Thus the subsequent acidification by acetic acid is required to displace the ammine ligands to allow the precipitation of the less soluble **2-7Ag**. The solvation of all the ions allows the formation of the less soluble **2-7Ag** which is observed to form by slow precipitation of a yellow solid on standing in solution over time (Scheme 2-20).

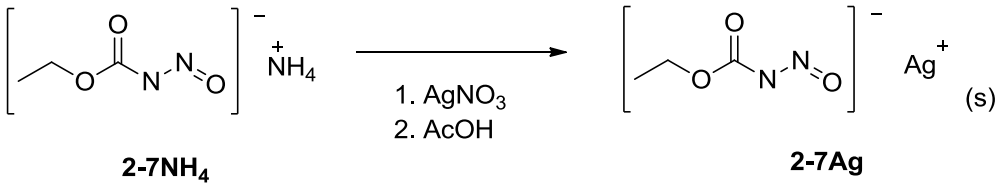

2-7NH$_4$ **2-7Ag**

Scheme 2-20. Precipitation of **2-7Ag**.

Compound **2-7Ag** is very unstable to moisture and isolation of this product has been unreliable even in the best of times. This is reflected in the less than satisfactory elemental analysis data obtained by Benin.[111] **2-7Ag** rapidly decomposes in moist conditions to give silver ethylcarbonate which can be observed when the yellow solids turned beige. The beige solids have been analyzed to be silver ethylcarbonate by IR spectroscopy. The likely side-product from the decomposition is nitrogen gas (Equation 2-2) similar to the decomposition of the free acid.

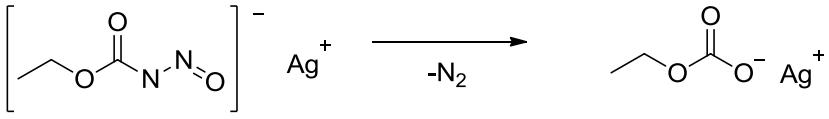

2-7Ag yellow solid beige solid

Equation 2-2. Decomposition of **2-7Ag**.

Prolonged exposure of **2-7Ag** to the acidic mother liquor causes the decomposition of **2-7Ag** when the solution starts turning black, indicating the formation of silver particles. Disturbing the solution during the precipitation process also causes the decomposition to accelerate. The observation of silver particles may indicate a redox reaction between the silver cation and the possible decomposition aldehyde product of **2-7** in solution (Scheme 2-21). Due to the difficulty of handing **2-7Ag**, it was decided that the next step of the reaction towards the synthesis of **2-7** would proceed without proper isolation of **2-7Ag**.

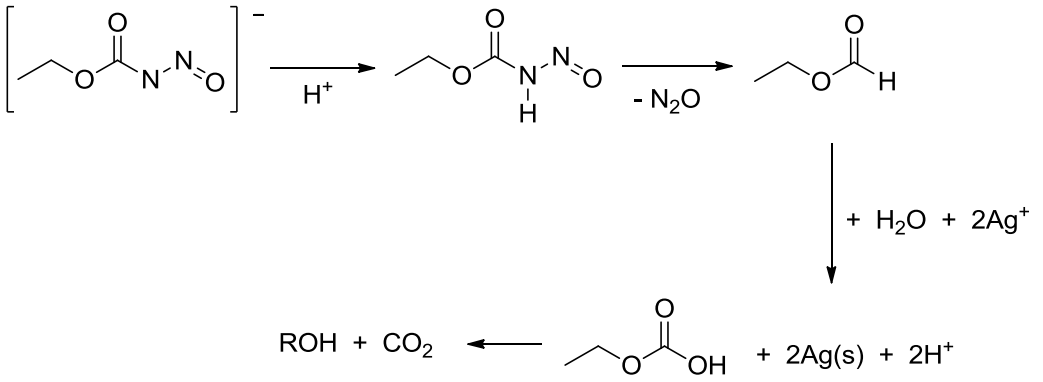

Scheme 2-21. Possible decomposition pathway to give silver particles.

In the original synthesis, a white precipitate is observed to form during the addition of acetic acid which subsequently dissolves. The possible sources of the white precipitate are silver acetate, silver hydroxide and zinc hydroxide as all ammonium and nitrate salts are soluble in aqueous solutions. The colour of the precipitate also rules out the presence of **[2-7]**$^-$. The white precipitate is likely to be zinc hydroxide as the acidification of the solution converts the soluble ammonium zincate to give the less soluble zinc hydroxide which reacts with additional acetic acid to form the soluble zinc acetate (Scheme 2-22).

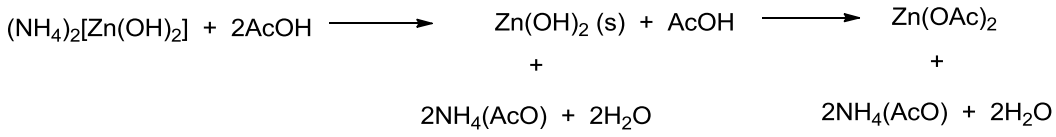

Scheme 2-22. Sequential acidification of ammonium zincate.

The next step of the reaction is to convert **2-7Ag** to **2-7Na** by cation metathesis with sodium chloride (Scheme 2-23). Since we were unable to determine the amounts of **2-7Ag** used for this step of the reaction exactly, the amount of sodium chloride used was in slight excess of the amount of silver nitrate added in the previous step. Vigorous shaking/stirring of **2-7Ag** was required to convert all the silver salt to give a yellow solution which was filtered through Celite.

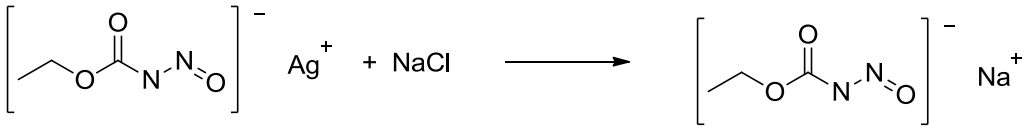

2-7Ag **2-7Na**

Scheme 2-23. Reaction of **2-7Ag** with NaCl.

The yellow filtrate was next extracted with CH_2Cl_2 which is acidified with concentrated sulfuric acid (Scheme 2-24). The extracts have to be dried with anhydrous $CaCl_2$ as anhydrous $MgSO_4$ seems to react with **2-7** which is observable due to the decrease in colouration of the solution. This could be related to the higher Lewis acidity of Mg^{2+} compared to Ca^{2+}. It is important to keep the solution cold at all times to prevent decomposition and also the low sublimation point of **2-7** makes it a very volatile solid. A dry atmosphere during this process is required to prevent moisture from condensing into the solution.

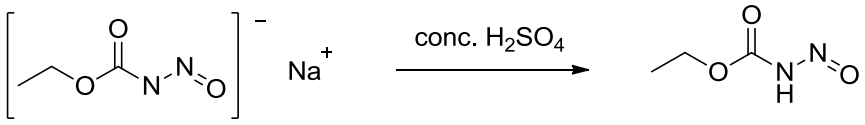

2-7Na **2-7**

Scheme 2-24. Formation of **2-7**.

The final steps in the purification and isolation of **2-7** require reduced pressure sublimation as there is always some residual acid or impurities that recrystallization is less efficient at removing as observed in previous cases with the N-nitroamides and N-nitrocarbamates. The yield of **2-7** at the end of the synthesis based on the amount of silver nitrate used is 34 % which is acceptable but pales in comparison to what was reported by Thiele (76 %).

The synthesis of **2-6** is similar to **2-7** however there are some important differences to take note. Both the salts and neutral form of **2-6** are much more soluble in water which requires careful use of ice and water during the multiple steps of the reaction. The precipitation of **2-6Ag** is less likely to proceed to completion compared to **2-7Ag** as the filtrate remains coloured compared to colourless in **2-7Ag** (Scheme 2-25).

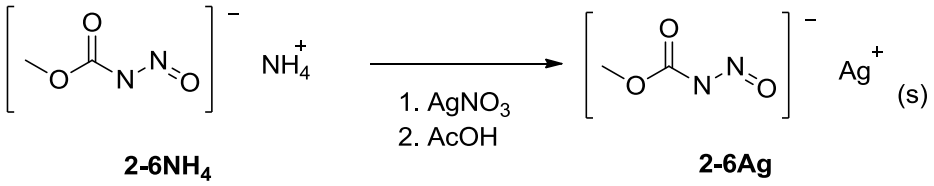

2-6NH$_4$ **2-6Ag**

Scheme 2-25. Formation of **2-6Ag**.

Compound **2-6Ag** also decomposes more readily than **2-7Ag** as black silver particles are is observed to form towards the end of the 15 min precipitation time. The increased solubility of **2-6** also requires the extraction solvent to be changed to the more polar ethyl acetate. All the above factors contribute to the much lower yield of **2-6** (15 %) as compared to **2-7**.

The low stability of the silver salt is the main crux to getting a better yield in the synthesis of the N-nitrosocarbamates. To that end, we have investigated if changing the proton source from acetic acid (*p*Ka = 4.78) for the reduction will improve the yields for this reaction. There is a need for balance in the strength of the acid that can be used for the reduction. Mineral acids are good proton donors but are not suitable as the method of isolation involves the precipitation of the less soluble silver salt from the aqueous media. Boric acid being a very weak acid was not effective as the Zn reduction step failed. Thus other organic acids were tested such as formic acid (*p*Ka = 3.77), propionic acid (*p*Ka = 4.87) and butyric acid (*p*Ka = 4.82). Formic acid was very efficient in the Zn reduction step but undergoes redox reactions with silver nitrate to give colloidal silver. Butyric acid was both a poor acid for the reduction stage and also undergoes rapid redox reaction with silver nitrate. Propionic acid was actually the best acid comparable to acetic acid. An advantage of propionic acid compared to acetic acid is that during the precipitation of the silver salt stage, **2-6Ag** and **2-7Ag** are more stable in propionic acid compared to acetic acid which most likely is due to the lower acidity of propionic acid. However a major problem associated with propionic acid is that the corresponding silver propionate has very similar solubility to **2-7Ag** and is actually less soluble than **2-6Ag**. This resulted in samples of N-nitrosocarbamates prepared with propionic acid to be contaminated with propionic acid after acidification with sulfuric acid. The boiling point of propionic

acid is 141 ^{o}C while the N-nitrosocarbamates have low melting points around 50 ^{o}C. Under reduced pressure environments, the boiling point and sublimation points of propionic acid and the N-nitrosocarbamates are very similar which prevents an efficient way of separating the mixtures.

2.6.1.4 N-nitro-*p*-tolylsulfonamide

The N-nitrosulfonamides are synthesized by nitration of sulfonamides with concentrated nitric acid (95 %, ρ = 1.48 g mL^{-1}) in concentrated sulfuric acid (Scheme 2-26).[112]

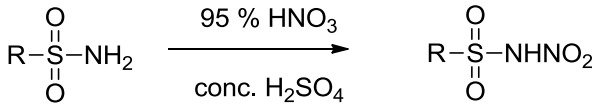

2-8: R = *p*-tolyl

Scheme 2-26. Synthesis of N-nitrosulfonamides.

More recent methods include the use of ammonium nitrate with concentrated sulfuric acid.[129] Most of the sulfonamides of interest are those of arylsulfonamides and it is surprising the nitration reaction is selective towards N-nitration instead of electrophilic aromatic nitration. This is most likely due to the deactivatating effect of the sulfonyl group on the electron-rich benzene ring towards electrophiles.

The N-nitrosulfonamides have similar properties to the N-nitrocarbamates in that there are susceptible to acid hydrolysis[130] (Scheme 2-27) (but not to the extent of N-nitroamides) and are relatively base stable.

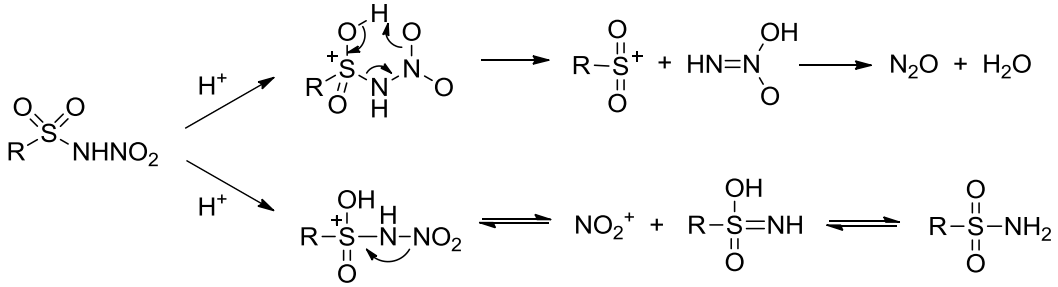

Scheme 2-27. Possible decomposition pathways of N-nitrosulfaonamides

There is some evidence that the release of NO_2^+ is possible.[131] The isolation of these compounds exploits the low solubility of the corresponding ammonium salts in the aqueous acid media. This enhanced stability is attributed to the less electrophilic nature of the sulfonyl group towards nucleophiles.

2.6.1.5 Anionic salts of the ligands

The silver salts for the N-nitro/nitroso compounds are synthesized by reaction with silver carbonate, Ag_2CO_3 (Scheme 2-28).

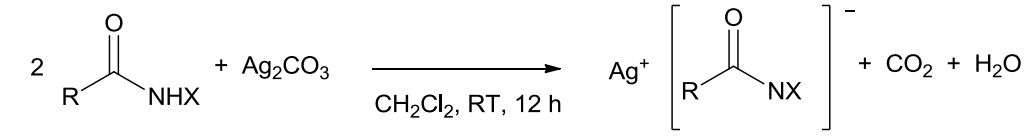

R	X	Compound
CH_3	NO_2	**2-2**
CH_3O	NO_2	**2-4**
C_2H_5O	NO_2	**2-5**
CH_3O	NO	**2-6**

R	X	Compound
CH_3	NO_2	**2-2Ag**
CH_3O	NO_2	**2-4Ag**
C_2H_5O	NO_2	**2-5Ag**
CH_3O	NO	**2-6Ag**

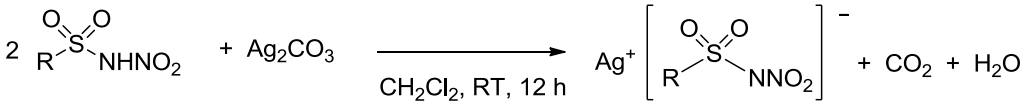

2-8 **2-8Ag**

R = *p*-tolyl

Scheme 2-28. Synthesis of silver salts of N-nitroamides, N-nitrocarbamates, N-nitrosocarbamates and N-nitro-*p*-tolylsulfonamides.

The heterogeneous suspension of silver carbonate reacted with the acidic amides which were soluble in dichloromethane overnight in the absence of light to generate the corresponding insoluble silver salts in good yield. This is in contrast to the poor yields obtained for **2-5Ag** when carried out in water.[110] All the silver salts are white solids which are relatively stable except for **2-6Ag** and **2-7Ag** which are yellow. Compound **2-6Ag** is actually friction sensitive when dry. Isolation of **2-6Ag** during the reduction of **2-5NH$_4$** is risk-free due to the moist condition of the salt. However isolation of **2-6Ag** from the above preparation requires special precaution as detonation of the substance occurred on retrieval of the product from the sintered glass frit due to friction.

The potassium salts of the N-nitro/nitroso compounds are obtained similarly by the reaction with bases (Scheme 2-29).

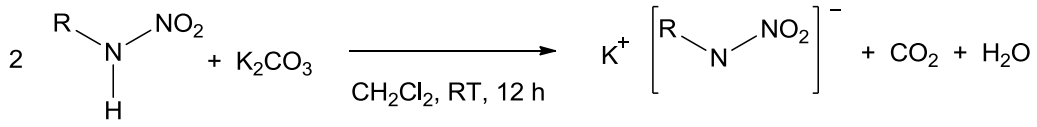

R	Compound
$CH_3C(O)$	**2-2**
p-tolylSO_2	**2-8**

R	Compound
$CH_3C(O)$	**2-2K**
p-tolylSO_2	**2-8K**

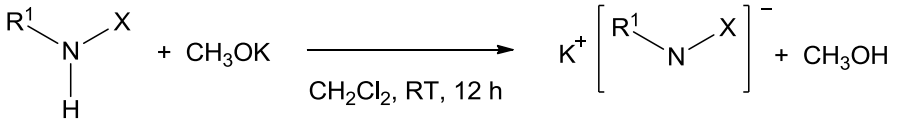

R^1	X	Compound
CH_3O	NO_2	**2-4**
CH_3O	NO	**2-6**

R^1	X	Compound
CH_3O	NO_2	**2-4K**
CH_3O	NO	**2-6K**

Scheme 2-29. Synthesis of potassium salts of N-nitroamides, N-nitrocarbamates, N-nitrosocarbamates and N-nitro-*p*-tolylsulfonamides.

With the N-nitroamides and N-nitro-*p*-tolylsulfonamides, crushed potassium carbonate was sufficient to generate the potassium salts in good purity. For the N-nitro/nitroso carbamates, potassium methoxide was used instead as there was always residual unreacted K_2CO_3 remaining which affected the purity of the products. Compound **2-5K** is obtained in good yields compared to the reported preparation in water using potassium hydroxide.[110] The potassium salts are soluble in water and insoluble in non-polar solvents with very limited solubility in alcohols such as methanol and ethanol. All the potassium salts are white with the exception of **2-6K** which is yellow similar to **2-6Ag**. Compound **2-6K** is also relatively soluble in methanol and comparatively hygroscopic. It has similar characteristics as **2-6Ag** which requires special attention during isolation due to detonation from friction.

An attempt to try to isolate **2-6K** directly from moist **2-6Ag** during the reduction of **2-4NH$_4$** using KI in dry methanol was not successful as precise amounts of the moist **2-6Ag** could not be determined easily. This led to contamination of excess KI in the **2-6K** samples which could not be separated easily.

Compound **2-8NH$_4$** was isolated by precipitation when aqueous ammonia was added to an aqueous solution of **2-8**.

2.6.2 Crystallography discussion

The compounds discussed so far have potential multiple bond character intra-molecularly which may give rise to various isomeric forms due to restricted bond rotation. This sort of feature has been mentioned briefly in the NMR spectroscopy section for the N-nitrosocarbamates.

2.6.2.1 Neutral ligands

The solid state structures of all the nitrogen acids are planar. The strong hydrogen bonds between the amide proton and the oxygen of the acyl group results in the high density values obtain for the crystals (Table 2-1). This strong H-bonding also causes the crystal packing to exhibit close intermolecular contacts (Figure 2-2).

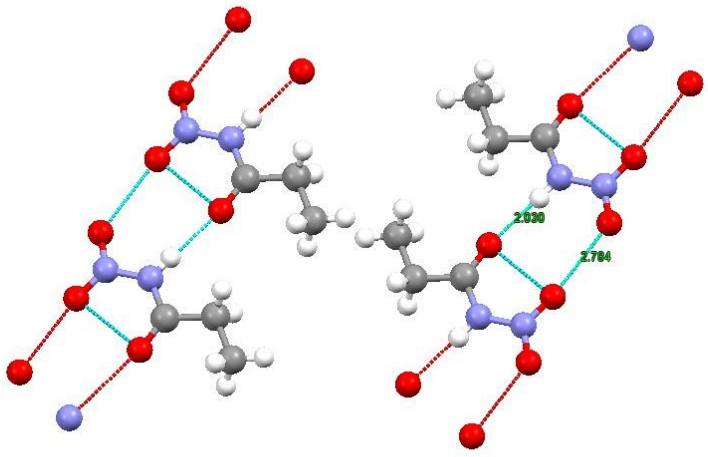

Figure 2-2. Crystal packing showing close intermolecular contacts from H-bonding in **2-3**.

The lack of disorder within the solid state determination for the possible isomers may be due to the above crystal packing effect especially for the N-nitrosocarbamates.

For the N-nitroamides and N-nitrocarbamates, the amidic bond gives rise to cis (Z), trans (E) isomers due to hindered rotation about the C-N bond (Figure 2-3).

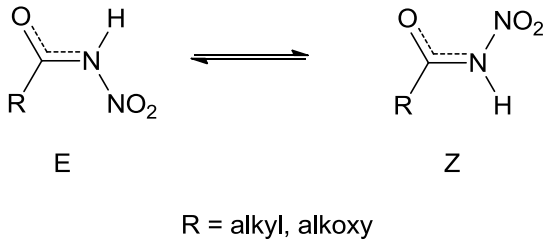

Figure 2-3. Cis (Z), trans (E) isomers of N-nitroamides and N-nitrocarbamates.

The two isomers are not detected in ^{1}H NMR spectroscopy which may be due to either the rate of rotation still being fast on the NMR timescale or to one isomer predominating in solution.

The solid state molecular structures for N-nitroamides, **2-2** and **2-3**, are shown in Figure 2-4 and Figure 2-5 respectively.

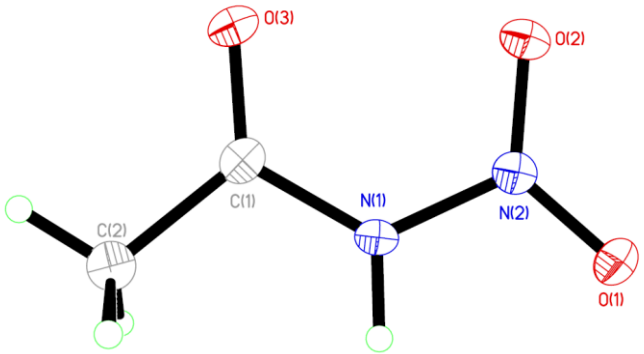

Figure 2-4. Molecular structure of **2-2**

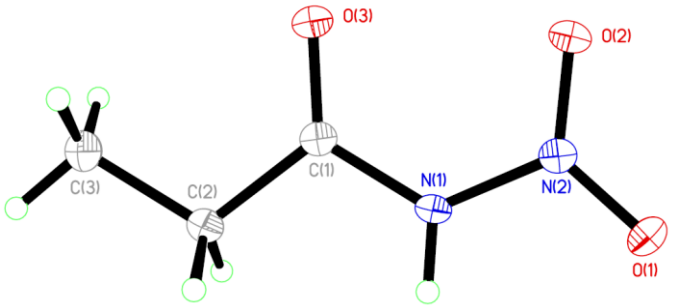

Figure 2-5. Molecular structure of **2-3**.

Compound **2-2** and **2-3** are shown to adopt the Z conformation in the solid state. However, Density functional theory (DFT) calculations carried out indicates that the most stable gas phase isomer is the E isomer (Figure 2-6).

E Z

	E	Z
Relative E (kcal mol^{-1})	0	0.4

Figure 2-6. Calculated relative energy levels of the isomers of **2-2**.

Similarly the solid state structures for the N-nitrocarbamates, **2-4** and **2-5**, are observed to take up the Z configurataion as shown in Figure 2-7 and Figure 2-8 respectively.

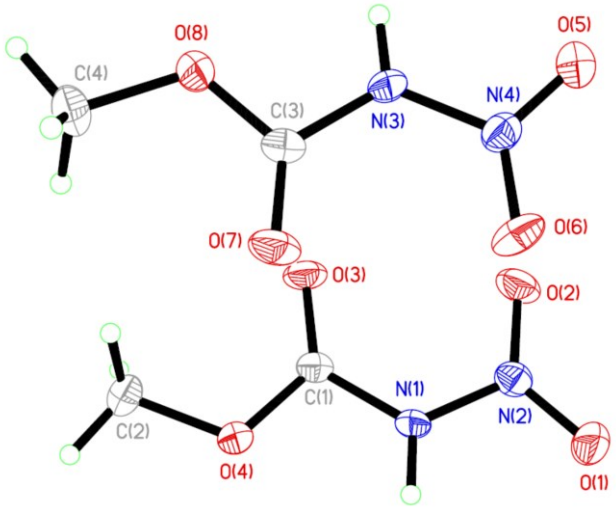

Figure 2-7. Molecular structure of **2-4** containing two independent molecules.

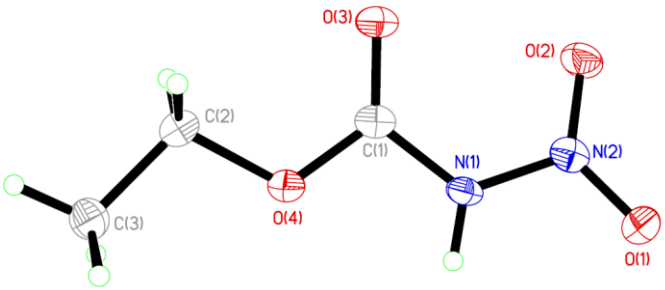

Figure 2-8. Molecular structure of **2-5**.

In the case of compound **2-4** there are 2 independent molecules in the asymmetric unit with both molecules in the cis conformation. DFT calculations for gas phase isomers also indicate the Z isomer to be the thermodynamic isomer which is similar to the solid state structure (Figure 2-9).

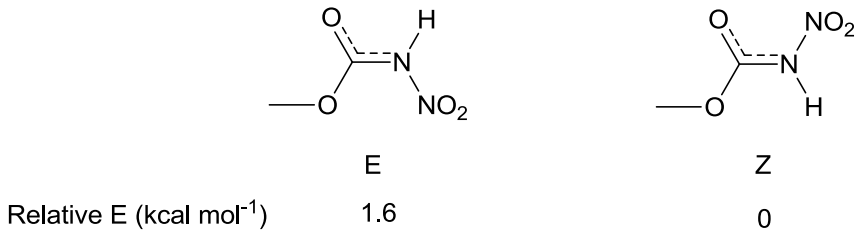

Figure 2-9. Calculated relative energy levels of isomers of **2-4**.

For the N-nitrosocarbamates, the presence of the NNO fragment adds an additional combination to the E/Z isomeric forms which is mentioned in the NMR section. Thus there are 2^2 combinations which give rise to four possible configurations of the N-nitrosocarbamates as shown in Figure 2-10. Following the convention at the start of this section, the isomers are described in the C-N, N-N configuration order.

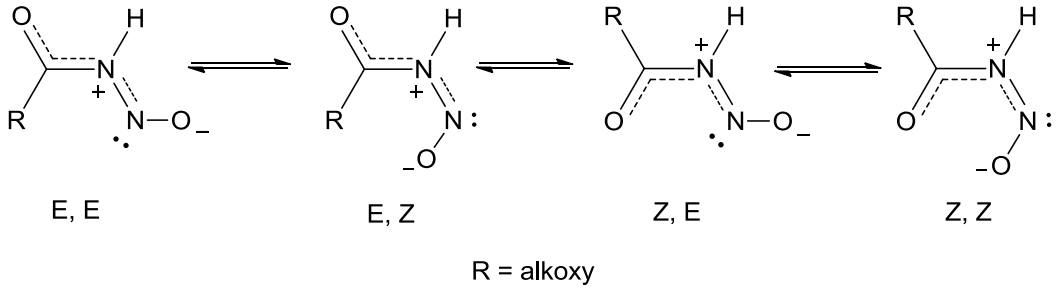

Figure 2-10. Possible isomers of N-nitrosocarbamates.

The solid state structures of the N-nitrosocarbamates, **2-6** and **2-7** are shown in Figure 2-11 and Figure 2-12 respectively.

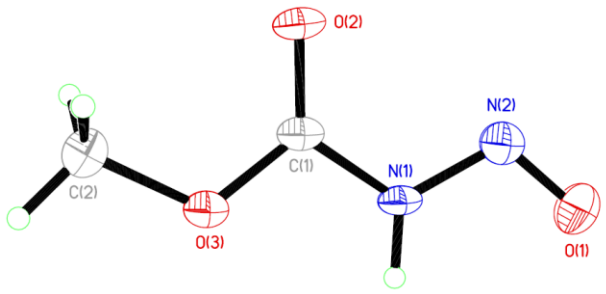

Figure 2-11. Molecular structure of **2-6**.

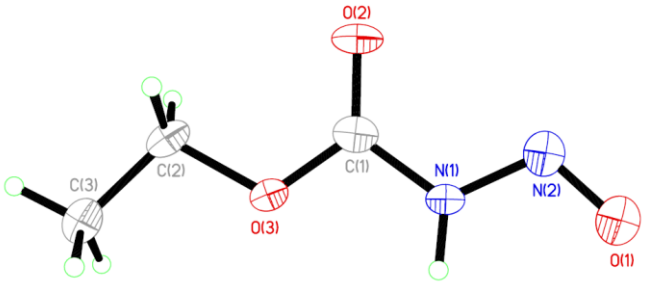

Figure 2-12. Molecular structure of **2-7**.

Compound **2-6** and **2-7** are both in (Z, E) configuration. DFT calculations of the four isomers arranged in increasing order of energy are shown in (Figure 2-13). The gas phase calculations indicate that the (E, Z) isomer is the most thermodynamically stable isomer while the E,E isomer is the least. The solids state structure equivalent, (Z, E) isomer is found to be 3.7 kcal mol^{-1} higher in energy in comparison to the most stable isomer.

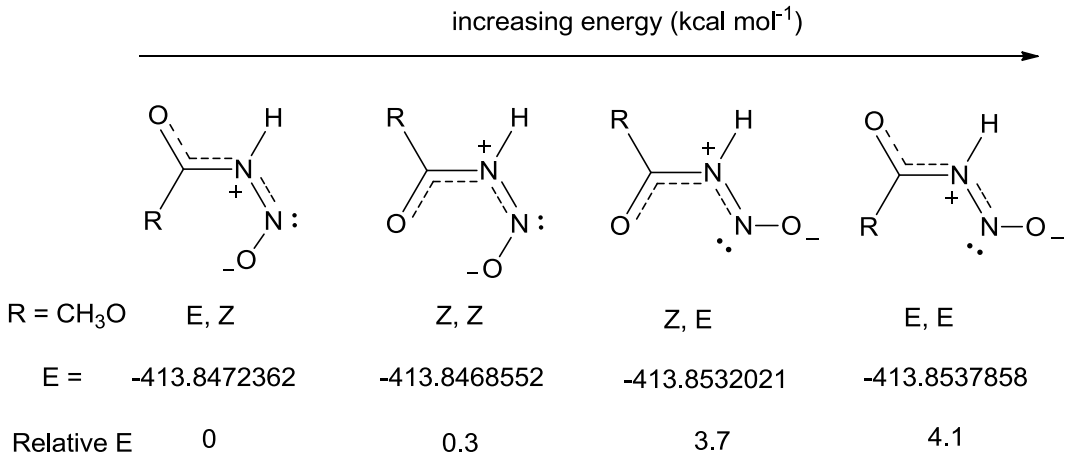

Figure 2-13. Isomers of **2-4** and their calculated relative energy levels.

The solid state structure of N-nitrosulfonamide **2-8** is shown in Figure 2-14. For compound **2-8** there are no configuration isomers due to the presence of the sulfonyl, SO_2, group.

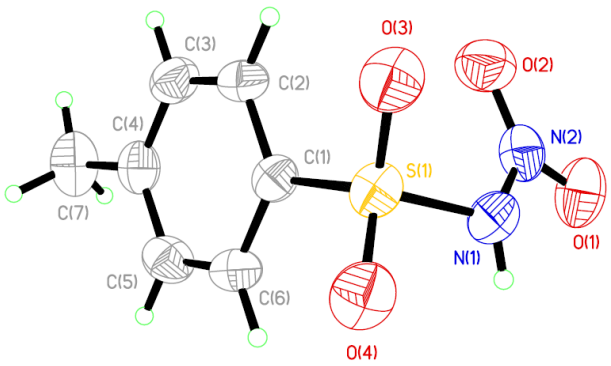

Figure 2-14. Molecular structure of **2-8**.

A list of selected bond lengths and bond angles of the free ligands of the nitrogen acids are presented in Table 2-3. In general all the molecules are co-planar with most of the dihedral angles around the amide/carbamate group at or close to 180°. The co-planar nature of the structures gives evidence of the overall conjugation across the acyl N-NO/NO_2 fragment. Such an observation is matched by the C-N bond lengths range of 1.38 to 1.40 Å and the N-N bond lengths range of 1.34 to 1.39 Å which indicates double bond character. An interesting observation in these series of compounds is that the N-nitrocarbamates **2-4** and **2-5** have slightly distorted co-planarity due to deviations from 0 or 180° in the dihedral angles of the C-C-N-O and C-N-N-O planes. This could be the result of competing conjugation requirements of the carbamate functional group. Increasing the alkyl chain of the alkoxy group reduces the planarity too. However this trend is not repeated for the N-nitrosocarbamates.

The only exception is **2-8** which is non-planar at O(1) – N(2) – N(1) – S(1) and O(3) – S(1) – N(1) – N(2) for the dihedral angles of -162.1(2)° and -63.9(2)° respectively due to the tetrahedral geometry of the sulfonyl group. The S-N bond of 1.6877(15) Å still indicates some degree of double bond character which implies limited conjugation across the $SNNO_2$ fragment.

Table 2-3: Selected bond lengths (Å) bond and torsion angles (deg) of N-nitroamides, N-nitrocarbamates, N-nitrosocarbamates and N-nitro-*p*-tolylsulfonamides.

Compound	**2-2**	**2-3**	**2-4**[a]	**2-5**	**2-6**[b]	**2-7**[b]	**2-8**[c]
N(1) – N(2)	1.3835(19)	1.3858(18)	1.382(3)/1.380(3)	1.385(2)	1.354(3)	1.347(4)	1.388(2)
N(1) – C(1)	1.389(2)	1.3949(19)	1.394(3)/1.396(3)	1.387(2)	1.385(3)	1.381(5)	1.6877(15)
O(1) – N(2)	1.2230(17)	1.2183(16)	1.222(3)/1.226(3)	1.216(2)	1.217(3)	1.220(4)	1.213(2)
O(2) – N(2)	1.2144(17)	1.2141(16)	1.212(3)/1.214(3)	1.2154(19)			1.213(2)
N(2) – N(1) – C(1)	125.47(13)	125.27(12)	124.5(2)/124.6(2)	123.87(14)	118.64(17)	118.7(3)	121.60(13)
O(2) – N(2) – O(1)	126.24(13)	126.42(12)	126.3(2)/126.8(2)	126.41(16)			127.18(18)
O(2) – N(2) – N(1)	119.62(13)	119.18(11)	119.7(2)/119.3(2)	118.41(15)			117.67(16)
O(1) – N(2) – N(1)	114.14(12)	114.40(11)	114.0(2)/113.9(2)	115.17(14)	112.76(19)	112.3(3)	115.14(17)
O(1) – N(2) – N(1) – C(1)	180.0(1)	180.0(1)	-178.2(2)/-178.8(2)	168.1(2)	180.0(2)	-180.0(3)	-162.1(2)
O(3) – C(1) – N(1) – N(2)	0.0(2)	0.0(2)	-1.3(4)/0.5(4)	-1.8(3)	0.0(3)	-0.0(6)	-63.9(2)

a. 2 independent molecules. O(5), O(6), O(7), O(8), N(3), N(4), C(3), C(4) in corresponding order for second molecule.

b. O(2) instead of O(3) for torsion angles.

c. S(1) instead of C(1).

The C-N and N-N bond lengths of the N-nitroamides and N-nitrocarbamates are very similar at around 1.40 and 1.38 Å respectively. However the C-N (1.39 Å) and N-N (1.35 Å) bond lengths in the N-nitrosocarbamates **2-6** and **2-7** are significantly shorter. The extent of this difference is greater in the N-N bond. This structural observation may be related to the N-nitrosocarbamates' propensity to decompose to release N_2. The N-O bond lengths in these series are almost uniform at approximately 1.22 Å which signifies N=O. For compound **2-8**, the N-N and N-O bond lengths are similar to the N-nitroamides and N-nitrocarbamates.

Comparison of the bond angles in the series of compounds (Table 2-3) shows that the N-nitro compounds are very similar, with the N-nitrosocarbamates exhibiting smaller angles between the C-N-N and N-N-O fragments. An interesting observation in the nitro compounds is that the N-N-O angles for the nitro group are asymmetric. The O(1) atom which is trans to the acyl group tends to have smaller N-N-O angles compared to O(2) atom cis to the acyl group.

There are extensive hydrogen bonds between the amide protons and the acyl oxygen atoms in the crystal array of the compounds. This interaction may have an effect such that the slightly less stable Z isomers (C-N bond) of the nitro/nitroso compounds are observed instead of the more stable trans isomers.

2.6.2.2 Anionic ligands

The anionic ligands of the above series of compounds are mostly isolated as the potassium salts. The solid state molecular structure of N-nitroamide **2-2K**, N-nitrocarbamate **2-4K** and N-nitrosocarbamate **2-6K** are shown in Figure 2-15, Figure 2-16 and Figure 2-17 respectively.

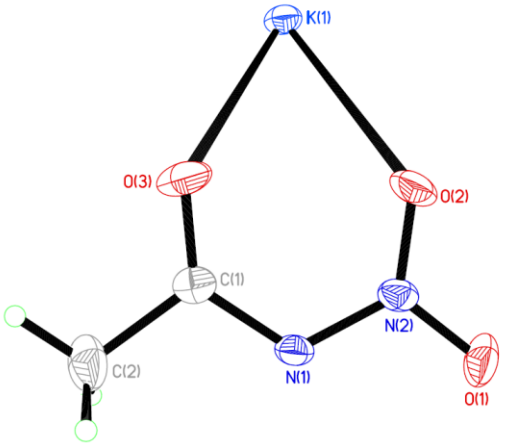

Figure 2-15. Molecular structure of **2-2K**. Other K atoms have been omitted.

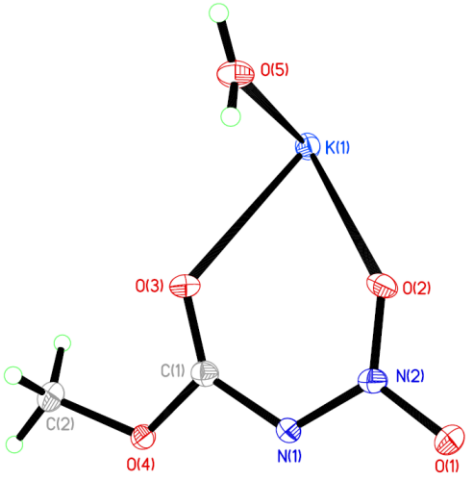

Figure 2-16. Molecular structure of **2-4K**. Other K atoms have been omitted.

For **2-6K**, the crystals crystallize in the $P2_1$ space group which is chiral. Compound **2-6K** is achiral such that it crystallizes as a racemeric twinned crystal. The selected bond length and bond angles of the anionic ligands are shown in Table 2-4.

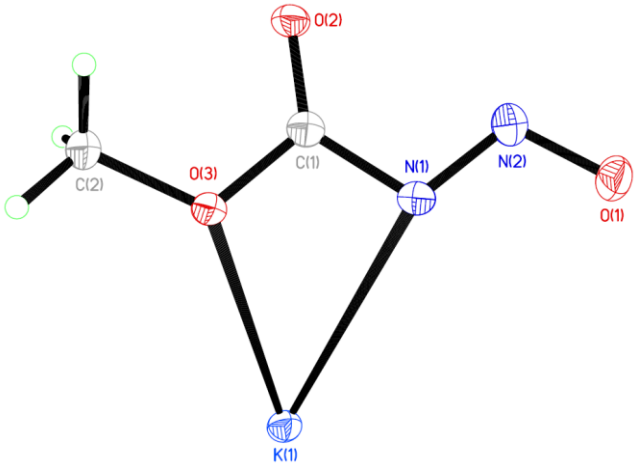

Figure 2-17. Molecular structure of **2-6K**. Other K atoms have been omitted.

In all the structures, there is no change in the configuration between the free acid form and the potassium salt. DFT calculation of the possible isomers of **2-6Li** indicate that the Z,Z isomer is the most stable form while the solid state structure (Z,E) that is observed is slightly higher in energy (Figure 2-18).

Computational analysis of the related diazotate anion had been carried out at the MP level.[111] The results of the stability of the different isomers are very different from the results by DFT. This may be due to the lower level calculations or the acid substituent instead of the ester.

Most of the structural features of the potassium salts are similar to the neutral compounds. However certain parameters are significantly different. The more significant differences are the decrease in N-N and increase in N-O bond lengths between the neutral ligands and the anionic salts. On average the N-N bond lengths are reduced by about 0.3 Å [**2-2** and **2-4** (1.38 Å) to **2-2K** and **2-4K** (1.35 Å), **2-6** (1.35 Å) to **2-6K** (1.32 Å)] while the N-O bond lengths have increased by approximately 0.23 Å [**2-2** and **2-4** (1.22 Å) to **2-2K** and **2-4K** (1.45 Å)]. For **2-6K**, the increase in the N-O bond length is almost 0.4 Å!

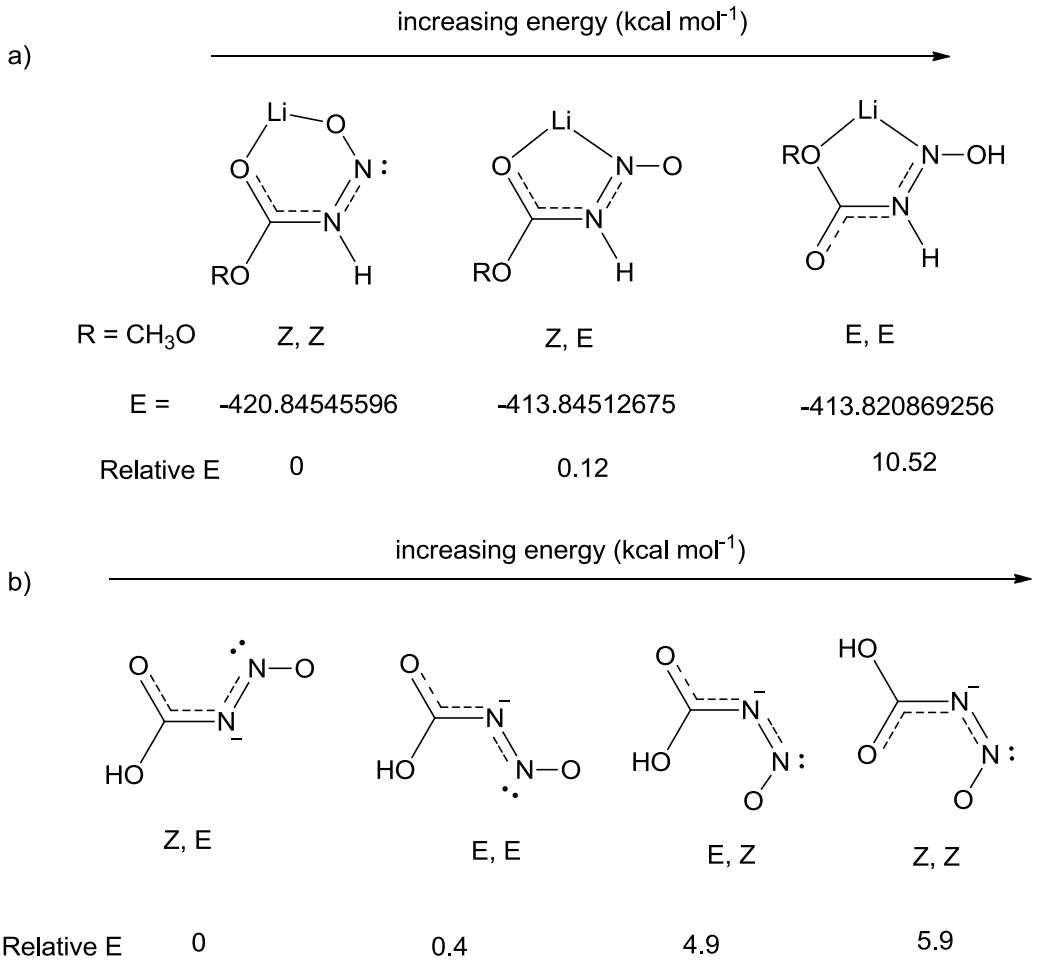

Figure 2-18. a) DFT calculations of isomers of **2-4Li**. B) MP calculations of isomers of diazotate anion.

Table 2-4: Selected bond length (Å), bond and torsion angles (deg) of potassium and ammonium salts of N-nitroamides, N-nitrocarbamates, N-nitrosocarbamates and N-nitro-*p*-tolylsulfonamide.

Compound	**2-2K**	**2-4K**	**2-6K**[a]	**2-8K**[b]	**2-8NH$_4$**[b]
N(1) – N(2)	1.352(4)	1.343(3)	1.321(3)	1.339(2)	1.331(3)
N(1) – C(1)	1.376(4)	1.384(3)	1.399(3)	1.6487(18)	1.641(2)
O(1) – N(2)	1.243(4)	1.257(3)	1.260(2)	1.250(2)	1.249(3)
O(2) – N(2)	1.243(4)	1.242(3)		1.256(2)	1.233(3)
N(2) – N(1) – C(1)	118.8(3)	117.9(2)	108.98(18)	115.55(13)	115.41(18)
O(2) – N(2) – O(1)	120.2(3)	120.5(2)		120.89(16)	120.6(2)
O(2) – N(2) – N(1)	125.4(3)	124.7(2)		123.13(16)	123.8(2)
O(1) – N(2) – N(1)	114.5(3)	114.8(2)	113.05(17)	115.97(15)	115.6(2)
O(1) – N(2) – N(1) – C(1)	178.7(3)	172.4(2)	177.6(2)	177.8(1)	178.8(2)
O(3) – C(1) – N(1) – N(2)	-3.8(6)	-8.8(5)	-2.2(3)	52.7(2)	53.2(2)

a. O(2) instead of O(3) for torsion angles

b. S(1) instead of C(1).

The structural changes from conversion of the neutral ligand to the anionic form indicate the possible strengthening of the N-N bond and weakening of the N-O bond of the NNO/NNO_2 fragment. There is some indication that the increasing charge separation of the NNO/NNO_2 fragment may be the result of increasing electron density on the oxygen atoms making them more nucleophilic which results in increase oxidative properties. The much larger change in **2-6K** gives some evidence of its stronger oxidation ability by the loss of the O atom of the nitroso fragment. The C-N bond change from the neutral ligand to the anionic form is less clear. With regards to the N-nitro compounds **2-2K** and **2-4K**, there is a decrease of 0.15 Å, while for N-nitroso compound **2-6K**, there is an increase in about 0.2 Å. The implication for such differences between these two groups may be that the acyl group is better able to stabilise the anionic NNO_2 fragment but actually destabilise the NNO fragment.

The other difference in converting the neutral ligand to the anionic salt is the slight increase in non-co-planarity of the C-C-N-N and C-N-N-O plane. This structural change can be thought of as a decrease in the conjugation between the NNO/NNO_2 fragments with the acyl group.

For the N-nitrosulfonamides salts **2-8K** and **2-8NH$_4$**, their molecular structures are shown in Figure 2-19 and Figure 2-20 respectively. The 2 K atoms are located on special positions which results in each having site occupancy of 0.5.

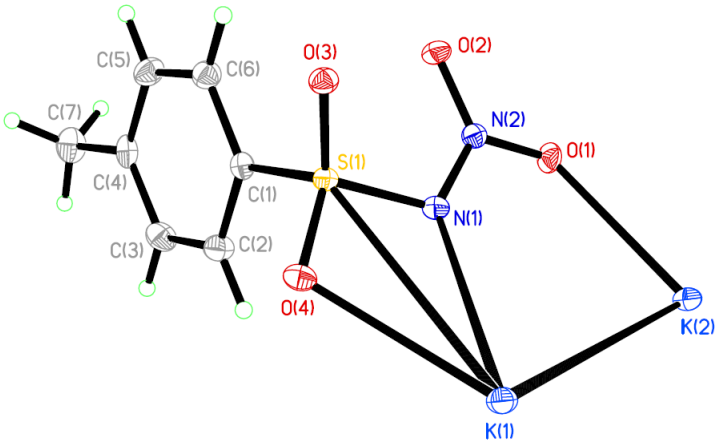

Figure 2-19. Molecular structure of **2-8K**. Other K atoms have been omitted.

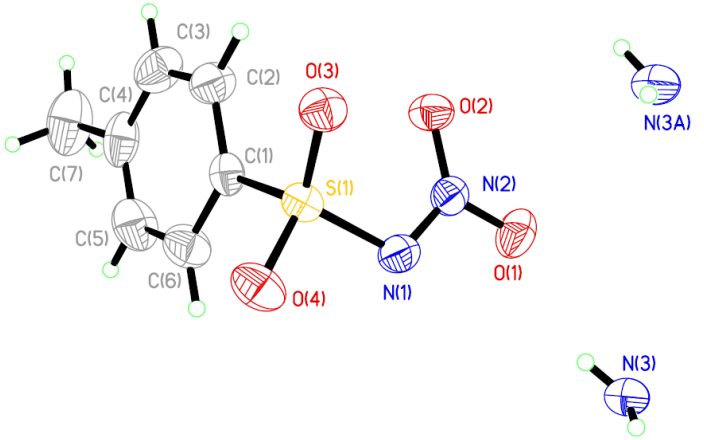

Figure 2-20. Molecular structure of **2-8NH$_4$** with disordered ammonium cations.

The structural changes of **2-8K** and **2-8NH$_4$** from **2-8** are similar to the other N-nitro compounds where there is a shortening of the N-S bond and increase in the N-O bond to mostly the same extent The structure of **2-8NH$_4$** is also shown to have a disordered ammonium cation.

The differences in the structural forms of the neutral and anionic salts do give us an insight into the possible changes on coordination of these ligands to transition metal complexes.

2.6.3 Spectroscopic properties of ligands

There is very limited spectroscopic information for the primary N-nitroamides, N-nitrocarbamates, N-nitrosocarbamates and N-nitrosulfonamide except for **2-5**[110] Most of the characterisations for these compounds were for the secondary compounds.[132] Furthermore the spectroscopic information is generally limited to boiling/melting points, elemental analysis, and electronic absorption information. There are some rare instances of limited infra-red characterisation of the N-nitroamides[119] and proton NMR of the analog of the salt of **2-7**.[111] There are however vast reports of the related nitrosamines, R_2NNO, and nitramines, R_2NNO_2, for which the NO and NO_2 spectroscopic information is similar.

2.6.3.1 NMR spectroscopy

Free ligand

The N*H* protons of the N-nitroamides, N-nitrocarbamates, N-nitrosocarbamates and N-nitrosulfonamides are acidic and are observed in ^{1}H NMR in the following range: N-nitroamides (**2-2** and **2-3**) 10.3 to 10.5 ppm; N-nitrocarbamates (**2-4** and **2-5**[110]) 9.9 to 10.1 ppm; N-nitrosocarbamates (**2-6** and **2-7**) 10.6 to 10.8 ppm; N-nitrosulfonamide **2-8** at 10.0 ppm. Compared to **2-1** (8.05 ppm), the amide protons are more de-shielded due to the presence of the acyl/sulfonyl functional groups. For simple nitramines,[133] the chemical shift effect on the α-H of the –$N(NO_2)$ group is similar to that of alkoxy substituents.[134] Therefore by taking into account the general chemical shifts of the related amides, carbamates and sulfonamides, the observed chemical shift of the N*H* proton of the N-nitro compounds are expected.

The alkyl substituents of the N-nitroamides, N-nitrocarbamates, N-nitrosocarbamates and N-nitrosulfonamides are all observed slightly downfield (approximately 0.2 to 0.4 ppm difference) from the generic region of the regular amides, esters or sulfonamide probably due to the inductive effect of the nitro or nitroso groups.

The ^{1}H NMR spectra of the N-nitrosocarbamates **2-6** and **2-7** are observed to have multiple sets of resonances in the alkyl region: **2-6**: 3.68, 3.91, 4.06 (ratio of 0.03:0.05:1 respectively); **2-7**: 1.35 and 4.35 (minor), 1.44 and 4.50 (major). This indicates the possible presence of several isomers in solution.[126c] In contrast the N-nitroamides, N-nitrocarbamates and N-nitrosulfonamide are observed to have only one isomer in solution. The N-nitrosocarbamates can be expressed as two resonance forms (Figure 2-21).

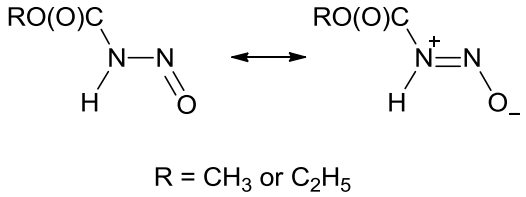

Figure 2-21. Two resonance forms of N-nitrosocarbamates.

The two resonance forms of N-nitrosocarbamates give rise to cis-trans isomers of the nitroso compound across the hindered N-N bond (Scheme 2-30).

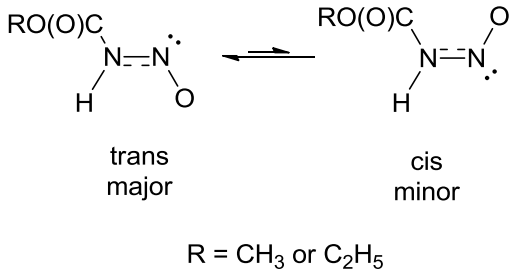

Scheme 2-30. N-nitroso compounds cis-trans isomers.

The barrier to rotation for the N-N bond is between 76 to 160 kJ mol^{-1} depending on the environment.[134] It has been established that in general, substituents trans to the oxygen of the nitroso are observed further downfield compared to cis substituents.[135] Furthermore, due to steric effects, the trans configuration is favoured, which is consistent with the observed spectra of **2-6** and **2-7**.

Compound **2-6** is observed to have three singlets in total. The additional minor singlet could be due to the presence of small amount of isomers from the hindered C-N rotation (Scheme 2-31).

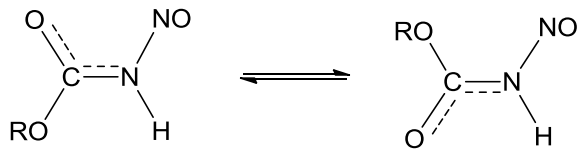

Scheme 2-31. Isomers of N-nitrosocarbamate from hindered C-N rotation.

Anionic salts

The ^{1}H NMR spectra of the potassium salts of N-nitroamides, N-nitrocarbamates, N-nitrosocarbamates and N-nitrosulfonamide are similar to the free ligand except for the resonance for the N*H* proton. In general, there is an upfield shift in the resonance signals of the alkyl substituents of approximately 0.5 to 0.8 ppm such that the signals falls within the generic region for amides, esters and sulfonamide. For N-nitrosocarbamate **2-6K**, the additional resonance signals corresponding to the isomers mentioned above are also observed.

2.6.3.2 Vibrational Spectroscopy

Free ligand

The N-nitroamides/carbamates/sulfonamides and N-nitrosocarbamates exhibit interesting infra-red bands in their IR spectrums. In particular, the presence of the acyl/sulfonyl and nitro/nitroso conjugated system gives rise to unqiue bands that do not reside in the usual ranges for the respective functional groups. Some suitable references that would help in the assignment of the vibrational bands include the regular amides[136] (N-C(O): 1695 cm^{-1}), carbamates[137] (N-C(O): 1690 - 1740 cm^{-1} and N-C(O)-O: 1050 cm^{-1}) and sulfonamides[136] (N-SO_2: 1155 – 1170 cm^{-1} symmetric), (SO_2-N: 1335 – 1370 cm^{-1} asymmetric). Other related functional groups would include the nitramines[134] which show two nitro bands at 1550 - 1630 cm^{-1} (asymmetric), 1274 - 1304 cm^{-1} (symmetric) and the nitrosamines[134, 138] which have nitroso related bands at 1421 – 1476 cm^{-1} (N=O), 1020 cm^{-1} (N-N).

For the N-nitroamides, the Amide 1 band is located around 1730 cm^{-1}, Amide 2 around 1443 – 1469 cm^{-1} and Amide 3 around 1140 – 1196 cm^{-1}. All the bands are relatively strong while the nitro bands are observed around 1610 - 1625 (asym) and 1305 – 1330 cm^{-1} (sym). A new strong band is observed around 1000 – 1100 cm^{-1} corresponding to the N-N bond stretch.

For the N-nitrocarbamates, the Amide 1 band is located around 1745 cm^{-1}, Amide 2 around 1450 – 1460 cm^{-1} and Amide 3 around 1220 – 1250 cm^{-1}. Similarly all the bands are relatively strong with the nitro bands in the same region as the N-nitroamides. Several new bands are also observed around the 900 to 1150 cm^{-1}. These bands are assigned to the carbamate stretch.[137] The lowest energy strong intensity band in this region, between 900 to 1000 cm^{-1}, is however better assigned to the N-N vibration mode. The IR bands of **2-5** match well with the literature assignment.[110]

For the N-nitrosocarbamate, the Amide 1 band is located around 1750 - 1760 cm^{-1}, Amide 3 around 1240 – 1260 cm^{-1}. The Amide 2 band overlaps with the NO bands and are located between 1400 and 1480 cm^{-1}. Multiple bands of medium

intensity are located in this region and could be due to the presence of the aci-form. Lastly between 900 and 1100 cm^{-1} are the carbamate and N-N stretch with the N-N band at the lowest energy between 900 and 1000 cm^{-1}. The bands at 1707s, 1619s, 1529s, 1615m, 1520m, 1393m, 1376m, 1329s, 1233m, 1205m could be due to the aci form isomer.

The N-nitrosulfonamide **2-8** is observed to have the sulfonyl vibration modes at 1392 cm^{-1} (asym) and 1170 cm^{-1} (sym). The nitro bands are in the same region as the N-nitroamides/carbamates. An additional strong band at 1085 cm^{-1} is also observed and corresponds to the N-N stretching mode.

In general, the bands assigned to the various acyl/sulfonyl bands are shifted to higher energy while those of the nitro and nitroso groups are very similar to the related to the nitramines and nitrosoamines.

Anionic salts

The anionic salts of the above ligands exhibit very simple vibrational spectra. Both the silver and potassium salts have similar or near identical vibration bands. In general there are several common strong bands. The first is the Amide band 1 observed around 1641 cm^{-1} for **2-2K/Ag** and 1680 cm^{-1} for the nitro/nitrosocarbamates salts. For the N-nitroamides/carbamates/sulfonamides, the common strong bands are between 1400 and 1460 cm^{-1} and between 1220 and 1290 cm^{-1} which most likely corresponds to the asymmetric and symmetric stretch of the nitro group. Strong bands near the 900 to 1105 cm^{-1} region are due to the N-N stretch for the N-nitro/nitroso amides/carbamates. Additional bands between 1110 and 1200 bands are also observed in the carbamate salts. Multiple bands of medium intensity are observed between 1300 and 1500 cm^{-1} which are most likely due to the nitroso stretch. The IR spectrum of **2-5Ag** is similar to that reported in literature.[110]

2.6.3.3 UV-visible spectroscopy

Free ligand

Most of the compounds are colourless which indicate the usual π → π* transition fall in the UV range with λ_{max} less than 400 nm. The N-nitrosocarbamates **2-6** and **2-7** however are yellow in both solution and solid states. The observed colour has been attributed to n → π* transition of the nitrogen lone pair on the nitroso functional group.[139] The UV-vis spectrum of **2-6** in the visible region is shown in Table 2-5 and Figure 2-22 and there is a distinct absorbance near 400 nm which gives rise to the intense yellow colour. Of interest is the fine vibronic coupling that is observed which is better defined in less polar solvents such as chloroform than polar solvents such as methanol for nitrosamines.[139a] Initially this fine structure was attributed to N-H vibronic effects in solution, but a control experiment with deuterated methanol did not give any difference in the absorbance spectrum (Table B-1, Figure B-1). The wavelength of maximum absorbance is also observed to be red-shifted in non-polar to polar solvents which is similar to the related nitrosoamines where the n → π* transition is sensitive to solvent effects.[140] The red-shift is in striking contrast to initial reports for n → π* transitions, where blue-shift in the wavelength of maximum absorbance occurs for solvents with increasing di-electric constants.[141] This effect was initially attributed to the fact that polar solvents are more able to stabilise ground states than excited states increasing in the energy gap for the transition. It has been shown instead that hydrogen bonding is the main cause in such phenomena.[142] On a related note, increasing the polarity of a solvent causes a red-shift in the wavelength for maximum absorbance for π → π* transitions which is also attributed to hydrogen bonding effects.[143] In the studies for the red-shift effect, the solute molecules were the hydrogen donors, while for the blue-shift effect, the solvent was the hydrogen donor. For compound **2-6**, as a strong acid, it can be considered to be a solute with hydrogen donors which will account for the red-shift effect. Therefore we believe that for red-shift versus blue-shift trends, the hydrogen donor potential of the solute plays a major role.[134] A similar vibronic

fine structure absorption feature is also present for **2-7** (Table B-2, Figure B-2). It has also been shown that this n → π* transition can be manipulated to alter the ratio of the cis-trans isomers of the nitrosamines.[144]

Table 2-5. λ_{max}, abs and Δν values of 3.2 mM **2-6** in CH_3OH and $CHCl_3$.

2-6 in CH_3OH			**2-6** in $CHCl_3$		
λ_{max} (nm)	ε (M^{-1} cm^{-1})	Δν (cm^{-1})	λ_{max} (nm)	ε (M^{-1} cm^{-1})	Δν (cm^{-1})
366	12.6	1348	368	21.3	1064
385	34.1	1036	383	43.0	857
401	61.6	956	396	75.0	981
417	88.5	1045	412	105.0	1016
436	76.7		430	88.7	

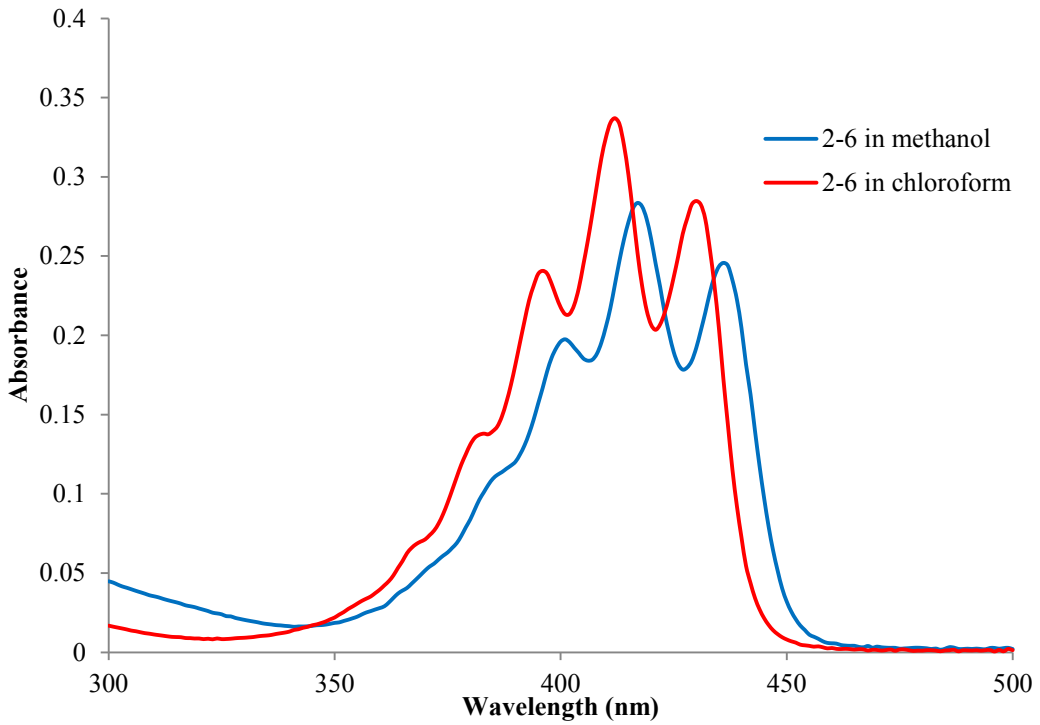

Figure 2-22. UV-vis absorption spectrum of 3.2 mM **2-6** in $CHCl_3$ (red) and CH_3OH (blue).

Anionic salts

The potassium salt **2-6K** is observed to have a less intense colouration and this is confirmed by the UV-vis spectrum which is shown to have an absorbance around 400 nm with lower absorption coefficients (Figure 2-23). The vibronic coupling absorption feature in **2-6** is also broadened out in **2-6K**.

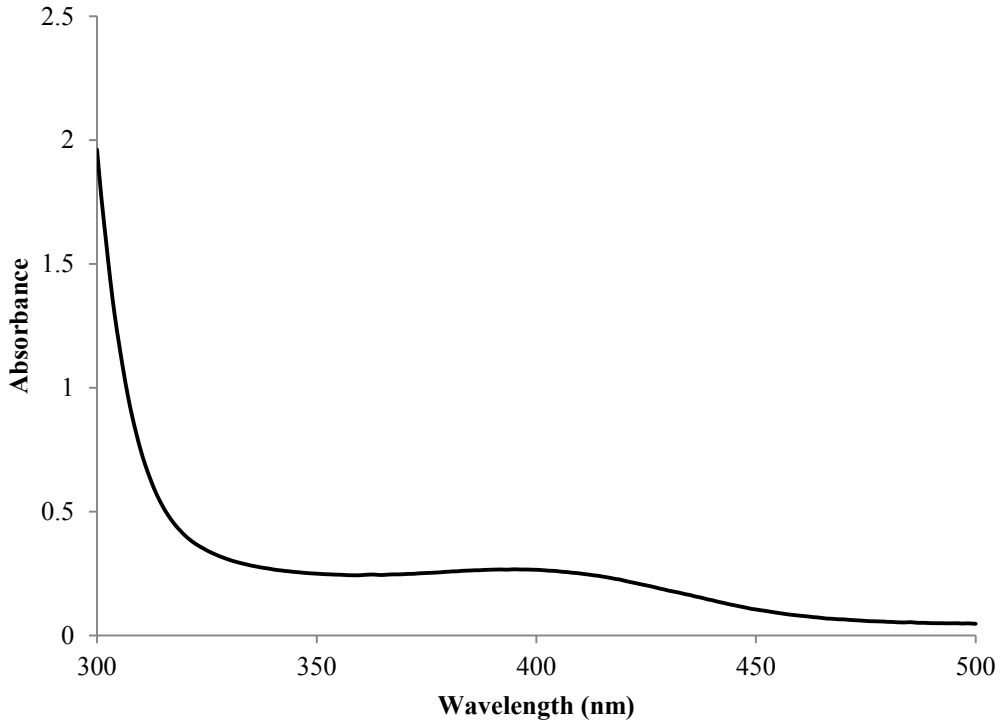

Figure 2-23. UV-vis absorption spectrum of 7.0 mM **2-6K** in CH_3OH. λ_{max} = 395 nm and ε = 37.9 L mol $^{-1}$ cm^{-1}.

2.7 Conclusion

The successful synthesis of **2-1** and the related N-nitroamides, N-nitrocarbamates, N-nitrosocarbamates and N-nitrosulfonamide gives us a series of the high oxidation nitrogen amides for reactivity studies. The acidic nature of these compounds provides access to the corresponding anionic salts such as potassium and silver which allow us to explore alternative reaction pathways.

Complete structural and spectroscopic determination of these compounds allows insight to subsequent coordination reactivity studies with the transition metal complexes.

Chapter 3: Iridium complexes of Nitrogen Acids

3.0 Introduction

Transition metals are able to support various oxidation states depending on the environment and the ligand coordination sphere. The ability to access multiple oxidation states allows the transition metals to undergo redox changes with the ligands or reagents during chemical transformation to effect catalysis of the chemical reactions. The application of this catalytic property has been the main basis of transition metal organometallic catalysis renaissance towards the end of the twenty-first century. The catalytic cycle can be broken into separate stages: mainly activation/coordination: addition/rearrangement (possibility of several repetitions) and release of the final substrates. Not all reactions of transition metal complexes are catalytic by default. The most common reactions by these complexes are usually coordination with the compounds of interest to generate new metal complexes which may be stable or metastable. The advantage of these new complexes is that they give rise to unstable ligand fragments that cannot exist in the uncoordinated form but are stabilised by the transition metal through coordination.

Third row transition metal complexes tend to be kinetically inert which allow the isolation of metastable forms of coordination complexes. The early transition metal complexes are electron-poor, oxophilic in nature and tend to extract hard ligands such as oxides and nitrides from coordinated ligands. Therefore the nitrogen acids of interest may not be suitable substrates for these metals. Late transition metals on the other hand are electron-rich, prefer softer ligands such as phosphines and thiolates and can undergo facile oxidative addition and reductive elimination.

The nitrogen acids contain electron-withdrawing nitro and nitroso groups which may have a great effect on the properties of the transition metal complexes upon coordination. To investigate the direct inductive effect of the nitrogen acids, the

trans-$Ir^{(I)}(Cl)(CO)(PPh_3)_2$ complex (**3-1**) or Vaska's complex is best suited for the task.[145] The chloride on **3-1** is labile and undergoes metathesis with silver salts to give silver chloride readily.[146] The acidic proton on the nitrogen acids allows us access to the silver salts of the nitrogen acids and by reaction with **3-1** will coordinate to the Ir center and replace the chloride. The nitrogen acid ligands if positioned trans to the carbonyl will affect the carbonyl stretch which in turn provides some information on the electronic nature of the nitrogen acid conjugate base. The coordinative unsaturated **3-1** is also prone to oxidative addition by various reagents such as O_2, CH_3I, H_2, Cl_2 and acids.[147]

The more reactive Ir(I) dinitrogen complex (**3-2**) is also coordinatively unsaturated but more electron deficient.[148] It is also able to undergo oxidative addition with the added advantage of a labile N_2 ligand which is readily displaced. The main disadvantage of **3-2** is that it decomposes rapidly on exposure to air and is metastable on extended periods in solution.[149]

The above Ir(I) complexes on successful reaction with the nitrogen acids will provide an insight into the chemical reactivity of this class of largely unknown compounds.

3.1 General Experimental

General: Except as noted, reagents and solvents are used as supplied commercially. Dry CH_3OH is distilled from freshly generated magnesium methoxide, dry $CHCl_3$ is distilled from $CaCl_2$, dry CH_2Cl_2 and CH_3CN are distilled from CaH_2, dry hexanes, pentanes, toluene and benzene are distilled from sodium benzophenone ketyl. ^1H and ^{31}P spectra are recorded on Varian Mercury 200, 400 or 500 MHz spectrometers. All chemical shifts are recorded in δ (ppm) relative to residual solvent signals for ^1H spectra and H_3PO_4 for ^{31}P spectra. Melting/decomposition points are measured by using a TA-Q2000 differential scanning calorimeter. The IR spectra are recorded in KBr disks by using ABB Bomem MB Series spectrometer with spectral resolution of 4 cm^{-1}. Elemental analyses are performed in the Elemental Analyses Laboratory at University of Montreal.

X-ray crystallography: Crystals are mounted on glass fibre with epoxy resin or Mitegen mounts using Paratone-N from Hampton Research and single-crystal X-ray diffraction experiments are carried out with a BRUKER SMART CCD or BRUKER APEX-II CCD diffractometer by using graphite-monochromated $Mo_{K\alpha}$ radiation (λ = 0.71073 Å) and KRYOFLEX for low temperature experiments. SAINT[105] is used for integration of the intensity reflections and scaling and SADABS[106] for absorption correction. Direct methods are used for structures that show pseudo-merohedral twinning, corrected using PLATON,[150] while Patterson maps are used for the rest of the structures to generate the initial solution. Non-hydrogen atoms are located by difference Fourier maps and final solution refinements are solved by full-matrix least-squares method on F^2 of all data, by using SHELXTL[105] software. The hydrogen atoms are placed in calculated positions.

Crystals of the Ir(I) carbonyl nitrogen acids and related amides are grown from CH_2Cl_2/CH_3OH layered solution at -21 ^oC except for $Ir^{(I)}(\eta^1$-$CH_3OC(O)NNO)(CO)(PPh_3)_2$ (**3-6**) which is grown from slow diffusion of pentanes into THF/CH_2Cl_2 solution at 5 ^oC. The crystals of

$Ir^{(I)}(N(NO_2)_2)(CO)(PPh_3)_2$ (**3-8**) and $Ir^{(I)}(Cl)(CO)(PPh_3)_2[Ag(N(SO_2CF_3)_2)]$ (**3-9**) co-crystallized with **3-1** and are manually separated. Crystallographic data and data collection parameters for the Ir(I) carbonyl nitrogen acids and related amides are shown in Table 3-1.

Crystals of the Ir(III) N-nitroamides and N-nitrocarbamates are grown from CH_2Cl_2/CH_3OH layered solutions at -21 ^oC. Crystallographic data and data collection parameters for the Ir(III) complexes are shown in Table 3-2.

Table 3-1: Crystallographic data for $Ir^{(I)}(\eta^1\text{-}X)(CO)(PPh_3)_2$ complexes and $Ir^{(I)}(Cl)(CO)(PPh_3)_2.Ag[N(SO_2CF_3)_2]$.

Compound	**3-3**	**3-4**	**3-5**	**3-6**	**3-7**	**3-8**	**3-9**
empirical formula	$C_{39}H_{33}IrP_2N_2O_4$ $.CH_2Cl_2$	$C_{39}H_{33}IrP_2N_2O_5$	$C_{40}H_{35}IrP_2N_2O_5$	$C_{39}H_{33}IrP_2N_2O_5$ $.OC_4H_8$	$C_{44}H_{38}IrP_2N_2O_5$ S	$C_{37}H_{30}IrP_2N_3O_5$	$C_{39}H_{30}IrP_2ClO.$ $AgNO_4F_6S_2$
T (K)	298(2)	298(2)	296(2)	100(2)	296(2)	100(2)	100(2)
fw (g mol^{-1})	932.76	863.81	877.84	919.92	960.96	850.78	1168.22
cryst sys	triclinic	monoclinic	monoclinic	triclinic	monoclinic	monoclinic	orthorhombic
space group	P-1	$P2_1/c$	$P2_1/c$	P-1	$P2_1/c$	$P2_1/c$	$P2_12_12_1$
a (Å)	9.892(7)	17.3160(11)	11.9228(8)	9.5341(12)	11.5792(17)	16.023(2)	11.9375(6)
b (Å)	11.307(8)	11.8362(7)	29.487(2)	11.6693(15)	17.291(3)	11.7437(16)	17.6813(8)
c (Å)	18.922(14)	19.8140(9)	10.5336(7)	18.640(2)	20.476(3)	19.480(2)	19.8625(9)
α (deg)	79.814(9)	90	90	76.9840(10)	90	90	90
β (deg)	87.192(9)	120.358(4)	94.6940(10)	87.842(2)	105.536(2)	116.840(9)	90
γ (deg)	66.851(9)	90	90	72.248(2)	90	90	90
V ($Å^3$)	1915(2)	3504.2(3)	3690.9(4)	1923.3(4)	3949.8(10)	3270.7(7)	4192.4(3)
Z	2	4	4	2	4	4	4
density (g cm^{-3})	1.618	1.637	1.580	1.589	1.616	1.728	1.851
abs coeff (mm^{-1})	3.752	3.949	3.750	3.602	3.563	4.230	3.948
No. of reflns collected	16440	38011	37704	16098	35556	32562	47725
No. of indep reflns	8366	7483	7054	5628	6509	6539	9838

Data/restraints/parameters	8366/0/460	7483/0/443	7054/0/451	5628/49/453	6509/0/496	6539/0/433	9838/0/523
Final R indices [$I > 2s(I)$] R1	0.0287	0.0380	0.0258	0.0500	0.0327	0.0351	0.0240
*w*R2	0.0700	0.0659	0.0496	0.1039	0.0606	0.0721	0.0499
R indices (all data) R1	0.0332	0.0614	0.0426	0.0751	0.0560	0.0546	0.0276
*w*R2	0.0714	0.0727	0.0546	0.1143	0.0668	0.0794	0.0508
Goodness-of-fit on F^2	1.031	1.055	1.016	1.046	1.006	1.057	1.006

Table 3-2: Crystallographic data of $Ir^{(III)}(\eta^2\text{-X})(H)(Cl)(PPh_3)_2$ complexes

Compound	**3-11**	**3-12**	**3-13**
empirical formula	$C_{38}H_{33}IrClP_2N_2O_3.$ CH_2Cl_2	$C_{39}H_{35}IrClP_2N_2O_3.$ CH_2Cl_2	$C_{38}H_{33}IrClP_2N_2O_4.$ CH_2Cl_2
T (K)	298(2)	298(2)	298(2)
fw (g mol^{-1})	940.20	954.23	956.18
cryst sys	triclinic	triclinic	triclinic
space group	P-1	P-1	P-1
a (Å)	10.8122(16)	11.2223(17)	9.1667(4)
b (Å)	12.4141(18)	12.3960(18)	12.1296(6)
c (Å)	15.610(2)	15.945(2)	18.5758(9)
α (deg)	69.852(2)	69.818(2)	84.3510(10)
β (deg)	76.836(2)	76.442(2)	76.8890(10)
γ (deg)	74.564(2)	74.736(2)	76.2610(10)
V ($Å^3$)	1874.5(5)	1983.1(5)	1951.85(16)
Z	2	2	2
density (g cm^{-3})	1.666	1.598	1.627
abs coeff (mm^{-1})	3.901	3.689	3.750
No. of reflns collected	16635	17642	22372
No. of indep reflns	8292	8754	8821
Data/restraints/parameters	8292/0/451	8754/0/460	8821/0/460
Final R indices [$I > 2s(I)$] R1	0.0300	0.0327	0.0246
*w*R2	0.0723	0.0823	0.0690
R indices (all data) R1	0.0366	0.0400	0.0265
*w*R2	0.0756	0.0878	0.0700
Goodness-of-fit on F^2	1.032	1.047	1.063

Experimental

$Li[N(SO_2CF_3)_2]$ is purchased from Acros Organics and used without purification. *trans*-$Ir^{(I)}(Cl)(CO)(PPh_3)_2$ (**3-1**),[151] $NH_4[N(NO_2)_2]$,[152] $K[N(NO_2)_2]$,[153] $Ag[N(NO_2)_2]$[154] and $H[N(SO_2CF_3)_2]$[155] are synthesized according to literature procedures. $Ag[N(SO_2CF_3)_2]$[156] is synthesized using Ag_2CO_3 instead of Ag_2O. The following reactions are carried out under strict exclusion of light due to the light sensitivity of the silver salts. *trans*-$Ir^{(I)}(Cl)(N_2)(PPh_3)_2$ (**3-2**) is synthesized as per literature method.[157]

3.2 Iridium(I) complexes of N-nitroamides/carbamates, N-nitrosocarbamates and N-nitrosulfonamides.

3.2.1 Synthesis of $Ir^{(I)}(\eta^1\text{-}CH_3C(O)NNO_2)(CO)(PPh_3)_2$ (3-3)

Complex **3-1** (0.080 g, 0.103 mmol) is dissolved in degassed $CHCl_3$ (5 mL) under an N_2 atmosphere. **2-2Ag** (0.022 g, 0.104 mmol) is added and stirred for 2 h at room temperature. A white precipitate is formed and is filtered through a Celite plug to give a yellow solution. The solvent is removed in *vacuo*, and the yellow residue recrystallized from CH_2Cl_2/CH_3OH to give yellow crystals of $Ir^{(I)}(\eta^1\text{-}CH_3C(O)NNO_2)(CO)(PPh_3)_2$ (**3-3**) (0.065 g, 0.0767 mmol, 75 % yield).

IR (cm^{-1}): 3077vw, 3053vw, 1968vs (CO), 1652m, 1491m, 1436m, 1224m, 1097m, 1027w, 747m, 694m, 521m.

Raman (cm^{-1}): 3065vw, 1970vw, 1591m, 1576vw, 1192vw, 1100m, 1030m, 1002vs, 618m, 571m, 255w

^1H NMR (200 MHz, $CDCl_3$) ppm: δ = 1.23 (s, 3H), 7.42 (m, PPh_3), 7.73 (m, PPh_3).

^{31}P NMR (81 MHz, $CDCl_3$) ppm: δ = 26.76 (s)

ESI-MS: 849.16 $[M]^+$

Elemental analysis calcd. for $C_{39}H_{33}N_2O_4P_2Ir.0.9CH_2Cl_2$ (924.31 g mol^{-1}) % C, 51.85; H, 3.79; N, 3.03. Found % C, 52.37; H, 3.22; N, 3.06.

3.2.2 Synthesis of $Ir^{(I)}(\eta^1\text{-}CH_3OC(O)NNO_2)(CO)(PPh_3)_2$ (3-4)

Complex **3-1** (0.030 g, 0.0385 mmol) is dissolved in degassed $CHCl_3$ (5 mL) under an N_2 atmosphere. **2-4Ag** (0.009 g, 0.0397 mmol) is added and stirred for 3 h at room temperature. A brown precipitate is formed and is filtered through a Celite plug to give a yellow solution. The solvent is removed in *vacuo*, and the yellow residue recrystallized from CH_2Cl_2/CH_3OH to give yellow crystals of $Ir^{(I)}(\eta^1\text{-}CH_3OC(O)NNO_2)(CO)(PPh_3)_2$ (**3-4**) (0.025 g, 0.0292 mmol, 76 % yield).

IR (cm^{-1}): 3055w, 2921w, 2851w, 1965vs (CO), 1875w, 1739s, 1683w, 1482m, 1435s, 1315w, 1230m, 1204s, 1181s, 1160m, 1096s, 1027w, 999w, 745m, 694vs, 611w, 521vs, 499m.

^1H NMR ($CDCl_3$) ppm: δ = 7.68 (m, PPh_3), 7.43 (m, PPh_3), 3.08 (s, 3H).

^{31}P NMR ($CDCl_3$) ppm: δ = 25.03 (s)

Elemental analysis calcd. for $C_{39}H_{33}N_2O_5P_2Ir$ (863.86 g mol^{-1}) % C, 54.17; H, 3.82; N, 3.24. Found % C, 54.19; H, 3.91; N, 3.13.

3.2.3 Synthesis of $Ir^{(I)}(\eta^1\text{-}C_2H_5OC(O)NNO_2)(CO)(PPh_3)_2$ (3-5)

Complex **3-1** (0.100 g, 0.128 mmol) is dissolved in degassed $CHCl_3$ (10 mL) under an N_2 atmosphere. **2-5Ag** (0.037 g, 0.154 mmol) is added and stirred for 3 h at room temperature. A brown precipitate is formed and is filtered through a Celite plug to give a yellow solution. The solvent is removed in *vacuo*, and the yellow residue recrystallized from CH_2Cl_2/CH_3OH to give yellow crystals of $Ir^{(I)}(\eta^1\text{-}C_2H_5OC(O)NNO_2)(CO)(PPh_3)_2$ (**3-5**) (0.100 g, 0.113 mmol, 88 % yield).

IR (cm^{-1}): 3055w, 2981vw, 2900vw, 1959vs (CO), 1912w, 1731s, 1688w, 1587w, 1572w, 1492m, 1481m, 1435s, 1388w, 1365w, 1292w, 1202s, 1185m, 1163m, 1096s, 1029w, 998m, 882w, 769w, 759m, 745m, 706m, 693w, 614m, 518s, 499m.

^{1}H NMR (200 Mhz, $CDCl_3$) ppm: δ = 0.99 (t, 3H, *J* = 7.1 Hz), 3.47 (q, 2H, *J* = 7.1 Hz), 7.43 (m, PPh_3), 7.72 (m, PPh_3).

^{31}P NMR (81 MHz, $CDCl_3$) ppm: δ = 26.22 (s)

ESI-MS: 900.84 $[M + Na]^+$

Elemental analysis calcd. for $C_{40}H_{35}N_2O_4P_2Ir$ (877.88 g mol^{-1}) % C, 54.67; H, 3.99; N, 3.19. Found % C, 54.45; H, 3.89; N, 3.13.

3.2.4 Synthesis of $Ir^{(I)}(\eta^1\text{-}CH_3OC(O)NNO)(CO)(PPh_3)_2$ (3-6)

Complex **3-1** (0.060 g, 0.0770 mmol) and **2-6Ag** (0.018 g, 0.0854 mmol) are added together in a reaction flask. Dry and degassed $CHCl_3$ (6 mL) is added under an N_2 atmosphere and stirred for 3 h at room temperature in an inert atmosphere glove box. A white precipitate is formed and is filtered through a Celite plug to give a bright yellow solution. The solvent is removed in *vacuo*, and the yellow residue recrystallized from dry and degassed CH_2Cl_2/pentanes to give yellow solids of $Ir^{(I)}(\eta^1\text{-}CH_3OC(O)NNO)(CO)(PPh_3)_2$ (**3-6**) (0.056 g, 0.0623 mmol, 86 % yield).

IR (cm^{-1}): 3055vw, 2949vw, 2841vw, 1968vs (CO), 1734w, 1702m, 1636w, 1480m, 1436m, 1400m, 1323m, 1262w, 1235w, 1185w, 1147m, 1093s, 1028w, 998w, 777w, 747m, 694m, 610m, 522s, 513m, 498m.

^{1}H NMR (200 MHz, $CDCl_3$) ppm: δ = 3.23 (s, 3H), 7.41 (m, PPh_3), 7.70 (m, PPh_3).

^{31}P NMR (81 MHz, $CDCl_3$) ppm: δ = 25.86 (s)

Elemental analysis calcd. for $C_{39}H_{33}N_2O_4P_2Ir$ (847.86 g mol^{-1}) % C, 55.19; H, 3.89; N, 3.30. Found % C, 55.04; H, 3.77; N, 3.43.

3.2.5 Synthesis of $Ir^{(I)}(C_7H_7SO_2NNO_2)(CO)(PPh_3)_2$ (3-7)

Complex **3-1** (0.030 g, 0.0385 mmol) and **2-8Ag** (0.013 g, 0.0403 mmol) are added together in a reaction flask. Dry and degassed $CHCl_3$ (5 mL) is added under

an N_2 atmosphere and stirred for 3 h at room temperature in an inert atmosphere glove box. A white precipitate is formed and is filtered through a Celite plug to give a bright yellow solution. The solvent is removed in *vacuo*, and the yellow residue recrystallized from dry and degassed CH_2Cl_2/CH_3OH to give yellow solids of $Ir^{(I)}(\eta^1\text{-}C_7H_7SO_2NNO_2)(CO)(PPh_3)_2$ (**3-7**) (0.025 g, 0.0257 mmol, 67 % yield).

IR (cm^{-1}): 3054vw, 2961vw, 2919vw, 2847vw, 1977vs (CO), 1596w, 1493s, 1482m, 1434s, 1339m, 1275m, 1154s, 1093s, 1013m, 922m, 812m, 744m, 693s, 661m, 605w, 589s, 542m, 516vs, 495m, 452w.

^1H NMR (200 MHz, $CDCl_3$) ppm: δ = 2.28 (s, 3H), 6.82 (d, 2H, *J*, = 8 Hz), 7.39 (m, p-tolyl and PPh_3), 7.64 (m, PPh_3).

^{31}P NMR (81 MHz, $CDCl_3$) ppm: δ = 24.60 (s)

Elemental analysis calcd. for $C_{44}H_{37}N_2O_5P_2SIr.0.75CH_2Cl_2$ (1023.72 g mol^{-1}) % C, 52.50; H, 3.79; N, 2.74; S, 3.13. Found % C, 52.84; H, 3.92; N, 2.60; S, 2.76.

3.2.6 Synthesis of $Ir^{(I)}(N(NO_2)_2)(CO)(PPh_3)_2$ (3-8)

Complex **3-1** (0.030 g, 0.0385 mmol) is dissolved in dry and degassed $CHCl_3$ (5 mL) and added into a dry CH_3CN (2 mL) solution containing $Ag[N(NO_2)_2]$ (0.010 g, 0.0421 mmol). A white precipitate appeared immediately (most likely some insoluble silver salt) and this is stirred overnight at room temperature under a N_2 atmosphere in an inert atmosphere glove box. The suspension is filtered through a Celite plug to give a bright yellow solution. The solvent is removed in *vacuo*, and the yellow oil recrystallized from dry and degassed CH_2Cl_2/CH_3OH to give brown crystals, $Ir^{(I)}(\eta^1\text{-}N(NO_2)_2)(CO)(PPh_3)_2$ (**3-8**) (0.0036 g, 0.0424 mmol, 11 % yield) contaminated with small amounts of yellow crystals of **3-1**.

IR (cm^{-1}): 3054vw, 2962vw, 2924vw, 2068w, 2024vw, 1981vs (CO), 1633w, 1588w, 1567s, 1480m, 1435s, 1385w, 1309w, 1264w, 1193s, 1158m, 1095s, 1057w, 998w, 967m, 827w, 746m, 693s, 607m, 521s, 514s, 500m, 423w.

^{1}H NMR (200MHz, $CDCl_3$) ppm: δ = 7.55 (m, PPh_3), 7.68 (m, PPh_3).

^{31}P NMR (81 MHz, $CDCl_3$) ppm: δ = 25.40

3.2.7 Synthesis of $Ir^{(I)}(Cl)(CO)(PPh_3)_2[Ag(N(SO_2CF_3)_2)]$ (3-9)

Complex **3-1** (0.030 g, 0.0385 mmol) is dissolved in dry and degassed $CHCl_3$ (5 mL) and added into a dry CH_3CN (2 mL) solution containing $Ag[C_7H_7SO_2NNO_2]$ (0.0156 g, 0.400 mmol). A white precipitate appeared immediately (most likely some insoluble silver salt) and stirred overnight at room temperature under a N_2 atmosphere in an inert atmosphere glove box. The suspension is filtered through a Celite plug to give a bright yellow solution. The solvent is removed in *vacuo*, and the yellow oil recrystallized from dry and degassed CH_2Cl_2/CH_3OH to give yellow crystals of $Ir^{(I)}(Cl)(CO)(PPh_3)_2[Ag(N(SO_2CF_3)_2)]$ (**3-9**) (0.017 g, 0.0146 mmol, 38 % yield) contaminated with small amounts of yellow crystals of **3-1**.

IR (cm^{-1}): 3058w, 2963w, 2918w, 2012s(CO), 1986m (CO), 1957w, 1627w, 1481w, 1436m, 1390m, 1356s, 1262m, 1197vs, 1133s, 1096vs, 1063m, 1026m, 997s, 805m, 747m, 693m, 613m, 569w, 513s, 461w.

^{1}H NMR (200 MHz, $CDCl_3$) ppm: δ = 7.43 (m, PPh_3), 7.51 (m, PPh_3), 7.68 (m, PPh_3).

^{31}P NMR (81 Mhz, $CDCl_3$) ppm: δ = 28.67 (s, minor) 23.82 (s, major)

Elemental analysis calcd. for $C_{39}H_{30}NS_2O_5F_6ClAgIr.CH_2Cl_2$ (1191.28 g mol^{-1}) % C, 40.33; H, 2.71; N, 1.18; S, 5.38. Found % C, 40.32; H, 2.63; N, 1.18; S, 5.21.

3.2.8 Synthesis of $Ir^{(I)}(CH_3C(O)NNO_2)(N_2)(PPh_3)_2$ (3-10)

Complex **3-3** (0.030 g, mmol) is dissolved in deoxygenated $CHCl_3$ containing small amounts of CH_3OH (2 mL) under an N_2 atmosphere and cooled to 0 ^{o}C. Compound *p*-nitrobenzoyl azide (mg, mmol), dissolved in degassed $CHCl_3$ (1 mL), is added and stirred for 15 min. The solvent is removed in *vacuo* to give yellow solids of $Ir^{(I)}(CH_3C(O)NNO_2)(N_2)(PPH_3)_2$ **3-10** (approx. 0.023 g).

IR (cm^{-1}): 3052vw, 2965vw, 2109vs (N_2), 1654m, 1559m, 1541m, 1507m, 1490m, 157w, 1436m, 1262m, 1211s, 1097s, 1022m, 801m, 746m, 695m, 516vs.

^{1}H NMR ($CDCl_3$) ppm: 1.25 (s, 3H), 7.42 (m, PPh_3), 7.75 (m, PPh_3)

^{31}P NMR (200 MHz, $CDCl_3$) ppm: δ = 22.93 (s)

3.3 Iridium(III) complexes of N-Nitroamides and N-nitrocarbamates

3.3.1 Synthesis of $Ir^{(III)}(\eta^2\text{-}CH_3C(O)NNO_2)(H)(Cl)(PPh_3)_2$ (3-11)

Complex **3-2** (0.110 g, 0.141 mmol), **2-2** (0.020 g, 0.192 mmol) and degassed $CHCl_3$ (5 mL) are mixed and stirred under an N_2 atmosphere. Bubbling is observed and the reaction mixture is stirred for 3 h. The reaction mixture is evacuated in *vacuo* to give yellow solids. The yellow solids are recrystallized from CH_2Cl_2/CH_3OH to give yellow crystals of $Ir^{(III)}(\eta^2\text{-}CH_3C(O)NNO_2)(H)(Cl)(PPh_3)_2$ (**3-11**) (0.104 g, 0.121 mmol, 86 % yield).

IR (cm^{-1}): 3056w, 2963vw, 2322vw, 2068vw, 1696m, 1572vw, 1514s, 1483m, 1435s, 1363w, 1261w, 1241w, 1198s, 1096s, 1035m, 806m, 745m, 707m, 695vs, 621w, 520vs, 504m.

Raman (cm^{-1}): 3067vw, 2326w, 1590m, 1190w, 1098m, 1030m, 1002vs, 891w, 704m, 617m, 542w, 255m.

^{1}H NMR (200 MHz, $CDCl_3$) ppm: δ = -31.78 (s, Ir-*H*, broad), 1.23 (s, 3H), 7.38 (m, PPh_3), 7.62 (m, PPh_3)

^{1}H NMR (400 MHz, $CDCl_3$) ppm: δ = -31.74 (s, Ir-*H*, broad), 1.25 (s, 3H)

^{1}H NMR (200 MHz, C_6D_6) ppm: δ = -31.22 (t, Ir-*H*, $J_{P\text{-}H}$ = 13.4 Hz), 1.47 (s, 3H), 6.92 (m, PPh_3), 7.88 (m, PPh_3)

^{1}H NMR (400 MHz, C_6D_6) ppm: δ = -31.22 (s, Ir-*H*, broad), 1.48 (s, 3H)

^{31}P NMR (81 MHz, $CDCl_3$) ppm: δ = 11.42 (s)

^{31}P NMR (81 MHz, C_6D_6) ppm: δ = 10.92 (s)

ESI-MS: 878.92 $[M + Na]^+$

Elemental analysis calcd. for $C_{38}H_{34}N_2O_3P_2ClIr.1.2CH_2Cl_2$ (958.24 g mol^{-1}) % C, 49.14; H, 3.83; N, 2.92. Found % C, 49.22; H: 3.74; N, 2.85.

An intermediate is observed from NMR and IR studies but never isolated. The spectra show a mixture of the intermediate and final product.

IR (cm^{-1}) new bands: 1567m, 1239s.

^{1}H NMR (200 MHz, $CDCl_3$) ppm: δ = -35.11 (t, Ir-*H*, J_{P-H} = 13.2 Hz), 1.36 (s, 3H)

^{11}H NMR (200 MHz, C_6D_6) ppm: δ = -34.28 (t, Ir-*H*, J_{P-H} = 13.4 Hz), 1.49 (s, 3H)

^{1}H NMR (400 MHz, C_6D_6) ppm: δ = -34.26 (t, Ir-*H*, J_{P-H} = 13.6 Hz), 1.49 (s, 3H)

^{31}P NMR (81 MHz, $CDCl_3$) ppm: δ = 14.56 (d, J_{P-H} = 10.9Hz)

With decoupler offset adjusted: 14.56 (s)

^{31}P NMR (200 MHz, C_6D_6) ppm: δ = 13.99 (s)

3.3.2 Synthesis of $Ir^{(III)}(\eta^2\text{-}C_2H_5C(O)NNO_2)(H)(Cl)(PPh_3)_2$ (3-12)

Complex **3-2** (0.156 mg, 0.200 mmol), **2-3** (0.028 g, 0.237 mmol) and $CHCl_3$ (5 mL) are mixed and stirred under an N_2 atmosphere. Bubbling is observed and the reaction mixture is stirred for 3 h. The reaction mixture is evacuated in *vacuo* to give yellow solids. The yellow solids are recrystallized from CH_2Cl_2/CH_3OH to give $Ir(\eta^2\text{-}C_2H_5C(O)NNO_2)(H)(Cl)(PPh_3)_2$ (**3-12**) (0.110 g, 0.126 mmol, 63 % yield)

Melting point: 131.4 ^{o}C

IR (cm^{-1}): 3056m, 2983w, 2937vw, 2311vw, 1720m, 1692m, 1509vs, 1482s, 1435vs, 1222m, 1168s, 1096s, 1061w, 999w, 753m, 744m, 706s, 695vs, 618vw, 522vs, 503m.

Raman (cm^{-1}): 3063vw, 2314vw, 1591w, 1190w, 1164w, 1099m, 1031m, 1002s, 855w, 706m, 618m, 543w, 318w.

^{1}H NMR (200 MHz, $CDCl_3$) ppm: δ = -31.65 (t, Ir-*H*, J_{P-H} = 14 Hz), 0.49 (t, 3H, *J* = 7 Hz), 1.44 (q, 2H, *J* = 7 Hz), 7.34 (m, PPh_3), 7.62 (m, PPh_3).

^{31}P NMR (81 MHz, $CDCl_3$) ppm: δ = 11.56 (s)

ESI-MS: 893.14 $[M + Na]^+$

Elemental analysis calcd. for $C_{39}H_{36}N_2O_3P_2ClIr.CH_2Cl_2$ (955.27 g mol^{-1}) % C, 50.24; H, 3.98; N, 2.93. Found % C, 50.15; H, 3.46; N, 2.99.

An intermediate is observed from NMR and IR studies but never isolated. The spectra show a mixture of the intermediate and final product.

^{1}H NMR (200 MHz, $CDCl_3$) ppm: δ = -34.87 (t, Ir-*H*, J_{P-H} = 13.4 Hz), 0.59 (t, 3H, *J* = 7 Hz), 1.60 (q, 2H, *J* = 7 Hz)

^{31}P NMR (81 MHz, $CDCl_3$) ppm: δ = 14.43 (d, J_{P-H} = 9.8 Hz)

3.3.3 Synthesis of $Ir^{(III)}(\eta^2\text{-}CH_3OC(O)NNO_2)(H)(Cl)(PPh_3)_2$ (3-13)

Complex **3-2** (0.015 g, 0.0192 mmol), **2-4** (0.003 g, 0.002 mmol) and degassed $CHCl_3$ (3 mL) are mixed and stirred under an N_2 atmosphere. Bubbling is observed and the reaction mixture is stirred for 3 h. The reaction mixture is evacuated in *vacuo* to give yellow solids. The yellow solids are recrystallized from CH_2Cl_2/CH_3OH to give yellow crystals of $Ir^{(III)}(\eta^2\text{-}CH_3OC(O)NNO_2)(H)(Cl)(PPh_3)_2$ (**3-13**) (0.012 g, 0.0133 mmol, 69 % yield).

IR (cm^{-1}): 3056w, 2953vw, 2920vw, 2850vw, 2298vw, 1747s, 1518m, 1483m, 1434s, 1266m, 1212m, 1185m, 1161w, 1097s, 1028w, 998w, 843w, 795w, 747m, 695s, 918vw, 520vs, 503m, 462w.

^{1}H NMR (200 MHz, $CDCl_3$) ppm: δ = -31.69 (t, Ir-H, J_{P-H} = 13.2 Hz), 2.97 (s), 7.34 (m, PPh_3), 7.62 (m, PPh_3).

^{31}P NMR (81 MHz, $CDCl_3$) ppm: δ = 9.97(s) with decoupler off (d, J_{P-H} = 4.5 Hz)

Elemental analysis calcd. for $C_{38}H_{34}N_2O_4P_2ClIr.CH_2Cl_2$ (957.23 g mol^{-1}) % C, 48.89; H, 3.76; N, 2.93. Found % C, 49.11; H, 3.62; N, 2.85.

Two intermediates are observed from NMR monitoring and new IR bands are observed to form and disappear. The intermediates are not isolated. The spectra show a mixture of the intermediates and final product.

IR (cm^{-1}): new bands at 1790 and 1620 cm^{-1}.

Intermediate A:

^{1}H NMR (200 MHz, $CDCl_3$) ppm: δ = -36.69 (t, Ir-*H*, J_{P-H} = 13.5 Hz), 3.43 (s, 3H).

^{31}P NMR (81 MHz, $CDCl_3$) ppm: δ = 14.43 (s).

Intermediate B:

^{1}H NMR (200 MHz, $CDCl_3$) ppm: δ = -25.95 (t, Ir-*H*, J_{P-H} = 13.4 Hz), 3.64 (s, 3H).

^{31}P NMR (81 MHz, $CDCl_3$) ppm: δ = 7.46 (s).

3.3.4 Synthesis of $Ir^{(III)}(\eta^2\text{-}C_2H_5OC(O)NNO_2)(H)(Cl)(PPh_3)_2$ (3-14)

Complex **3-2** (0.010 g, 0.100 mmol), **2-5** (0.014 g, 0.104 mmol) and degassed $CHCl_3$ (5 mL) are mixed and stirred under an N_2 atmosphere. Bubbling is observed and the reaction mixture is stirred for 3 h. The reaction mixture is evacuated to give yellow solids. The yellow solids are recrystallized from CH_2Cl_2/hexanes to give yellow solids, $Ir^{(III)}(\eta^2\text{-}C_2H_5OC(O)NNO_2)(H)(Cl)(PPh_3)_2$ (**3-14**) (0.053 g, 0.060 mmol, 60 % yield).

IR (cm^{-1}): 3056w, 2988vw, 2923vw, 1747m, 1517m, 1483m, 1435s, 1207s, 1207s, 1095vs, 1028w, 999w, 745m, 695vs, 542m, 522vs.

^{1}H NMR (200 MHz, $CDCl_3$) ppm: δ = --31.80 (t, Ir-*H*, J_{P-H} = 13.6 Hz), 0.88 (t, 3H, *J* = 7.2 Hz), 3.32 (q, 2H, *J* = 7.2 Hz), 7.40 (m, PPh_3), 7.64 (m, PPh_3)

^{1}H NMR (400 MHz, $CDCl_3$) ppm: δ = --31.81 (t, Ir-*H*, J_{P-H} = 14 Hz), 0.87 (t, 3H, *J* = 8 Hz), 3.32 (q, 2H, *J* = 8 Hz), 7.39 (m, PPh_3), 7.65 (m, PPh_3)

^{1}H NMR (200 MHz, C_6D_6) ppm: δ = -30.88 (t, Ir-*H*, J_{P-H} = 13.5 Hz), 0.61 (t, 3H, *J* = 7.2 Hz), 3.23 (q, 2H, *J* = 7.2 Hz), 6.96 (m, PPh_3), 7.87 (m, PPh_3)

^{1}H NMR (400 MHz, C_6D_6) ppm: δ = -30.91 (t, Ir-*H*, J_{P-H} = 12 Hz), 0.61 (t, 3H, *J* = 8 Hz), 3.23 (q, 2H, *J* = 8 Hz), 6.96 (m, PPh_3), 7.87 (m, PPh_3)

^{31}P NMR (81MHz, $CDCl_3$) ppm: δ = 10.35 (s)

^{31}P NMR (81MHz, C_6D_6) ppm: δ = 10.71 (s)

ESI-MS: 884.96 $[M - H]^+$

Elemental analysis calcd. for $C_{39}H_{36}N_2O_4P_2ClIr.0.3C_6H_{14}$ (912.20 g mol^{-1}) % C, 53.72; H, 4.44; N, 3.07. Found % C, 53.30; H, 4.82; N, 2.58.

Two intermediates are observed from NMR studies but never isolated. The spectra show a mixture of the intermediates and final product.

Intermediate A:

^{1}H NMR (200 MHz, $CDCl_3$) ppm: δ = -36.16 (t, Ir-*H*, J_{P-H} = 13.2 Hz), 0.99 (t, 3H, *J* = 8 Hz), 3.92 (q, 2H, *J* = 7 Hz).

^{31}P NMR (81 MHz, $CDCl_3$) ppm: δ = 13.92 (s).

Intermediate B:

^{1}H NMR (200 MHz, $CDCl_3$) ppm: δ = -25.96 (t, Ir-*H*, J_{P-H} = 13.7 Hz), 1.36 (t, 3H, *J* = 7 Hz), 4.05 (q, 2H, *J* = 7.3 Hz).

^{31}P NMR (81 MHz, $CDCl_3$) ppm: δ = 7.26 (s).

3.4 Reactivity studies of **3-11**

3.4.1 Reaction with CO

Complex **3-11** (0.030 g, 0.035 mmol) is dissolved in $CHCl_3$ (5 mL). CO is vigorously bubbled into the solution at 5 atmospheres. The yellow solution turned pale yellow after 10 min. The solvent is removed in *vacuo*, and the pale yellow solids recrystallized from CH_2Cl_2/hexanes to give pale yellow solids which contain isomers of $Ir^{(III)}(CH_3C(O)NNO_2)(H)(Cl)(CO)(PPh_3)_2$ (**3-15**) (0.030 mg, 0.034 mmol, 97 % yield).

IR (cm^{-1}): 3056w, 2962vw, 2185vw (broad), 2047m (CO), 1695vw, 1648vw (broad), 1511m, 1483m, 1435s, 1362w, 1262w, 1188m, 1095s, 1029m, 1000m, 745m, 694vs, 524vs

^1H NMR (400 MHz, $CDCl_3$) ppm: δ = -8.31 (t, Ir-*H*, J_{P-H} = 16 Hz, minor isomer = 0.05), -7.68 (t, Ir-*H*, J_{P-H} = 12 MHz, major isomer = 0.56), -7.54 (t, Ir-*H*, J_{P-H} = 12 MHz, minor isomer = 0.39), 1.15 (s, 3H, minor isomer = 0.41), 1.57 (s, 3H, major isomer = 0.59)

^{31}P NMR (81 MHz, $CDCl_3$) ppm: δ = 3.61 (s, minor isomer = 0.43), 3.92 (s, major isomer = 0.57)

Upon leaving the reaction mixture in solution overnight, **3-11** is regenerated, as confirm by the loss of the 2047 cm^{-1} band. ^{31}P NMR shows only the appearance of a single resonance at 11.45 ppm. Repeated CO bubbling regenerated the three isomers of **3-15** again.

3.4.2 Reaction with $P(CH_3)_2Ph$

Complex **3-11** (0.060 g, 0.070 mmol) is dissolved in dry $CHCl_3$ (5 mL). $P(CH_3)_2Ph$ (21 μL, 0.147 mmol) is added and stirred for 3 h. The solution turned slightly pale yellow over time and the solvent is removed in *vacuo*. The oil that

remained contains isomers of $Ir^{(III)}(CH_3C(O)NNO_2)(H)(Cl)(P(CH_3)_2Ph)_3$ (**3-16**) (approx. 0.043 g).

^1H NMR (200 MHz, $CDCl_3$) ppm: - 21.48 (dt, Ir-*H*, $J_{cis\ P\text{-}H}$ = 19.2 Hz, $J_{cis\ P\text{-}H}$ = 12.2 Hz, minor isomer = 0.10), -19.96 (dt, Ir-*H*, $J_{cis\ P\text{-}H}$ = 19.8 Hz, $J_{cis\ P\text{-}H}$ = 12.2 Hz, major isomer = 0.42), -19.68 (t, Ir-*H*, $J_{P\text{-}H}$ = 13.2 Hz minor isomer = 0.18), -11.63 (dt, Ir-*H*, $J_{trans\ P\text{-}H}$ = 157.8 Hz, $J_{cis\ P\text{-}H}$ = 16.0 Hz, minor isomer = 0.30)
^{31}P NMR (81 MHz, $CDCl_3$) ppm: -44.37 (s, free $P(CH_3)_3Ph$), three isomers = 0.82; -34.56 (t, $P(CH_3)_2Ph$, $J_{cis\ P\text{-}trans\ P}$ = 19.9 Hz), -20.12 (d, PPh_3, $J_{trans\ P\text{-}cis\ P}$ = 19.9 Hz), -4.38 (s, free PPh_3), 35.13 (s, minor isomer = 0.18)

3.4.3 Reaction with methyl trifluoromethanesulfonate

Complex **3-11** (0.050 g, 0.058 mmol) is dissolved in dry CH_3CN (4 mL) under a N_2 atmosphere. Methyl trifluoromethanesulfonate (7 μL, 0.064 mmol) is added and stirred for 2 h. The reaction mixture is observed to change from pale yellow to colourless. The solvent is removed in *vacuo* to give white-brown solids which are recrystallized from CH_3CN/ether to give $Ir^{(III)}(H)(Cl)(CH_3CN)_2(PPh_3)_2$ (**3-17**) (18 mg, 0.022 mmol, 37 % yield).

IR (cm^{-1}): 3059w, 3024vw, 3005vw, 2990vs, 2931vw, 2296vw, 2272vw, 2251vw, 1483m, 1435s, 1270vs, 1224m, 1187m, 1154m, 1096m, 1031s, 999m, 753m, 709m, 695s, 638s, 524vs, 504m.
^1H NMR (200 MHz, $CDCl_3$) ppm: -20.67 (t, Ir-*H*, $J_{P\text{-}H}$ = 12.3 Hz), 1.91 (s, 3H), 2.00 (s, 3H), 7.46 (m. PPh_3), 7.69 (m, PPh_3)
^{31}P NMR (81 MHz, $CDCl_3$) ppm: 4.43 (s)

3.5 Results and Discussion

3.5.1 Ir(I) complexes of nitrogen acids and related amides

3.5.1.1 Synthesis of Ir(I) complexes of nitrogen acids and related amides

The nitrogen acids N-nitroamides, N-nitrocarbamates, N-nitrosocarbamates and N-nitrosulfonamides have electronegative nitro and nitroso functional groups that may exhibit unusual π-accepting properties. For comparison studies, related amides with electron-withdrawing functional groups such as dinitramide and bistriflimide have been synthesized.

Silver dinitramide, $Ag[N(NO_2)_2]$, requires a multi-step synthesis starting from the nitration of nitramide and multiple cation metatheses to give the silver salt as shown in Scheme 3-1.

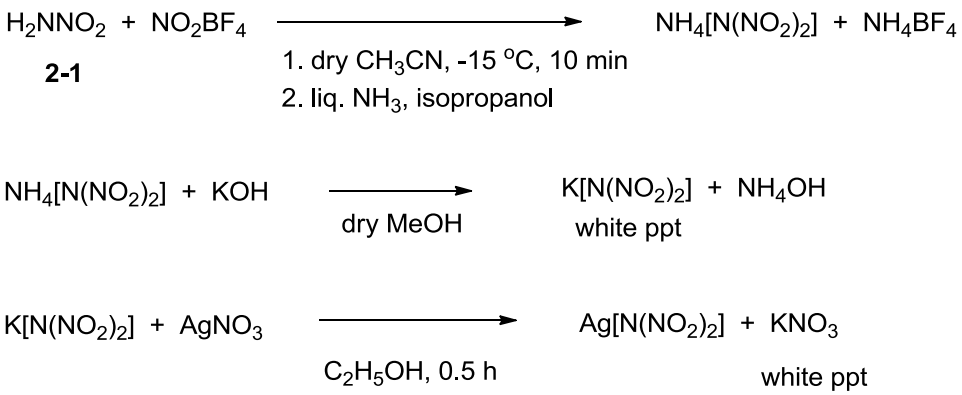

Scheme 3-1. Synthesis of $Ag[N(NO_2)_2]$ from **2-1**.

The free dinitramide acid, $HN[N(NO_2)_2]$, is very unstable, undergoes decomposition which is explosive and is never isolated in the absence of solvent. Dinitramide acid is a strong acid and reacts with base and carbonates to give corresponding metal salts $M^{n+}[N(NO_2)_2]_n$. However due to its explosive nature, the usual reaction pathway of dintramide acid with silver oxide or carbonate is avoided. All dinitramide salts are sensitive to shock and should be handled with caution especially when dry!

The silver bistriflimide salt is synthesized from the reaction of the super acid, bistrifluoromethanesulfonic acid (generated from lithium bistriflimide with conc.

H_2SO_4), with silver carbonate (Scheme 3-2). The silver salt is extremely hygroscopic.

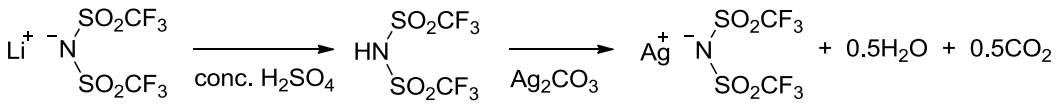

Scheme 3-2. Synthesis of $Ag[N(SO_2CF_3)_2]$.

Several attempts at generating the silver bistriflimide salt from the reaction of trifluoromethanesulfonic anhydride with benzyl amine and subsequent hydrolysis with ethanol and silver oxide was unsuccessful.[158]

The Ir(I) carbonyl complexes of the nitrogen acids and related amides are synthesized from the reaction of **3-1** and the corresponding silver salts (Scheme 3-3).

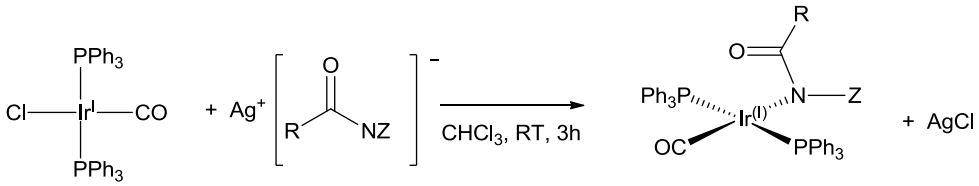

3-1

R	Z	Compound
CH_3	NO_2	**2-2Ag**
CH_3O	NO_2	**2-4Ag**
C_2H_5O	NO_2	**2-5Ag**
CH_3O	NO	**2-6Ag**

R	Z	Complex
CH_3	NO_2	**3-3**
CH_3O	NO_2	**3-4**
C_2H_5O	NO_2	**3-5**
CH_3O	NO	**3-6**

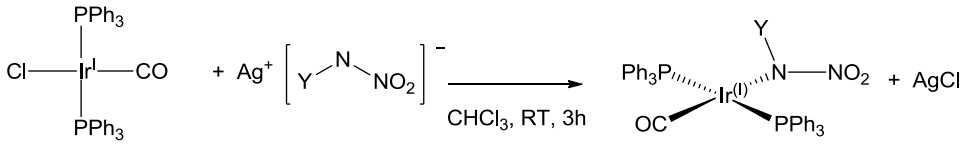

3-1

Y	Compound
p-tolylSO$_2$	**2-8Ag**
NO_2	$Ag[N(NO_2)_2]$

Y	Complex
p-tolylSO$_2$	**3-7**
NO_2	**3-8**

Scheme 3-3. Synthesis of $Ir^{(I)}(\eta^1\text{-X})(CO)(PPh_3)_2$.

The new Ir(I) carbonyl complexes containing the nitrogen acids and related amides were obtained in good yields except for **3-8**. Complex **3-8** was always obtained as a mixture of **3-1** and **3-8** with **3-8** as a minor component. A significant amount of triphenylphosphine oxide is also observed in the ^{31}P NMR spectrum

during the isolation process which indicates oxidation of the phosphine ligand of **3-1**. There seems to be a competition between silver chloride formation and oxidation of the triphenylphosphine ligand of **3-1**. The reaction is complicated by the mostly insoluble silver dinitramide salt.

The complexes are stable to oxygen in the solid state. Complexes **3-3**, **3-4**, **3-5**, **3-6** containing the amide or carbamate substituents are stable to oxygen in solution while complexes **3-7** and **3-8** readily react with oxygen in the air to form the O_2 adducts in solution similar to **3-1**. The reduced reactivity of complexes **3-3**, **3-4**, **3-5**, **3-6** to O_2 is unusual for the derivatives of Vaska's complex and may be correlated to the electron-withdrawing nature of the nitro/nitroso conjugate bases. All the new complexes have similar solubility properties as **3-1** which are recrystallized from CH_2Cl_2/CH_3OH solvent systems except for **3-6** which contains the nitroso substituent and is soluble in most solvents except for alkanes.

The reaction of silver bistrisflimide with **3-1** did not result in the displacement of the chloride anion by the bistriflimide anion to give AgCl. An unexpected Vaska's complex silver bistriflimide adduct, **3-9**, was instead isolated with significant amounts of **3-1** (Scheme 3-4).

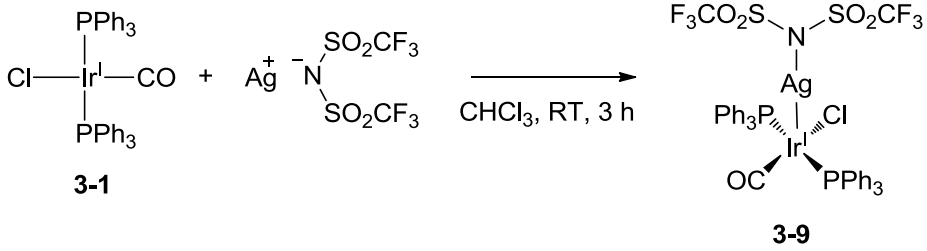

3-1 **3-9**

Scheme 3-4. Reaction of silver bistriflimide with **3-1**.

Changing the reaction conditions such as solvent to benzene or toluene and refluxing the reaction mixtures did not cause the displacement of the chloride ligand by the bistriflimide anion. The silver bistriflimide salt is relatively insoluble in the reaction solvents used but becomes more soluble after reflux. Complex **3-9** is not the first Ag-adduct of Vaska's complex. There are at least two examples of such Ag-adducts mainly with anionic carborane clusters such as **3-17** and **3-18** (Figure 3-1).[159] These clusters are poorly coordinating and bulky which may account for the unsuccessful silver metathesis reactions.

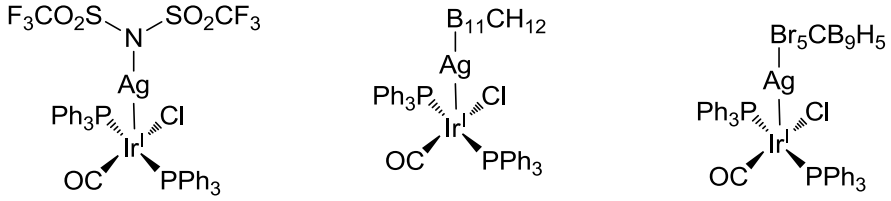

3-9 **3-18** **3-19**

Figure 3-1. Vaska complex with adducts of silver anions.

There are also other examples of silver adducts with Ir complexes and in almost all cases the silver salt contains poorly coordinating or electron-withdrawing anions such as trifluoromethanesulfonate ($CF_3SO_3^-$), difluorophosphinate ($P(O)F_2O^-$) or trifluoracetate ($CF_3CO_2^-$).

The mechanism of the silver metathesis reactions with **3-1** is still poorly understood as there are several possible pathways for halide displacement. The most probable mechanism likely involves the initial dissociation of the chloride ligand followed by the formation of AgCl which precipitates out of solution completing the metathesis reaction. This mechanism is supported by the halide substitution reactions for Vaska's complex that have been carried out using ten-fold excess reagents such as NaI, NaBr, NaN_3, etc to allow the exchange of the chloride ligand for the iodide, bromide or azide ligand.[149]

However the unsuccessful reaction of $Ag[N(SO_2CF_3)_2]$ with **3-1** may hint that another reaction mechanism is possible. As **3-1** is coordinatively unsaturated and electron-rich, a plausible mechanism can be an electrophilic attack of the silver cation on the Ir center followed by nucleophilic attack of the anion on the Ir center which eventually results in elimination of silver halide. In such cases, if the anion is a poor nucleophile or has electron withdrawing substituents, the displacement reaction will be unsuccessful. Finally, the coordination unsaturation and electron-rich Ir(I) center, an alternative and more probable mechanism may involve oxidative addition across the bond of the silver cation and the anion with subsequent reductive elimination of silver halide (Scheme 3-5). The appropriate mechanism for the reaction may very well depend on the bonding nature of the silver salt, with ionic forms preferring the displacement substitution and more covalent forms undergoing the redox pathway.

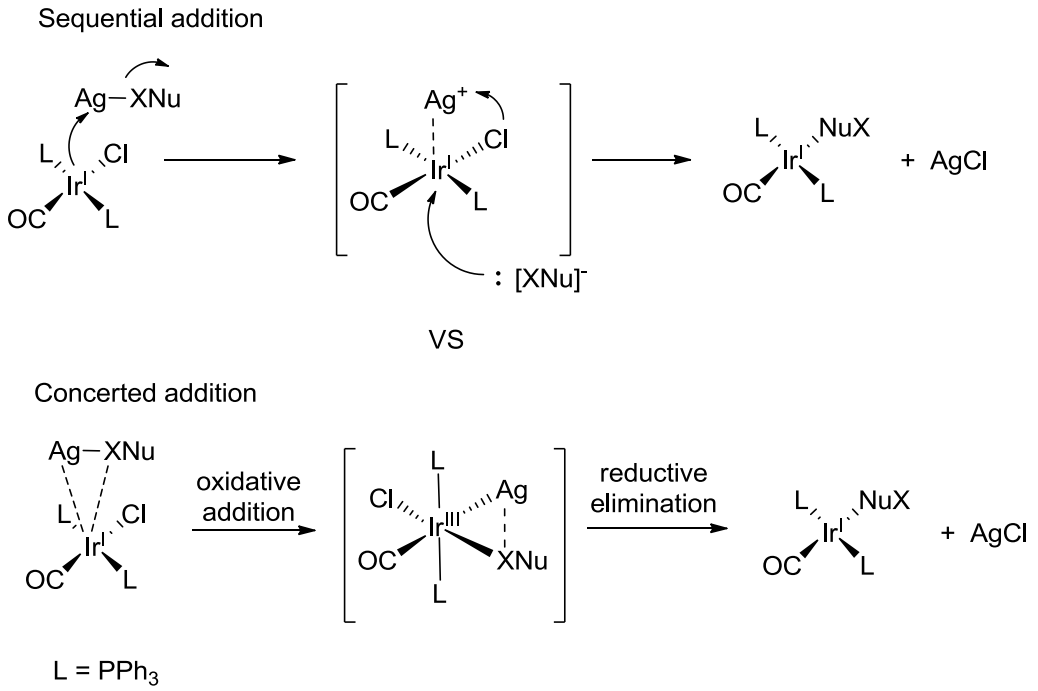

Scheme 3-5. Possible mechanisms of silver metathesis reactions with Vaska complex.

Silver salts forming transition metal Ag-metal adducts are not the only unusual adducts reported before. There are also reports of thallium salts forming similar adduct-type complexes. In particular examples involving Ir complexes, there was an observed luminescent effect of these Tl-Ir adducts (Figure 3-2).[160]

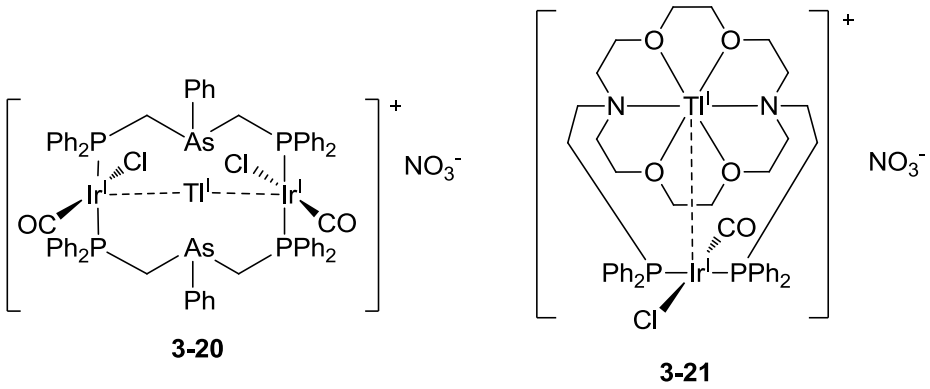

Figure 3-2. Complexes of Ir-Tl adducts with luminescent properties.

The reaction of $Tl[N(SO_2CF_3)_2]$ (generated from bistrifluoromethanesulfonic acid and thallium carbonate) with **3-1** in various solvents such as $CHCl_3$, CH_2Cl_2, toluene and benzene generated such possible Tl-Ir adducts (Scheme 3-6).

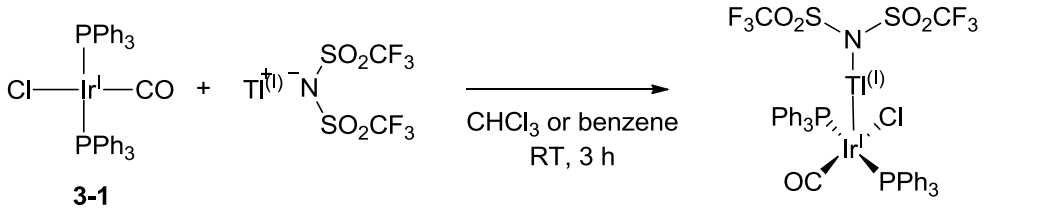

3-1

Proposed pink solution complex

Scheme 3-6. Reaction of **3-1** with $Tl[N(SO_2CF_3)_2]$ in $CHCl_3$ or benzene.

Concentration of the solvent of the fully dissolve yellow-orange reaction mixture of $Tl[N(SO_2CF_3)_2]$ and **3-1** gave an intense pink solution which on dilution gave the same yellow-orange solution. The process is reversible and when the solvent is fully removed, solids of both **3-1** and $Tl[N(SO_2CF_3)_2]$ remained.

3.5.1.2 Crystallograpic and spectroscopic properties

The molecular structures of **3-3**, **3-4**, **3-5**, **3-6**, **3-7** and **3-8** are shown in Figure 3-3, Figure 3-4, Figure 3-5, Figure 3-6, Figure 3-7 and Figure 3-8 respectively. All the structural parameters were obtained by full least squares refinement without any restraints except for **3-6**. The crystals of **3-6** were grown from slow diffusion of pentanes into a solution of **3-6** in THF/CH_2Cl_2 and were often very small or microcrystalline (less than 0.01 mm). The dataset used for the structure determination was collected from the largest possible crystal obtained but only diffracted to $2\theta = 46.90^{o}$, slightly short of the ideal $2\theta = 50^{o}$ requirement. Nevertheless the number of unique reflections obtained was more than twelve times the number parameters fulfilling the minimum ratio of 9:1. The diffraction data was solved with least squares restraints such as ISOR, SIMU, DELU, which are used to affect the thermal parameters, and SADI, which affects the bond lengths of the atoms, on the atoms of the THF molecule as there is a slight disorder with a CH_2Cl_2 molecule that was left out.

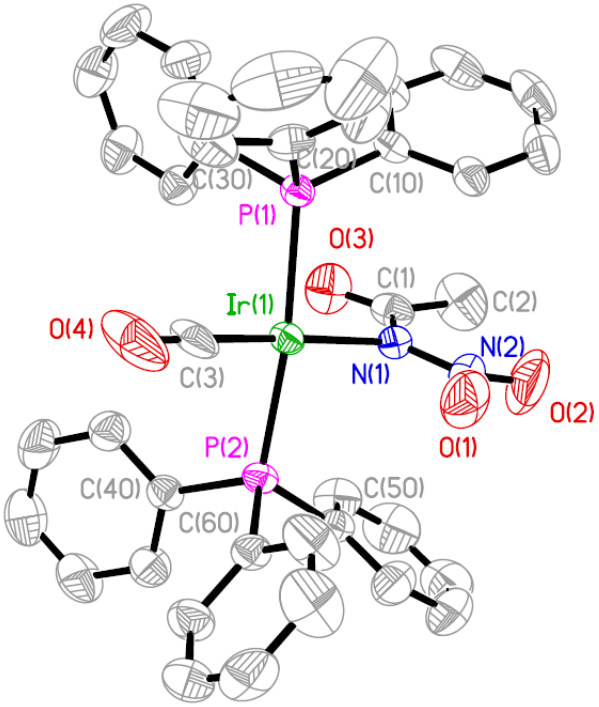

Figure 3-3. Molecular structure of **3-3**. Hydrogen atoms and solvent molecules have been omitted for clarity.

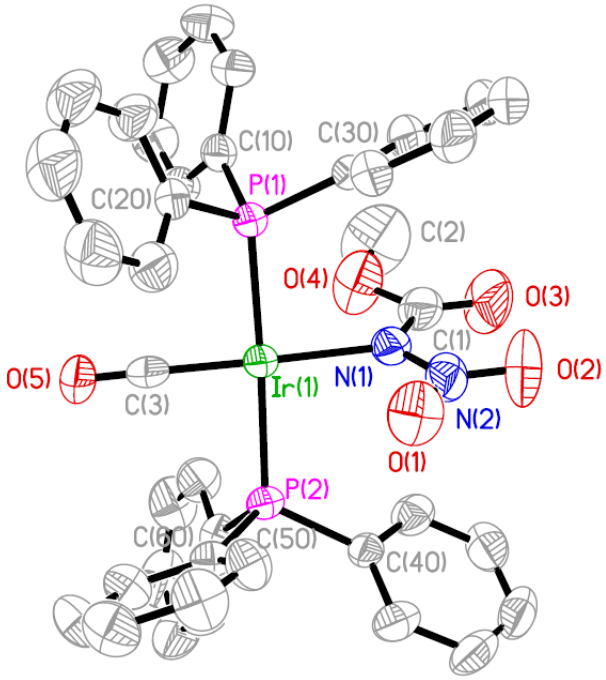

Figure 3-4. Molecular structure of **3-4**. Hydrogen atoms have been omitted for clarity.

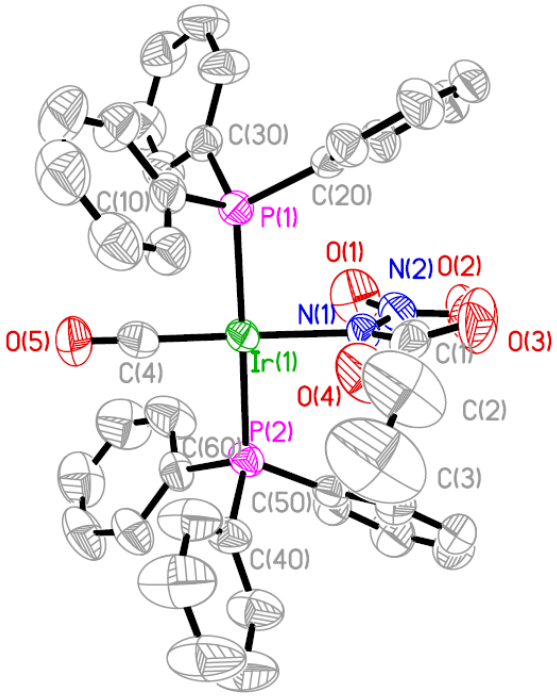

Figure 3-5. Molecular structure of **3-5**. Hydrogen atoms have been omitted for clarity.

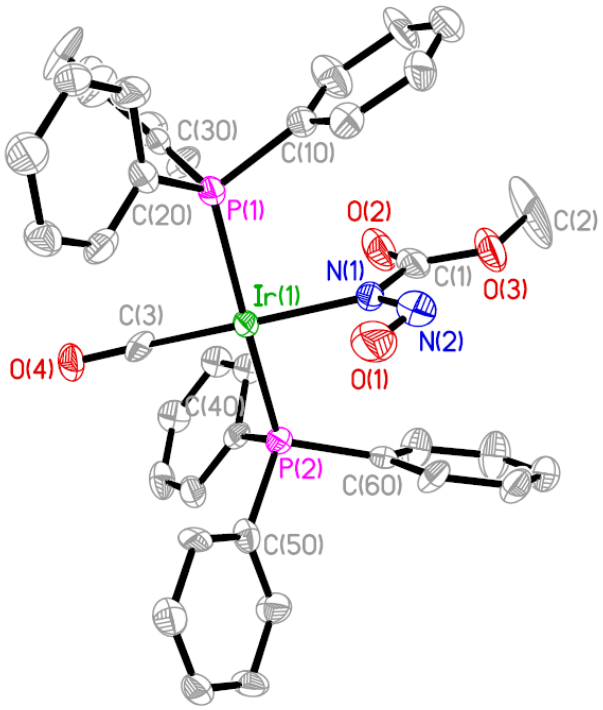

Figure 3-6. Molecular structure of **3-6**. Hydrogen atoms and solvent molecules have been omitted for clarity.

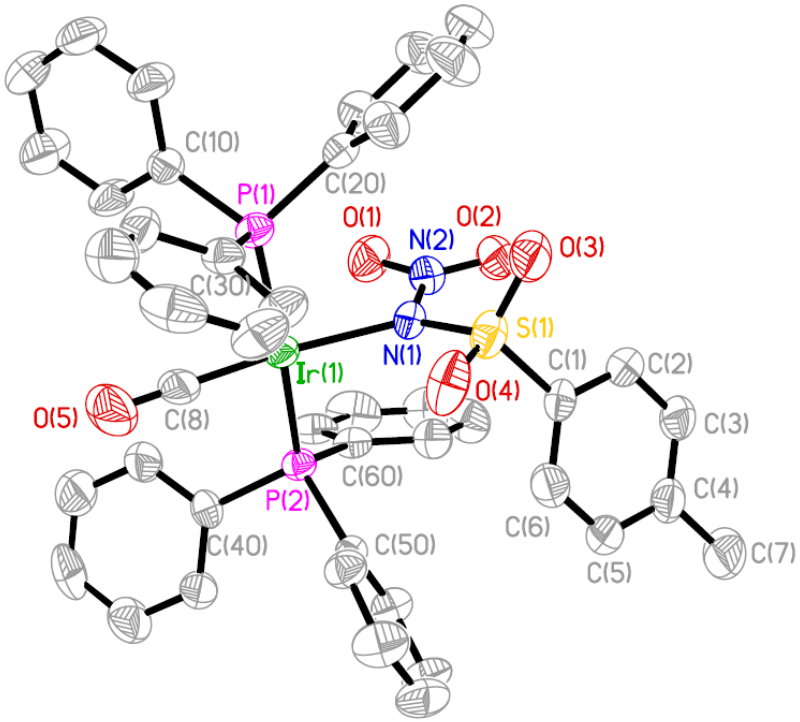

Figure 3-7. Molecular structure of **3-7**. Hydrogen atoms have been omitted for clarity.

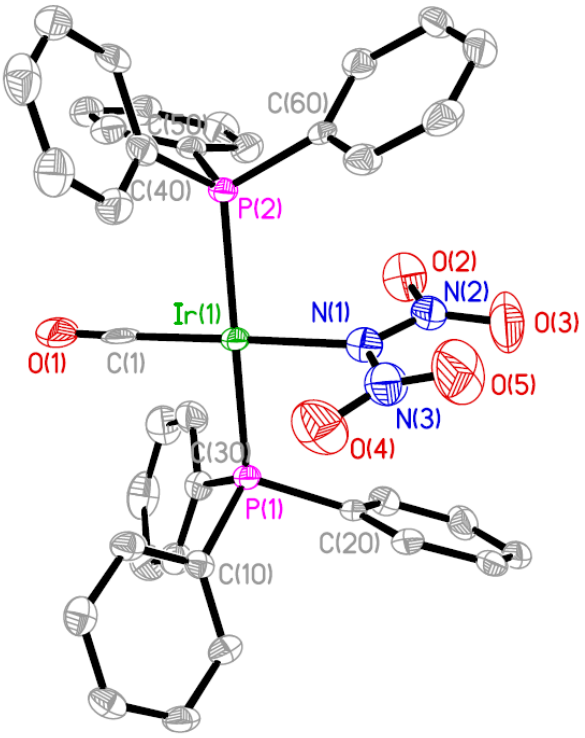

Figure 3-8. Molecular structure of **3-8**. Hydrogen atoms have been omitted for clarity.

The Ir complexes in the above structures have *trans*-square planar geometry with the triphenylphosphine ligands trans to each other while the carbonyl (CO) ligand is trans to the respective amides of interest. The conjugate base of the nitrogen acids is coordinated to the Ir center through the nitrogen of the amide function. The trans arrangement of the conjugate base of the nitrogen acid to the carbonyl ligand induces a strong electronic effect on the carbonyl ligand mostly through the dπ orbital interactions. This effect is most easily observed in the IR stretching frequency of the CO ligand. The reduction in the electron donating ability of the Ir center (due to competition from the π-accepting ligand trans to the CO) from the dπ orbitals into the π* orbitals of the carbonyl ligand increases the bond order of the CO ligand. This results in the shift of the Ir-CO stretch to higher wavenumbers (closer to free CO stretch of 2147 cm^{-1}). The CO stretching frequency, υ(CO), of **3-3**, **3-4**, **3-5**, **3-6**, **3-7** and **3-8** are listed in Table 3-3.

In general there is a shift to higher wavenumbers in υ(CO) on coordination of the new N-nitro/nitroso amide/carbamate/sulfonamide ligands. This observation

corresponds to the general idea that the presence of the electron-withdrawing nitro and nitroso functional groups on the ligands makes them π-accepting in nature.

To better discuss the π-acidic effect of ligands on transition metals, a molecular orbital diagram analysis will be useful. The simplified molecular orbital (M.O.) diagram of the d^8 square planar Ir(I) Vaska complex is shown in Figure 3-9.

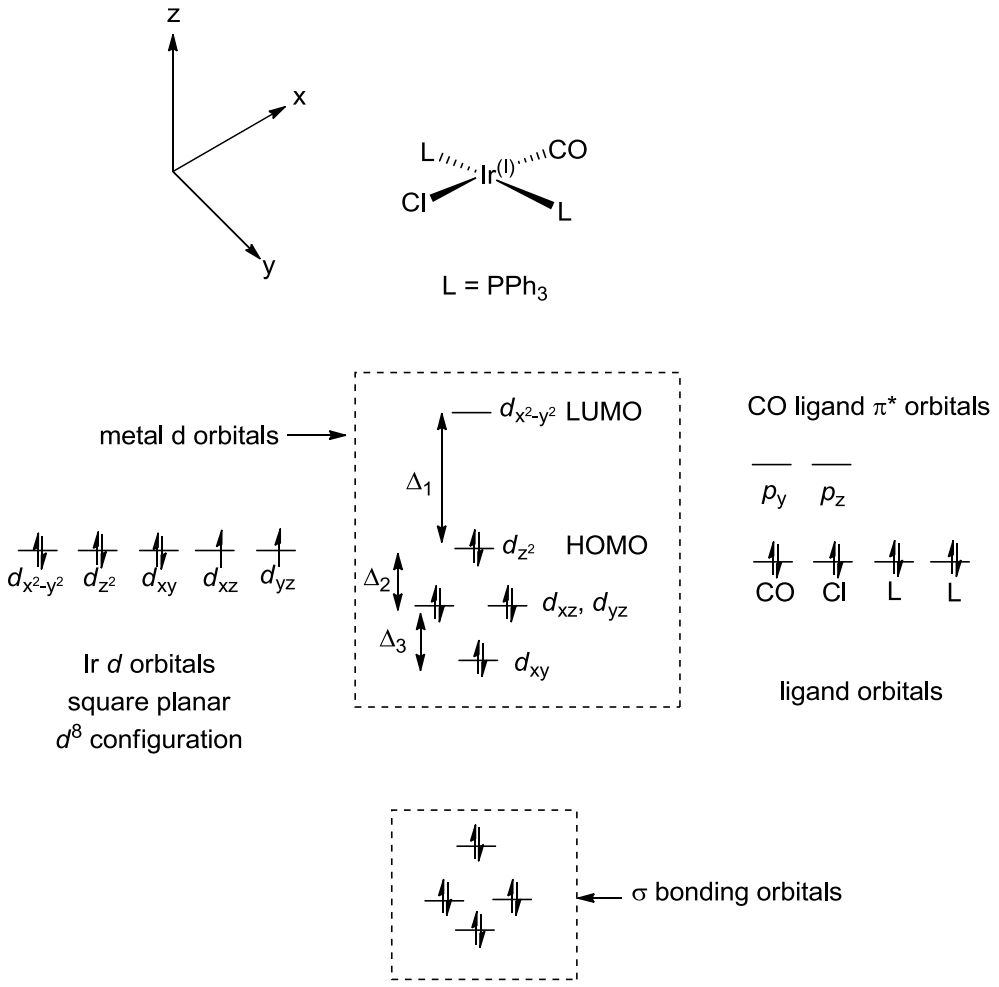

Figure 3-9. Simplified molecular orbital diagram of d^8 trans-$Ir^{(I)}(Cl)(CO)(PPh_3)_2$. It is assume that the four ligands are homoleptic with similar σ-interaction with the Ir center. The π* orbital interaction of the CO ligand with the Ir dπ orbitals are not shown.

Table 3-3: υ(CO)(cm^{-1}), bond length (Å), bond and torsion angles (deg) of $Ir^{(I)}(\eta^1\text{-}X)(CO)(PPh_3)_2$ complexes and $Ir^{(I)}(Cl)(CO)(PPh_3)_2.Ag[N(SO_2CF_3)_2]$.

Compound	**3-3**	**3-4**[a]	**3-5**[b]	**3-6**[c]	**3-7**[d]	**3-8**[e]	**3-9**[f]
υ(CO)	1968	1965	1959	1968	1977	1981	2011,1987
Ir(1) - C(3)	1.804(4)	1.814(6)	1.821(4)	1.803(10)	1.786(6)	1.865(6)	1.857(4)
Ir(1) - N(1)	2.111(3)	2.131(4)	2.114(3)	2.092(8)	2.146(4)	2.104(5)	2.6074(3)
C(3) - O(4)	1.141(5)	1.127(6)	1.125(4)	1.176(10)	1.152(6)	1.060(7)	1.138(5)
N(1) - N(2)	1.363(4)	1.351(6)	1.367(4)	1.330(12)	1.367(6)	1.343(7)	1.607(3)
N(1) - C(1)	1.393(5)	1.377(7)	1.384(5)	1.407(13)	1.673(4)	1.449(7)	1.615(3)
N(2) – O(1)	1.233(5)	1.225(6)	1.220(4)	1.260(11)	1.237(5)	1.200(6)/1.247(7)	
N(2) – O(2)	1.221(5)	1.229(6)	1.221(4)		1.222(5)	1.245(6)/1.189(6)	
C(3) – Ir(1) – N(1)	175.17(18)	176.6(3)	176.78(15)	179.5(4)	170.7(2)	174.5(2)	78.47(12)
O(4) – C(3) – Ir(1)	177.3(5)	177.8(7)	178.8(4)	178.8(8)	178.6(6)	177.7(7)	178.0(3)
O(1) – N(2) – N(1) – C(1)	175.7(4)	-179.6(5)	-169.9(3)	-179.4(8)	-171.2(4)	-172.5(5)	
O(3) – C(1) – N(1) – N(2)	177.1(3)	4.1(9)	12.6(6)	-178.9(9)	48.8(4)	15.8(8)	

a. O(5) instead of O(4).

b. C(4) instead of C(3) and O(5) instead of O(4).

c. O(2) instead of O(3).

d. C(8) instead of C(3), O(5) instead of O(4) and S(1) instead of C(1).

e. C(1) instead of C(3), O(1) instead of O(4), O(2) and O(4) instead of O(1), O(3) and O(5) instead of O(2), N(3) instead of C(1) and O(5) instead of O(3).

f. C(1) instead of C(3), Ag(1) instead of N(1), O(1) instead of O(4), S(1) instead of N(2) and S(2) instead of C(1).

The ligand field stabilisation energy (LFSE) is indicated by Δ_1 which is the energy level difference between the $d_{x^2-y^2}$ and the d_{z^2} orbitals of the Ir center. The LFSE can be considered to be the gap between the highest occupied molecular orbital (HOMO) and lowest unoccupied molecular orbital (LUMO) for the square planar d^8 metal complex. The strongly π-accepting ligand CO has π* orbitals for interactions with the Ir *d* orbitals. In this case the p_y and p_z π* orbitals are in the same orientation as the *d*π orbitals, d_{xy} and d_{xz} respectively. This causes the stabilisation of the similarly oriented *d*π orbitals such that the d_{xz} and d_{yz} orbitals are no longer degenerate with d_{xy}. The strength of the *d*π-π* interaction between the Ir center and the CO ligand is dependent on the overlap extent of the molecular orbitals (Figure 3-10).

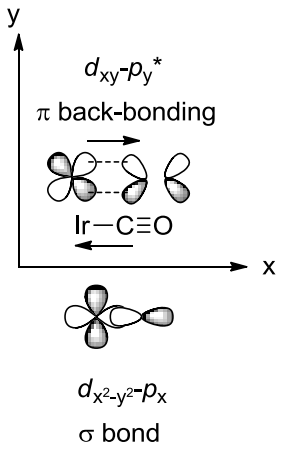

Figure 3-10. σ bonding and π back-bonding in Ir-CO bond interactions.

For π orbitals, the extent of the orbital overlap is also dependent on the σ bond interaction of the ligand, such that the stronger the σ interaction of the ligand results in better overlap of the π*-*d*π orbital giving a stronger π*-*d*π interaction. This type of σ-π* synergy effect is present for π-accepting ligands and contributes to the overall decrease in the energy levels of the d_{z^2}, d_{xz}, d_{yz} and d_{xy} orbitals. The decrease in energy levels of the HOMO increases the LFSE and makes the transition complex less reactive towards oxidative addition reactions.

The introduction of an additional π-accepting ligand trans to the CO ligand which is similar to the Ir(I) nitrogen acid complexes shown above result in competition for π-backbonding from the Ir *d*π orbitals to the π* orbitals of the CO and nitrogen

acid ligand. The nitrogen acids have a delocalised π system that generates its own π* orbital. From the solid state structures obtained, the nitrogen acid ligands are aligned to the z-axis. This would result in the π* orbital to be in the xy plane with the x-axis as the Ir-CO σ bond. Therefore there will be competition for π-backbonding from the d_{xy} orbital of the Ir center. For a simple double bond π-acidic ligand, the competition would result in a much weaker M-C bond interaction. However the CO ligand has a triple bond which has an additional orthorgonal p_z*- d_{xz} interaction. The π-backbonding effect for the CO ligand can be compensated from increased π-backbonding from the p_z*- d_{xz} interaction. The presence of weak π-donors such as Cl ligand helps to mitigate the π-backbonding competition. The overall outcome is that the Ir-CO stretch is not easily analyzed.

The strength of the π-accepting nature of these ligands may be inferred from the extent of the shift in the υ(CO) stretch of the starting Vaska's complex which is at 1954 cm^{-1} in KBr matrix.

The reduced π-basicity of the nitrogen acids may also play a role in the increase of υ(CO) for the Ir(I) carbonyl nitrogen acid complexes. The presence of electron-withdrawing nitro/nitroso functional groups will also stabilised the filled *p*π orbitals of the nitrogen acid ligands which makes it less available for interaction with the Ir *d*π orbitals in comparison to the chloride anion in **3-1**. This will result in reduced π-basicity of the ligand *trans* to the carbonyl ligand, which strengthens the carbonyl bond. It is therefore likely that a combination of the increased π-accepting and reduced π-donating properties of the nitrogen acids result in the increased in υ(CO) for the Ir(I) carbonyl nitrogen acid complexes.

Complex **3-8** with dinitramide as the ligand has the highest υ(CO) among the new Ir(I) carbonyl nitrogen acid complexes at 1981 cm^{-1}. This is not surprising as dintramide contains two nitro groups. The free acid of dintramide is known to be a very strong acid as the dinitramide anion is a very weak conjugate base from the inductive effect of the nitro groups on the amide nitrogen atom. The N-nitrosulfonamide Ir complex **3-7** has the next highest υ(CO) value at 1977 cm^{-1}. This is followed by N-nitrosocarbamate Ir complex **3-6** and N-nitroamide Ir

complex **3-3** which have similar υ(CO) values and are the next highest after **3-7** and **3-8**. Lastly the N-nitrocarbamates Ir complex **3-4** and **3-5** have the lowest υ(CO) values in the whole series. The observed υ(CO) values gives a general trend of the π-acidic properties of the ligands as shown in Figure 3-11.

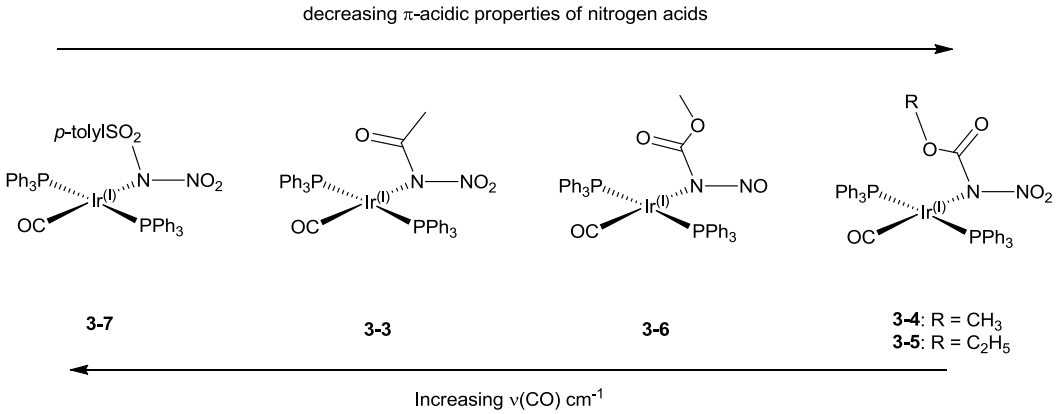

Figure 3-11. General trends of the Ir(I) carbonyl nitrogen acids.

The sulfonamide has greater electron-withdrawing properties than the carboxamide which in turn is stronger than the carbamates. The nitroso group has also greater electron-withdrawing effect than the nitro group from direct comparison between **3-4** and **3-6**.

There have been a few studies of analogues of Vaska's complex where the chloride ligand is substituted for various anionic ligands some of which contain electron withdrawing groups such as fluoride,[161] nitrite,[161a, 162] cyano,[161a] isocyanate,[161a, c, 162] trifluoroacetate,[161c] perchlorates,[146, 163] benzotriazole[164] and even the psuedohalaogen, nitrosodicyanomethanide.[165] In all the examples except for fluoride, the υ(CO) stretch was higher than Vaska complex between 1965 to 1990 cm^{-1}. The fluoride stretch is unexpectedly low at around 1945 to 1957 cm^{-1} depending on the matrix is Nujol or solvent $CHCl_3$.

Vaska's complex adds O_2 reversibly by oxidative addition to give the Ir(III) O_2-complex and the nature of the anionic ligand affects the rate of the oxidative addition of O_2. It has been found that electron-donating anions increase the rate of the addition while electron-withdrawing anions decrease the rate.[147c, 161c] This reactivity is similarly observed for **3-3**, **3-4**, **3-5** and **3-6** where handling solutions of these complexes under aerobic conditions did not result in detectable

formations of the Ir(III) O_2 adducts by ^{31}P NMR, IR spectrooscopy or elemental analysis. However solutions of **3-7** and **3-8** are surprisingly reactive, especially for **3-7**, which rapidly takes up O_2 observed by rapid change in solution colour from yellow to orange and a new band in the IR at 2030 cm^{-1} corresponding to $\upsilon(O_2)$ and a new ^{31}P resonance signal at 3.28 ppm. This is very surprising as these complexes have the two highest υ(CO) values in the series. There may be some evidence of a geometry induced electronic effect that the anionic ligand imposed on the complex that give rise to the observed reactivity as the solid state structures of both **3-7** and **3-8** are shown to have the largest non-linear C(carbonyl)-Ir-N(1) angle at 170.7(2) and 174.5(2)^o respectively (Table 3-3). The increasingly bent C(carbonyl)-Ir-N(1) angle changes the geometry of the Ir complex towards trigonal bypyrimidal and is likely to increase the d_{z^2} orbital (Figure 3-9) or HOMO energy level causing an increase in the reaction coordinate towards oxidative addition of O_2.

The bond lengths (Table 3-3) of the conjugate base of the nitrogen acids in the Ir(I) complexes follow the general trend of the potassium salt of the nitrogen acids in Chapter 2. The N(1)-N(2) bond lengths are shorter and the N(1)-C(1)/S(1) bond lengths are longer in the new Ir(I) complexes when compared to the free acid forms. The N(2)-O(1)/O(2) bond lengths are also longer in the Ir(I) complexes compared to the free acid which is similar to the potassium salts. The O(1)–N(2)–N(1)–C(1) torsion angles for the nitrogen acid ligands have increased deviation from 180^o which implies reduced conjugation between the 'NNO_2/NNO' fragment and the acyl fragment of the ligand. This is structural change is also observed in the potassium salts. An increase in the alkyl chain on the acyl fragment is observed to lead to an increase in the non-planarity.

The Ir-C(carbonyl) and the C(carbonyl)-O bond lengths of the determined solids state structures are inaccurate due to both the truncation effects of the neighbouring heavy Ir atom and the linear form of the CO ligand. Which makes the location of the C(carbonyl) atom inaccurate. Therefore the use of these bond lengths to evaluate the strength of the Ir-CO interaction and the π-backbonding effect is not appropriate. An example would be the very short CO bond length of

3-7 at 1.060(7) Å which is shorter than the measured gas phase CO molecule bond length of 1.127 Å. The ν(CO) stretch measured in the KBr matrix would have minimum effect from the crystal packing due to inversion centers present in the space group determinations of structures. The chiral space group $P2_12_12_1$ for **3-9** has no inversion center and is observed to have a splitting of the ν(CO) band probably derived from the lattice packing.

In general the conformation of the nitrogen acid ligand coordinated to the Ir center exhibits different configuration isomers compared to both the free acid and the potassium salts. In chapter 2 it was mentioned that there are two possible conformations for the N-nitroamides/carbamates, E or Z, and four for the N-nitrosocarbamates (E, E), (E, Z), (Z, E) and (Z, Z). Based on conventions, the E/Z isomerism for ligands coordinated to transition metal complexes may be different from the free acid or the conjugate base anions (Figure 3-12).

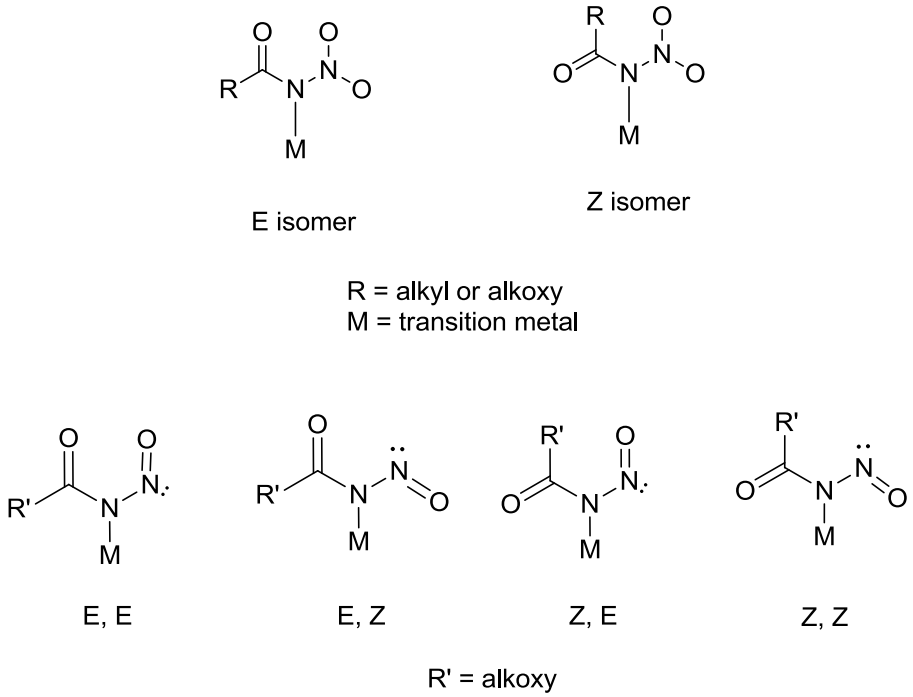

Figure 3-12. Possible configuration isomers for Ir(I) nitrogen acid complexes.

For **3-4** and **3-5**, the nitrogen acid ligand has the E configuration which is similar to both the free acid and the conjugate base potassium salt. For **3-3**, the N-nitroacetamide ligand is observed to adopt the Z configuration which differs from both the free acid and potassium salt. Lastly for **3-6**, the N-

nitrosomethylcarbamate ligand is observed to take up the (Z, Z) configuration while the free acid and conjugate base potassium salt has the (Z, E) configuration.

The solid state structure of **3-8** is observed to have unusual bond parameters of the dinitramide ligand. The first unusual feature is that the two NO_2 groups are non-planar to each other with a deviation approximately 15.8°. The second unusual feature is that there are unsymmetrical N-O bond lengths within the same nitro group! These types of structural features are apparently common for the dinitramide ligand and have been observed in other metal complexes.[154b]

The reaction of **3-1** with $Ag[N(SO_2CF_3)_2]$ gave the unusual bimetallic silver adduct **3-9** which the molecular structure is shown in Figure 3-13.

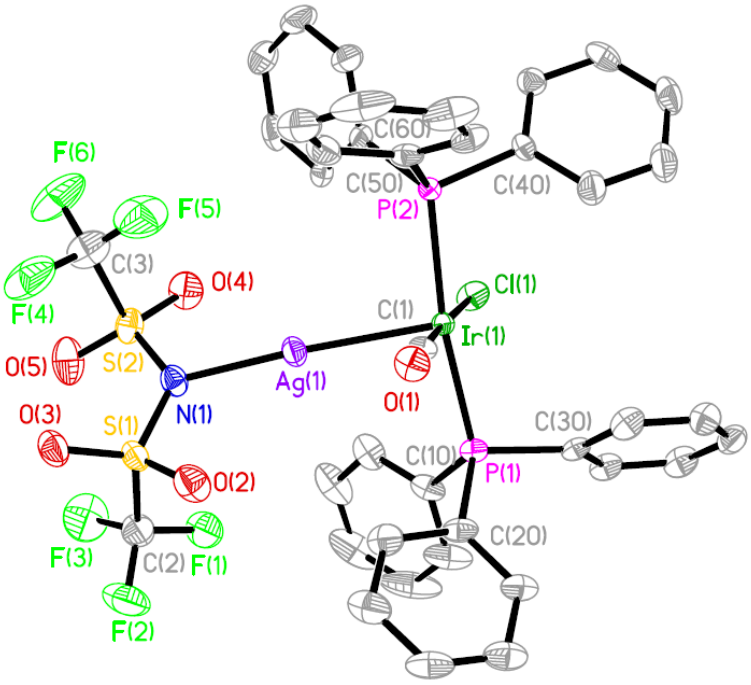

Figure 3-13. Molecular structure of **3-9**. Hydrogen atoms have been omitted for clarity.

The geometry around the Ir center is that of a square pyramidal with the triphenylphosphines, chloride and carbonyl ligands forming the square base and the silver bistriflimide salt in the apical position pyramid. The Ag(1)-Ir(1) bond length is 2.6074(3) Å which indicates some Ir-Ag interaction. The position of the silver cation is along the z-axis of the original Vaska's complex likely due to interaction with the d_{z^2} HOMO orbital.

3.5.1.3 Synthesis of $Ir^{(I)}(CH_3C(O)NNO_2)(N_2)(PPh_3)_2$ (3-10)

Complex **3-3** is treated with *p*-nitrobenzoyl azide to generate *trans*-$Ir^{(I)}(CH_3C(O)NNO_2)(N_2)(PPh_3)_2$, **3-17** (Scheme 3-7).

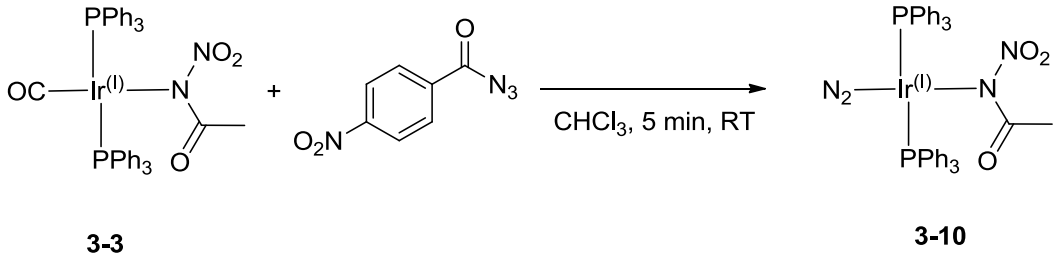

3-3 **3-10**

Scheme 3-7. Synthesis of **3-10**.

The above synthesis is adapted from the reaction of Vaska's complex to generate **3-2**.[148, 157, 166] A new band at 2109 cm^{-1} is observed together with the loss of the band at 1968 cm^{-1} which is assigned to the CO stretch. The new IR band falls in the same region as other M-N_2 complexes and is tentatively assigned to the N_2 ligand. This is further verified by a new ^{31}P resonance signal at 22.93 ppm similar to **3-2** which appears at 22.3 ppm. Bubbling of CO into a chloroform solution of **3-10** regenerates **3-3** with the reappearance of CO stretch at 1965 cm^{-1} and ^{31}P resonance signal at 23.76 ppm. The regeneration of **3-3** from CO addition is similar to the reactivity of **3-2** which regenerates **3-1**.[166] The isolation of **3-10** was however unsuccessful as **3-10** is very soluble under these reaction conditions. Addition of alkanes such as hexanes or pentanes only resulted in the precipitation of the carbamate ester side product (Scheme 3-8). Cooling the reaction mixture to -78 ^{o}C gave a mixture of the carbamate ester and **3-10**.

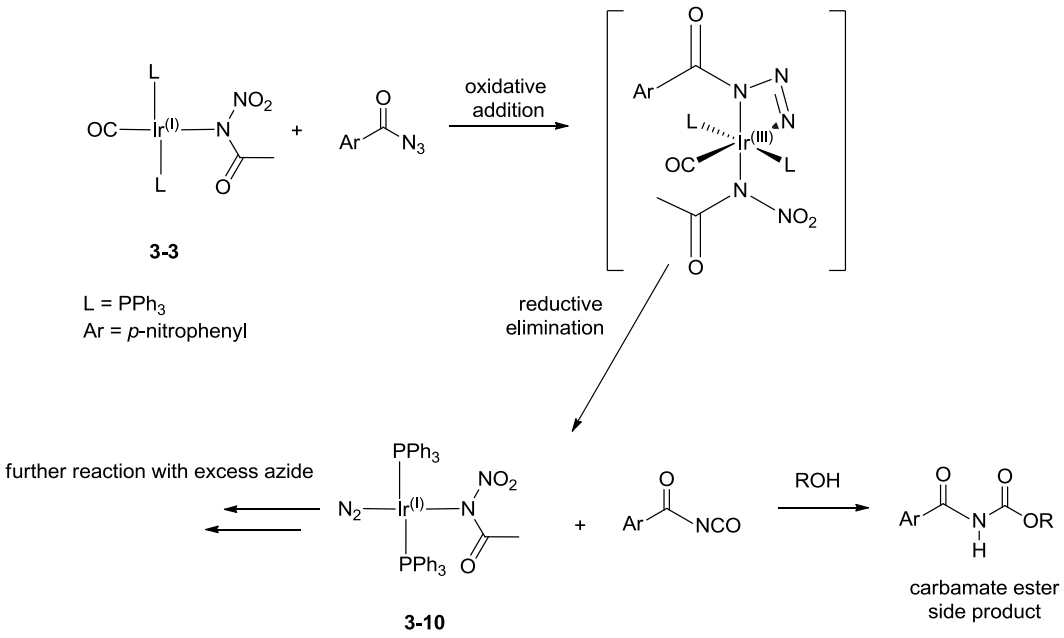

Scheme 3-8. Proposed reaction of **3-3** with *p*-nitrobenzoyl azide.

The Ir(I) N_2 complexes synthesized using the above methodology requires rapid isolation by precipitation from the reaction mixture as further reactions with the excess azide or the carbamate esters generated results in the displacement of the N_2 ligand.[166-167] It is noteworthy that **3-10** is relatively stable in solution even on exposure to air. This is in contrast to the N_2 complexes similar to **3-2**. This phenomenon may be related to the same kinetic stability of **3-3** towards O_2 observed in the previous section.

3.5.2 Ir(III) complexes of N-nitroamides and N-nitrocarbamates

3.5.2.1 Synthesis of Ir(III) complexes of N-nitroamides and N-nitrocarbamates

The N-nitroamides, N-nitrocarbamates, N-nitrosocarbamates and N-nitrosulfonamides are termed nitrogen acids since the amide proton is acidic as demonstrated in Chapter 2. In addition these species are π-accepting due to the delocalized and low energy of their π* orbitals.

Vaska's complex was initially reacted with **2-2** and **2-8** to investigate if this class of acids is able to undergo oxidative addition across the Ir(I) carbonyl complex to generate a new series of Ir(III) complexes containing these unusual nitrogen acid ligands. The reaction mixtures were monitored over time by ^{31}P NMR and show that the reactions were not going to completion with significant amounts of **3-1** remaining after prolonged reaction times even after heating the mixtures to reflux. New ^{31}P NMR singlet signals are observed at 25.01 and -1.17 ppm. In the ^{1}H NMR, a triplet at -15.39 ppm corresponding to Ir hydride and a singlet at 1.25 ppm for the CH_3 group of the coordinated ligand are observed. When more **2-2** is added, the spectrum became more complicated by the appearance of multiple new resonances. We believe that some extent of oxidative addition occurred, but the newly formed Ir(III) carbonyl complexes are unstable and undergo various reductive elimination and rearrangements to give the starting ligands and other products. The implication for the above observations is that the reaction could be reversible or in equilibrium initially and with additional stoichiometry of **2-2** leads to product inhibition from the formation of small amounts of base derived from some decomposition of **2-2**. The reaction of **3-1** with **2-8** was similar to **2-2** where three sets of singlet resonances at 6.78, -1.25 and -12.67 ppm were observed in ^{31}P NMR in addition to **3-1**. The ^{1}H NMR spectrum was observed to give three sets of Ir hydride triplet with resonances at -21.04, -15.36 and -13.25 ppm. Overtime, the ^{31}P NMR spectrum became more complicated with the

addition of multiple new signals and the ^{1}H NMR was observed to have only a single low intensity Ir hydride triplet at -15.34 ppm.

The conclusion of the above observations indicates that the N-nitroamide **2-2** and N-nitrosulfonamide **2-8** have *p*Ka values lower than the mineral acids such as HCl. The reason is that it has been established that the extent of oxidative addition of an acid to **3-1** is related to the strength of the acid (*p*Ka) or the coordinating ability of the conjugate base.[168] In comparison with the strong organic acids such as trifluoroacetic acid and pentadifluoropropionic acid, **2-2** and **2-8** have similar acid strength as the fluoroalkyl acids react reversibly with **3-1** to give multiple isomers[147d] as observed in **2-8** and to a lesser extent **2-2**. Therefore with the above results we can come to the conclusion that the *p*Ka value of **2-8** is less than that of **2-2**. Complex **3-2** and **3-1** have similar reactivity and **3-2** is able to undergo similar oxidative addition reactions with acids. The N_2 ligand is labile which makes **3-2** more reactive. The disadvantage of **3-2** is that it is metastable in solution such as $CHCl_3$ over time and easily decomposes when exposed to air in solution.

The nitrogen acids N-nitroamides **2-2**, **2-3**, N-nitrocarbamates **2-4** and **2-5** were reacted with **3-2** (Scheme 3-9).

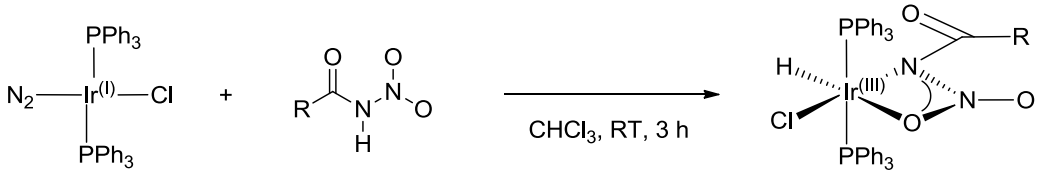

R	Compound
CH_3	**2-2**
C_2H_5	**2-3**
CH_3O	**2-4**
C_2H_5O	**2-5**

R	Complex
CH_3	**3-11**
C_2H_5	**3-12**
CH_3O	**3-13**
C_2H_5O	**3-14**

Scheme 3-9. Reaction of **3-2** with N-nitroamides and N-nitrocarbamates.

In all of the above reactions, vigorous evolution of gas was observed during the start of the reaction which is most likely from the loss of N_2. The reaction mixture was stirred at room temperature over 3 h during which the colour turned from a

deep yellow to pale yellow. This corresponds to the formation of an Ir(III) species which has a larger d-d transition energy shifting the absorbance to the UV region. The successful reaction of **3-2** with the N-nitroamides/carbamates differs from that of **3-1** with the same ligands because the loss of the labile N_2 ligand facilitates the bidentate coordination of the nitrogen acids which is not possible for the carbonyl complex. In addition, during the course of the reaction, reaction intermediates are observed in the ^{31}P and ^{1}H NMR spectra which will be discussed later.

Similar reactions of **3-2** with N-nitrosocarbamate **2-6** and N-nitrosulfonamide **2-8** were also carried out (Scheme 3-10).

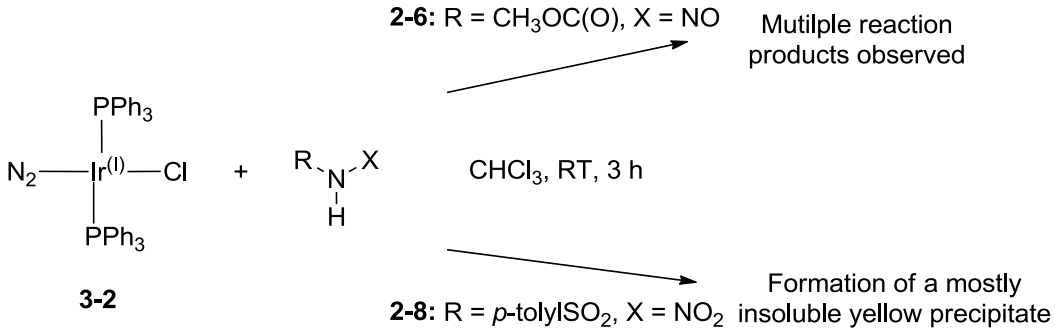

Scheme 3-10. Reaction of **3-2** with **2-6** and **2-8**.

The same observation of a gas evolution was also noted in the above reactions which most likely correspond to the loss of the N_2 ligand. For the reaction with **2-6** however, multiple product resonances were observed in the ^{31}P NMR over the course of the reaction. For the reaction with **2-8**, slow precipitation of a yellow precipitate appears over time. The recrystallization of this yellow precipitate was not possible as it is insoluble in most solvents other than strongly coordinating solvents such as pyridine and DMSO. The reaction monitoring details for the synthesis of these Ir(III) complexes will be discussed in the next section.

The change of solvent from $CHCl_3$ to benzene causes the reaction of **3-2** with **2-2**, **2-3** and **2-4** to be slower such that longer reaction times are required for the reaction to be complete. Therefore it is very likely that polar solvents are more favourable for the oxidative addition step due to their ability to stabilized charged or highly polar intermediates.

3.5.2.2 Crystallographic, spectroscopic properties

Crystallographic and molecular structural discussion

The molecular structures of **3-11**, **3-12** and **3-13** are shown in Figure 3-14, Figure 3-15 and Figure 3-16 respectively. In all of the three examples, the new Ir (III) complexes have a distorted octahedral geometry with the triphenylphosphines trans to each other. The Ir(III) complexes are shown to have an unexpected bidentate coordination of the N-nitroamide/carbamate conjugate base through the nitrogen on the amide functionality and the oxygen of the nitro group. The nitrogen acid conjugate bases form a four-membered Ir-N-N-O chelate ring. The chloride ligand is positioned trans to the N atom of the amide group with Cl(1)-Ir(1)-N(1) = 172.6(1)^{o} for **3-11**. The metal hydride derived from the oxidative addition is not located by the diffraction model, but inferred from spectroscopic means as discussed below and it is located trans to the oxygen atom of the nitro group. Large crystals and neutron diffraction experiments are required to unambiguously locate metal hydrides.

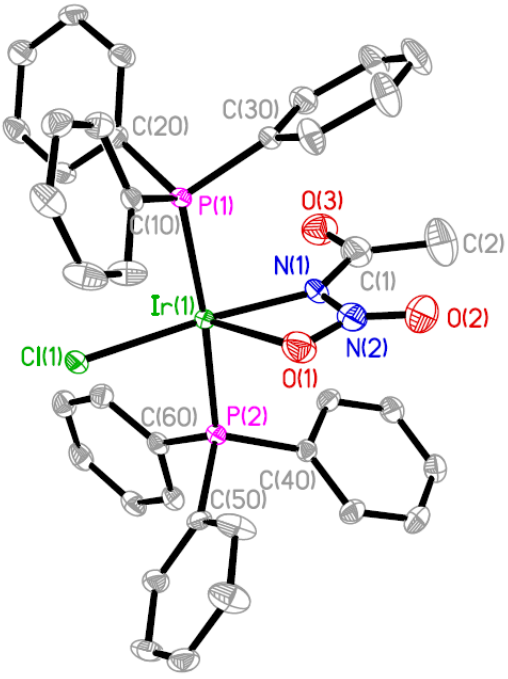

Figure 3-14. Molecular structure of **3-11**. Hydrogen atoms and solvent molecules have been omitted for clarity.

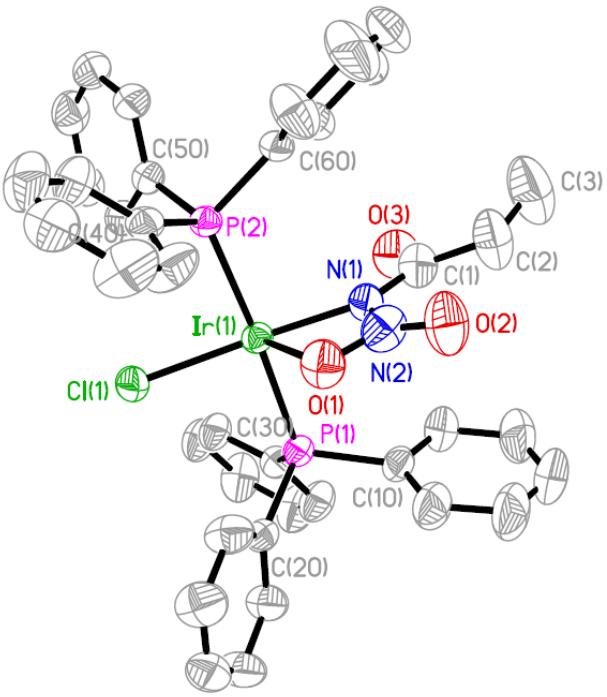

Figure 3-15. Molecular structure of **3-12**. Hydrogen atoms and solvent molecules have been omitted for clarity.

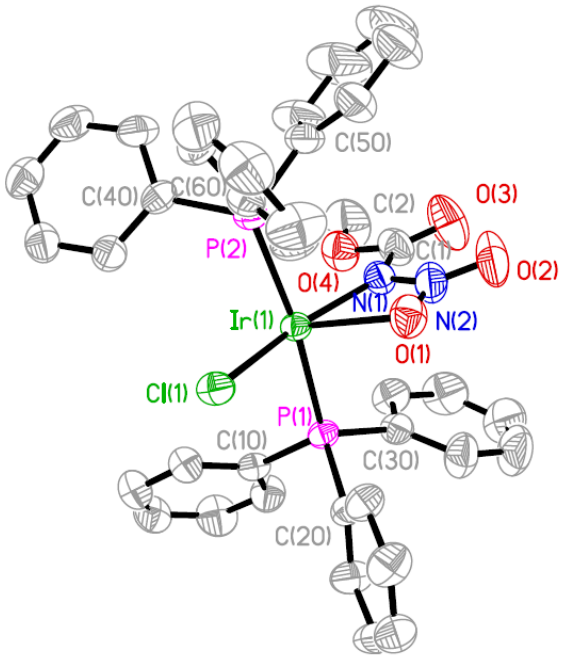

Figure 3-16. Molecular structure of **3-13**. Hydrogen atoms and solvent molecules have been omitted for clarity.

The most interesting aspect of the solids state structures for the complexes is that one of the oxygen atoms of the nitro group out-competes the acyl oxygen that is present in **3-11** and **3-12** as well as an additional methoxy subsituent in **3-13** for coordination to the Ir center. When considering the alkyl and alkoxy group as a single entity, there are six possible bidentate coordination isomers with trans PPh_3 which arises from firstly the N-O/O-O chelate, secondly, the position of nitrogen/oxygen atom trans to the metal hydride and lastly the oxygen atom of the nitro/acyl group that is bound to the Ir center (Figure 3-17).

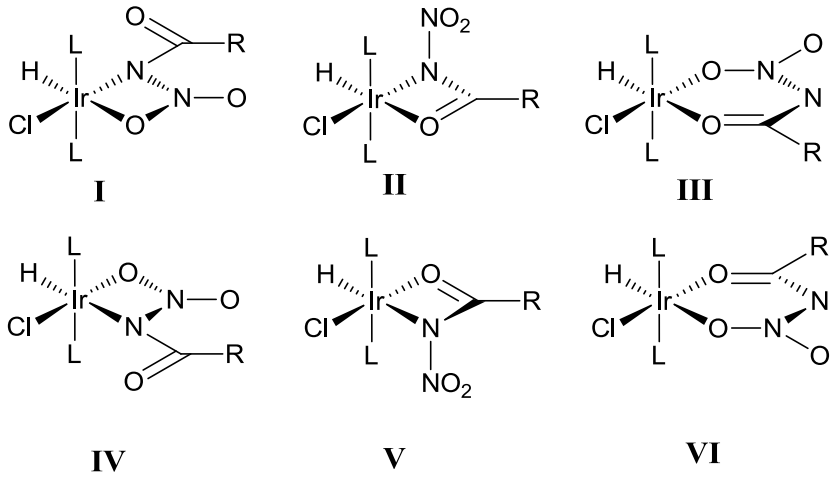

Figure 3-17. Possible coordination isomers of the Ir(III) complexes.

For **3-13**, the oxygen of the alkoxy group can also coordinate to the Ir center producing four additional possible isomers. The observed mode of coordination is unique for a couple of reasons. The first is that the oxygen on the acyl functionality is not the preferred coordinating site to the Ir center. There are substantially greater numbers of cases of acyl group coordination e.g. metal-acetylacetonyl ligands (acac) compared to nitro group coordination as there are only a few examples where nitro groups coordinate to transition metal center. Within these reports the nitro group coordination is through the oxygen of the nitro group.[169] Even in examples where nitro groups are present in the ligands, the preferred coordination to the metal centers is through other functional groups.[169a, 170] The second reason is that between a four or six-membered cyclic structure that can be adopted by the bidentate coordination, a six-membered

chelate is usually more favourable. The new Ir(III) complexes however adopts the four-membered chelate ring.

Another type of isomerism that is encountered between the Ir(III) complexes involves the nitrogen acid ligands. In chapter 2 and the Ir(I) complexes section, it was mentioned that there are two possible conformations for the N-nitroamides/carbamates, E or Z. Based on conventions, the E/Z isomerism for ligands coordinated to transition metal complexes may be different from the free acid or the anionic salts (Figure 3-18).

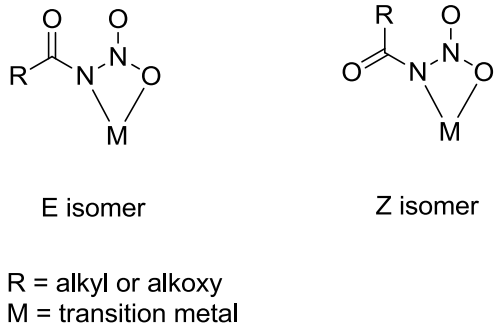

Figure 3-18. E/Z isomers of nitrogen acids ligand coordinated to transition metal.

For **3-11** and **3-12**, the N-nitroamide conjugate base is observed to be the Z isomer while for **3-13** the ligand conformation is the E isomer. The conformation of the N-nitroamide ligands in **3-11** and **3-12** differs from that of the free acid **2-2**, **2-3** respectively and the potassium salt **2-2K**. For the N-nitrocarbamate ligand in **3-13**, the conformation is the same as the free acid **2-4** and the potassium salt **2-4K**.

The selected structural data for **3-11**, **3-12** and **3-13** are shown in Table 3-4. The Ir(1)-N(1) bond length for all three complexes are approximately 2.04 Å which corresponds to a regular Ir-N single bond. The Ir(1)-O(1) bond lengths of the three complexes are more than 2.33 Å which is longer than most Ir-O single bonds and indicates a weak Ir-O bond. The reason for the observed structural feature may be due to the trans influence of the hydride ligand.[171] The N(1)-N(2) bond lengths of **3-11** and **3-13** decreased on coordination to the Ir center, similar to the Ir(I) complexes, in comparison to the free acid **2-2** and **2-4** while to a smaller extent when compared to the potassium salts **2-2K** and **2-4K**. For **3-12**,

the N(1)-N(2) bond length is almost similar to that of **2-3**. The N(1)-C(1) bond lengths of **3-11** and **3-13** both increased which differs significantly from **2-2K** and **2-4K** where there is an actual decrease in the bond lengths compared to **2-2** and **2-4**. For **3-12** a reverse in the trend is observed as the N(1)-C(1) bond length actually decreases compared to **2-3**. For the Ir(I) complexes, the increase in N-C bond length is also seen in **3-3**, but for **3-4**, the trend is reversed. It is very likely that the N-C bond lengths are subtly affected by the ligand trans to the nitrogen acids. In the Ir(I) complexes, the π accepting carbonyl ligand may play a role modulating the N-C bond changes between the N-nitroamide versus the N-nitrocarbamate. For the Ir(III) complexes, the Cl ligand will have a more direct σ interaction which accounts for the less variable N-C bond lengths across the series.

Table 3-4: Selected bond lengths (Å), bond and torsion angles (deg) of $Ir^{(III)}(\eta^2\text{-}X)(H)(Cl)(PPh_3)_2$ complexes.

Compound	**3-11**	**3-12**	**3-13**
Ir(1) – N(1)	2.030(3)	2.042(4)	2.050(3)
Ir(1) – O(1)	2.329(3)	2.357(4)	2.323(3)
N(1) – N(2)	1.372(5)	1.389(6)	1.349(4)
N(1) – C(1)	1.398(6)	1.372(7)	1.405(5)
N(2) – O(1)	1.287(5)	1.298(6)	1.275(4)
N(2) – O(2)	1.199(5)	1.193(6)	1.223(4)
O(1) – Ir(1) – N(1)	59.26(12)	59.38(16)	58.80(11)
Ir(1) – N(1) – N(2)	101.2(2)	101.3(3)	100.4(2)
N(1) – N(2) –O(1)	109.4(3)	109.6(4)	110.8(3)
N(2) – O(1) – Ir(1)	90.1(2)	89.7(3)	89.97(19)
O(1) – N(2) – N(1) – C(1)	173.7(4)	-179.9(5)	178.3(4)
O(3) – C(1) – N(1) – N(2)	-174.3(4)	173.3(5)	-1.2(7)

The N-O bond lengths in **3-11**, **3-12** and **3-13** differ significantly between the N(2)-O(1) coordinated versus the N(2)-O(2) free by at least 0.5 Å. This shows that on coordination, the N-O bond is weakened. The bite angle of the Ir-N(1)-N(2)-O(1) chelate is only approximately 60^{o} which is very acute compared to other five or six-membered rings. Lastly the torsion angles of the ligand between the nitro fragment and the amide/carbamate section of the ligand is close to 180^{o} indicating planarity between the two sections of the ligand. The increase in the alkyl group length for N-nitroamides in **3-11** to **3-12** seems to have no effect in decreasing the conjugation between the nitro group and the amide section while for the N-nitrocarbamates in the Ir(I) complexes, the increase in the alkoxy group in **3-4** to **3-5** reduces the conjugation of nitro fragment with the carbamate section as the torsion angles in **3-5** diverge from 180^{o}.

NMR spectroscopy

The ^{31}P NMR spectroscopy of the Ir(III) complexes all show a single resonance signal which corresponds to a single isomer in solution. With the default NMR parameters, the resonance usually appears as a doublet with a separation of 4 to 10 Hz. The appearance of the coupling is due to the coupling of the Ir hydride (Ir-H) to the phosphorus ligand through the Ir metal. This is uncommon as the default ^{31}P NMR operates as $^{31}P\{^{1}H\}$ NMR where the proton signals are decoupled by saturation through broadband decoupling. In our situation, the location of the Ir hydride is at substantially upfield regions and requires an adjustment of either the power of the decoupler or re-centering of the decoupler offset to decouple the Ir hydride efficiently.

In the ^{1}H NMR spectrum, the resonance signals for the triphenylphosphine ligands are located as two sets of multiplets between 6.7 to 8 ppm. The alkyl and alkoxy groups are also located upfield compared to the free acid. The Ir hydride resonance is located between -30 to -40 ppm and appears as a broad signal in $CDCl_3$ for **3-11** but as triplets for **3-12**, **3-13** and **3-14**. The observation of the Ir-H resonance signal confirms the presence of a metal hydride which is not located in the X-ray diffraction experiments. However the appearance of a broad signal for

the Ir-H resonance in **3-11** is unexpected. A broad signal is usually due to some dynamic processes that are happening to the substrates in solution. In the case of **3-11**, the dynamic process is solvent dependent (Figure 3-19).

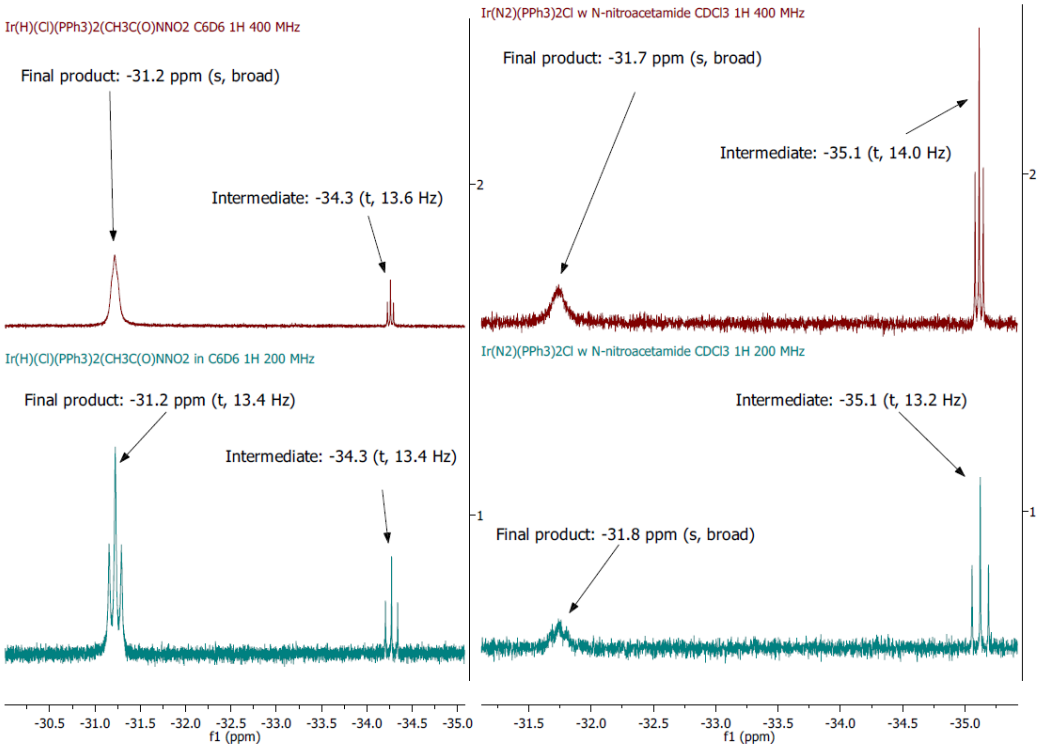

Figure 3-19. Variable field ^{1}H NMR in C_6D_6 (left) and $CDCl_3$ (right) for Ir-H region of **3-11**.

In $CDCl_3$, at the effective field of 200 MHz, the Ir hydride signal is very broad, but this sharpens slightly when the effective field is increased to 400 MHz. When C_6D_6 is used instead, the Ir hydride signal is observed to be a triplet at the effective field of 200 MHz. When the effective field is increased to 400 MHz, the same signal is now observed as a broad signal. The difference in the Ir hydride resonance signals is related to the rate of the dynamic process with respect to the NMR time scale. From Equation 3-1, when the exchange ratio $R >> \Delta\nu_0$, the system is in the fast exchange regime while when $R << \Delta\nu_0$, the system is in the slow exchange regime. Therefore the triplet signal that is observed in the C_6D_6 200 MHz spectrum could either be at the fast exchange limit or the slow exchange limit.

$R = k/\Delta\nu_0$

k = total rate constant (s^{-1})

$\Delta\nu_0$ = difference in frequency between two exchanging signals (Hz)

Equation 3-1. Exchange ratio R.

By increasing the effective field of the ^1H NMR, we are increasing $\Delta\nu_0$ of the dynamic process. Since the total rate constant k is unchanged, the exchange ratio R will be decreased which leads to a smaller difference between R and $\Delta\nu_0$. If the dynamic process observed is at the fast exchange regime, a decrease in the R value and increase in the $\Delta\nu_0$ value may cause it to fall towards the coalescence point or into the slow regime which will result in a change in the line-shape of the resonance that is observed. If the dynamic process is in the slow exchange regime, there will be no change in the line-shape of the resonance signal. From Equation 3-2, as the effective field is increased, $\Delta\nu_0$ is increased which leads to a larger k_c. This causes the coalescence temperature of the dynamic process to increase.

$k_c = [\pi[2(\Delta\nu_0)^2]^{1/2}$

k_c = total rate constant at coalescence

Equation 3-2. Total rate constant k at coalescence.

The increase in the coalescence temperature for a higher effective field NMR together with the change in line-shape from triplet to broad resonance means that in C_6D_6 the dynamic process observed is at the fast exchange limit. In $CDCl_3$, the dynamic process is also at the fast exchange limit and at the lower effective field of 200 MHz NMR, is closer to the coalescence temperature which gives a broader signal that broadens as the effective field is increased. The additional metal hydride resonance that is located further upfield at around -35 ppm in Figure 3-19 is a separate species that is not interacting with the product resonance at -30 ppm as the resonance signals broaden and resolve independently. This upfield resonance is assigned to an intermediate that will be discussed in later sections.

From the collective Ir hydride resonances observed for **3-11**, **3-12**, **3-13** and **3-14**, it is very likely that an increase in the alkyl chain length or change to an alkoxy chain length causes the rate of the dynamic process to increase such that all the triplet resonances observed are actually in the fast exchange region. This is

supported to some extent since the Ir hydride resonance signal in **3-12** is close to being a broad signal. Low temperature ^{1}H experiment for these substrates may provide a definitive answer to the above question.

Since the broad resonance is observed for the Ir hydride and not in the other proton resonance nor in the ^{31}P NMR, it is very likely that the dynamic process affects the Ir-H environment. We proposed that this dynamic process is due to the labile O atom coordination trans to the hydride (Scheme 3-11). The reason for such a phenomenon could be due to the strong trans effect of the hydride ligand.[171]

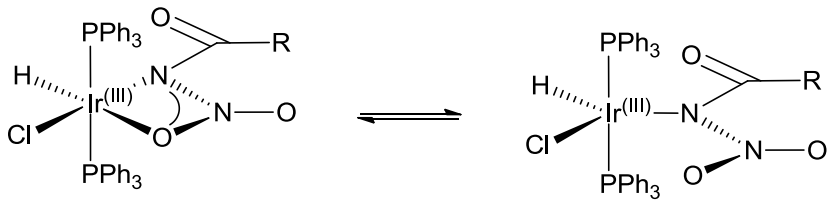

Scheme 3-11. Proposed labile coordination of O atom to Ir center.

The repeated coordination and dissociation of the O atom trans to the Ir hydride will cause the hydride to 'see' both forms of the complexes, giving rise to the broad signal.

The related Ir(III) carboxylate complex synthesized from the reaction of **3-2** with acetic acid is proposed to give a similar bidentate ligand (Scheme 3-12).[172]

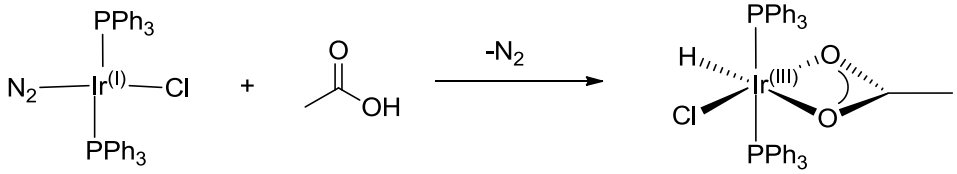

3-2 **3-22**

Scheme 3-12. Synthesis of Ir(III) acetate complex **3-22**.

Complex **3-22** is formed from the oxidative addition of acetic acid with **3-2**. It is reported that the ν(Ir-H) stretch is observed at 2304 cm^{-1} and the IR bands at 1535, 1445, 1423 and 1412 cm^{-1} are from a coordinated bidentate carboxylate vibrations. The complex is characterized only by IR and elemental analysis. By repeating the synthesis of **3-22**, it is confirmed that a ν(Ir-H) band is observed at 2307 cm^{-1} with similar bands at 1538, 1417 and 1189 cm^{-1} corresponding to the

acetate ligand. The ^{31}P NMR spectrum of **3-22** shows a single singlet resonance signal at 13.98 ppm which indicates a single species is present. The ^{1}H NMR spectrum of **3-22** shows resonances in the aromatic region between 7.30 and 7.80 ppm for the triphenylphosphine, 1.25 ppm for the methyl group and a well-resolved triplet with J_{P-H} of 13.8 Hz at -33.15 ppm. The Ir hydride signal observed in **3-22** is in great contrast with that of **3-11** and provides more evidence for the dynamic behavior of **3-11** in solution.

Vibrational Spectroscopy

The vibrational spectra of **3-11**, **3-12** and **3-13** have unusual bands associated with the coordinated ligand. Of great interest is the low intensity Ir-H stretch for **3-11** and **3-12** at 2322 and 2311 cm^{-1}. For **3-13** a weak band is observed at 2298 cm^{-1} and is assigned to ν(Ir-H). A possible reason for the very low intensity ν(Ir-H) band could be that the stretch is strongly coupled to the coordinated nitrogen acid. It could also be that there is great thermal motion of this hydride such that the stretching band is almost non-existent. There is however a medium intensity band observed around 805 cm^{-1} in **3-11**, **3-12** and **3-13** which can be assigned to the ν(Ir-H) bending mode. For **3-11** and **3-12** the new bands observed are at 1690 cm^{-1} for the Amide 1 band, 1509 cm^{-1} for $\upsilon(NO_2)_{asym}$, 1220 to 1261 cm^{-1} for $\upsilon(NO_2)_{sym}$ and 1160 to 1200 cm^{-1} for υ(N-N).

For the N-nitrocarbamate complexes, **3-13** and **3-14** new bands are observed at 1750 cm^{-1} for the Amide 1 band, 1518 cm^{-1} for $\upsilon(NO_2)_{asym}$, 1260 cm^{-1} for $\upsilon(NO_2)_{sym}$ and 1212 to 1185 cm^{-1} for υ(N-N).

3.5.2.3 Reaction intermediates

In the course of **3-2** reaction with **2-2**, a reaction intermediate is observed to form initially which slowly converts into the final product. This intermediate can be observed using ^{31}P (Figure 3-20), ^{1}H NMR (Figure 3-21) and IR (Figure 3-22) spectroscopy techniques.

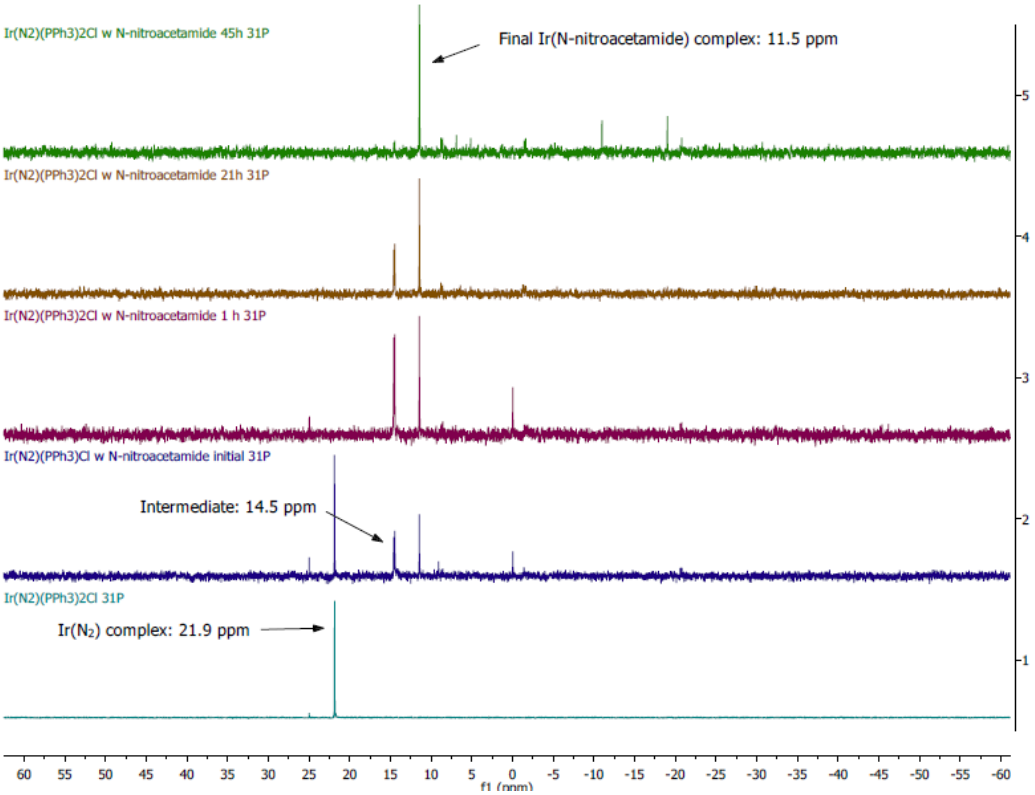

Figure 3-20. ^{31}P NMR reaction monitoring of **3-2** with **2-2** in $CDCl_3$.

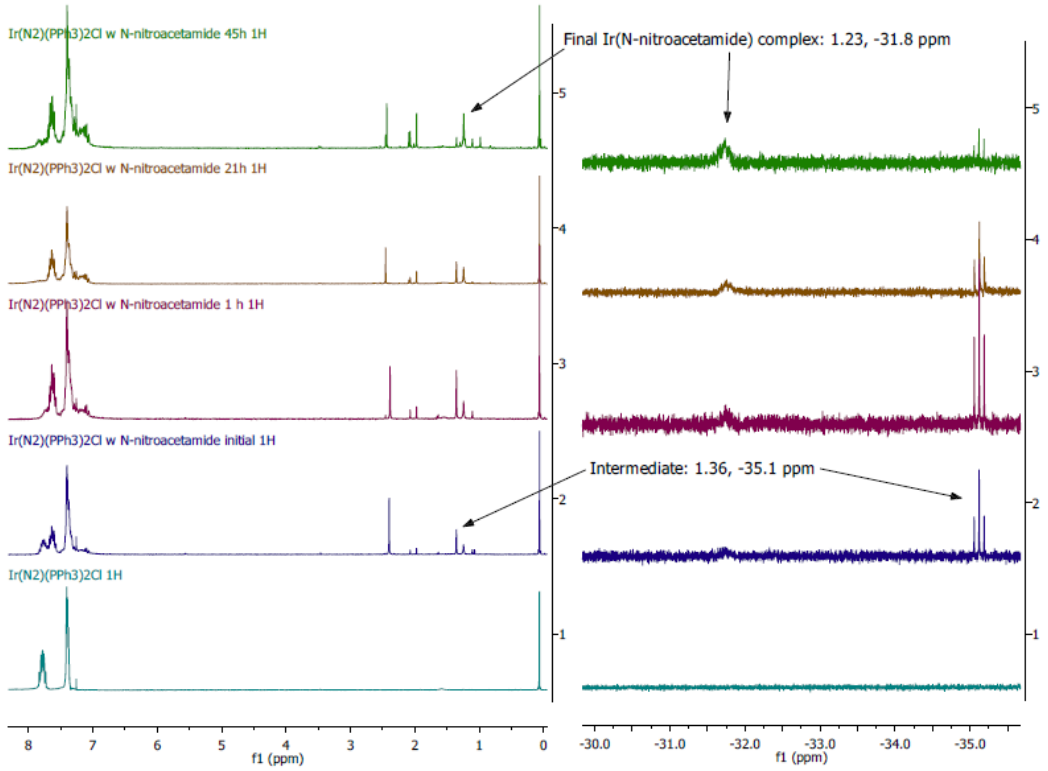

Figure 3-21. ^{1}H NMR reaction monitoring of **3-2** with **2-2** in $CDCl_3$.

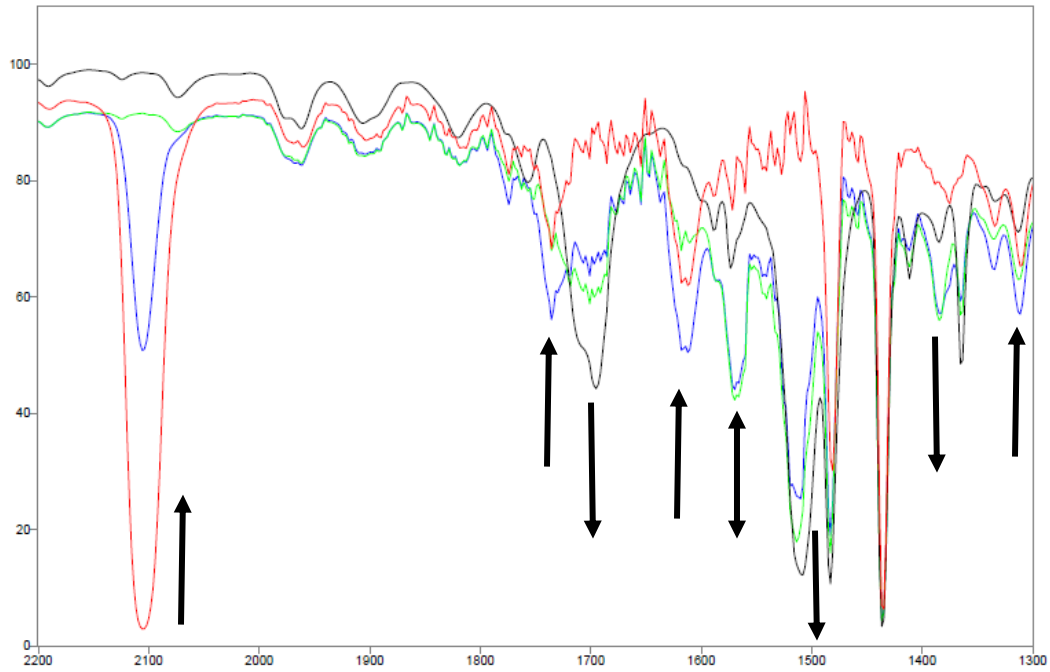

Figure 3-22. Solution IR spectra for the reaction of **3-2** with **2-2** between 2200 to 1300 cm^{-1}. Reaction carried out at -10 ^{o}C in $CHCl_3$ over 24 h. Aliquots taken at the following time intervals: Red: Initial **3-2** complex immediately after addition of **2-2**; Blue: after 15 min; Green: after 1.5 h; Black: after 17 h.

In ^{31}P NMR, a resonance signal at 14.5 ppm is observed to form initially together with the resonance signal at 11.5 ppm. The 14.5 ppm signal increases and subsequently decreases over time to give only the signal at 11.5 ppm. Thus the signal at 14.5 ppm corresponds to an intermediate that slowly converts to **3-11** with the resonance at 11.5 ppm. The similar trend is also observed in the ^{1}H NMR where the resonance signals at 1.36 and -35.1 ppm assigned to the intermediate are observed to increase and subsequently decrease to resonance signals at 1.23 and -31.8 ppm observed in **3-11**.

The multiple solution IR spectra of the reaction mixture over time gave the most information regarding the functional group changes taking place over time. It is shown that the band at 2104 cm^{-1} corresponding to the N_2 band in **3-2** disappears which indicates the loss of N_2 ligand. Similar bands at 1736 and 1610 cm^{-1} which belongs to **2-2** and a band near 1300 cm^{-1} are also observed to decrease overtime. The band at 1570 cm^{-1} is observed to increase initially but decrease over the course of the reaction. Finally bands at 1695, 1510 and 1360 cm^{-1} are observed to increase over time. These bands correspond to the bands in **3-11**.

The conclusion of the observed vibrational changes above is that the band at 1570 cm^{-1} most likely corresponds to the intermediate that is observed in the ^{31}P and ^{1}H NMR spectra. Comparing the IR bands in some carboxamide complexes[173] and the related Ir(III) carboxylate complexes,[172] the 1570 cm^{-1} band can be assigned to a coordinated acyl ligand. Thus a mechanism involving initially an acyl intermediate, **3-23A** or **3-23B**, can be proposed which subsequently isomerises to the thermodynamically stable **3-11** (Scheme 3-13). The ^{31}P NMR resonance signal of **3-22** at 13.97 ppm is also very close to that of the intermediate **3-23** at 14.56 ppm.

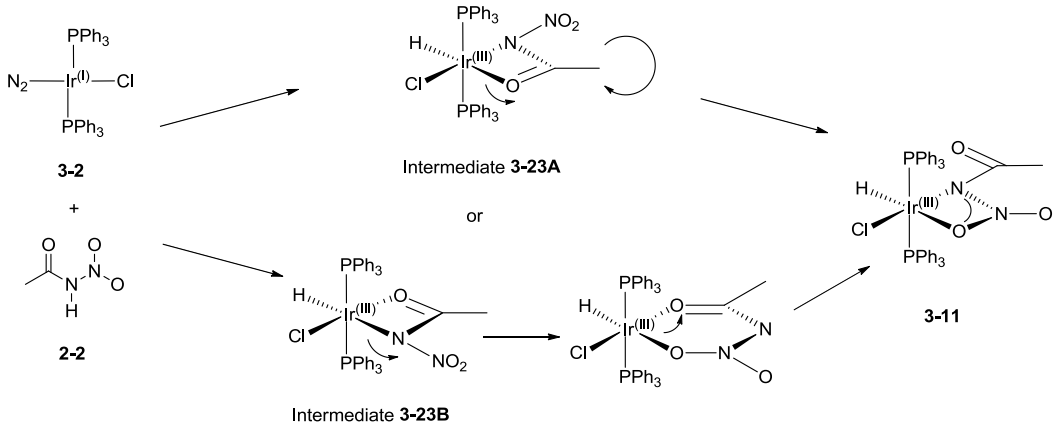

Scheme 3-13. Proposed reaction mechanism of **3-2** with **2-2** to form initially intermediate **3-23** to finally give **3-11**.

The difference in the intermediates **3-23A** and **3-23B** is that the nitrogen is trans to the chloride ligand in **3-23A** and trans to the Ir hydride in **3-23B**. For intermediate **3-23A**, a dissociation followed by rotation around the Ir –N bond would generate **3-11**. For intermediate **3-23B**, the stepwise dissociation of the Ir-N bond followed by formation of a six-membered metallacycle and subsequent dissociation of the the Ir-O(acyl) bond would give **3-11**. Without more information it would be difficult to determine which of the intermediates is more plausible.

The reaction of **3-2** with **2-4** has also been monitored by ^{31}P NMR (Figure 3-23), ^{1}H NMR (Figure 3-24) and IR spectroscopy (Figure 3-25) and reveals a possible formation of two intermediates which eventually converts to the product **3-13**.

The ^{31}P NMR is observed to show two intermediates; A at 14.4 ppm and B at 7.5 ppm with intermediate B in greater proportion. Both these intermediates are observed to disappear within 3 h to give **3-13** which has the resonance signal at 10.0 ppm. Similarly in ^{1}H NMR resonances corresponding to the intermediates are observed; A at 3.4 and -36.7 ppm and B at 3.6 and -26.0 ppm with B in greater proportion. These resonances disappear over time to give resonance signals at 3.0 and 35.7 which is assigned to **3-13**.

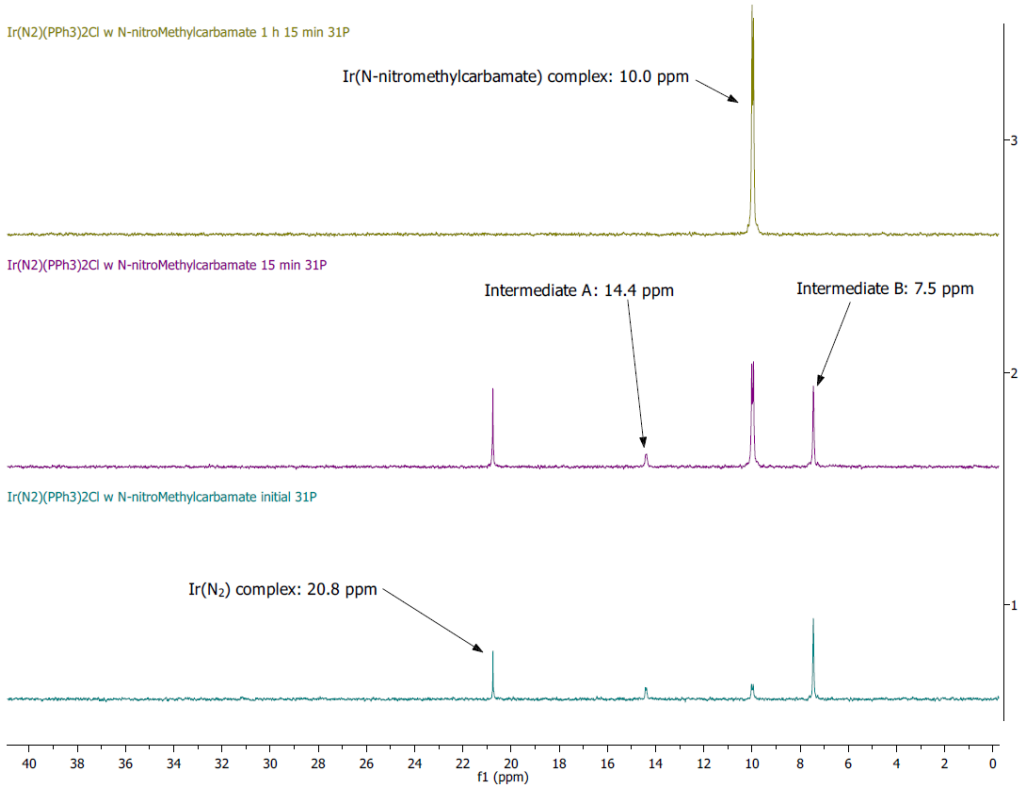

Figure 3-23. ^{31}P NMR reaction monitoring of **3-2** with **2-4** in $CDCl_3$.

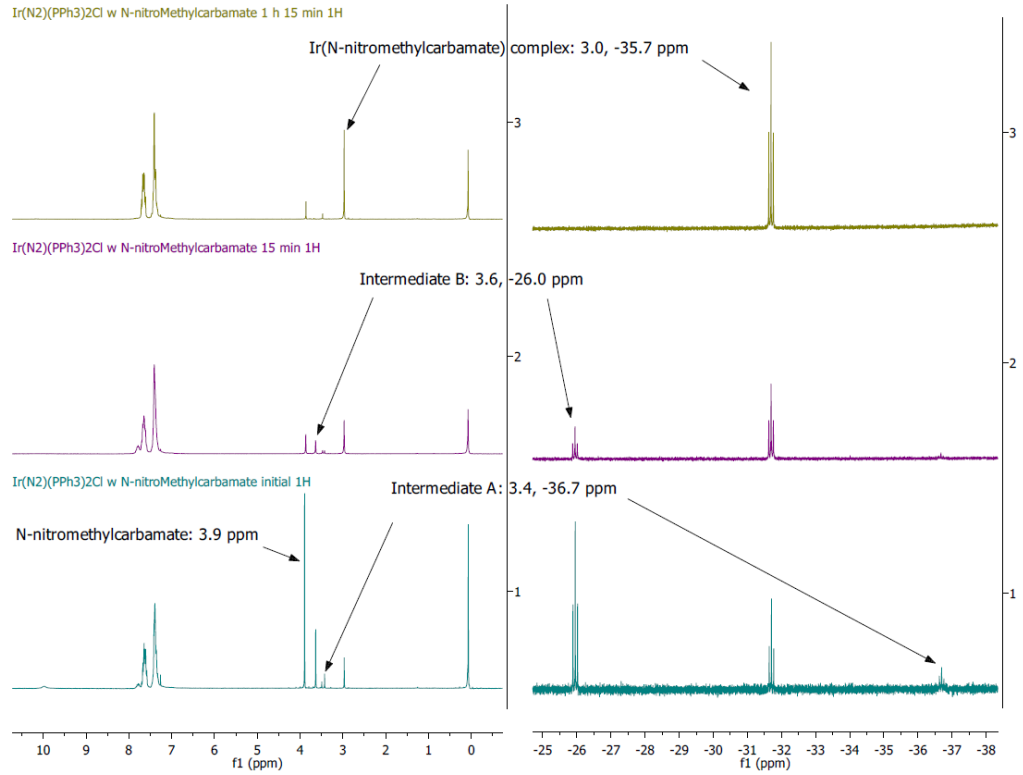

Figure 3-24. ^{1}H NMR reaction monitoring of **3-2** with **2-4** in $CDCl_3$.

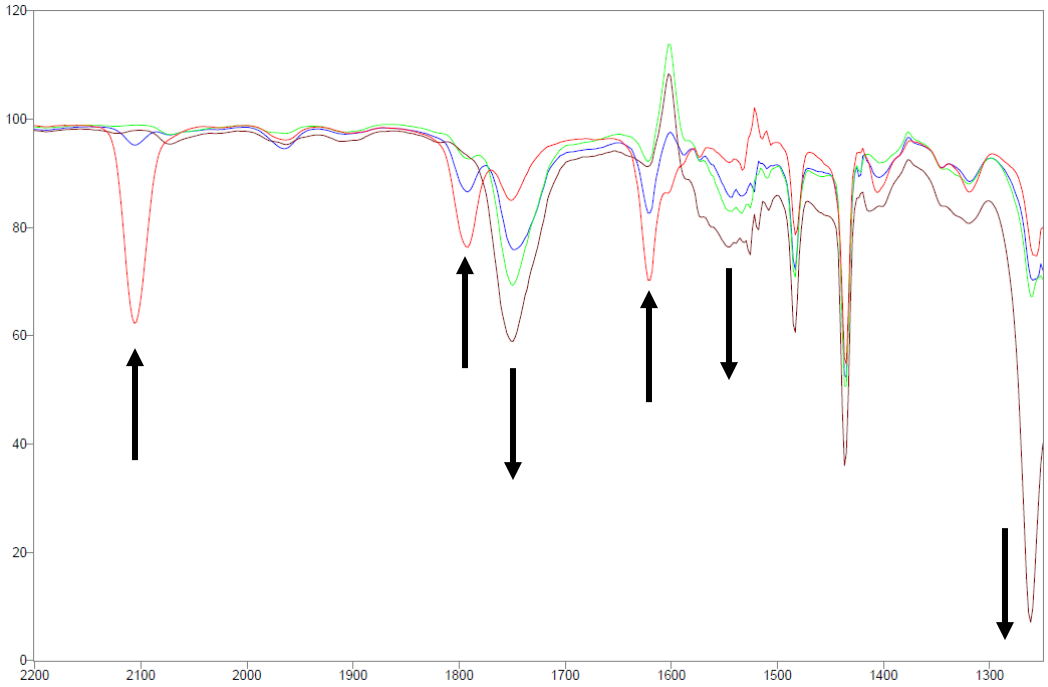

Figure 3-25. Solution IR spectra for the reaction of **3-2** with **2-4**. Reaction carried out at -10 ^{o}C in $CHCl_3$ over 21 h. Aliquots taken at the following time intervals: Red: Initial **3-2** complex with **2-4**; Blue: 45 min after addition of **2-4**; Green: after 3 h; Brown after 21 h.

The solution IR monitoring formation of **3-13** reveals some similar changes observed in the synthesis of **3-11**. The decrease of the 2104 cm^{-1} band of the starting N_2 ligand with concurrent decrease in the 1790 and 1620 cm^{-1} bands are assigned to **2-4**. The increase in the bands at 1750 and 1260 cm^{-1} and the general increase in the bands between 1570 and 1500 cm^{-1} are due to the formation of **3-13**. In this case, no initial increase and subsequent decrease and loss of any bands could be observed. A possible reason is that the rate of reaction of **3-2** with **2-4** is much more rapid than that of **3-2** with **2-2**. This is shown by the rapid loss of the 2104 cm^{-1} band and the overall time scale of the transformations. In the reaction of **3-2** with **2-2**, the reaction time monitored in NMR is over 24 h long while that for **3-2** with **2-4** is observed to be complete within 2 h! Thus despite starting the solution IR experiment at -10 ^{o}C, the rate of conversion between the intermediates to **3-13** was too rapid for observation.

The ^{31}P NMR resonance signal for intermediate A has similar chemical shift to intermediate **3-23** observed in the system of **3-11**. It is probable that these

intermediates are similar. The new intermediate B that is observed could be another coordination isomer of **3-13** that forms kinetically but converts into the thermodynamically stable **3-13**. This intermediate B is also the preferred kinetic product in this reaction from the larger proportions present during the reaction period. It is not known if intermediates A and B interconvert between them to give **3-13**. A proposed mechanism of the synthesis of **3-13** is shown in Scheme 3-14.

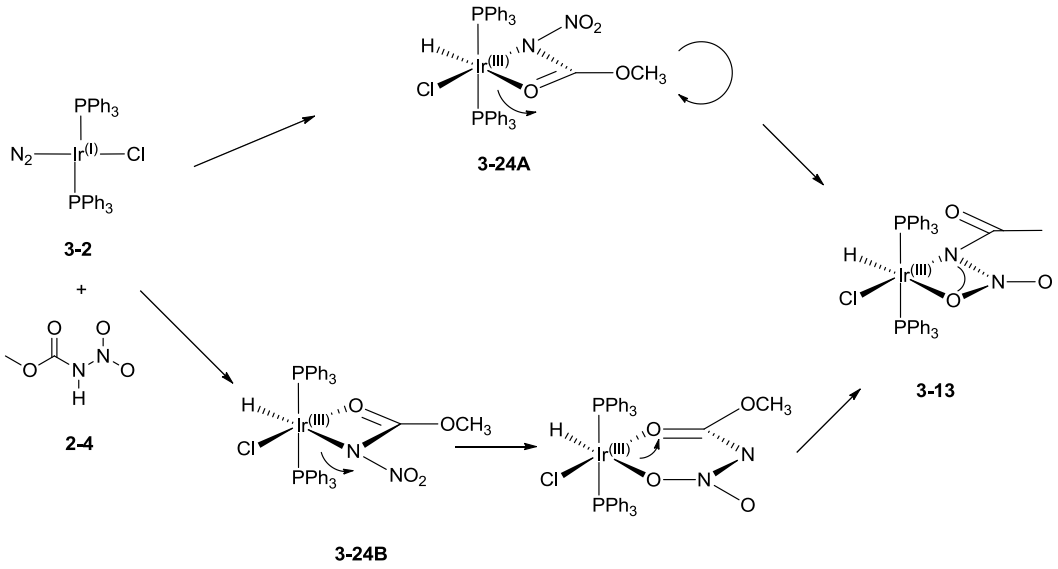

Scheme 3-14. Proposed reaction mechanism of **3-2** with **2-4** to form initially intermediates **3-24A** and/or **3-24B** to finally give **3-13**.

As per the proposed mechanism of for the synthesis of **3-11**, the reaction of **3-2** with **2-4** may involve the intermediate **3-24A** which has the amide nitrogen trans to the chloride ligand. Dissociation of the Ir-O bond followed by rotation about the Ir-N bond will generate **3-13**. The reaction may also proceed by the formation of intermediate **3-24B** which has the nitrogen trans to the Ir hydride. Intermediate **3-24B** then undergoes stepwise dissociation of the Ir-N bond followed by coordination of the oxygen of the nitro group to give a six-membered metallacycle which subsequently the Ir-O(acyl) bond dissociates to give **3-13**. Both of these intermediates may actually be present as there are two intermediates A and B observed during the course of the reaction. The key difference between the formation of **3-11** versus that of **3-13** is that the rate of conversion of the

intermediates in **3-13** is much faster than that of **3-11**. This difference may be driven by the alkoxy versus the alkyl functional group or may be due to the pK_a of the free acids. However even with this information, it is not possible to determine the actual intermediates present.

We have been unsuccessful in obtaining the crystal structure solution for **3-14**, however from the ^{31}P and ^{1}H NMR reaction monitoring results (Figure C-1 and Figure C-2 respectively) together with the IR results of the isolated solids, it is determined that **3-14** has similar reaction intermediates and product geometry as **3-13**. Thus the structure of **3-14** is very likely an analogue of **3-13** with an ethoxy group.

The reaction of **3-2** with **2-6** was also studied by ^{31}P, ^{1}H NMR and IR spectroscopy monitoring (Figure 3-26, Figure 3-27 and Figure 3-28 respectively).

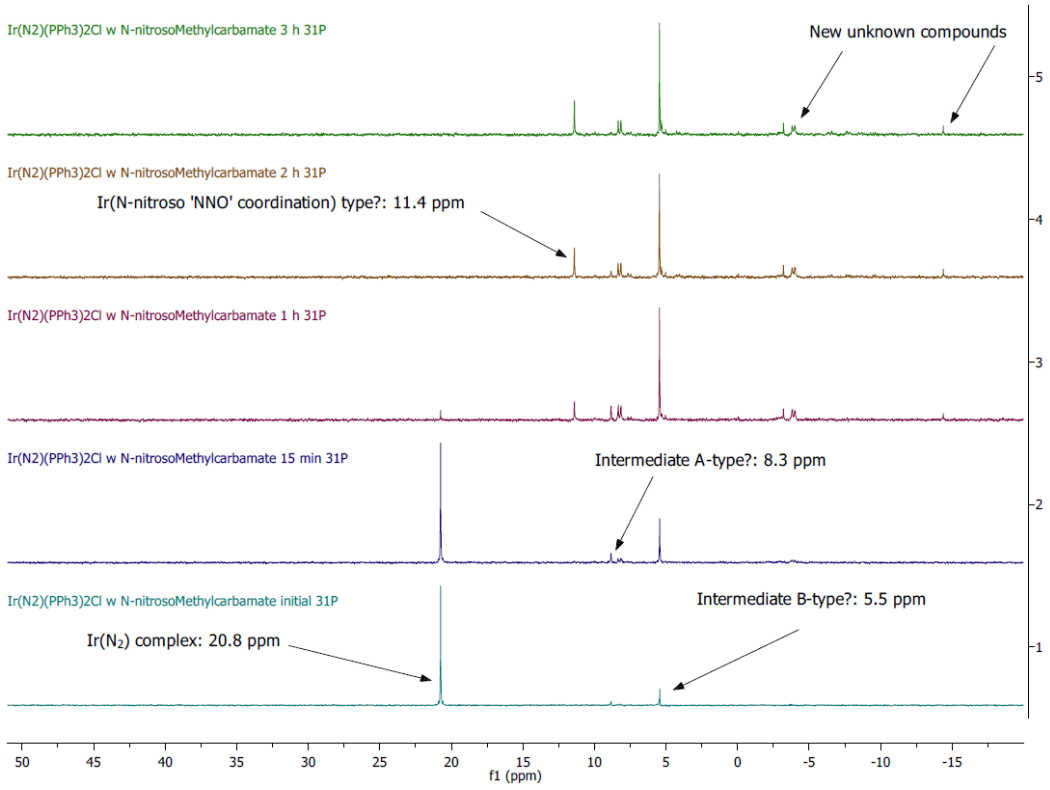

Figure 3-26. ^{31}P NMR reaction monitoring of **3-2** with **2-6** in $CDCl_3$.

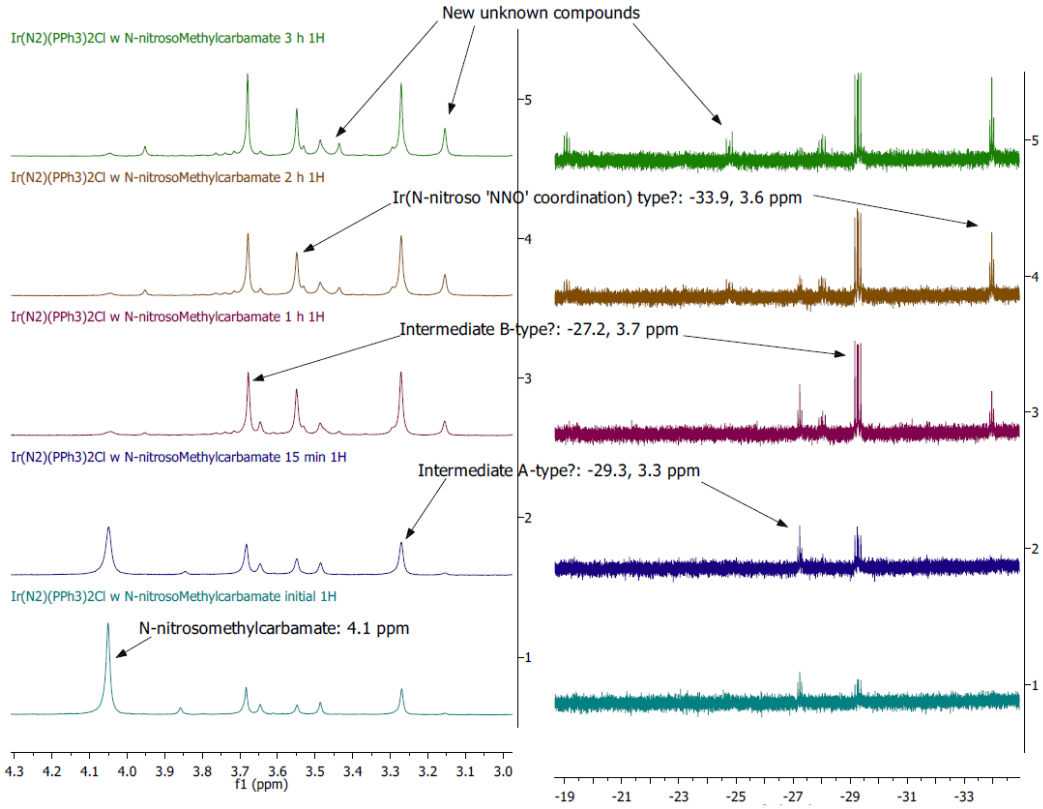

Figure 3-27. ^{1}H NMR reaction monitoring of **3-2** with **2-6** in $CDCl_3$.

In the ^{31}P and ^{1}H NMR spectra, the initial stage of the reaction seems to be very similar to that of **3-13** where two intermediates are observed; intermediate A with ^{31}P signal at 8.3 ppm, ^{1}H signals at 3.3, -29.3 ppm and intermediate B with ^{31}P signal at 5.5 ppm, ^{1}H signals at 3.7, -27.2 ppm. These initial resonances however do not resolve over time to give a single set of signals that correspond to a single isomer or product but instead become more complicated as the reaction proceeds. A new set of resonances with ^{31}P signal at 11.4 ppm, ^{1}H signals at 3.6 and -33.9 ppm have similar chemical shifts compared to **3-11** and **3-13**. This set of resonances may correspond to the analogue Ir(III) N-nitrosomethylcarbamate complex.

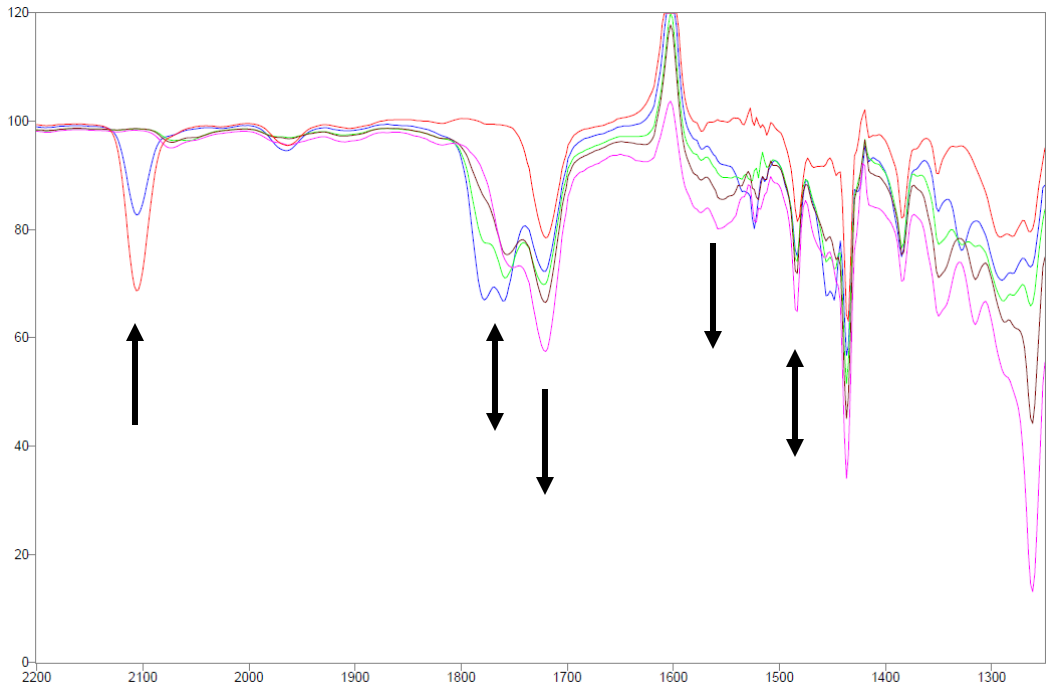

Figure 3-28. Solution IR spectra for the reaction of **3-2** with **2-6**. Reaction carried out at -10 °C in $CHCl_3$ over 20 h. Aliquots taken at the following time intervals: Red: Initial **3-2** complex with **2-6**; Blue: 15 min after addition of **2-6**; Green: after 1 h; Brown: after 3 h; Pink after 18 h**.**

The solution IR spectra of the reaction indicate the same disappearance of the 2104 cm^{-1} band which is the loss of the N_2 ligand. There is an initial increase and subsequent decrease in bands between 1780 and 1750 cm^{-1} and also in the band at 1450 cm^{-1}. The bands close to 1780 and 1450 cm^{-1} are likely to be from **2-6** however the additional band located near 1750 cm^{-1} is new. The reaction terminates with new bands at 1720 and between 1580 and 1500 cm^{-1}. The final IR spectrum may represent a mixture of Ir(III) N-nitrosomethylcarbamate isomers that are observed in the NMR spectra.

The ^{31}P and ^{1}H NMR (Figure C-3 and Figure C-4 respectively) of **3-2** with **2-6** in C_6D_6 was also monitored as the acidity of $CDCl_3$ may play a role in the decomposition of the reaction products. However, the reaction intermediates and eventual unknown product mixtures are very similar between the two solvent systems.

Finally the reaction of **3-2** with **2-8** was also tracked using ^{31}P, ^{1}H NMR and IR spectroscopy (Figure 3-29, Figure 3-30. Figure 3-31).

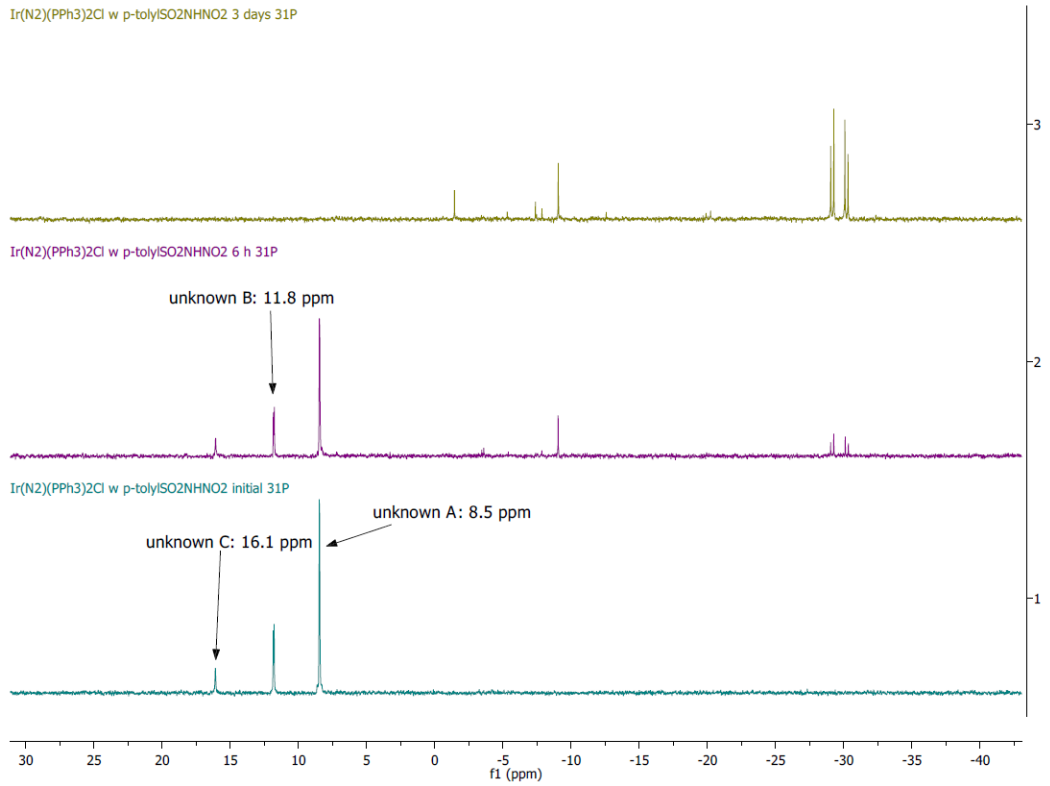

Figure 3-29. ^{31}P NMR reaction monitoring of **3-2** with **2-8** in $CDCl_3$.

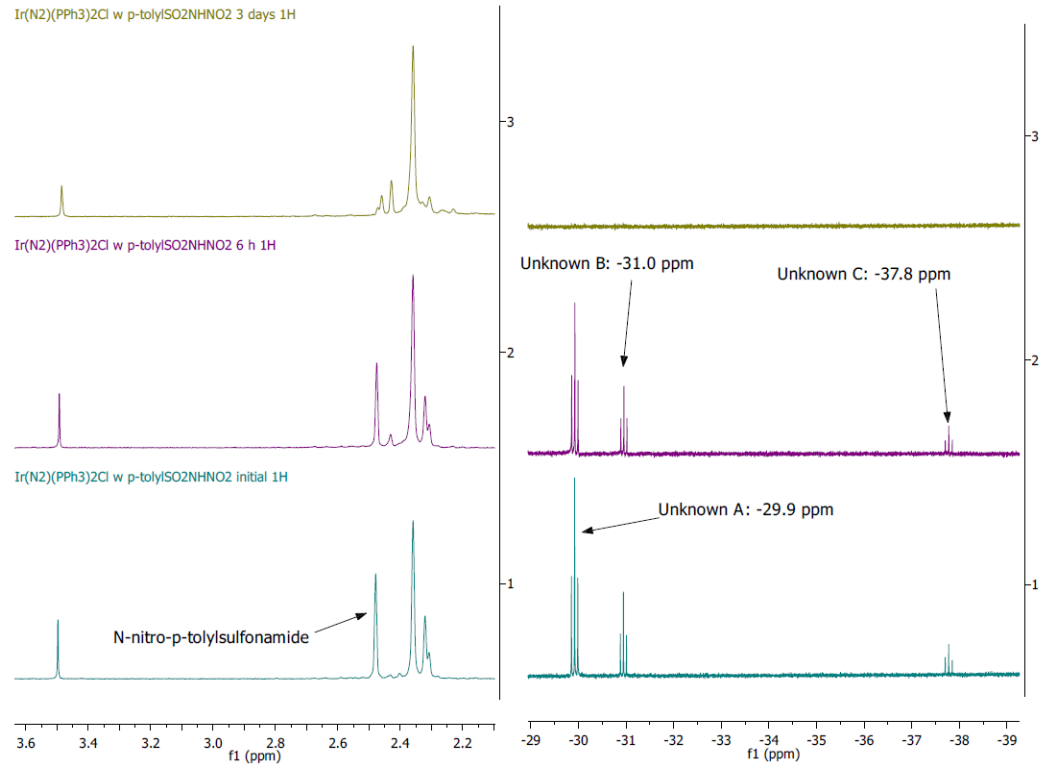

Figure 3-30. ^{1}H NMR reaction monitoring of **3-2** with **2-8** in $CDCl_3$.

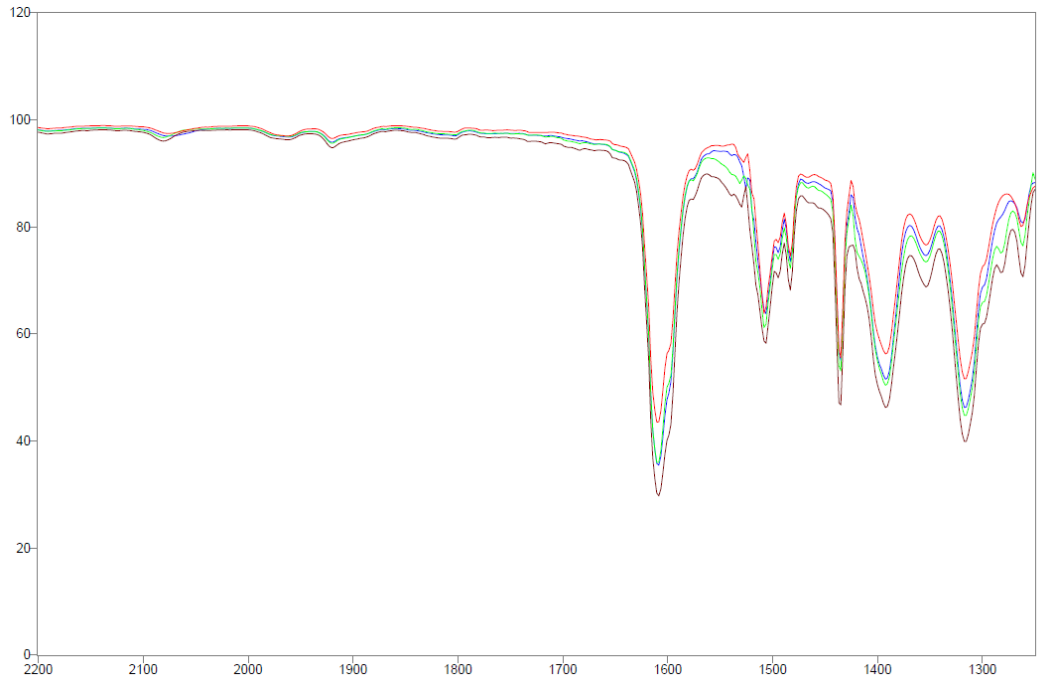

Figure 3-31. Solution IR spectra for the reaction of **3-2** with **2-8**. Reaction carried out at -10 ^{o}C in $CHCl_3$ over 20 h. Aliquots taken at the following time intervals: Red: Initial **3-2** complex; Blue: 15 min after addition of **2-8**; Green: after 3 h; Brown: after 19 h.

In both the ^{31}P and ^{1}H NMR spectra, three sets of resonances with different intensities are observed. The observation of hydride signals in the upfield region of the ^{1}H NMR indicates the oxidative addition has been successful, giving rise to Ir hydride complexes. However over time these hydride signals disappear with concurrent new ^{31}P signals that includes a AB pattern doublet of doublets ($^{2}J_{P\text{-}P}$ = 84.24 and 18.63 Hz) which indicates inequivalent phosphines. The precipitation of the reaction products may very well represent the formation of dimers or oligomeric complexes.

The solution IR spectra do not give much information except that the bands all represent similar terminal products. The reaction of **3-2** with **2-8** is very rapid such that on addition of **2-8**, the loss of the N_2 ligand is immediate as the 2104 cm^{-1} band is not even observed.

From all the reaction monitoring results obtained for the N-nitroamides, N-nitrocarbamates, N-nitrosocarbamate and N-nitrosulfonamide, based on the rate of reaction of the nitrogen acids with **3-2**, it may be possible to approximate the *p*Ka

values of the nitrogen acids in decreasing order: N-nitroamide > N-nitrocarbamate > N-nitrosocarbamate > N-nitrosulfonamide. This trend differs slightly from the π-accepting properties of the nitrogen acids (Figure 3-11) discuss above in the section for Ir(I) complexes. The rate of reaction of the nitrogen acids could also be affected by the strength of the π-accepting character, where the stronger π-acid reacts at a faster rate.

3.5.2.4 Reactivity studies of $Ir^{(III)}(\eta^2\text{-}CH_3C(O)NNO_2)(H)(Cl)(PPh_3)_2$ (3-11)

With CO

The reaction of **3-11** with CO gives a single new broad IR band at 2047 cm^{-1} which is assigned to the newly added carbonyl ligand of the new Ir(III) carbonyl complex **3-15**. The Ir hydride stretch which is not observed in **3-11** is observed as a low intensity broad band centered at 2185 cm^{-1}. The ^{31}P and ^{1}H NMR spectra however show that there are more than one isomers of **3-15**. In the ^{31}P NMR spectrum, two resonance signals are observed with unequal intensity. In the ^{1}H NMR, three Ir hydride triplet resonances are observed, with two signals that are significantly stronger and the third weaker in a ratio of 0.56:0.39:0.05 respectively. Thus there are three isomers of **3-15** which is possible depending on the site of CO addition (Scheme 3-15).

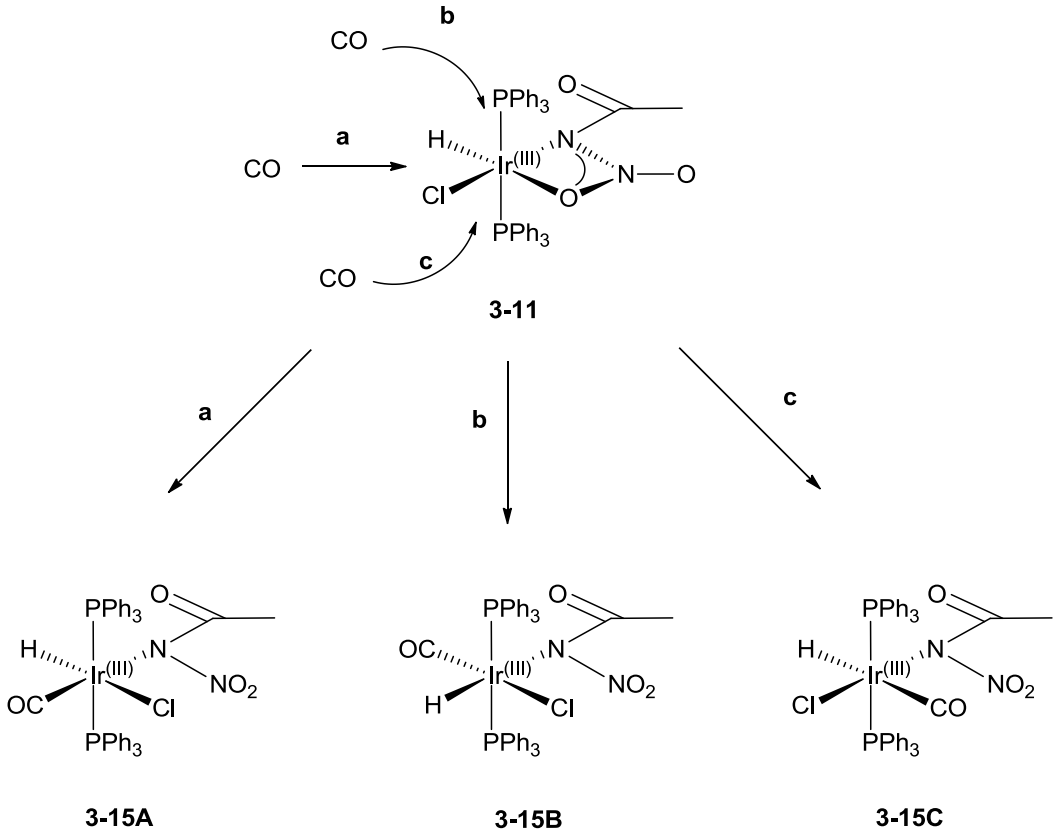

Scheme 3-15. Possible CO addition coordination isomers with **3-11**.

The related Ir(III) carboxylate complexes also undergo CO addition (Scheme 3-16).[172] The reaction of **3-22** with CO gives **3-25** which is reported to form only one isomer based on IR analysis of the Ir-H, Ir-Cl and Ir-CO stretches. The trans labilisation effect of CO[174] on the Ir hydride affects ν(Ir-H) stretch which is found at 2112 cm^{-1} which is much lower than that of **3-22** at 2307 cm^{-1}. The observation of hydridocarbonyl vibrational coupling[175] also supports a trans H-Ir-CO structure from isotopic analysis using $^{1}H/^{2}D$ Ir hydride samples. The ^{31}P single singlet resonance at 5.41 ppm, ^{1}H NMR signals of singlet at 1.06 ppm for the methyl group and triplet at -7.83 ppm (14 Hz) for the Ir hydride indicate the presence of only a single isomer for **3-25**.

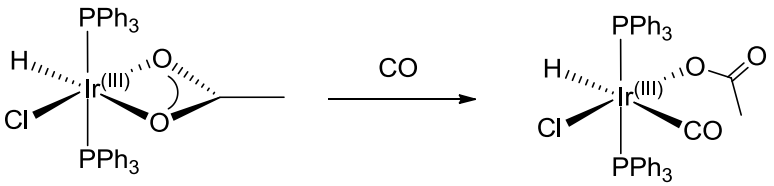

3-22 **3-25**

Scheme 3-16. CO addition to **3-22** to give **3-25**.

The formation of multiple isomers in **3-15** compared to **3-25** could be due to the labile coordination of the oxygen of the nitro group. Without additional information, it is not possible to assign the isomers of **3-15** to the observed ^{31}P and ^{1}H signals to allow determination of the distribution of the isomers. ^{13}CO labelling may help in the identification of **3-15C** from trans ^{1}H-Ir-^{13}CO coupling but this may be hampered by an unexpected phenomenon discussed next.Complex **3-15** is metastable and on standing in solution over time, the CO ligand is lost from all three isomers and **3-11** is regenerated. The addition of CO again regenerates **3-15** which eventually loses CO again when left in solution. The loss of CO from an Ir(III) complex is very unusual as d^6 Ir(III) complexes are usually inert. The loss of CO is most likely due to two factors. The first is that the electron withdrawing N-nitroacetamide ligand causes the Ir(III) center to be electron deficient and competes for π-backbonding from the metal center to the carbonyl ligand. Secondly the bidentate nature of the N-nitroacetamide ligand

allows efficient chelation to the Ir center. These two factors together may play a role in the labile nature of the carbonyl ligand. The CO addition reaction to **3-11** to give isomers of **3-15** is in contrast to the reaction of **3-1** with **2-2** (Scheme 3-17). The first reaction results in formation of isomers that reversibly lose the CO ligand while the second reaction gives incomplete conversion of the starting complex **3-1** which with additional stoichiometric amounts of **2-2** generate multiple products. Furthermore **3-15** does not undergo reductive elimination to give **3-1** and **2-2**.

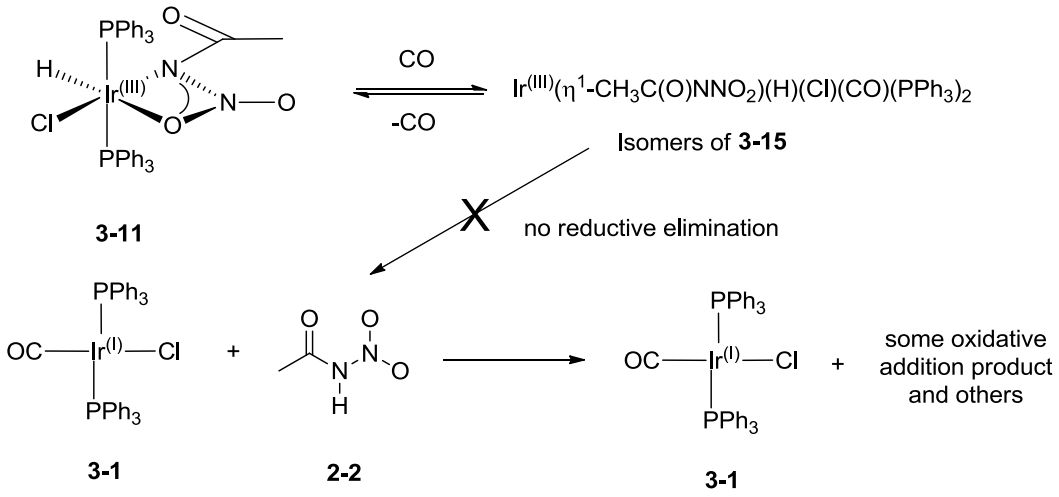

Scheme 3-17. Reaction of **3-11** with CO versus reaction of **3-1** with **2-2**.

With $P(CH_3)_2Ph$

The reaction of **3-11** with one equivalent of $P(CH_3)_2Ph$ did not allow the reaction to go to completion. Most of the starting complex, **3-11**, is still present after stirring overnight. Several new ^{31}P NMR resonance signals were observed, one of which with significant intensity at -4.38 ppm belongs to free PPh_3. A set of doublet and triplet signals with similar coupling constants of 19.9 Hz in the ^{31}P NMR spectrum represents a phosphine ligand that is positioned cis to two identical and trans phosphine ligands. It is very likely that the substitution of the PPh_3 ligand of **3-11** is occurring such that a single substitution results in both PPh_3 ligands to be substituted. This is supported by the absence of two sets of doublets that have large coupling constants being observed in the ^{31}P NMR for

inequivalent trans phosphines. The substituted phosphine complex **3-16A** also undergoes further nucleophilic addition of an additional $P(CH_3)_2Ph$ molecule preferentially to give the isomers **3-16B**, **3-16C** and **3-16D**. This is evidenced by the appearance of three sets of doublet of triplet resonance signals and a single triplet in the upfield region of the ^1H NMR spectrum. With excess $P(CH_3)_2Ph$ added, total conversion of **3-11** occurs to give the four species of complexes (Scheme 3-18). The single Ir hydride triplet is assigned to the $P(CH_3)_2Ph$ substituted **3-16A** as it is not coupled to any additional phosphine.

One of the doublet of triplet ^1H signals for the Ir hydride complexes have a significantly large doublet coupling constant of 158 Hz. This isomer is most likely **3-16D** which has the hydride located trans to the dimethylphenylphosphine ligand. The remaining two doublet of triplet Ir hydride signals have the hydride located cis to the equatorial phosphine and the assignment of the signals assumes that $P(CH_3)_2Ph$ preferentially adds from the less hindered site. Therefore **3-16B** is formed in larger proportions than **3-16C**. The three complexes, **3-16B-D**, will have identical ^{31}P NMR signals and is assigned to the doublet and triplet resonance signals.

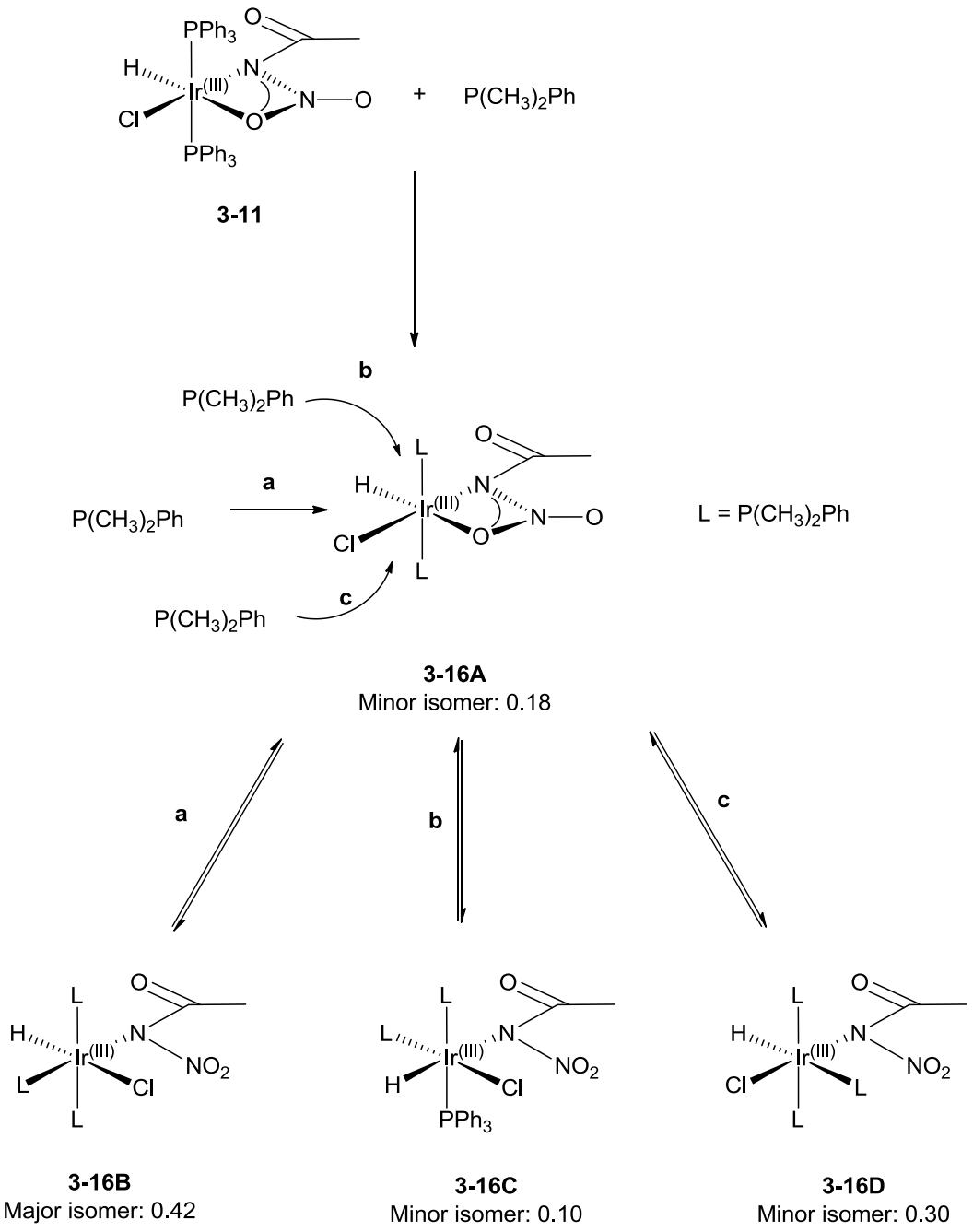

Scheme 3-18. Proposed reaction isomers of **3-16** from the addition of $P(CH_3)_2Ph$ to **3-11** with fractional proportions.

In a similar reaction, addition of dimethylphenylphosphine to the Ir(III) carboxylate complexes,[172] only one isomer with the trans H-Ir-$P(CH_3)_2Ph$ structure, **3-26**, is obtained (Scheme 3-19). In the original article this isomer is confirmed by ν(Ir-Cl). The repeated synthesis of **3-26** confirms the presence of

ν(Ir-H) at 2187 cm^{-1}. The ^{31}P NMR contains two sets of resonances; a doublet at -2.77 ppm (13.5 Hz) assigned to $P(CH_3)_2Ph$ and a triplet of doublet at -42.50 ppm assigned to PPh_3 from coupling to both the P (13.5 Hz) and CH_3 groups (7.3 Hz) in $P(CH_3)_2Ph$. The results from the ^{31}P and ^{1}H NMR indicates only one isomer is formed.

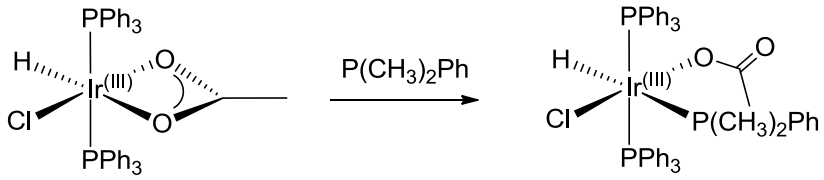

3-22 **3-26**

Scheme 3-19. Addition of $P(CH_3)_2Ph$ to **3-22** to give **3-26**.

The reactivity studies of **3-22** are in great contrast with **3-11** with regards to CO and $P(CH_3)_2Ph$ addition. In both the CO and $P(CH_3)_2Ph$ additions to **3-22** only one ligand is added to generate single isomers which are stable. For **3-11**, the addition of CO generates isomers of **3-15** which on prolonged duration in solution loses CO and regenerates **3-11**. With $P(CH_3)_2Ph$ addition, PPh_3 substitution by $P(CH_3)_2Ph$ is observed which preferentially adds an additional $P(CH_3)_2Ph$ to give isomers of **3-16**. The above reactivity for **3-11** can be attributed to both the electron withdrawing nature of the N-nitroacetamide ligand and the labile coordination of the oxygen atom of the nitro group observed earlier from the ^{1}H NMR of the Ir hydride resonance. It seems that the trans labilising effect of the Ir hydride[171] in **3-11** is not sufficient to enforce the formation of a single isomer for nucleophiles.

With methyl triflate

The reaction of methyl triflate with **3-11** results in the loss of the N-nitroacetamide ligand, **2-2**, to give the bis(acetonitrile) Ir(III) complex **3-17** (Scheme 3-20).

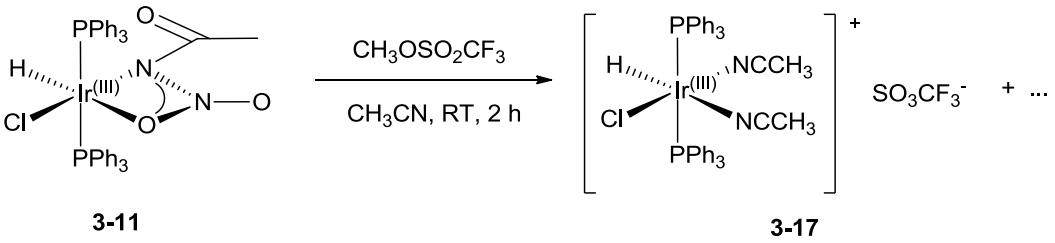

3-11 **3-17**

Scheme 3-20. Reaction of methyl triflate with **3-11** to form **3-17**.

The IR spectrum of **3-17** shows multiple weak bands in the 2270 cm^{-1} region which can be assigned to the coordinated acetonitrile ligands and the Ir hydride stretch. The appearance of the bands at 1270, 1154, 1031 and 638 cm^{-1} confirms the presence of the triflate anion. The bands at 1695, 1514, 1262, 1198 and 621 cm^{-1} are missing indicating the loss of the coordinated N-nitroacetamide ligand. The ^{31}P spectrum shows only a single singlet at 4.43 ppm and the ^{1}H NMR spectrum has only a single triplet at -20.67 ppm for the Ir hydride indicating a single species. New singlets at around 1.90 and 2.00 ppm can be assigned to the coordinated CH_3CN ligands. A crystal structure solution for **3-17** has been obtained but due to the poor quality of the diffraction data, the structure is not of publication quality (Table C-1, Figure C-5).

The methylation of **3-11** only occurs in acetonitrile and is unsuccessful in other solvents such as $CHCl_3$ and benzene. The use of alternative methylating agents such as CH_3I and dimethylsulfoxide did not change the reaction outcome in other solvents. It is very likely that coordination of the acetonitrile ligand to **3-11** is necessary for the methylation reaction to occur and is related to the proposed labile behaviour of the coordinated oxygen atom of the nitro group. It is interesting that successful methylation of the N-nitroacetamide ligand results in the loss of the methlylated ligand through substitution by acetonitrile. We have not been able to isolate the methylated N-nitroacetamide ligand but proposed the methylation site to be on the oxygen atom of the nitro group.

3.6 Conclusion

Ir(I) nitrogen acids complexes

New Ir(I) nitrogen acid complexes **3-3**, **3-4**, **3-5**, **3-6**, **3-7** and **3-8** have been synthesized from the reaction of **3-1** with **2-2Ag**, **2-4Ag**, **2-5Ag**, **2-6Ag**. **2-8Ag** and $Ag[N(NO_2)_2]$. The new complexes have square planar geometry with the carbonyl ligand trans to the nitrogen acids. The reaction of **3-1** with $Ag[N(SO_2CF_3)_2]$ did not undergo silver metathesis but instead formed a rare Vaska's silver adduct, **3-9**. Complex **3-9** has the silver bistriflimide ligand located at the axial axis forming a five coordinate square pyramidal complex. It is very likely that the bistriflimide anion is a poorer ligand compared to the dinitramide anion. The ν(CO) stretch of all the complexes are higher than 1954 cm^{-1} of the Vaska's complex indicating that they are all strong π-acceptors which compete with the carbonyl ligand for electron density from the electron-rich Ir(I) center.

Conversion of **3-3** into the dinitrogen complex is shown to give a new Ir(I) N_2 complex containing the **2-2**. This new N_2 complex is uncharacteristically stable to decomposition compared to **3-2**. However due to difficulty in purification, isolation of **3-10** was not successful.

Ir(III) nitrogen acids complexes

Compounds **2-2**, **2-3**, **2-4** and **2-5** undergo oxidative addition with **3-2** to give new Ir(III) hydrido nitrogen acid complexes **3-11**, **3-12**, **3-13** and **3-14** respectively. The Ir(III) complexes all feature an unusual four-membered N,O chelate with the nitrogen of the amide and the oxygen of the nitro group to the Ir center. The hydride ligand is also located trans to the oxygen atom. The new Ir(III) complexes exhibit interesting and unique vibrational bands.

The ^1H NMR spectrum for **3-11** is observed to have solvent-dependent line shape behaviour for the metal hydride resonance which can also be observed on varying the effective field. This effect is proposed to be due to the labile Ir-O bond and is believed to undergo rapid coordination and release in solution. The fluxional

behaviour of the nitrogen acid in **3-11** is believed to contribute to the unusual reactivity with nucleophiles such as CO and $P(CH_3)_2Ph$ to give multiple isomers. Of significance is the ability of the Ir(III) carbonyl complex **3-15** to lose the carbonyl ligand over time in solution. Ir(III) complexes with a labile carbonyl are rare but there are precedence of labile CO on transition metal complexes such as the d^6 $Re^{(I)}(\eta^1\text{-}CH_3CO_2)(CO)_3(PPh_3)_2$ complex.[176] The presence of three π-accepting CO ligands causes the Re center to be electron-deficient which affects one of the CO ligands to be labile. Thus the electron-withdrawing effect of the N-nitroacetamide ligand may be the reason for the loss of CO and substitution of PPh_3 by $P(CH_3)_2Ph$. The methylation reaction of **3-11** is only possible in acetonitrile and results in the loss of the **2-2** with the formation of the bis(acetonitrile) complex **3-17**.

The reaction profiles for the nitrogen acids with **3-2** were also monitored using solution IR, ^1H and ^{31}P NMR spectroscopy. It is observed that in the reaction of **3-2** with **2-2**, a single intermediate was observed to form which slowly converts to the final **3-11**. A proposed structure for this intermediate was made based on the change in solution IR bands over time and with comparison with other reports. Similar phenomena are observed in the reaction of **3-2** with both **2-4** and **2-5** however there are two intermediates observed. The reaction rate was significantly more rapid which prevented decent solution IR analysis of the intermediates. Nonetheless, similarities of one of the intermediates allow us to propose possible structures of the intermediates.

The reaction of **3-2** with N-nitrosocarbamate **2-6** gave multiple products which from monitoring the reaction indicate that the initial reaction intermediates are similar to that observed in **2-4** and **2-5**. The reaction rate is also very rapid but on prolonged reaction times, multiple products are observed. Similarly, the reaction of **3-2** with **2-8** started with few products but progressively multiple different side products is formed. The reaction residue slowly precipitates out of solution which may be due to the formation of insoluble oligomers. The reaction rate of **2-8** with **3-2** is the most rapid.

We have successfully synthesized a series of Ir(I) and Ir(III) complexes containing the nitrogen acids coordinated to the Ir center. Preliminary reactivity studies indicate much unusual chemical reactivity. It is our eventual goal to deprotect the nitrogen acids from the acyl groups to allow the study of nitrous oxide precursors.

Chapter 4: Rhenium complexes of Nitrogen Acids

4.0 Introduction

The successful synthesis of a series of Ir(I) carbonyl nitrogen acids and the unique coordination and reactivity of the Ir(III) N-nitroamide and N-nitrocarbamate complexes provide us with some information with regards to their chemical reactivity. The reaction methodologies of silver salt metathesis and oxidative addition to an electron-rich Ir(I) center are useful pathways to the above complexes.

The presence of the strong trans-directing hydride in the Ir(III) nitrogen acid complexes may play a role in the unusual reactivities of the Ir(III) nitrogen acid complexes towards nucleophiles and electrophiles. $[Re^{(I)}(CH_3CN)_2(CO)_2(PPh_3)_2](X)$ (**4-3**: X = ClO_4, **4-7**: X = BF_4) complexes are suitable complexes for displacement study with the nitrogen acid salts as the acetonitrile ligands are labile and can be substituted for the conjugate base of the nitrogen acids. $Re^{(I)}(H)(CO)_2(PPh_3)_3$ (**4-5**) contains a basic hydride which can react with acids. The CO ligands in the complexes are coordinative inert compared to hydride ligands and **4-3**, **4-5** and **4-7** are also Re(I) d^6 complexes that tend to be kinetically inert. There are also reports of Re complexes that are able to activate carbon dioxide [177] and form coordination complexes with N_2.[178]

4.1 General Experimental

General: All reagents and solvents are used as supplied commercially. Dry CH_3OH is distilled from freshly generated magnesium methoxide, dry $CHCl_3$ is distilled from $CaCl_2$, dry CH_2Cl_2 is distilled from CaH_2, dry hexanes, pentanes and benzene are distilled from sodium benzophenone ketyl. ^1H and ^{31}P spectra are recorded on Varian Mercury 200, 400 or 500 MHz. All chemical shifts are recorded in δ (ppm) relative to residual solvent signals for ^1H spectra and H_3PO_4 for ^{31}P spectra. Melting/decomposition points are measured by using a TA-Q2000 differential scanning calorimeter. The IR spectra are recorded in KBr disks by using ABB Bomem MB Series spectrometer with a spectral resolution of 4 cm^{-1}. Elemental analyses are performed in the Elemental Analyses Laboratory at University of Montreal.

X-ray crystallography: Crystals are mounted on glass fibres with epoxy resin or Mitegen mounts using Paratone-N from Hampton Research and single-crystal X-ray diffraction experiments are carried out with a BRUKER APEX-II CCD diffractometer by using graphite-monochromated $Mo_{K\alpha}$ radiation (λ = 0.71073 Å) and KRYOFLEX for low temperature experiments. SAINT[105] is used for integration of the intensity reflections and scaling and SADABS[106] for absorption correction. For large and unusual unit cell parameters, CELL_NOW[179] was used to check the viability of the suggested lattice and subsequent space group solution. Direct methods are used for structures with the rhombohedral space group R-3 while Patterson maps are used for the rest of the structures to generate the initial solution. Location of non-hydrogen atoms are carried out using Fourier difference maps with the refinements solved by full-matrix least-squares method on F^2 of all data using SHELXTL[105] software. The hydrogen atoms positions are placed in calculated positions.

Diffraction quality crystals of **4-7** and **4-12** are grown from CH_2Cl_2 solutions layered with pentanes at -21 ^oC. Diffraction quality crystals of **4-9**, **4-10** and **4-11** are grown from slow diffusion of either pentanes or petroleum ether into CH_2Cl_2 solutions at 5 ^oC over a week. The crystals of **4-9** and **4-10** contain large solvent

channels which require low temperature collection of the diffraction data to prevent loss of the solvates. The crystal structure of **4-11** contains two non-identical independent molecules. Crystallographic data and data collection parameters are shown in Table 4-1.

Table 4-1: Crystallographic data for $Re^{(I)}(\eta^2\text{-}X)(CO)_2(PPh_3)_2$.

Compound	**4-8**	**4-9**	**4-10**	**4-11**	**4-12**
empirical formula	$C_{40}H_{33}ReP_2N_2O_5$	$C_{40}H_{33}ReP_2N_2O_6.2.33CH_2Cl_2$	$C_{40}H_{33}ReP_2N_2O_5.2.33CH_2Cl_2$	$2(C_{40}H_{33}ReP_2N_2O_6).CH_2Cl_2$	$C_{45}H_{37}ReP_2N_2O_6S.2CH_2Cl_2$
T (K)	293(2)	100(2)	100(2)	100(2)	296(2)
fw (g mol^{-1})	869.82	1083.98	1067.98	1824.57	1151.82
cryst sys	triclinic	rhombohedral	rhombohedral	monoclinic	monoclinic
space group	P-1	R-3	R-3	$P2_1/c$	$P2_1/c$
a (Å)	10.9821(16)	45.476(3)	44.739(4)	11.1714(7)	15.411(4)
b (Å)	12.4685(18)	45.476(3)	44.739(4)	46.877(3)	12.131(3)
c (Å)	14.339(2)	11.9001(7)	12.0464(9)	17.9886(8)	25.065(6)
α (deg)	91.368(8)	90	90	90	90
β (deg)	108.094(7)	90	90	128.081(3)	96.007(13)
γ (deg)	111.615(7)	120	120	90	90
V ($Å^3$)	1713.7(4)	21313(2)	20881(3)	7415.1(7)	4660.2(19)
Z	2	18	18	4	4
density (g cm^{-3})	1.686	1.520	1.529	1.634	1.642
abs coeff (mm^{-1})	3.688	2.941	3.000	3.483	3.001
No. of reflns collected	66092	62827	62856	85200	19268
No. of indep reflns	17143	8285	8231	17490	9814

Data/restraints/parameters	17143/0/451	8285/90/541	8231 / 170 / 515	17490 / 411 / 986	9814/0/568
Final R indices [$I > 2s(I)$] R1	0.0592	0.0445	0.0575	0.0538	0.0391
*w*R2	0.1549	0.1237	0.1518	0.1106	0.0852
R indices (all data) R1	0.0853	0.0611	0.0863	0.0807	0.0662
*w*R2	0.1746	0.1329	0.1668	0.1208	0.0990
Goodness-of-fit on F^2	1.156	1.044	1.053	1.066	1.041

4.2 Rhenium complexes of N-Nitroamides

Experimental

$Re^{(v)}(O)(Cl)_3(PPh_3)_2$ (**4-1**),[180] $Re^{(I)}(Cl)(CO)_3(PPh_3)_2$ (**4-2**),[181] $[Re^{(I)}(CH_3CN)_2(CO)_2(PPh_3)_2](ClO_4)$ (**4-3**),[182] $Re^{(I)}(\eta^2-NO_2)(CO)_2(PPh_3)_2$ (**4-4**),[182] $Re^{(I)}(H)(CO)_2(PPh_3)_3$ (**4-5**),[182] and $Re^{(VII)}(H)_7(PPh_3)_2$ (**4-6**)[183] are synthesized by literature methods. $[Re^{(I)}(CH_3CN)_2(CO)_2(PPh_3)_2](BF_4)$ (**4-7**) is synthesized using $AgBF_4$ instead of $AgClO_4$.

4.2.1 Reaction of $Re^{(VII)}(H)_7(PPh_3)_2$ (4-6) with 2-2

$ReH_7(PPh_3)_2$ (**4-6**) (0.030 g, 0.042 mmol) and **2-2** (0.005 g, 0.048 mmol) are placed in 50 mL flask. THF (5 mL) is added into the reaction flask and stirred for 3 h. The solvent is removed to give brown solids (approx. 0.023 g).

IR (cm^{-1}): 3056w, 1964w, 1894w, 1731w, 1668m, 1615m, 1587w, 1573w, 1480m, 1434s, 1183m, 1119m, 1092m, 909m, 748s, 722s, 694vs, 541s, 521m.

^1H NMR (200 MHz, CD_2Cl_2) ppm: 2.27 (s), 2.14 (s), 2.03 (s), 1.98 (s), -4.90 (t) starting complex.

^{31}P NMR (200 MHz, CD_2Cl_2) ppm: 37.58 (s), 31.30 (s), 30.95 (s, major, **4-6**), 22.15 (s), -4.40 (s, free PPh_3).

4.2.2 Synthesis of $Re^{(I)}(\eta^2-CH_3C(O)NNO_2)(CO)_2(PPh_3)_2$ (4-8)

Reaction with **4-3**

Complex **4-3** (0.030 g, 0.032 mmol) and **2-2K** (0.0045 g, 0.032 mmol) are placed in 50 mL flask. CH_3OH or C_2H_5OH (5 mL) is added and the reaction brought to reflux under N_2. The reflux is continued for 1 h during which the white suspension turned into a bright yellow solution. The solvent is removed and the residue is extracted with CH_2Cl_2 (10 mL) and filtered through a glass frit. The

solution is concentrated to *ca.* 1 mL and pentanes (20 mL) are added to give orange crystals of $Re^{(I)}(\eta^2\text{-}CH_3C(O)NNO_2)(CO)_2(PPh_3)_2$ (**4-8**) (0.019 g, 0.022 mmol, 69 % yield) after 2 days.

Reaction with **4-5**

Complex **4-5** (0.030 g, 0.029 mmol) and **2-2** (0.003 g, 0.030 mmol) were added into a 50 mL flask. Toluene (10 mL) is added and the reaction heated to 60 ^oC for 2 h under N_2. The colourless solution turned bright yellow during the course of the reaction. The solvent is removed and the mixture recrystallized from CH_2Cl_2/pentanes to give orange crystals of $Re^{(I)}(\eta^2\text{-}CH_3C(O)NNO_2)(CO)_2(PPh_3)_2$ (**4-8**) (0.012 g, 0.014 mmol, 47 % yield).

IR (cm^{-1}): 3055w, 1942vs (CO), 1867vs (CO), 1691m, 1511s, 1481m, 1434s, 1363w, 1257m, 1216s, 1093s, 1028m, 751m, 743s, 693s, 611m, 517s.

^1H NMR (200 MHz, $CDCl_3$,) ppm: δ = 1.33 (s, 3H,), 7.40 (m, PPh_3), 7.46 (m, PPh_3).

^{31}P NMR (81 MHz, $CDCl_3$) ppm: δ = 28.00 (s).

ESI: 893 $[M + Na]^+$

Elemental analysis calcd. for $C_{40}H_{33}N_2O_5P_2Re$ (869.87 g mol^{-1}) % C, 55.18; H, 3.79; N, 3.22. Found % C, 55.32; H, 3.92; N, 3.09.

4.2.3 Synthesis of $Re^{(I)}(\eta^2\text{-}CH_3OC(O)NNO_2)(CO)_2(PPh_3)_2$ (4-9)

Complex **4-6** (0.050 g, 0.053 mmol) and **2-4K** (0.009 g, 0.057 mmol) were placed in a 50 mL flask. Dry CH_3OH (6 mL) is added and the reaction brought to reflux under N_2. The reflux is continued for 30 min during which the white suspension turned into a bright yellow solution. The solvent is removed and the residue extracted with CH_2Cl_2 (10 mL) followed by filtration through sintered glass filter. The CH_2Cl_2 solvent is removed in *vacuo* to give yellow solids of $Re^{(I)}(\eta^2\text{-}CH_3OC(O)NNO_2)(CO)_2(PPh_3)_2$ (**4-9**) (0.038 g, 0.043 mmol, 80% yield).

IR (cm^{-1}): 3056w, 2956vw, 1936vs (CO), 1860vs (CO), 1745m, 1636m, 1513m, 1482m, 1435s. 1324m, 1263w, 1231m, 1184m, 1119m, 1093s, 908m, 745m, 724m, 695vs, 542m, 517s.

^{1}H NMR (200 MHz, $CDCl_3$,) ppm: δ = 3.38 (s, 3H,), 7.40 (m, PPh_3), 7.49 (m, PPh_3)

^{31}P NMR (81 MHz, $CDCl_3$) ppm: δ = 27.36 (s)

Elemental analysis calcd. for $C_{40}H_{33}N_2O_6P_2Re.0.55CH_2Cl_2$ (932.60 g mol^{-1}) % C, 52.22; H, 3.69; N, 3.00. Found % C, 52.01; H, 4.00; N, 3.22.

4.2.4 Synthesis of isomers of $Re^{(I)}(\eta^2$-$CH_3OC(O)NNO)(CO)_2(PPh_3)_2$

Room temperature reaction

Complex **4-6** (0.030 g, 0.032 mmol) is dissolved in dry CH_2Cl_2 (2 mL) and added to a solution of **2-6K** (0.006 g, 0.038 mmol) in dry CH_3OH (6 mL) in a 50 mL flask. The white suspension was stirred overnight during which the suspension turned into a bright yellow. The solvent is removed and the residue extracted with CH_2Cl_2 (10 mL) followed by filtration through a sintered glass filter. The CH_2Cl_2 solvent is removed to give yellow solids containing isomers of $Re^{(I)}(\eta^2$-$CH_3OC(O)NNO)(CO)_2(PPh_3)_2$ (**4-10**) (0.020 g, 0.023 mmol, 72 % yield).

IR (cm^{-1}): 3055w, 2964wv, 2924w, 1942vs (CO), 1864vs (CO), 1750m, 1633m (broad), 1481m, 1434s, 1384m, 1311m, 1261m, 1181m, 1094s, 1029m, 9109m, 804e, 746m, 695s, 518s.

^{1}H NMR (200 MHz, $CDCl_3$) ppm: 3.00 (s, 3H, major isomer), 3.46 (s, 3H, minor isomer), 7.38 (m, PPh_3), 7.48, (m, PPh_3)

^{1}H NMR (500 MHz, $CDCl_3$) ppm: 3.07 (s, 3H, minor isomer = 0.21), 3.41 (s, 3H, major isomer = 0.79), 7.39 (m, PPh_3), 7.52 (m, PPh_3)

^{31}P NMR (81 MHz, $CDCl_3$) ppm: 23.74(s, minor isomer = 0.24), 29.01 (s, major isomer = 0.76)

^{31}P NMR (202 MHz, $CDCl_3$) ppm: δ = 23.74 (s, minor isomer = 0.19), 29.03 (s, major isomer = 0.81)

Reflux reaction

Complex **4-6** (0.030 g, 0.032 mmol) and **2-6K** (0.006 g, 0.038 mmol) were placed in 50 mL flask. Dry CH_3OH (6 mL) is added and the reaction heated to 60 ^oC for 45 min. The white suspension turned into a bright yellow suspension. The solvent is removed and the residue extracted with CH_2Cl_2 (10 mL) and filtered through a glass frit. The CH_2Cl_2 solvent is removed in *vacuo* to give orange solids containing isomers of $Re^{(I)}(\eta^2\text{-}CH_3OC(O)NNO)(CO)_2(PPh_3)_2$ (**4-11**) (0.021 g, 0.024 mmol, 75 % yield).

IR (cm^{-1}): 3054w, 1952vw, 1950vs (CO), 1870vs (CO), 1748m, 1556m, 1481m, 1434s, 1419m, 1327s, 1266m, 1185m, 1158m, 1093s, 1066s, 998m, 995m, 744s, 695vs, 634m, 515vs.

^1H NMR (200 MHz, $CDCl_3$) ppm: δ = 3.07 (s, 3H, major isomer = 0.83), 3.41 (s, 3H, minor isomer = 0.17), 7.40 (m, PPh_3), 7.48 (m, PPh_3)

^1H NMR (500 MHz, $CDCl_3$) ppm: δ = 3.07 (s, 3H, major isomer = 0.83), 3.41 (s, 3H, minor isomer = 0.17), 7.38 (m, PPh_3), 7.47 (m, PPh_3)

^{31}P NMR (81 MHz, $CDCl_3$) ppm: δ = 23.73 (s, major isomer = 0.78), 29.03 (s, minor isomer = 0.22)

^{31}P NMR (202 MHz, $CDCl_3$) ppm: δ = 23.74 (s, major isomer = 0.82), 29.03 (s, minor isomer = 0.18)

A sample containing a mixture of both the room temperature and reflux reactions was sent for elemental analysis.

Elemental analysis calcd. for $C_{40}H_{33}N_2O_5P_2Re.0.8CH_2Cl_2$ (937.83 g mol^{-1}) % C, 52.25; H, 3.72; N, 2.99. Found % C, 52.49; H, 3.75; N, 2.68.

4.2.5 Synthesis of $Re^{(I)}(\eta^2–C_7H_7SO_2NNO_2)(CO)_2(PPh_3)_2$ (4-12)

Method with **4-3**

Complex **4-3** (0.070 g, 0.074 mmol) and **2-8K** (0.030 g, 0.118 mmol) were placed in 50 mL flask. CH_3OH or C_2H_5OH (6 mL) is added and the reaction brought to reflux under N_2. The reflux is continued for 1 h during which the white suspension turned into a bright yellow solution. The solvent is removed and the residue extracted with CH_2Cl_2 (10 mL) followed by filtration through a glass frit. The solution is concentrated to *ca.* 1 mL and pentanes (20 mL) are added to give orange crystals of $Re^{(I)}(\eta^2–C_7H_7SO_2NNO_2)(CO)_2(PPh_3)_2$ (**4-12**) (0.053 g, 0.054 mmol, 73 % yield) after 2 days.

Method with **4-5**

Complex **4-5** (0.050 g, 0.049 mmol) and **2-8** (0.013 g, 0.058 mmol) were added into a 50 mL flask. Toluene (10 mL) is added and the reaction heated to 60 ^oC for 2 h under N_2. The colourless solution turned bright yellow during the course of the reaction. The solvent is removed and the mixture recrystallized from CH_2Cl_2/pentanes to give orange crystals of $Re^{(I)}(\eta^2–C_7H_7SO_2NNO_2)(CO)_2(PPh_3)_2$ (**4-12**) (0.028 g, 0.029 mmol, 59 % yield).

IR (cm^{-1}): 3058w, 1947vs, 1881vs, 1871vs, 1595w, 1518s, 1482m, 1434s, 1351m, 1233m, 1186m, 1162m, 1094m, 1029w, 898w, 813w, 747m, 696s, 658s, 596s, 544m, 516vs.

^1H NMR (200 MHz, $CDCl_3$) ppm: δ = 2.33 (s, 3H), 6.89 (d, 2H, J = 8.2 Hz), 7.17, (d, 2H, J = 8.4 Hz), 7.45 (m, PPh_3), 7.52 (m, PPh_3)

^{31}P NMR (81 MHz, $CDCl_3$) ppm: δ = 28.68 (s)

Elemental analysis calcd. for $C_{45}H_{37}N_2SO_6P_2Re.0.65CH_2Cl_2$ (1037.24 g mol^{-1}) % C, 52.86; H, 3.72; N, 2.70; S, 3.09. Found % C, 52.29; H, 4.02; N, 2.42; S, 3.79.

4.2.6 Reaction of $Re^{(I)}(Cl)(CO)_3(PPh_3)_2$ (4-2) with 2-2Ag

Complex **4-2** (0.027 g, 0.033 mmol) and **2-2Ag** (0.007 g, 0.034 mmol) were placed in a 50 mL flask. CH_2Cl_2 (7 mL) is added into the flask and the reaction brought to reflux for 24 h. The reaction mixture was allowed to cool and filtered to remove silver chloride and the solvent is removed by vacuum evaporation to give yellow solids (approx. 0.020 g).

IR (cm^{-1}): 2958m, 2871m, 1939m, 1927m, 1896m, 1850m, 1730vs, 1587w, 1434vs, 1409vs, 1367m, 1314vs, 1227m, 1204s, 1178ms, 1095m, 1009m, 979w, 784m, 695m, 516m.

^1H NMR (200 MHz, $CDCl_3$) ppm: 3.43 (s, major), 3.65 (s, major), 7.37 – 7.44 (m)

^{31}P NMR (81 MHz, $CDCl_3$) ppm: 33.70 (s, major), 32.41 (s), 30.34 (s), 28.00 (s, major), 10.20 (s, **4-2**)

4.3 Results and Discussion

4.3.1 Synthesis and spectroscopic characterisation of Re(I) nitrogen acids

The reaction of **4-6** with **2-2** was not successful even though **4-6** is a strong base with strong reducing properties. Significant amounts of the starting complex remain even after addition of additional amounts of **2-2** which result in only small amounts of new ^{31}P resonance signals in the ^{31}P NMR spectrum, one of which corresponds to free triphenylphosphine ligand.

The Re(I) complexes are d^6 metal complexes which tend to be kinetically inert. Substitution of the ligands through acid base reaction is possible with some of the monohydrido Re complexes. Therefore a new series of Re(I) complexes containing a single hydride or labile ligands were used for reaction with the nitrogen acids. The Re(I) nitrogen acids complexes can be synthesized by two separate pathways (Scheme 4-1).

The reaction of either **4-3** or **4-7** with the potassium salts of the N-nitroamides/carbamates/sulfonamides results in the displacement of the labile acetonitrile ligand and elimination of either $KClO_4$ or KBF_4 respectively to give the Re(I) nitrogen acid ligands **4-8**, **4-9** and **4-12**. The alternative reaction pathway involves the reaction of **4-5** with the free nitrogen acids **2-2** and **2-8**. The reaction is an acid-base reaction between the nitrogen acids and the basic hydride of **4-5** and involves the evolution of H_2 and displacement of PPh_3. Both reactions give rise to a definite colour change from colourless to yellow on coordination of the nitrogen acid ligands. The salt metathesis preparation is more efficient and gives cleaner reaction mixtures compared to the acid-base reaction due to the shorter reaction times and better reaction yields. The purification of the Re(I) nitrogen acids from the acid-base preparation is harder because of the similar solubility of the complexes and PPh_3.

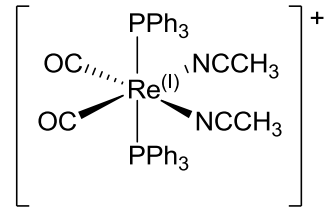

X	Complex
ClO_4^-	**4-3**
BF_4^-	**4-7**

X +

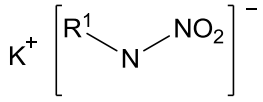

R^1	Compound
$CH_3C(O)$	**2-2K**
$CH_3OC(O)$	**2-4K**
p-tolylSO_2	**2-8K**

R^4OH, reflux, 30 min

$R^4 = CH_3, C_2H_5$

↓ - KX, $2(CH_3CN)$

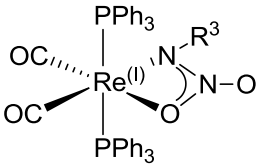

R^3	Complex
$CH_3C(O)$	**4-8**
$CH_3OC(O)$	**4-9**
p-tolylSO_2	**4-12**

toluene, 60 °C, 2 h

↑ - H_2, PPh_3

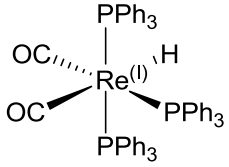

4-5

+

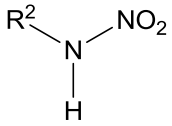

R^2	Compound
$CH_3C(O)$	**2-2**
p-tolylSO_2	**2-8**

Scheme 4-1. Synthesis of **4-8**, **4-9** and **4-12**.

The reaction of **4-7** with **2-6K** is interesting as under different reactions conditions, slightly different reaction products are obtained (Scheme 4-2).

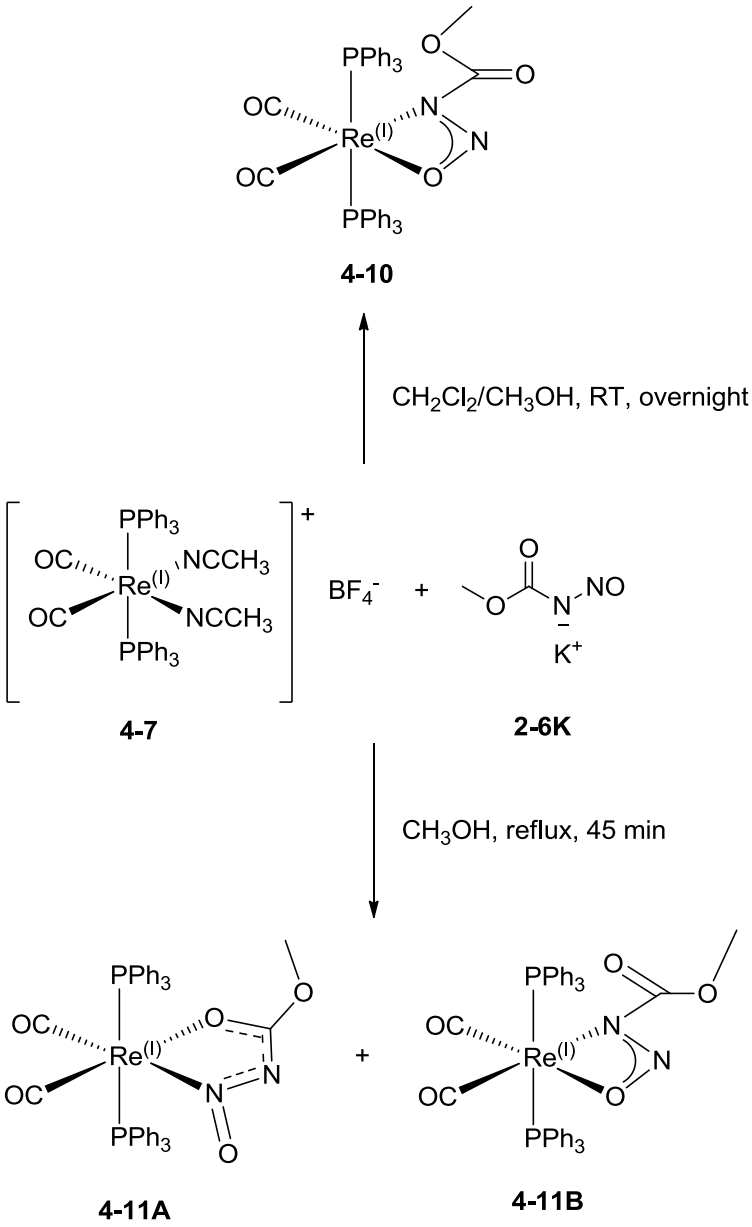

Scheme 4-2. Reaction of **4-7** with **2-6K** under different reaction conditions.

The reaction of **4-7** with **2-6K** at room temperature gives mostly complex **4-10**. The colourless suspension is observed to turn yellow over 10 h. The ^{31}P NMR spectrum shows the major resonance signal at 29.03 ppm with other minor resonance signals some of which are broad. The ^{1}H NMR spectrum is quite complicated with a major signal at 3.41 ppm which is assigned to the methyl

group of the coordinated N-nitrosomethylcarbamate ligand. The IR spectrum has two bands at 1942 and 1864 cm^{-1} for ν(CO) which is similar to that observed for **4-8** and **4-9**. Additional bands at 1750, 1326 and 1070 cm^{-1} are assigned to the Amide I, $\nu(NNO)_{sym}$, $\nu(NNO)_{asym}$ and ν(N-N) respectively.

When the same reaction is carried out under reflux for an hour, the reaction mixture is observed to change from colourless to yellow-orange. The ^{31}P NMR spectrum has a new major resonance at 23.73 ppm with other minor resonances present, one of which is at 29.03 ppm (approx. 0.20 fraction) which corresponds to **4-10**. In the ^{1}H NMR spectrum a new major singlet at 3.07 ppm is also observed. The IR bands for ν(CO) in **4-11** is observed at 1950 and 1870 cm^{-1}, which is different from that in **4-10**. However there is still a much weaker intensity 1748 cm^{-1} band that can still be observed from **4-10** which may be assigned to the isomer **4-11B** discussed in the next section. New bands at 1556, 1419, 1158 and 1066 cm^{-1} are assigned to the Amide I band, $\nu(NNO)_{sym}$, $\nu(NNO)_{asym}$ and ν(N-N) respectively for the new coordination isomer **4-11A**, which is discussed in the next section.

The identification of the ^{31}P signal at 23.73 ppm and ^{1}H signal at 3.41 ppm allowed us to note that small amounts of **4-11A** was also observed (approx. 0.20 fraction) in the room temperature reaction.

The reaction of **4-2** with **2-2Ag** by silver chloride metathesis to obtain **4-8** did not proceed to give only one product. The ^{31}P NMR spectrum is observed to have a signal at 28.00 ppm which can be assigned to **4-8** however significant amounts of other ^{31}P resonance signals were also observed. From the IR spectrum, multiple ν(CO) bands were observed at 1850, 1896, 1926 and 1939 cm^{-1}. The 1850 and 1936 cm^{-1} bands are very similar to the $Re^{(I)}(\eta^2\text{-}CH_3CO_2)(CO)_2(PPh_3)_2$ complex[176] that has been reported at 1850 and 1930 cm^{-1}. Therefore it may be probable that the reaction of **4-2** with **2-2Ag** may have resulted in partial hydrolysis of the conjugate base of **2-2** to the acetate anion.

4.3.2 Crystallographic and structural forms discussion

The molecular structures of **4-8**, **4-9**, **4-10** and **4-12** are shown in Figure 4-1, Figure 4-2, Figure 4-3 and Figure 4-4 respectively.

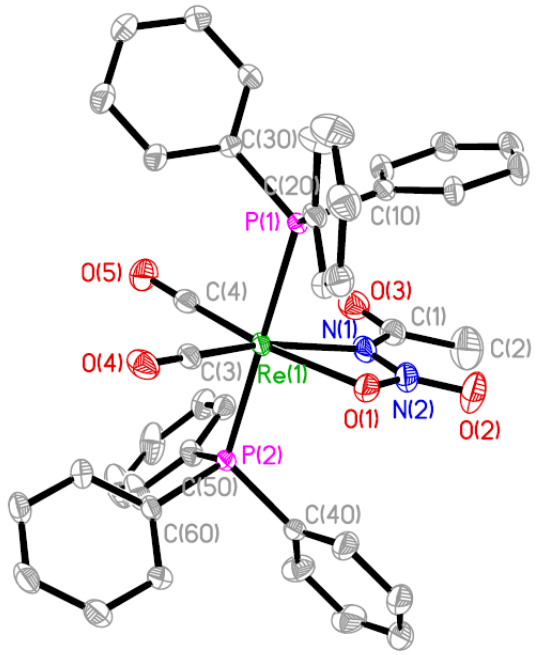

Figure 4-1. Molecular structure of **4-8**. Hydrogen atoms have been omitted for clarity.

The new Re complexes **4-8**, **4-9**, **4-10** and **4-12** have a distorted octahedral geometry around the Re center. The N-nitroamides/carbamates/sulfonamides and N-nitrosocarbamates have identical bidentate coordination through the nitrogen atom of the amide and the oxygen atom of the nitro/nitroso group to the Re center which is similar to the Ir(III) complexes **3-11**, **3-12** and **3-13**. The isomer associated with the coordination in **4-8**, **4-9**, **4-10** and **4-12** are the same as the anionic potassium salt structures of **2-2K**, **2-4K**, **2-6K** and **2-8K** which is the Z isomer for **4-8**, **4-9**, **4-12** and the (Z,E) isomer for **4-10**. From the NMR spectroscopic techniques, it could be observed that the crystals obtained for **4-10** contain about 0.2 mole fraction of **4-11A** (Figure 4-7).

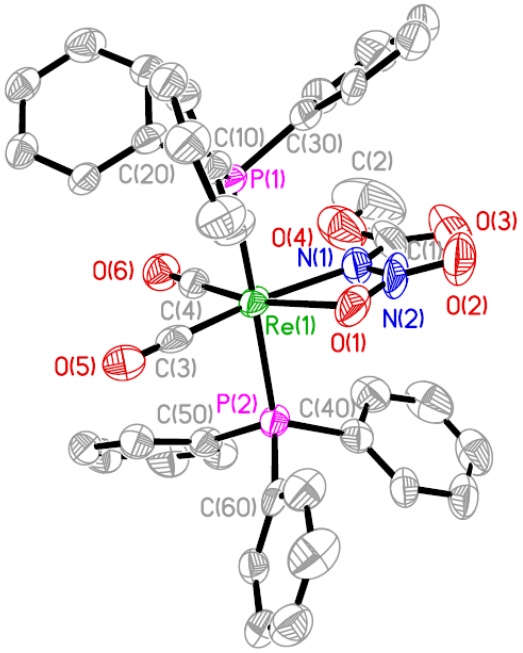

Figure 4-2. Molecular structure of **4-9**. Hydrogen atoms and solvent molecules have been omitted for clarity.

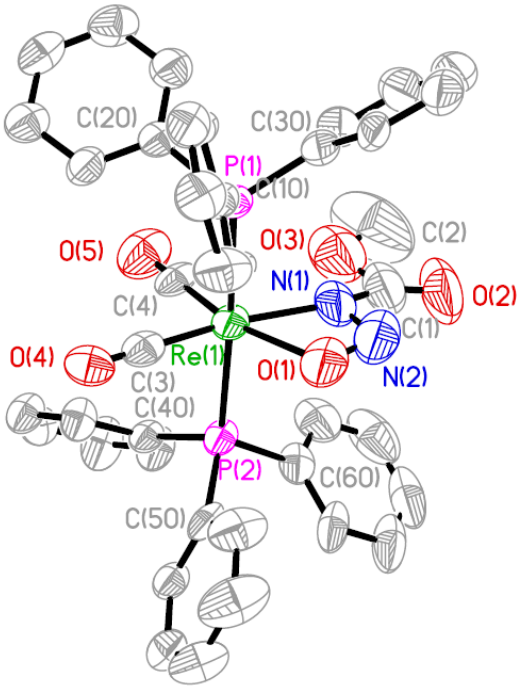

Figure 4-3. Molecular structure of **4-10**. Hydrogen atoms and solvent molecules have been omitted for clarity.

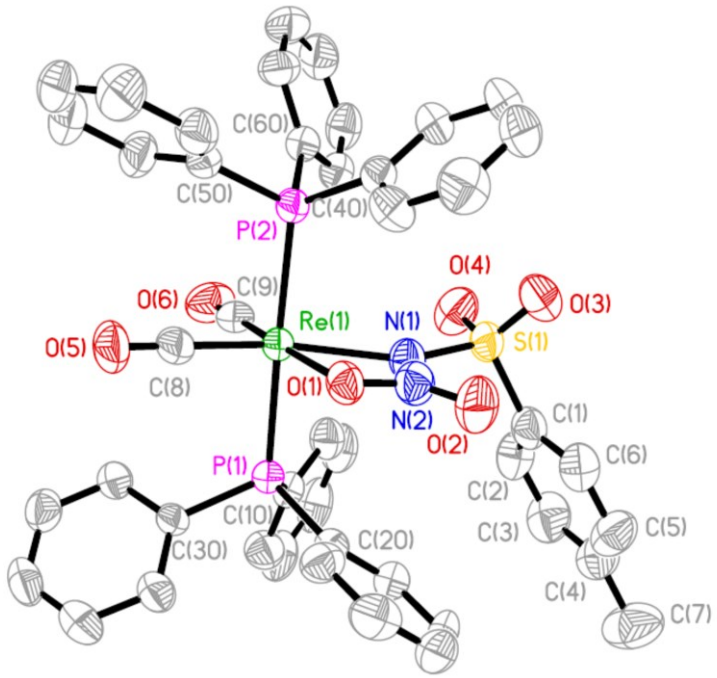

Figure 4-4. Molecular structure of **4-12**. Hydrogen atoms have been omitted for clarity.

The crystal structures of **4-9** and **4-10** have the unusual rhombohedral space group R-3. The unit cell parameter settings for this space group contains two edges of equal length with α and β angles equal to 90° while γ is at 120°. The R-3 space group has two possible settings as it falls under the trigonal/hexagonal crystal systems. The large unit cell volume of greater than 20000 Å^3 only allows the hexagonal setting to be used as there are eighteen general positions versus only six general positions per unit cell assuming a single Re complex in the asymmetric unit cell. The two identical edges of the unit cell in **4-9** and **4-10** are more than 44 Å in length which can almost be considered a super lattice.

The solid state packing arrangement in **4-9** is shown in Figure 4-5 along the shorter edge, the c-axis. Complex **4-10** has similar packing arrangements to Figure 4-5.

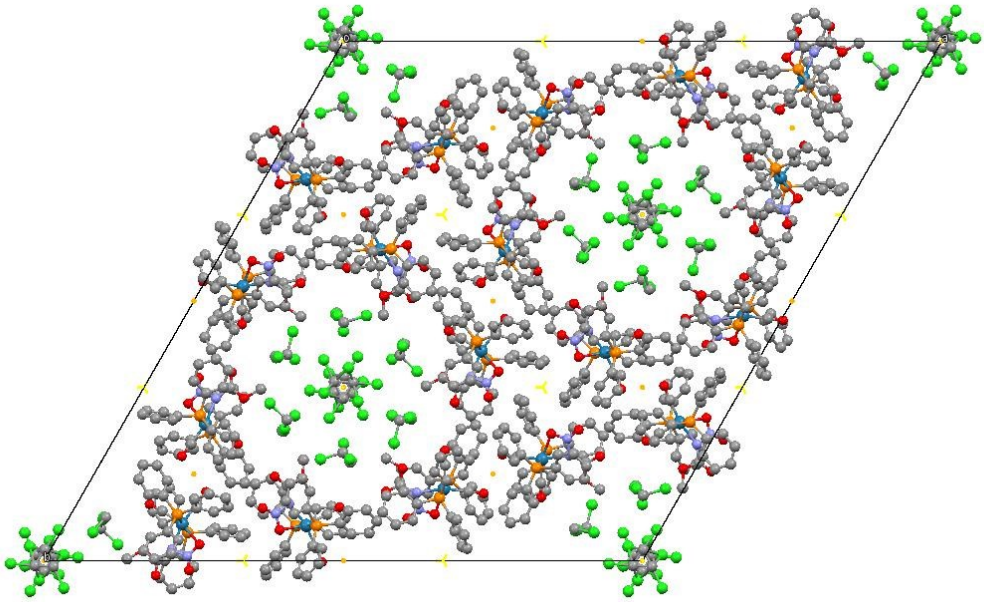

Figure 4-5. Crystal packing of **4-9** in R-3 along the c-axis.

In the above figure, the Re complexes are arranged in a circular pattern with six Re complexes per group generating wide solvent channels. The model for the crystal structure based on the diffraction data suggest up to forty-two molecules of CH_2Cl_2 per unit cell with fourteen molecules of CH_2Cl_2 located within each solvent channel! There are eighteen symmetry operators in the hexagonal R-3 with the inversion and three-fold rotation axis operators clearly defined by the CH_2Cl_2 molecules located at the four axes perpendicular to the ac plane and in the middle of the channels while the Re complexes are replicated by the three-fold rotoinversion axis located between the empty spaces external to the solvent channels. The crystallographic packing arrangement is similar to that obtained by Müller *et al*.[184] with a trigonal R-3 space group. However the diameter of the solvent channel in **4-9** is only 14.1 Å compared to 28 Å in their example. A close inspection of the crystallographic packing diagram in Figure 4-5 shows that the Re complexes are arranged such that the carbonyl ligands, which are hydrophobic, are orientated approximately 60^o towards each other within the 'walls' of the channel and also towards sections of 'walls' of the other channels to complete the macro arrangement. The channels are inscribed by the hydrophilic

ester section of the N-nitrocarbamate ligands (or nitroso in **4-10,** Figure D-1) oriented towards the center of the channels. This particular arrangement serves to allow hydrogen bond linkages between the oxygen atoms of the ester group and the hydrogen atoms of the dichloromethane solvates which give rise to the stability of this unusual crystallographic macrostructure.

The R-3 space group is related to the triclinic space group P-1 in that the three-fold and six-fold rotation axes are missing. The end result is that the P-1 unit cell has only half the cell length of the identical edges and only a third of the volume of the R-3 unit cell (Table D-1). With only an inversion center as the symmetry operator, there are three independent molecules in the asymmetric unit which generates a single solvent channel per unit cell (Figure 4-6).

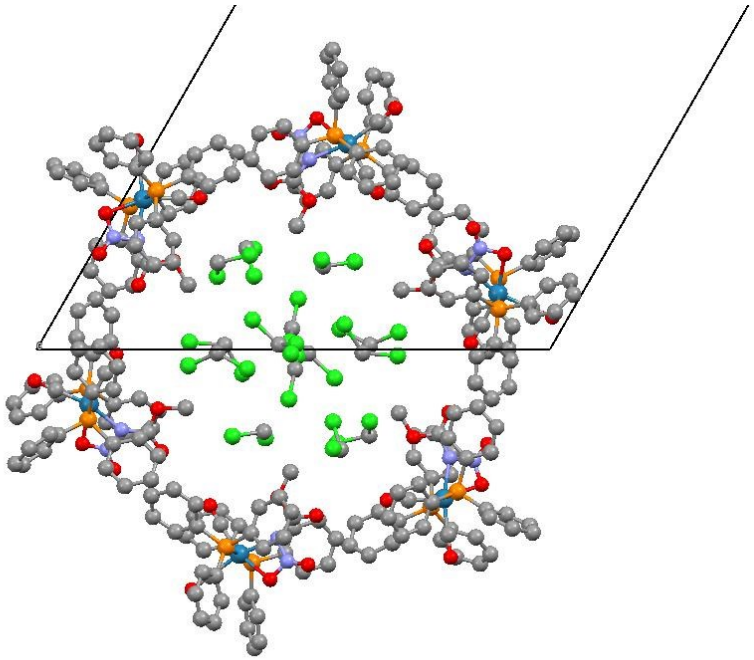

Figure 4-6. Crystal packing of **4-9** in P-1 along the c-axis.

The solvent channel in the P-1 space group contains up to fourteen CH_2Cl_2 molecules per unit cell too. The difference between the R-3 or P-1 setting is dependent on whether there is a true three-fold rotoinversion symmetry relationship between the Re complexes and also between the CH_2Cl_2 molecules. The case of global psuedosymmetry[185] may arise if the three-fold and six-fold symmetry between the Re complexes, CH_2Cl_2 in the R-3 setting is not real. The

choice of the space group would be dependent on the diffraction spot pattern. For the triclinic space group, P-1, there are no general reflection conditions required for the diffraction spot array while the space group, R-3, has several general reflection conditions such as systematic absences of $-h + k + l = 3n$ in the *hkil* zone, $-h + k = 3n$ in the hki0 zone and others which are required to be observed in the diffraction spot pattern. The solvent molecules are rarely found to be in an ordered arrangement. Therefore the arrangement of the Re complexes have a much greater effect on assigning the correct space group. Due to the large volume of solvent space located within the channels, there are multiple possible arrangements of the CH_2Cl_2 molecules. With the relatively heavy element Cl of the CH_2Cl_2 molecule, the disordered arrangement of these molecules can greatly affect the diffraction data at higher angles as was observed in the organic compound example by Müller *et al*.[184] For complex **4-9** and **4-10**, the situation is much better as the third row transition element Re together with the phosphorus in the phosphine ligands are also able to contribute to the diffraction data at high angles. The outcome is that we do not observe significant streaking of the diffraction spots in the high angle regions. Regardless of the remarkably good data sets that are obtained in **4-9** and **4-10**, it is still important to provide a suitable model for the arrangement of the CH_2Cl_2 molecules within the channels as they do contribute significantly to the diffraction data obtained from the presence of the Cl atoms. It is likely that these molecules are highly disordered and during the course of the least squares refinement process, distance constraints, DFIX, of 1.79 Å had to be used on the C-Cl bond lengths. This is in addition to the least squares restraints on the atomic distance esds such as SADI but also the least squares restraints ISOR, SIMU and DELU which affects the thermal parameters of the carbon and chloride atoms of CH_2Cl_2. In essence the bond parameters of the CH_2Cl_2 molecules in **4-9** and **4-10** are not suitable for analysis.

The X-ray diffraction solution for **4-11** contains two independent Re complexes that are different isomers of **2-6** coordinated to the Re center as shown in Scheme 4-2 (Figure 4-7). The solid state molecular structure of **4-11A** and **4-11B** are shown in Figure 4-8 and Figure 4-9 respectively.

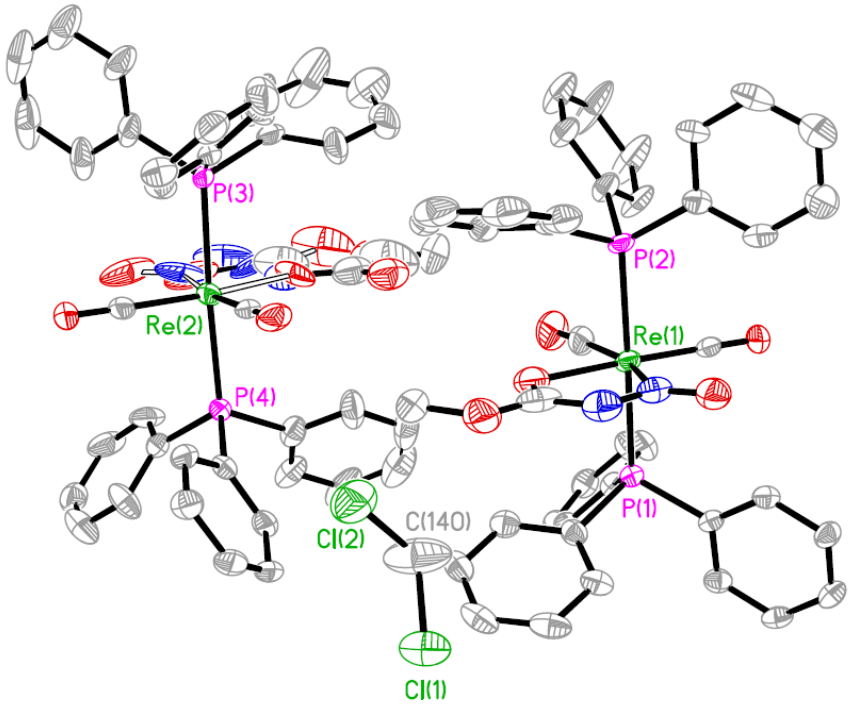

Figure 4-7. Solid state diagram of **4-11** with two independent Re complexes, **4-11A** (right) and **4-11B** (left). A CH_2Cl_2 solvate is also shown.

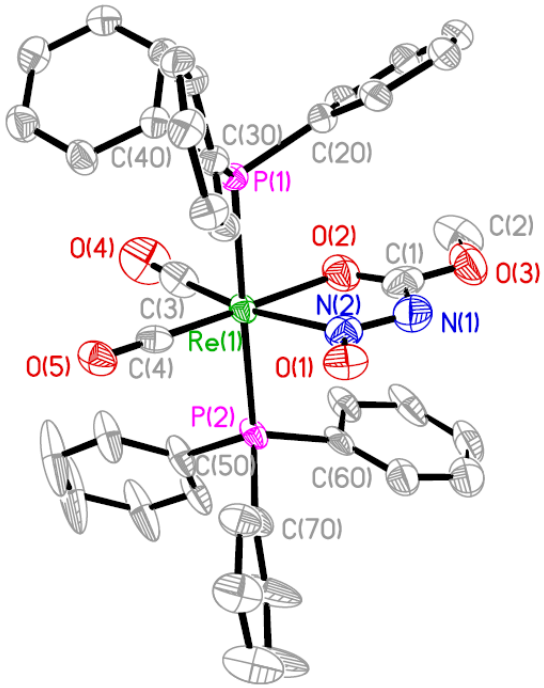

Figure 4-8. Molecular structure of **4-11A**. Hydrogen atoms and solvent molecules have been omitted for clarity.

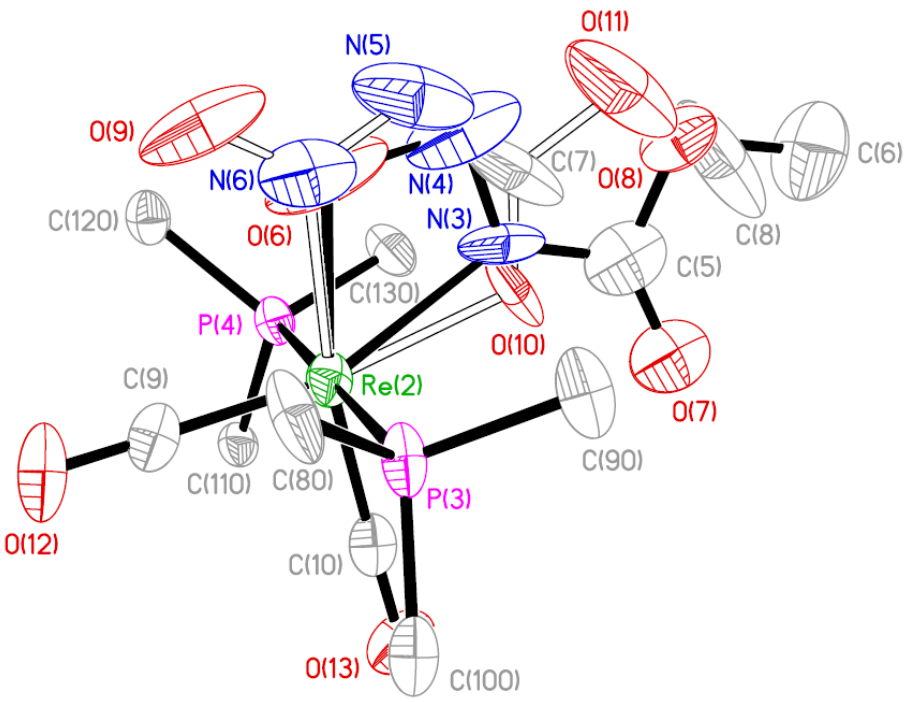

Figure 4-9. Molecular structure of **4-11B** with highlight on the disorder of the ligand. Full black lines refer to four-membered ring coordination. White lines refer to five-membered coordination. Phenyl rings of PPh_3 not shown and hydrogen atoms and solvent molecules have been omitted for clarity.

The structure of **4-11A** shows an unprecedented coordination isomer of **4-10** with regards to our current work on the coordination chemistry of the nitrogen acids. Structure **4-11A** has the same distorted octahedral coordination around the Re center with cis carbonyl and trans triphenylphosphine ligands. The N-nitrosocarbamate ligand is still bidentate but coordinated to the Re center through the oxygen atom of the acyl group and the nitrogen of the nitroso group! In normal circumstances, this form of coordination is expected for ligands with acyl functional groups as mention in Chapter 3. However with regards to the series of nitrogen acid coordination complexes that has been mentioned in both Chapter 3 and the above sections of Chapter 4, this structural isomer is definitely unexpected.

In a case of serendipity, the second Re complex in the X-ray structure model of **4-11** contains disordered isomers of both **4-11A** and the (E,E) ligand isomer of **4-10**, **4-11B** (Figure 4-9, Figure 4-10).

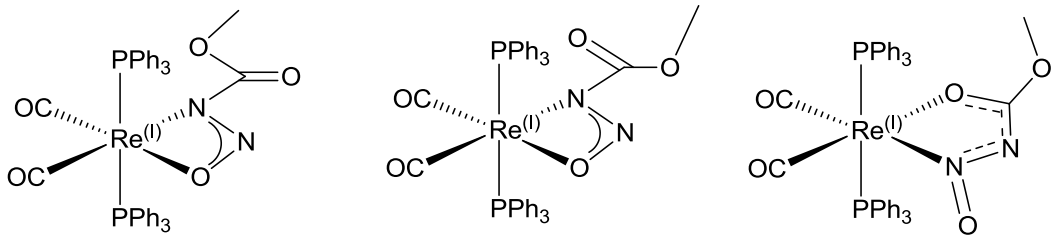

Figure 4-10. Coordination isomers of **2-6** in $Re^{(I)}(\eta^2$-$CH_3OC(O)NNO)(CO)_2(PPh_3)_2$ complexes.

The model for the diffraction data of **4-11** indicates approximately 1:1 ratio or 50% probability of either structure **4-11A** or structure **4-11B** in the second disordered Re complex. Due to the severe disorder encountered, several least squares restraints such as ISOR, SIMU, DELU for the thermal parameters and SADI for the bond lengths are required to model the disorder. In addition, a constraint, EADP to O(9) atom of **4-11B**, was applied to the O(6) atom of **4-11B** to restrict the anisotropic thermal parameters of the O(6) atom turning non-positive definite.

The solid state structural observations of **4-11** could be a 'frozen frame' of the transformations occurring in the reaction of **4-7** with **2-6K** over time. From the observations in the ^{31}P, ^{1}H NMR, IR spectroscopy and X-ray diffraction data, we proposed a possible sequence of transformations occurring between **4-7** and **2-6K** over time where the kinetic product is **4-10** while the final thermodynamic product is **4-11A**. Complex **4-11B** is an intermediate that is not observed in the NMR spectroscopic techniques (Scheme 4-3).

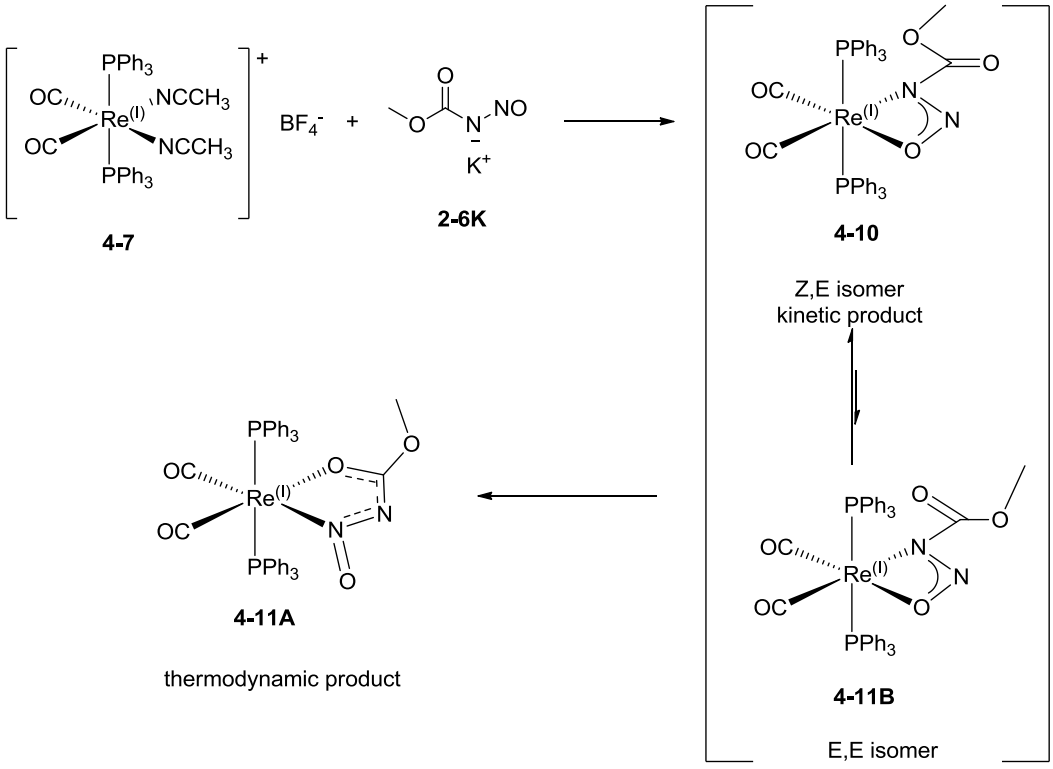

Scheme 4-3. Proposed transformations in reaction of **4-7** with **2-6K**.

Some evidence of the proposed transformations is observed in the ^{31}P NMR and ^{1}H NMR spectrums of the room temperature and reflux condition reactions where the resonance signals for **4-10** and **4-11A** are observed in fractional amounts corresponding to reaction conditions in the reaction mixtures and crystal dissolutions of both reaction conditions. There were other minor resonance signals present especially in the ^{31}P spectrum, however these signals are not observed together in both reaction conditions which may allow the assignment of signals to **4-11B**. It could be possible that **4-11B** is in equilibrium with **4-10** in solution but not observed due to rapid exchange and just happen to co-crystallize with **4-11A**. Once the crystals of **4-11** are dissolved, the signals of **4-11B** appear as **4-10**.

The transformation process from **4-10** to **4-11A** is not understood. However, one could consider a 'simplified' pathway of conversion from **4-10** to **4-11A** to involve total ligand dissociation from one side of the complex followed by coordination of the ligand from the opposite side of the N-

nitrosomethylcarbamate ligand. This obviously is unlikely to occur. The rearrangement may follow instead a similar pathway as $Re^{(I)}(\eta^2\text{-}NO_2)(CO)_2(PPh_3)_2$, **4-4**,[182] where CO addition creates N and O coordination isomers of the nitrite ligand either by one ended dissociation followed by coordination or a dimeric intermediate. This type of transformation is common for transition metal nitrite complexes.[186] These possible reaction mechanisms are better expressed in Scheme 4-4 for our present system.

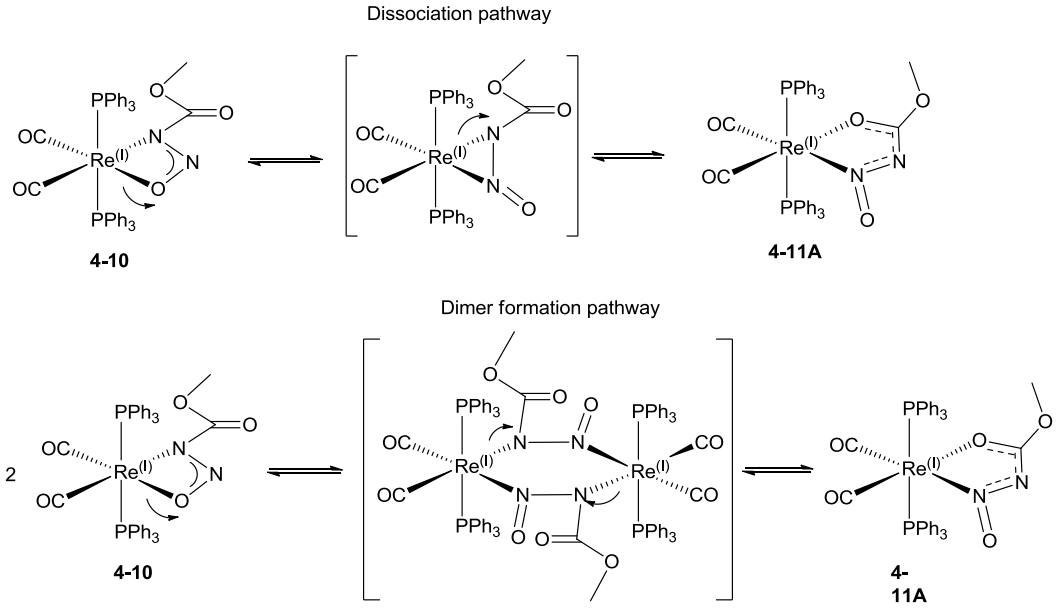

Scheme 4-4. Possible mechanisms of transformation of **4-10** to **4-11A** based on analogy of **4-4** by Grundy *et al*.[182]

The reaction of $Re^{(I)}(\eta^2\text{– }NO_2)(CO)_2(PPh_3)_2$ (**4-4**) with HCl gives two products, $Re^{(I)}Cl(CO)_3(PPh_3)_2$, **4-2** and $Re^{(I)}(Cl)_2(NO)(CO)(PPh_3)_2$, **4-12**, which seems to indicate that the reaction proceeds by a dimer formation of the Re complexes to allow the formal transfer of one of the carbonyl ligands to the other Re complex.

The selected bond lengths, bond and torsion angles of the Re(I) nitrogen acid complexes are shown in Table 4-2. For the N-nitro nitrogen acid ligands **4-8**, **4-9** and **4-12**, the N(1)-N(2) bond lengths are shorter than the N(1)-C(1) bond lengths which are similar to **3-11** and **3-13**. The N(2)-O(1) bond lengths are also longer than the N(2)-O(2) bond lengths due to coordination to the Re center which is also similar to the Ir (III) complexes. The torsion angles for O(1) – N(2) – N(1) – C(1)/S(1) and O(3) – C(1)/S(1) – N(1) – N(2) are close to 180° which means the

ligands are also mostly planar. In general, the Re(1)-N(1) bond length is slightly shorter than the Re(I)-O(1) bond lengths.

For **4-10**, the N(1)-N(2) and N(2)-O(1) bond lengths are 1.477 and 1.403 Å respectively, which is long. This could be due to the unmarked disorder with isomer **4-11A** which is observed in the ^{31}P and ^{1}H NMR spectrums in small amounts, approximately 20 %. Least square restraints ISOR, SIMU and DELU have been applied to the nitrogen acid ligand in **4-10** to reduce the effects of **4-11A** disorder. Therefore some of the bond lengths for **4-10** are not a true representation of the actual bond lengths. For **4-11A**, the N(1)-N(2) bond length at 1.320(9) Å and also the N(1)-O(1) nitrosyl bond length at 1.190(7) Å indicate double bond character. The O(2)-C(1) bond length of the coordinated acyl group is only slightly longer at 1.248(9) Å.

Table 4-2: Selected bond lengths (Å), bond and torsion angles (deg) of $Re^{(I)}(\eta^2\text{-}X)(CO)_2(PPh_3)_2$.

Compound	**4-8**	**4-9**[a]	**4-10**	**4-11A**[b]	**4-11B**[c]	**4-12**[d]
Re(1) – N(1)	2.213(4)	2.151(6)	2.117(10)	2.127(6)	2.25(4)	2.239(4)
Re(1) – O(1)	2.211(4)	2.203(5)	2.189(9)	2.176(5)	2.13(4)	2.182(4)
N(1) – N(2)	1.339(7)	1.351(11)	1.477(17)	1.320(9)	1.31(3)	1.349(6)
N(1) – C(1)/S(1)	1.383(6)	1.378(12)	1.238(19)	1.358(10)	1.39(4)	1.653(4)
N(2) – O(1)	1.270(6)	1.295(10)	1.403(17)	1.190(7)	1.47(4)	1.273(6)
N(2) – O(2)	1.226(6)	1.204(8)				1.210(6)
Re(1) – C(3)	1.870(4)	1.896(7)	1.902(11)	1.918(8)	1.884(7)	1.872(6)
Re(1) – C(4)	1.880(5)	1.886(6)	1.900(10)	1.881(7)	1.897(7)	1.872(6)
C(3) – O(4)	1.159(5)	1.162(7)	1.136(11)	1.159(9)	1.166(8)	1.146(6)
C(4) – O(5)	1.142(6)	1.154(7)	1.170(11)	1.171(8)	1.162(8)	1.134(7)
O(1) – Re(1) – N(1)	57.64(16)	59.2(3)	65.3(5)	73.3(2)	55.9(11)	57.94(15)
Re(1) – N(1) – N(2)	95.3(3)	96.3(6)	94.0(9)	118.0(5)	104(2)	93.7(3)
N(1) – N(2) –O(1)	109.6(4)	108.7(6)	107.5(10)	111.7(7)	95(3)	109.6(4)
N(2) – O(1) – Re(1)	97.5(3)	95.6(4)	93.2(8)	125.0(8)	104.6(18)	98.7(3)
C(1) – O(2) – Re(1)				112.1(6)		
O(1) – N(2) – N(1) – C(1)/S(1)	178.0(4)	-175.2(6)	-177.3(10)	179.8(6)	-179(4)	169.4(3)
O(3) – C(1)/S(1) – N(1) – N(2)	-174.8(4)	8.9(14)	-175.5(9)	-1.4(10)	172(3)	-43.7(5)

a. O(5) instead of O(3) and O(6) instead of O(4).

b. N(2) instead of N(1), O(2) instead of O(1), Re(1) – N(2) – N(1), N(2) – N(1) – C(1), N(1) – C(1) –O(2), O(2) instead of O(3)

c. Isomer of **4-9** and similar sequence, labels are just bigger numbers.

d. C(8) instead of C(3), C(9) instead of C(4), O(5) instead of O(4) and O(6) instead of O(5).

4.4 Conclusion

The Re(I) nitrogen acids complexes can be synthesized from two methods: 1) from salt metathesis reactions between the cationic Re(I) complexes **4-3** and **4-7** with the potassium salts **2-2K**, **2-4K**, **2-6K** and **2-8K**, and 2) from acid base reactions between **4-5**, which contains a basic Re hydride, with the free acid **2-2** and **2-8**. The salt metathesis method is more efficient as purification through elimination of the side product potassium salt is easier. The Re nitrogen acid complexes containing the nitro groups **4-8**, **4-9** and **4-12** have similar bidentate coordination geometry with the Ir(III) complexes **3-11**, **3-12** and **3-13** through the amide nitrogen and the oxygen atom of the nitro group.

The reaction of **4-7** with the **2-6K** gives two different products depending on the reactions conditions. The kinetic product **4-10** is observed to form when the reaction is carried out at room temperature while the thermodynamic product **4-11A** is observed when the reaction is carried out under reflux conditions. On standing in solution for long periods, it is observed that greater amounts of **4-11A** is formed from **4-10**. During the crystallization process of **4-11A**, some amount of **4-11B** is observed which is a configuration isomer of **4-10**. Complex **4-11B** is most likely an intermediate from **4-10** that co-crystallizes out of solution during the slow conversion process. Complex **4-10** has similar coordination mode with the Ir(III) complexes and Re(I) complexes **4-8**, **4-9** and **4-12**. Complex **4-11A** is the first complex that coordinates to the nitrogen of the nitrosyl fragment and the oxygen of the acyl fragment encountered in the coordination chemistry of the nitrogen acids in our work. This unique coordination mode provides more insight into the different chemistry between the N-nitro nitrogen acids and the N-nitroso nitrogen acids.

Complexes **4-9** and **4-10** both crystallize in an unusual space group R-3 which gives a large unit cell containing eighteen molecules. Within the unit cell there are two solvent channels walled by six Re complexes that can contain up to fourteen CH_2Cl_2 molecules. This unexpected crystal packing may be driven by the

hydrogen bonding effects between the dichloromethane molecules and the ester section of the ligand in **4-9** and **4-10**.

Chapter 5: Activation of Benzotriazole Derivatives

5.0 Introduction

The 1,2,3-triazoles have risen in prominence in recent times since the rediscovery of the 1,3-Huisgen dipolar addition of azides to alkynes[187] by Sharpless et. al. in 2001[188] (Scheme 5-1). This hetero-cycloadditon reaction, named the 'Click' reaction has found numerous incorporation in new materials, chemical biological probes, and an array of new reagents due to its selectivity and mild reaction conditions in the presence of a Cu(I) catalyst.[189] In order to increase the versatility of triazoles, it would be of synthetic interest if the triazole framework can be further exploited such that eventual multiple reaction transformations can be carried out.

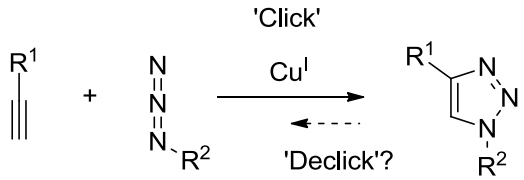

Scheme 5-1. 1,3-Huisugen dipolar addition.

Promoting a retro-1,3-dipolar addition of the triazole to the initial azide and alkyne Scheme 5-1 is strongly enthalpically unfavored and the only example reported is the unusual ultrasound promoted retro addition of a triazole which results from a long chain alkyne and azide.[190] Although the generality of the ultrasound reaction is an open question,[191] the case for developing an unclicking method remains compelling.

5.1 General Experimental

General: All reagents and solvents are used as supplied commercially. Dry CH_3OH is distilled from freshly generated magnesium methoxide, dry $CHCl_3$ is distilled from $CaCl_2$, dry CH_2Cl_2 is distilled from CaH_2, dry dimethylacetamide (DMA) is refluxed with BaO and distilled under reduced pressure. Dry hexanes and pentanes are distilled from sodium benzophenone ketyl. ^{1}H and ^{31}P spectra are recorded on Varian Mercury 200, 400 or 500 MHz spectrometers, ^{19}F spectra on Varian Mercury 200, 300 or 500 Mhz spectrometers and ^{13}C spectra on a Varian Mercury 300 Mhz spectrometer. All chemical shifts are recorded in δ (ppm) relative to residual solvent signals for ^{1}H and ^{13}C spectra, CF_3COOH for ^{19}F spectra and H_3PO_4 for ^{31}P spectra. Melting/decomposition points are measured by using a TA-Q2000 differential scanning calorimeter. The IR spectra are recorded in KBr disks by using ABB Bomem MB Series spectrometer with spectral resolution of 4 cm^{-1}. UV/visible spectra were measured using a HP 8453 Diode Array spectrophotometer from HP Elemental analyses are performed in the Elemental Analyses Laboratory at University of Montreal.

X-ray crystallography: Crystals are mounted on Mitegen mounts using Paratone-N from Hampton Research and X-ray diffraction experiments are carried out with a BRUKER APEX-II CCD diffractometer by using graphite-monochromated $Mo_{K\alpha}$ radiation (λ = 0.71073 Å) and KRYOFLEX for low temperature experiments. SAINT[105] is used for integration of the intensity reflections and scaling and SADABS[106] for absorption correction. The initial electron density maps are solved by Patterson vector maps followed by difference Fourier maps for the position of light non-hydrogen atoms. Final refinements are optimized using full-matrix least-squares method on F^2 of all data, by using SHELXTL[105] software. The hydrogen atoms positions are placed in calculated positions. Crystallographic data and data collection parameter solutions are shown in Table 5-1.

Table 5-1: Crystallographic data for **5-7** and **5-8** complexes.

Compound	**5-7**	**5-8**
empirical formula	$C_{46}H_{34}IrP_2ClN_3O_2F_9S.$ CH_2Cl_2, C_5H_{12}	$C_{48}H_{38}IrP_2ClN_6O_2S.$ CH_2Cl_2, $2CH_3OH$
T (K)	100(2)	100(2)
fw (g mol^{-1})	1310.48	1193.44
cryst sys	triclinic	monoclinic
space group	P-1	$P2_1/c$
a (Å)	9.5662(14)	11.5727(7)
b (Å)	11.5285(17)	17.7144(11)
c (Å)	25.311(4)	23.4260(14)
α (deg)	84.534(2)	90
β (deg)	89.423(2)	93.6100(10)
γ (deg)	74.541(2)	90
V ($Å^3$)	2677.9(7)	4792.9(5)
Z	2	4
density (g cm^{-3})	1.625	1.654
abs coeff (mm^{-1})	2.816	3.117
No. of reflns collected	25461	54128
No. of indep reflns	9421	11147
Data/restraints/parameters	9421/419/769	11147/0/583
Final R indices [$I > 2s(I)$] R1/wR2	0.0545/0.1461	0.0459/0.1173
R indices (all data) R1/wR2	0.0563/0.1470	0.0499/0.1205
Goodness-of-fit on F^2	1.235	1.045

Theoretical methods:

Gaussian03 was used for all calculations with B3LYP density functional theory and the triple zeta basis set 6-311++g**. All ground stacks are checked for non-position frequencies and solvent effects were determined using a polarized continuum model.

5.2 Synthesis of Ir diazo/diazene complexes.

Experimental

The benzotriazoles 1-[(nonafluorobutane)sulfonyl]-1H-benzotriazole (**5-1**),[192] 1,1′-sulfonylbis(benzotriazole) (**5-2**),[193] 1-nitro-1,2,3-benzotriazole (**5-3**),[194] 1-cyano-benzotriazole (**5-4**),[195] 1-*p*-nitrophenylsulfonyl-1,2,3-benzotriazole (**5-5**), and 1-*p*-tolylsulfonyl-1,2.3-benzotriazole (**5-6**), are prepared with modification to known literature methods. DMA.HCl,[196] **3-1**[151] and **3-2**[157] are prepared by literature methods.

5.2.1 Synthesis of $Ir^{(I)}(\eta^1\text{-}NNPhNSO_2C_4F_9)(Cl)(PPh_3)_2$ (5-7) .

Complex **3-2** (0.195 g, 0.25 mmol) and **5-1** (0.100 g, 0.25 mmol) are dissolved in degassed $CHCl_3$ (10 mL). The solution turned dark green rapidly with vigorous effervescence. The reaction mixture is allowed to stir for an hour and the solvent removed in *vacuo* until dryness. The dark-green residue is recrystallized from dry CH_2Cl_2/pentanes to give dark green crystals of $Ir^{(I)}(\eta^1\text{-}NNPhNSO_2C_4F_9)(Cl)(PPh_3)_2$ (**5-7**) (0.225 g, 0.195 mmol, 78 % yield).

IR (KBr, cm^{-1}): 3057w, 2960w, 2923w, 2856w, 1880m, 1482m, 1464m, 1436m, 1321m, 1297m, 1234s, 1190m, 1149s, 1097s, 1028m, 1010m, 982m, 825w, 746s, 709m, 693s, 582m, 573m, 520s.

^1H NMR (200 MHz, $CDCl_3$) ppm: δ = 6.11 (dd, 1H, *J* = 8.0, 1.6 Hz), 6.35, (td, 1H, *J* = 7.7, 1.2 Hz), 6.97 (td, 1H, *J* = 7.8, 1.4 Hz), 7.14 (m, 1H), 7.36 (m, PPh_3), 7.84 (m, PPh_3).

^{19}F NMR (470 MHz, $CDCl_3$) ppm: δ = -80.86 (t, 3F, *J* = 9.4 Hz), -112.70 (tq, 2F, *J* = 14.1, 4.7 Hz), -121.32 (m, 2F), -125.95 (m, 2F).

^{31}P NMR (81 MHz, $CDCl_3$) ppm: δ = 16.26 (s).

UV ($CHCl_3$ λ_{max}, nm (ε, M^{-1} cm^{-1})): 242 (60000), 290sh (34000), 405 (5400), 600 (266).

Elemental analysis calcd. for $C_{46}H_{34}N_3O_2F_9SP_2ClIr$ (1153.45 g mol^{-1}) %: C, 47.85; H, 2.95; N, 3.64; S, 2.77. Found: C, 47.87; H, 3.01; N, 3.53; S, 2.63.

5.2.2 Synthesis of $Ir^{(III)}(\eta^3$-NNPhNSO$_2$Btz)(Cl)(PPh$_3$)$_2$ (5-8)

A solution of **3-2** (0.050 g, 0.064 mmol) in degassed chloroform (10 mL) is cooled down to 0 °C under nitrogen. While stirring, (0.019 g, 0.064 mmol) of **5-2** in degassed chloroform (1 mL) is added via a syringe. After an additional 3 h of stirring at ambient temperature the solvent is evaporated to give quantitative yield. Deep red crystals of $Ir^{(III)}(\eta^3$-NNPhNSO$_2$Btz)(Cl)(PPh$_3$)$_2$ (**5-8**) are obtained from recrystallization in CH_2Cl_2/CH_3OH.

IR (KBr, cm^{-1}): 3057w, 2960w, 2915w, 2855w, 1591w, 1484m, 1459m, 1435s, 1320m, 1272w, 1233w, 1158s, 1093s, 927m, 915m, 863w, 793w, 743s, 707m, 694s, 593w, 560w, 522s.

^{1}H NMR (200 MHz, $CDCl_3$) ppm: δ = 6.66 (t, 1H, *J* = 7.5 Hz), 7.03 (m, 1H + PPh_3), 7.34 (t, 2H, *J* = 7.3 Hz), 7.52 (m, 2H + PPh_3), 7.75 (q, 2H, *J* = 9 Hz)

^{31}P NMR (81 MHz, $CDCl_3$) ppm: δ = -13.08 (s).

UV ($CHCl_3$ λ_{max}, nm (ε, M^{-1} cm^{-1})): 270 (31000), 490 (1100).

MS (ESI^+), *m/z*: calcd. for [$C_{48}H_{38}N_6O_2SP_2ClIr$] M 1051.54; found: [M – [PPh_3] + H]$^+$ 790.69 (95%); [M + H]$^+$ 1052.62 (50%).

Elemental analysis calcd. for $C_{48}H_{38}N_6O_2SP_2ClIr.2CH_3OH$ (1112.59 g mol^{-1}) %: C, 53.78; H, 4.15; N, 7.53; S, 2.87. Found: C, 54.17; H, 3.92; N, 7.58; S, 2.54.

5.2.3 IR solution monitoring formation of complex 5-8

A solution of **3-2** (0.010 g, 0.013 mmol) in degassed $CHCl_3$ (3 mL) is cooled down to -10 °C under nitrogen. **5-2** (0.004 g, 0.013 mmol) in cold degassed $CHCl_3$ (0.5 mL) is added via a syringe with stirring. Aliquots of the reaction mixture are removed, placed in a solution IR cell and recovered, at intervals over a period of 3 h.

5.2.4 Reaction of 3-2 with 5-3

Complex **3-2** (0.030 g, 0.0385 mmol) and **5-3** (0.007 g, 0.043 mmol) are dissolved in degassed $CHCl_3$ (5 mL). The solution turned reddish-brown over a period of 2 min. The reaction mixture is allowed to stir for 2 hour and the solvent removed in *vacuo* to give red-brown solids (approx. 0.020g).

IR (cm^{-1}): 3055w, 1625m, 1482m, 1471m, 1435s, 1280m, 1264m, 1218m, 1095m, 1025w, 744m, 694vs.
^1H NMR (200 MHz, $CDCl_3$) ppm: δ = 8.17 (t, 1H, *J* = 7.7 Hz), 7.87 (dd, 1H, *J* = 7.6 Hz, 2 Hz), 7.51 (m), 7.31 (s), 7.35 (s), 7.25(m), 7.12 (t, 1H, *J* = 7.4 Hz), 7.02 (d, 1H, *J* = 5.8 Hz)
^{31}P NMR (81 MHz, $CDCl_3$) ppm: δ = -6.16 (s).

5.2.5 Reaction of 3-2 with 5-4

Complex **3-2** (0.030 g, 0.0385 mmol) and **5-4** (0.006 g, 0.042 mmol) are dissolved in degassed $CHCl_3$ (5 mL). The solution turned orange-red with vigorous effervescence. The reaction mixture is allowed to stir for 30 min and the solvent removed in *vacuo* to give red solids (approx. 0.024 g).

IR (cm^{-1}): 3056w, 2961w, 2257m, 2194m, 2170m, 1624w, 1602m, 1573w, 1482m, 1433m, 1260m, 1091s, 1025m, 798m, 742s, 692vs.
^1H NMR (200 MHz, $CDCl_3$) ppm: δ = 7.80 (m, 1H), 7.56 (m), 7.30 (m), 6.93 (td, 1H, *J* = 7.3 Hz, 1.8 Hz), 6.42 (td, 1H, *J* = 7.5 Hz, 1.4 Hz), 6.01 (dd, 1H, *J* = 8.4 Hz, 1.2 Hz)
^{31}P NMR (81 MHz, $CDCl_3$) ppm: δ = -10.68 (s).

5.2.6 Reaction of 3-2 with 5-5

Complex **3-2** (0.030 g, 0.0385 mmol) and **5-5** (0.012 g, 0.039 mmol) are dissolved in degassed $CHCl_3$ (5 mL). The solution turned reddish-brown over 10 min. The reaction mixture is allowed to stir for 2 h and the solvent removed in *vacuo* to give red-brown solids (approx. 0.020 g).

IR (cm^{-1}): 3055w, 2960w, 1604w, 1526m, 1483m, 1434m, 1348m, 1189m, 1094m, 1029m, 744s, 693vs, 521vs.
^{31}P NMR (81 MHz, $CDCl_3$) ppm: δ = 4.94, (major, s), 3.81 (s), 1.59 (s), -3.17 (d, J = 7.45 Hz), -3.17 (s), -12.90 (d, J = 7.45 Hz)

5.2.7 Reaction of 3-2 with 5-6

Complex **3-2** (0.030 g, 0.0385 mmol) and **5-6** (0.008 g, 0.041 mmol) are dissolved in degassed $CHCl_3$ (5 mL). There is no visible reaction and the reaction mixture is allowed to stir for 2 h and the solvent removed in *vacuo* to give a mixture of brown and yellow solids which are identified as the starting Ir complex.

5.3 Reactivity studies of **5-7** and **5-8**.

5.3.1 Reaction of complex 5-8 with nucleophiles.

Reaction of **5-8** with CO.

Complex **5-8** (0.030 g, 0.0285 mmol) is dissolved in $CHCl_3$ (5 mL) and CO was bubbled into the solution for 30 min. No visible reaction was observed and the solvent removed in *vacuo* to give the starting Ir complex in quantitative yield.

Reaction of complex **5-8** with pyridine.

Complex **5-8** (0.030 g, 0.0285 mmol) is dissolved in $CHCl_3$ (5 mL) and pyridine (1.5 mL, 0.0372 mmol, 0.025 mM $CHCl_3$ solution) was added. No visible reaction was observed and the solvent removed in *vacuo* to give the starting Ir complex in quantitative yield.

5.3.2 Reaction of complex 5-7 with nucleophiles.

Reaction of **5-7** with CO

Complex **5-7** (0.030 g, 0.026 mmol) was dissolved in degassed $CHCl_3$ (5 mL) and CO is bubbled into the solution for 15 min. The dark-green solution slowly turned yellow during the course of the reaction. The solvent is removed in *vacuo* to give quantitative yellow solids which were identified as **3-1**.

IR (KBr, cm^{-1}): 1953vs

^{31}P NMR (81 MHz, $CDCl_3$) ppm: $\delta = 24.86$ (s)

Reaction of **5-7** with pyridine

Complex **5-7** (0.030 g, 0.026 mmol) is dissolved in degassed $CHCl_3$ (5 mL) and cooled to -78 ^{o}C. Pyridine (1.5 mL, 0.0372 mmol, 0.025 mM $CHCl_3$ solution) is added into the solution and the dark-green solution turned orange-yellow immediately. The reaction mixture is stirred for 2 h and the solvent removed in *vacuo* to give orange-red residue (approx. 0.026 g).

IR (KBr, cm^{-1}): 1609w, 1587w.

^{31}P NMR (81 MHz, $CDCl_3$) ppm: δ = -15.57 (s), etc.

Reaction of **5-7** with $P(CH_3)_3$

Complex **5-7** (0.030 g, 0.026 mmol) is dissolved in dry $CHCl_3$ (5 mL) and $P(CH_3)_3$ (55 µl, 0.0275 mmol, 0.5 M in toluene) is added. The dark-green solution turned orange immediately and is left to stir for 2 h. The solvent is removed in *vacuo* to give orange solids (approx. 0.025 g).

IR (KBr, cm^{-1}): 1632w, 1587w.

^{31}P NMR (81 MHz, $CDCl_3$) ppm: δ = -42.90 (s), etc.

Reaction of **5-7** with $P(CH_3)_2Ph$

Complex **5-7** (0.060 g, 0.052 mmol) is dissolved in dry $CHCl_3$ (5 mL) and $P(CH_3)_2Ph$ (105 µl, 0.053 mmol, 0.5 M in toluene) is added. The dark-green solution turned red immediately and is left to stir for 2 h. The solvent is removed in *vacuo* to give red-orange solids (approx. 0.050 g).

IR (KBr, cm^{-1}): 1604w, 1570m.

^{31}P NMR (81 MHz, $CDCl_3$) ppm: δ = -35.12 (s), -35.32 (s), -42.30(s), -42.49 (s).

Reaction of **5-7** with PPh_3

Complex **5-7** (0.018 g, 0.016 mmol) is dissolved in degassed $CHCl_3$ (5 mL) and PPh_3 (0.004 g, 0.016 mmol) is added. The dark-green solution turned red-brown immediately and is left to stir for 2 h. The solvent is removed in *vacuo* to give red-brown solids (approx. 0.015 g).

IR (KBr, cm^{-1}): 1627w, 1587w.

^{31}P NMR (81 MHz, $CDCl_3$) ppm: δ = 6.18 (s), -1.50 (s), -2.46 (s), -5.24 (free PPh_3), -14.39 (s), etc.

Reaction of **5-7** with *p*-tolylSO$_2$NC

Complex **5-7** (0.030 g, 0.026 mmol) is dissolved in dry $CHCl_3$ (5 mL) and *p*-tolylSO$_2$NC (0.005 g, 0.027 mmol) is added. The dark-green solution turned red immediately and is left to stir for 2 h. The solvent is removed in *vacuo* to give red solids (approx. 0.028 g).

IR (KBr, cm^{-1}): 1624w, 1596w.

^{31}P NMR (81 MHz, $CDCl_3$) ppm: δ = -5.30 (s), -7.26 (s), -9.62 (s), -13.12(s), -15.26 (s)

Reaction of **5-7** with sodium diethyldithiocarbamate

Complex **5-7** (0.030 g, 0.026 mmol) is dissolved in degassed $CHCl_3$ (5 mL) and sodium diethyldithiocarbamate (0.006 g, 0.0266 mmol) is added. The dark-green solution turned red immediately and is left to stir for 2 h. The solvent is removed in *vacuo* to give brown-red solids (approx. 0.021 g).

IR (KBr, cm^{-1}): 1628w, 1599w.

^{31}P NMR (81 MHz, $CDCl_3$) ppm: δ = -12.23 (s), -12.77(s), -12.93 (s), -13.14(s), -14.79 (s), -19.03 (s).

Reaction of **5-7** with $AgBF_4$

Complex **5-7** (0.030 g, 0.026 mmol) is dissolved in dry $CHCl_3$ (5 mL) and $AgBF_4$ (0.006 g, 0.0308 mmol) is added. The dark-green solution is stirred for 2 h and turned brown over time and a white ppt formed. The solution is filtered through a Celite pad and the brown filtrate evaporated to give brown solids (0.018 g, 0.0150 mmol, 57 % yield).

IR (KBr, cm^{-1}): 3060w, 2960w, 2924w, 1794m, 1676w, 1638m, 1587w, 1484m, 1437vs, 1382 m, 1351m, 1238vs, 1192s, 1141s, 1097vs, 1062s, 1031s, 747m, 711m, 694vs, 582m, 523vs, 515s.

^{1}H NMR (200 MHz, $CDCl_3$) ppm: δ = 7.68 (m, PPh_3), 7.47 (m, PPh_3), 7.04 (m, PPh_3), 6.89 (m, 1H), 6.79 (m, 1H).
^{19}F NMR (470 MHz, $CDCl_3$) ppm: δ = -80.72 (m, 3F), -110.65 (m, 2F), -121.02 (s, 2F), -125.94 (m, 2F), -152.11 (s, B*F*$_4$).
^{31}P NMR (81 MHz, $CDCl_3$) ppm: δ = -16.73 (s) 5.96 (s, minor), 4.97 (s, minor), -15.29 (s, minor).

Reaction of **5-7** with DMA.HCl

Complex **5-7** (0.030 g, 0.026 mmol) is dissolved in dry $CHCl_3$ (5 mL) and DMA.HCl (0.007 g, 0.0566 mmol) is added. The dark-green solution turned bright red immediately and is left to stir for 1 h. The solvent is removed in *vacuo* to give bright vermillion solids which are recrystallized from CH_2Cl_2/CH_3OH to give $Ir^{(III)}(\eta^1$-$HNNPhNHSO_2C_4F_9)(Cl)_3(PPh_3)_2$ (**5-9**) (0.025 g, 0.020 mmol, 78 % yield).

IR (KBr, cm^{-1}): 3437ss, 3069w, 2964w, 2924w, 1632m, 1485s, 1434vs, 1240vs, 1191vs, 1141s, 1091vs, 1031s, 804m, 744m, 695vs, 522vs, 515vs.
^{1}H NMR (200 MHz, $CDCl_3$) ppm: δ = 13.34 (s, N*H*), 8.36 (s, N*H*), 7.93 (m, PPh_3), 7.51 (m, 1H), 7.47 (m, 1H), 7.19 (m, PPh_3), 6.89 (m, 1H), 6.03 (d, 1H, *J* = 8.6 Hz).
^{19}F NMR (470 MHz, $CDCl_3$) ppm: δ = -80.64 (t, 3F, *J* = 9.6 Hz), -111.55 (t, 2F, *J* = 13.4 Hz), -120.95 (s, 2F), -125.87 (t, 2F, *J* = 12.5 Hz).
^{31}P NMR (81 MHz, $CDCl_3$) ppm: δ = -19.89 (s).
Elemental analysis calcd. for $C_{46}H_{36}N_3O_2F_9P_2SCl_3Ir$ (1226.37 g mol^{-1}), %: C, 45.01; H, 2.94; N, 3.42; S, 2.61. Found: C, 44.94; H, 2.99; N, 3.36; S, 2.58.

5.4.1 Dimroth rearrangements of benzotriazoles.

The azo-triazole equilibrium (also called Dimroth or amidine rearrangement) in Scheme 5-2 is prevalent in many polyaza-heterocycles and has been observed using spectroscopic methods.[197] Regitz *et al*. using ^{1}H NMR spectroscopy to monitor the composition of isomers present observed that the diazo form, **5-10b**, is favoured when the substituent R^1, R^2 contains electron-donating groups and the amine substituent R^3 contains electron-withdrawing groups. The triazole isomer, **5-10a**, is favoured when both R^1, R^2 are electron-withdrawing and R^3 is electron-donating.[197b]

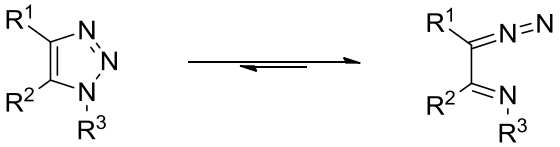

5-10a **5-10b**

R^1, R^2, = Electron-donating group (EDG)
R^3 = Electron-withdrawing group (EWG)

Scheme 5-2. Dimroth or Amidine rearrangement of triazoles.

Such phenomenom for benzotriazole and its derivatives are however rare. Katrizky *et al*. reported using custom designed benzotriazoles with different substituents on both the phenyl and triazole ring which under thermal conditions gave rearrangement products that are postulated to derive from the Dimroth intermediate (Scheme 5.3).[198] Reports describing nucleophiles such as amines, secondary amines, deprotonated malonates and cresols to effect addition products on benzotriazoles containing electron-withdrawing groups on the triazole ring are known, presumably by the Dimroth intermediate.[192, 194, 199]

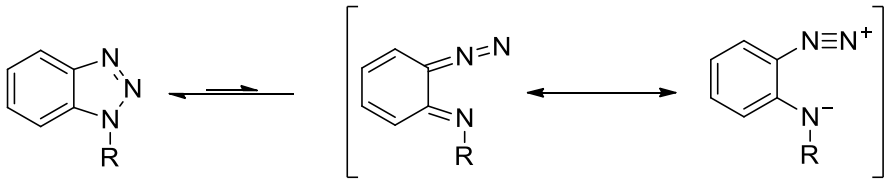

R = Electron-withdrawing group (EWG)

5-11a **5-11b**

Scheme 5-3: Dimroth rearrangement benzotriazoles.

In all the above reports, direct spectroscopic evidence for the equilibrium intermediate **5-11b** has never been observed. There are however indications in the literature for the presence of **5-11b** for electron withdrawing substituents on N1 of a benzotriazole. One early article for 1-cyanobenzotriazole reported a solvent dependent yellow solution which had a λ_{max} = 435 nm in ethanol.[197a]

In our initial studies of **5-1**, we have noticed a faint yellowish tint of its solutions, the intensity dependent on the solvent. Such colouration was reversible between the solid state and solutions. Based on such observations, we carried out careful and methodical sampling of **5-1** in various solvents (Table 5-2).

Table 5-2: Visible absorption bands of **5-1** and related triazoles in different solvents

Compound	Solvent	Dielectric constant, ε	λ_{max}[a], nm	Absorption[b] (M^{-1} cm^{-1})	λ_{max}[b], nm	Oscillator Strength[b]	Relative Energy[b,c] (kcal M^{-1})
5-1	Gas Phase		-	-	409.08	0.1450	8.5
	Hexanes	1.88	-	–	412.51	0.1783	6.5
	Chloroform	4.81	-	–	409.27	0.1825	4.7
	Ethyl Acetate	6	411	17.2			
	DMF	36.7	403	1204			
	Acetonitrile	37.5	408	334	404.64	0.1763	3.3
	DMSO	47	402	2015	405.60	0.1811	3.3
	Propylene carbonate	64.9	406	482			
	Water	78.39	-	-	404.18	0.1756	3.2
	Formic acid	58.5	396	484			
5-2	DMF	36.7	411	160			
	DMSO	47	404	452			
5-3	DMSO	47	430	0.43(5)			
5-4[197a]	C_2H_5OH	24	435	3.5			

a. Experimental Visible band only from freshly prepared solutions measured at room temperature. This is the absorbance at the λ_{max}.

b. Theoretical Values for the electronic spectra were calculated from time dependent density functional theory, B3LYP/6-311++g**.

c. Relative energies corresponds the difference in energy between **5-1a** and **5-1b** for each solvent.

There is a marked solvent dependent correlation on the wavelength and intensity of the solutions. Solvents with high dielectric constants exhibit a general increase in the energy of the transition and extinction. The band at ~400 nm is similar in energy to those found in arenediazonium species,[200] and for which the isolated salts often have $\varepsilon \sim 10^3$-10^4 M^{-1} cm^{-1}. The absorbance observed for **5-1b** is weaker due to the position of the **5-1a**/**5-1b** equilibrium. We have attempted to

gauge this by calculating the differences in the relative energies of the two isomers in these media, the right hand column of Table 5-2. Although the triazole isomer **5-1a** is always theoretically favoured, more polar solvents are predicted to stabilize the zwitterionic polar isomer more, and this shift in the equilibrium would rationalize observed absorption trends. Attempts to confirm the presence of **5-1b** in these mixtures by IR spectroscopy have been hampered by overlapping solvent and triazole bands and thus another structural method was sought to confirm the **5-1a/5-1b** equilibrium.

Spectroscopic evidence for the Dimroth equilibrium is found however in the proton and fluorine variable temperature NMR for solutions of **5-1.** At room temperature, these solutions are consistent with the presence of a single species, or the high temperature limit of a fast exchange. In prior work, high temperature NMR spectroscopy was used to examine the DMF solution of **5-1** and neither new signals nor significant broadening of any of the resonances was observed.[192] However, if these solutions in polar solvents are cooled, the ^{19}F NMR spectra, Figure 5-1, exhibit marked temperature dependence with cooling leading to coalescence at -46 ˚C followed by the emergence of a low temperature limit spectra with two signals observed for the α-CF_2 fluorines[201] in a 5:1 ratio. These resonances have a significant difference in the chemical shifts for **5-1a** and **5-1b** whereas the remaining three fluorines exhibit limited broadening or splitting on cooling (Table E-1). Analysis of these spectra give $\Delta G^{\ddagger} = 11$ kcal mol^{-1}. This low barrier and solvent effect is consistent with the NMR results previously reported by Regitz for non-annulated triazoles.[202] Under the same conditions ^{1}H NMR spectra reversibly broaden in DMF (Figure E-1) on cooling and the ^{19}F spectra remain unaltered in CD_2Cl_2 (Figure E-2). Thus at room temperature the NMR of these solutions correspond to the high temperature limit where the observed resonances are the weighted averages of the equilibrated **5-1a** and **5-1b**, and at low temperatures polar solvents are required to stabilize and enrich the population of **5-1b** so the equilibrium in Scheme 5-3 can be observed.

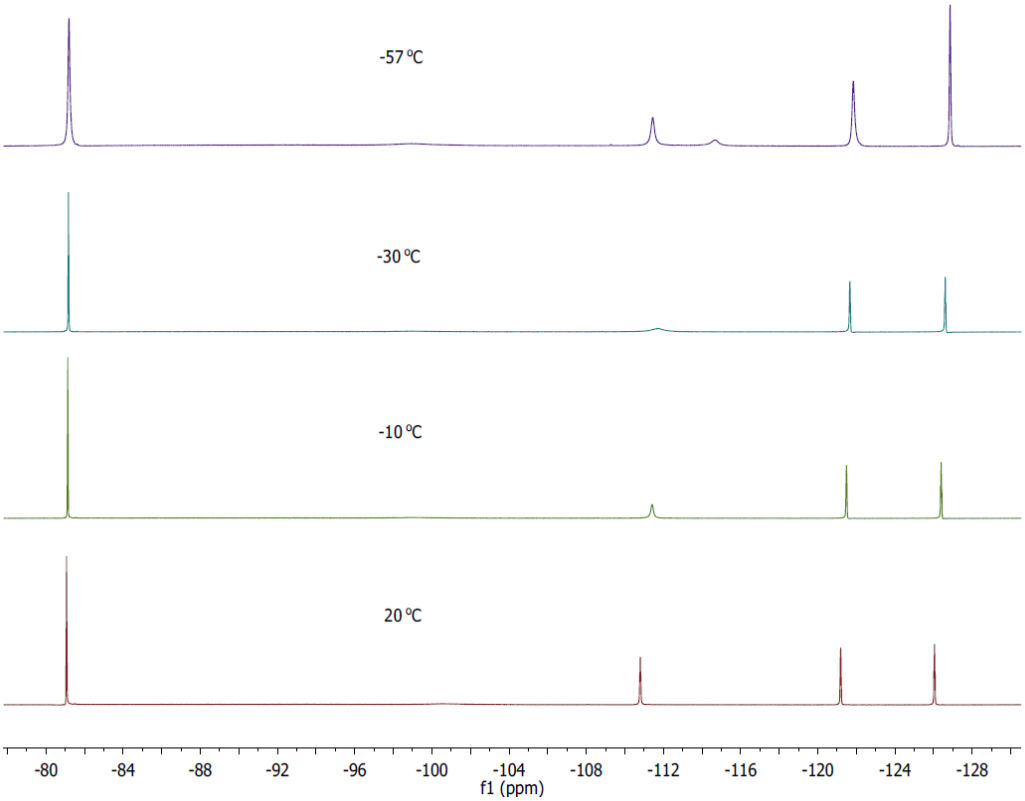

Figure 5-1. ^{19}F NMR of **5-1** in DMF-d_7 at different temperatures.

Theoretical density functional calculations, B3LYP/6-311++G** for **5-1** gives two ground state structures for **5-1a** and **5-1b** which differ by 8.5 kcal mol^{-1} in the gas phase and 3.3 kcal mol^{-1} in DMSO (Table 5-2). A stationary state with an out-of-plane $C_4F_9SO_2$ group on N1 is found 12.9 kcal mol^{-1} above the triazole isomer and internal reaction coordinate calculations indicate that the isomerization of **a** to **b** through this transition state involves lengthening of the N1-N2 bond, and shortening and linearization of the N2-N3 bond. Polar solvents are expected to both stabilize the charges which develop in the ring opening and in isomer **5-1b**. The theoretical predictions are remarkably close to the experiment for the dynamic behaviour. The conclusion is that for electron withdrawing substituents on N1 the Dimroth rearrangement is accessible at low and room temperatures for benzotriazole. For other triazoles, those with electron donating substituents on the ring, this equilibrium is also observed under these conditions for less electron withdrawing substituents.[203] The implication is that

with suitable choice of triazole substitutents, the Dimroth rearrangement represents a powerful tool to declick or otherwise transform clicked triazoles.

From the UV-vis spectra (Table 5-2) obtained from some of the benzotriazole derivatives, reactivity studies of *p*-nitrophenylSO$_2$Btz and *p*-tolylSO$_2$Btz with nucleophiles were carried out (Scheme 5-4). Electron withdrawing groups on N1 such as C$_4$F$_9$SO$_2$, BtzSO$_2$, NO$_2$, CN and *p*-nitrophenylsulfonyl give addition products from nuclephiles. Substituents such as *p*-tolylsulfonyl, which are not electron-negative, result in the substitution of the benzotriazole ring, releasing free benzotriazole.

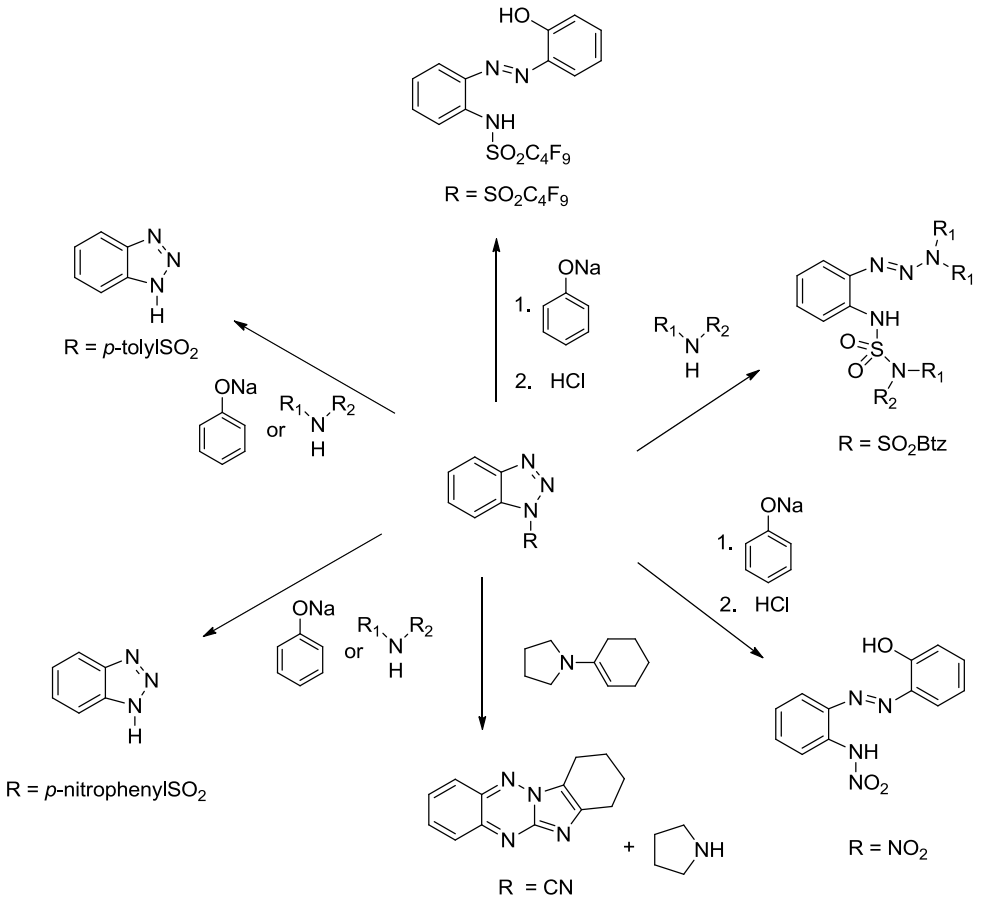

Scheme 5-4. Reaction products of benzotriazole derivatives with various nucleophiles (this work and others).[192, 194, 199b, c]

5.4.2 Synthesis of Ir diazo/diazene complexes

With the results collected in Scheme 5-4, we sought to investigate if low valent organometallic complexes can be used to stabilise and trap the Dimroth ring open isomer in Scheme 5-3. The Ir(I) carbonyl complex or Vaska complex was the initial choice for these experiments due to its relative stability, kinetic inertness of Ir(I) and coordination unsaturation. There has only been one other example of an Ir benzotriazole complex and it was synthesized through a thallium salt metathesis.[164] We found that the reactions of **3-1** with **5-1**, **5-2**, and **5-3** are complicated with unreacted starting complex even when excess ligand is used. We postulate the activation of the benzotriazle ring to be a reversible process in these cases and therefore proceeded to try other complexes. The iridium(I) dinitrogen complex, **3-2**, has many properties of Vaska complex but also a nitrogen ligand which is labile. To this end **3-2** is reacted with **5-1**, **5-2**, **5-3**, **5-4**, **5-5** and **5-6** (Scheme 5-5).

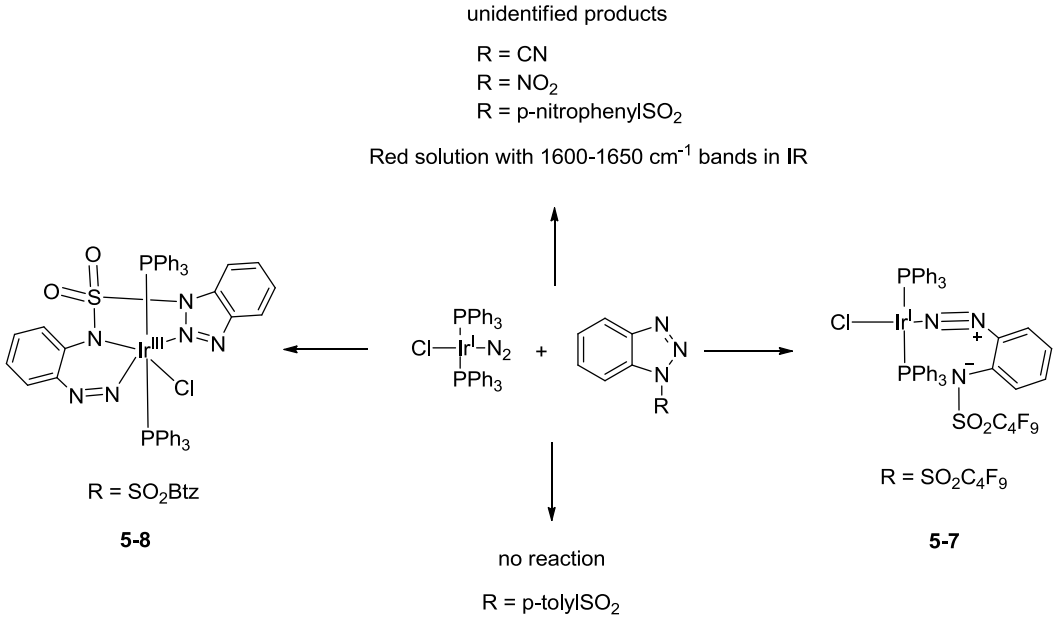

Scheme 5-5. Reaction of **3-2** with selected benzotriazole derivatives.

The reaction of **5-1** with **3-2** at room temperature produces a rapid effervescence of gas and immediate color change to dark green. Subsequent isolation of complex **5-7** gave intensely blackish-green crystals. The molecular structure of **5-**

7 shows a ring-opened benzotriazole in zwitterionic form[204] coordinated to the Ir(I) metal center through the diazo portion of the benzotriazole ring in a monodentate fashion (Figure 5-2). Of particular note is the relatively short diazonium-like N(2)-N(3) bond length of 1.165(9) Å and close to linear N(3)-N(2)-Ir bond angle of 171.5(7)˚ (Table 5-3) . The corresponding new ν(NN) band is at 1880 cm^{-1} in the IR spectrum for **5-7**. In contrast for the free non coordinated trifluoromethyl analog of **5-1b**, density function theory predicts an N-N bond length of 1.120666 Å and a ν(NN) band at 2238.4 cm^{-1}. Clearly the new diazo ligand in **5-7** is an excellent π-acid with coordination of Ir(I) leading to considerable π-backbonding to the ligand.

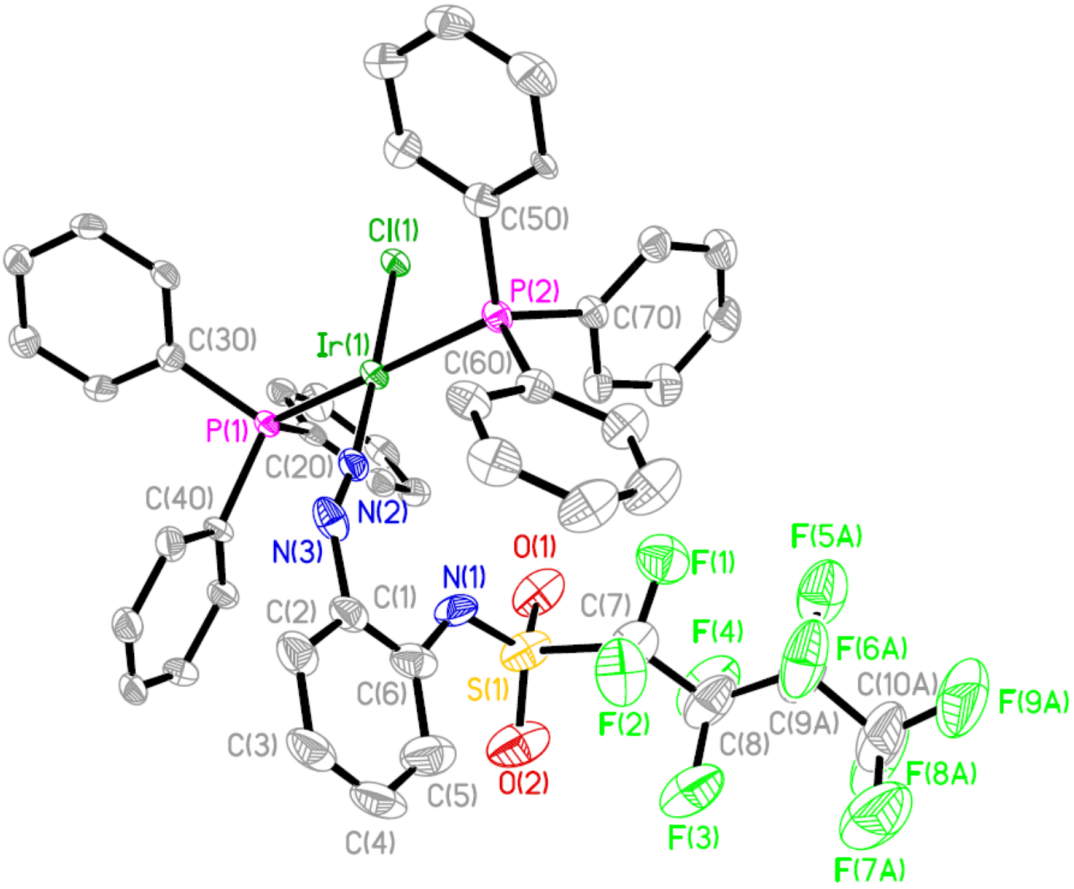

Figure 5-2. Molecular structure of **5-7**. Hydrogen atoms have been omitted for clarity.

For the transition metal complexes containing diazo/zwitterionic-diazo ligands which have been reported, the diazo bond lengths range between 1.163(7)-

1.224(6) Å.[204a, 205]. The diazo ligands are commonly N-bound to the metal in a η^1 manner. There are only a few unusual examples where the diazo ligand is bound in a π-form.[206] The long Ir(1)-N(1) separation, 3.762(7)Å, suggests little interaction of the sulfonyl substituted nitrogen and the iridium.

In common with many Vaska type complexes, **5-7** is relatively stable in the solid state but exhibits oxygen and light sensitivity in solution. Upon standing in solution and exposed to light, decomposition products which show the loss of the 1880 cm^{-1} band and a new band at 1626 cm^{-1} are observed.

There are numerous reports of aryldiazenido complexes and various structural forms have been isolated[200, 207] (Figure 5-3).

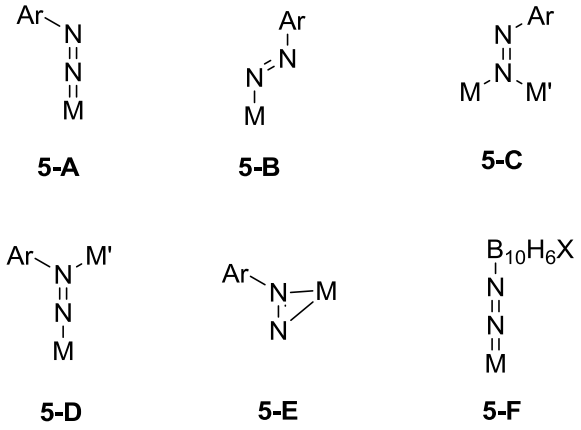

Figure 5-3. Some common structural forms of aryldiazenido complexes.

The more common are the singly-bent, **5-A**, which corresponds to the diazo form and the doubly-bent, **5-B**, the diazene form. Complex **5-7** falls into the category of **5-A**.

In contrast with the relatively simple substitution of dinitrogen for diazo ligand in **5-7** it is possible that coordination would lead to complete formal two electron transfer to the new ligand to give rise to an Ir(III) chelate complex. In part this happens when **3-2** is treated with **5-2**. As with **5-7**, this triazole has been shown to be able to undergo nucleophilic ring-opening,[193] and it exhibits some solvatochromism in polar solvents to give a new band at ~ 410 nm (Table 5-2). When **5-2** was added to **3-2** at 0 °C, a vigorous evolution of gas is coupled with an

immediate color change to dark green. The reaction mixture slowly turned wine red over the course of 3 h at room temperature (Scheme 5-6).

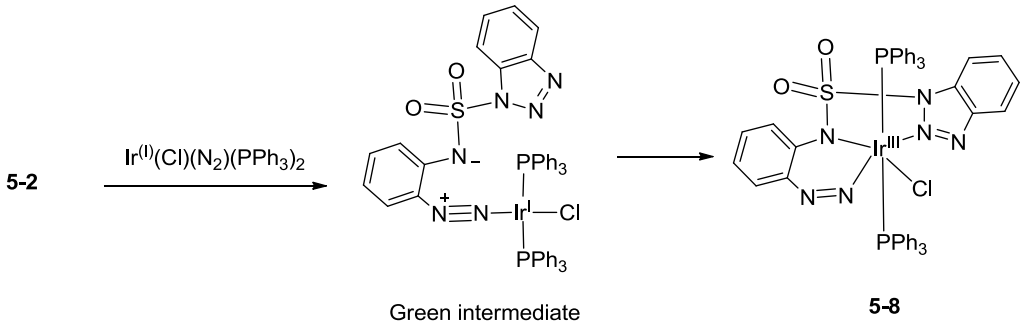

Scheme 5-6. Reaction of Btz_2SO_2 with *trans*-$Ir^{(I)}(N_2)(Cl)(PPh_3)_2$.

The ultimate red product isolated, **5-8**, contains an opened triazole which is bound as a chelate and includes an unusual doubly-bent cis diazene[196] (Figure 5-4). The second heterocycle is a coordinated but unmodified benzotriazole. From single X-ray crystallography all nitrogens are bound in meridonal geometry. The N(2)-N(3) bond lengths and N(2)-N(3)-Ir(1) bond angles reveal the ring-opened triazole fragment to be similar to the more commonly known doubly bent trans diazene, **5-B**, (Figure 5-3, Table 5-3).[200, 208]

The identity of the diazo-green intermediate in Scheme 5-6 is supported by the solution IR spectra shown in Figure 5-5. The intense dinitrogen stretch at 2105 cm^{-1} from the starting material dinitrogen disappears immediately on addition of **5-2** and is correlated with appearance of new diazonium bands 1887 and 567 cm^{-1}. Over 2.5 h these bands, due to the intermediate in Scheme 5-6, disappear and lead to new bands at 1602 and 593 cm^{-1} which correspond to the final product **5-8**.

The reaction with **5-3** results in the formation of a reddish-brown solution over 30 min which may indicate the presence of a diazene-like species. The ^{31}P NMR spectrum initially gives a single species while the over time a new ^{31}P signal appears at -9.28 ppm and also some triphenylphosphine oxide coupled with the loss of the 1625 cm^{-1} band indicates the complex is unstable and decomposes. Reaction of the unstable complex with CO did not stabilize the complex too.

When **5-4** was added **3-2**, an immediate colour change to bright red shows the presence of a formation of a diazo/diazene species. The ^{1}H and ^{31}P spectra

indicates mostly a single compound and the IR gave new bands around 1600 cm^{-1}. However the band at 2200 cm^{-1} is also present and broad. Over time, signals at -12.93, -9.67, -16.21, -16.47 ppm in the ^{31}P NMR spectrum means that the compound is not stable and is undergoing further reaction. The ^{1}H NMR spectrum also shows new resonances in the aromatic region.

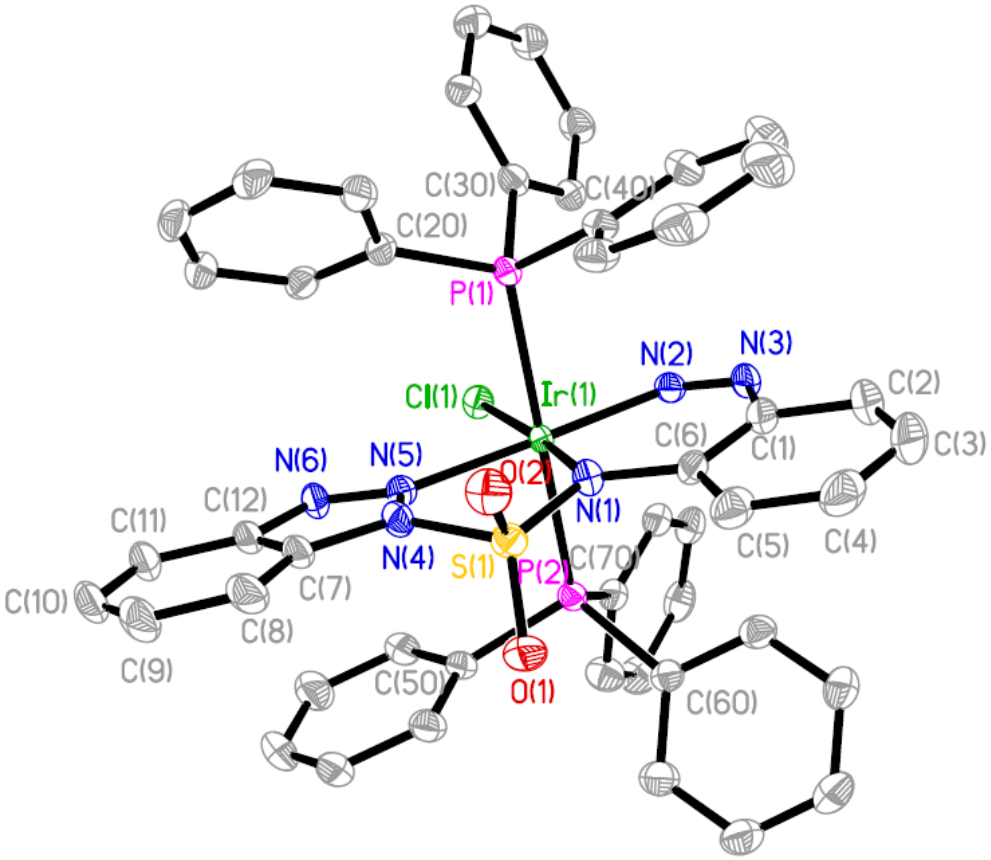

Figure 5-4. Molecular structure of **5-8**. Hydrogen atoms have been omitted for clarity.

The reaction of **5-5** with **3-2** gave a red-brown solution over 2 h. Initially a single species was observed in the ^{31}P NMR, but over time multiple signals are observed. A new IR band at 1603 cm^{-1} indicates a new diazo-like species. The new band at 1526 cm^{-1} is due to the nitro group.

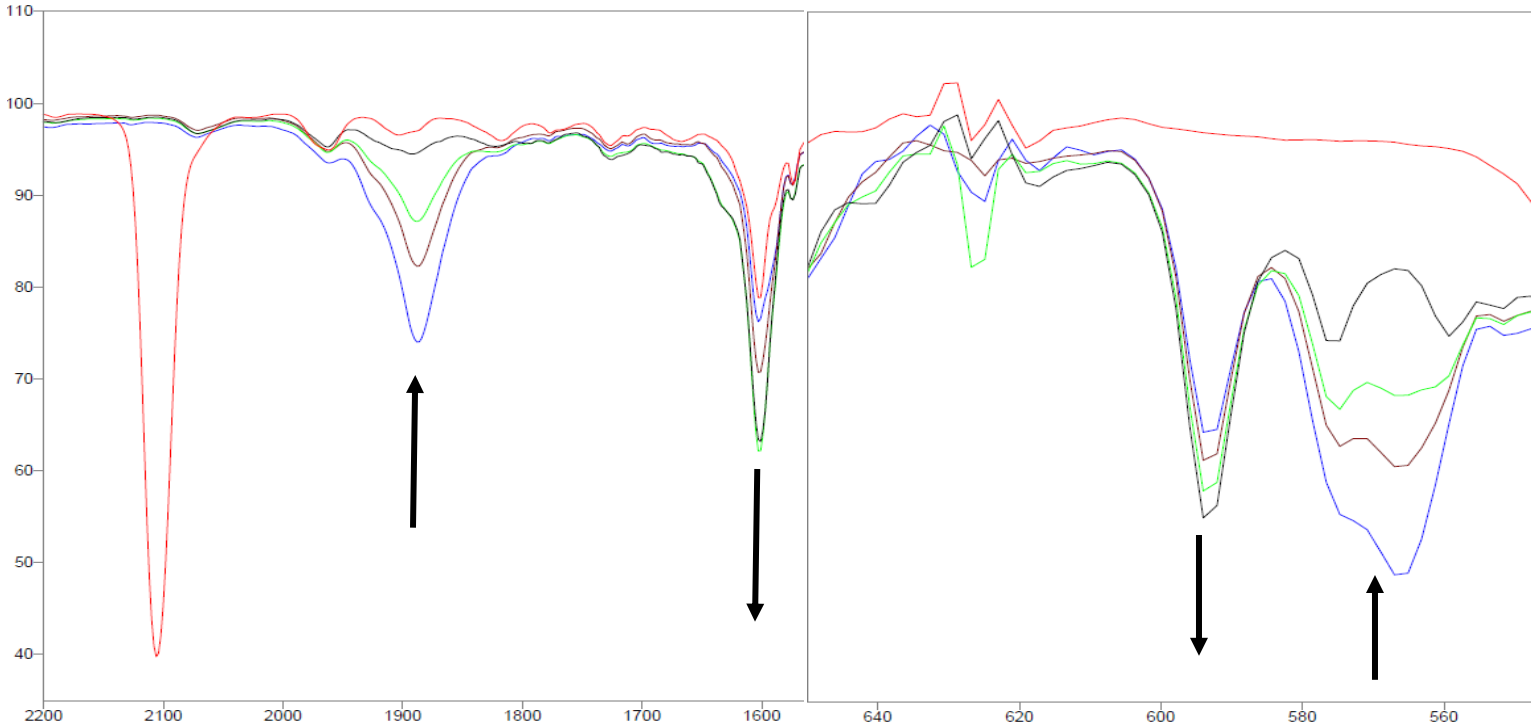

Figure 5-5. Solution IR spectra for the reaction of **3-2** with **5-2**. Reaction carried out at -10 ^{o}C in $CHCl_3$ over 2.5 h. Aliquots taken at the following time intervals: Red: Initial **3-2** complex; Blue: Immediately after addition of **5-2**; Brown: after 45 min ; Green: after 1.5 h ; Black: after 2.5 h.

In all the above reactions of benzotriazole derivatives with electron-withdrawing substituents at N1 (e.g. CN, NO_2 and *p*-nitrophenylSO_2), the appearance of IR bands in the 1600 cm^{-1} region suggest a common rapid coordination to **3-2** (Scheme 5-6) to give diazene products which are followed by subsequent reactions leading to complex product mixtures. **5-6** did not react with **3-2**, similar to its reaction with nucleophiles in Scheme 5-4 correlating with the less electron-withdrawing nature of the *p*-tolylsulfonyl group.

This strategy of trapping the ring opened Dimroth intermediate has been applied once before and this was to the reaction 1,2,3-thiadiazole, not a triazole, with iron carbonyls (Scheme 5-7).[209] In this case the Dimroth equilibrium is more favoured for the ring opened form and the resulting dinuclear product has a bridging diazo ligand.

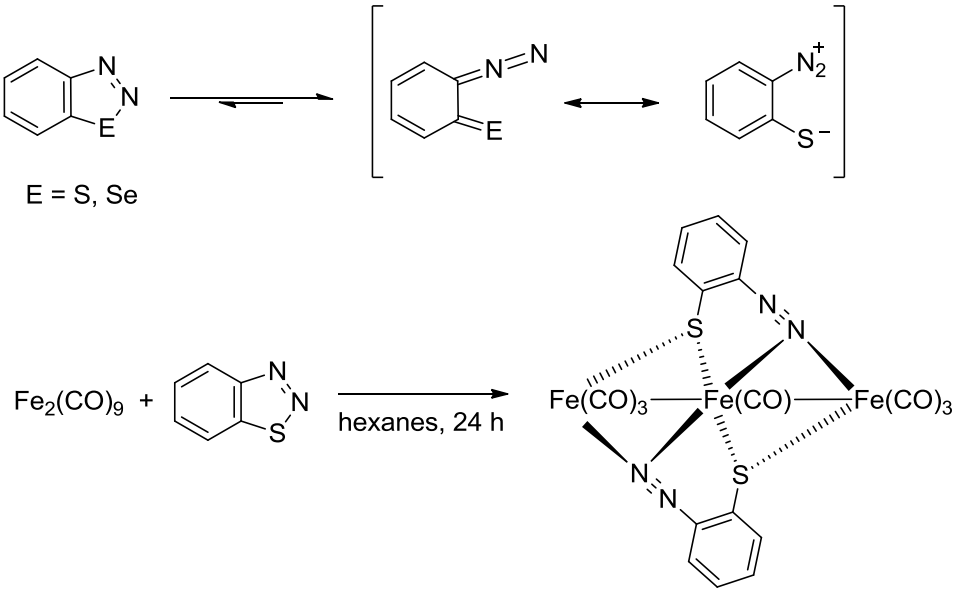

Scheme 5-7. Dimroth ring opening of 1,2,3-benzothiadizole and reaction with $Fe_2(CO)_9$.

X-Ray refinement and structural comparison between **5-7** and **5-8**

Crystals of **5-7** were obtained from CH_2Cl_2/pentanes solution at -21 ^oC. The diffraction model required restraints for the perfluorobutyl substituent, CH_2Cl_2 and pentane solvent molecules due to disorder. The final solution contain a large electron density peak and hole located near the disordered alkyl fluorines which

can be attributed to poor absorption correction as the crystals were very thin plates. The opacity of the crystals made selection of a suitable crystal difficult. Crystals of **5-8** were grown from CH_2Cl_2/CH_3OH solution at -21 ^oC. Severe disorder of the solvent molecules was also encountered. Both crystals lose solvent easily which required low temperature and a dense matrix such as N-paratone oil for data collection. Selected bond lengths and bond angles are shown in Table 5-3.

The N(3)-N(2)-Ir(1) and N(2)-N(3)-C(1) bond angle in **5-7** is almost 180^o and 137^o respectively thus described as singly bent while in **5-8** both are close to 120^o and suitably referred as doubly-bent.[200, 207b] The Ir-N(2) bond length of **5-7** is much shorter than **5-8** emphasizing the double bond character of the M-N bond in the singly-bent, **5-A**, as compared to the doubly-bent **5-B** (Figure 5-3).There are also structural differences in the phenyl group of the diazo (**5-7α**)/diazene (**5-8α**) ligand reflecting the conjugation effect of the diazo/diazene on the aromaticity of the phenyl ring (Figure 5-6).

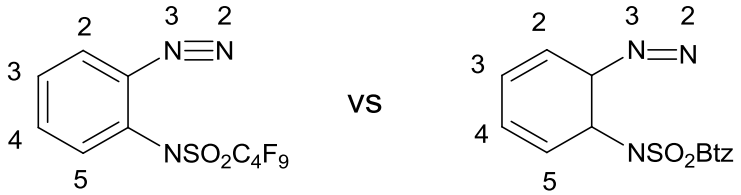

5-7α **5-8α**

Figure 5-6. Conjugation difference between **5-7α** and **5-8α**.

In **5-7**, there are alternate short and long C-C bonds in the phenyl group while in **5-8** there is a distinct difference between C-C bonds located away from the diazene compared to the C-C bonds closest. In both cases, the S(1)-N(1) bonds are remarkably short, indicating double bond character. This also implies the stabilisation effect of the electron-withdrawing group on the ring-opened triazole system.

Table 5-3: Selected bond lengths (Å) and torsion angles (deg) of **5-7** and **5-8**.

Compound	**5-7**	**5-8**
Ir(1)-N(2)	1.791(6)	1.991(4)
Ir(1)-N(1)		2.075(4)
Ir(1)-N(5)		2.107(4)
S(1)-N(1)	1.536(8)	1.600(4)
S(1)-C(7)/S(1)–N(4)[a]	1.867(11)	1.713(5)
N(1)-C(6)	1.420(13)	1.407(6)
N(2)-N(3)	1.165(9)	1.244(7)
N(3)-C(1)	1.410(11)	1.444(8)
C(1)-C(2)	1.401(13)	1.410(8)
C(2)-C(3)	1.360(14)	1.371(11)
C(3)-C(4)	1.403(18)	1.382(11)
C(4)-C(5)	1.388(17)	1.392(8)
C(5)-C(6)	1.405(14)	1.415(8)
C(6)-C(1)	1.386(14)	1.418(8)
N(3)-N(2)-Ir(1)	171.5(7)	124.9(4)
N(2)-N(3)-C(1)	139.2(8)	127.4(5)

a) S(1)-C(7) for **5-7**, S(1)-N(4) for **5-8**

5.4.3 Reactivites studies of Ir diazo/diazene complexes

The isolation of **5-7** and **5-8** allows us to further investigate the reactivity of the new diazo/diazene complexes to various reagents. Complex **5-8** is air stable and exhibits no reactivity to both CO and pyridine additions at room temperature. This is not surprising as Ir(III) complexes are known to be relatively inert. Together with the tris-chelate form of **5-2** and a coordination saturated Ir center, any substitution or addition reactions to the complex are unlikely under these conditions.

The reactivity of **5-7** is in great contrast to **5-8**. Carbon monoxide addition results in the loss of **5-1** and the formation of **3-1** on extended bubbling of CO gas. This demonstrates that CO is a better π-acid compared to the ring-open diazo **5-1b** for the electron–rich Ir(I) center. The reaction of **5-7** with other nucleophiles such as pyridine, $P(CH_3)_3$, $P(CH_3)_2Ph$, PPh_3, p-tolylisocyanate and sodium diethyldithiocarbamate results in rapid colour change and shows multiple ^{31}P NMR signals (Scheme 5-8).

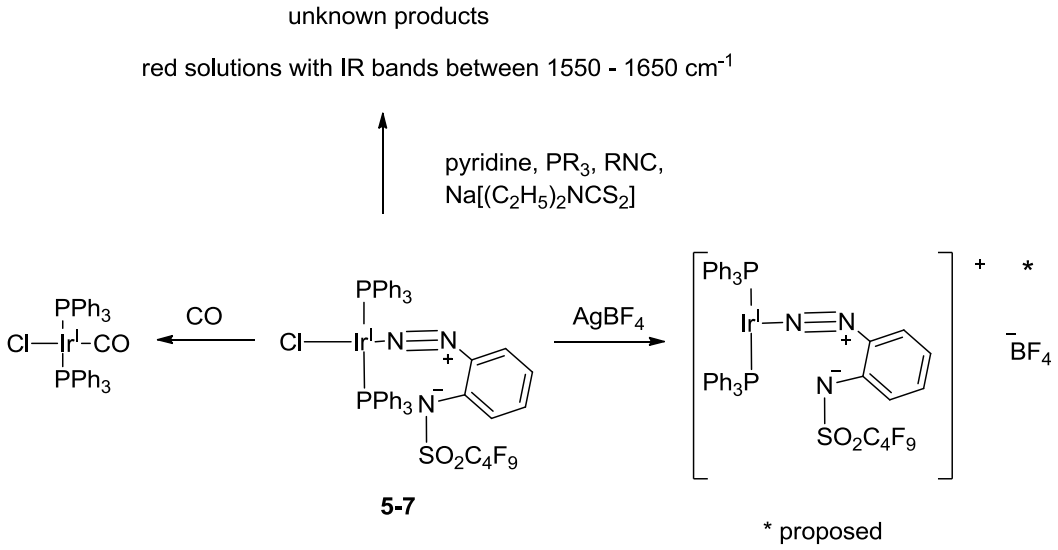

Scheme 5-8. Complex **5-7** reaction with various reagents.

These spectroscopic observations may mean the formation of multiple isomers based on PPh_3 substitution and formation of complex mixtures of Ir(I) complexes. The possible conversion of the diazo to a new diazene ligand is compelling as the band at 1880 cm^{-1} disappears and new bands appears between 1550 to 1650 cm^{-1}

corresponding to diazene complexes.[200] Such reactivity patterns have been observed in the Ir complexes containing zwitterionic diazo ligands and the conversion to diazene ligands based on the appearance of new IR bands between 1500 to 1650 cm^{-1} have been suggested.[205b] The reaction of $AgBF_4$ with **5-7** gave mostly a major product that shows an IR band at 1794 cm^{-1}. This band most likely corresponds to a diazo stretch shifted to lower energy from the increase back-bonding of the Ir(I) center. The loss of the chloride is confirmed by the appearance of a new ^{19}F signal at -152 ppm assign to the BF_4 anion. However the complex is very unstable, decomposing over time in solution to give multiple IR bands around the 1600 cm^{-1} region.

There has been only one structurally characterized example of a conversion of a diazo ligand to a diazene ligand. The conversion was carried out using oxidative addition of one equivalent of HCl to the Ir(I) center containing a diazoketone ligand (Scheme 5-9).[196]

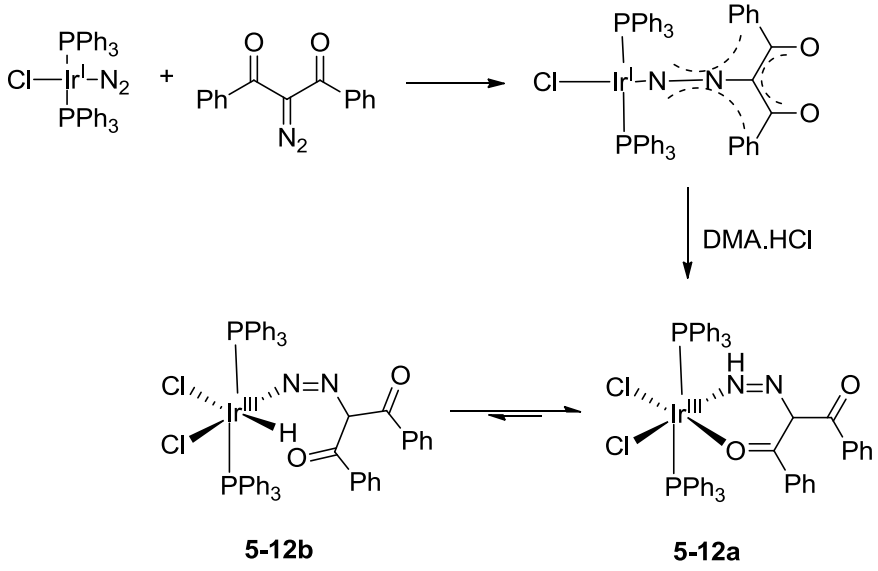

5-12b **5-12a**

Scheme 5-9. Synthesis of Ir-diazoketone **5-12**.

The molecular structure **5-12a** shows a bidentate N,O-bound cis diazene complex with the nitrogen closest to the Ir protonated. The authors also reported a minor isomer **5-12b** which is in equilibrium in solution with **5-12a** in approximate ratio of 15:1. Isomer **5-12b** contains a Ir-H which is observed in the ^1H NMR as a triplet at -15 ppm. However there was no observable Ir-H stretch in the IR

spectrum due to the weak intensity of the Ir-H vibration and small amounts of the species. This is in contrast to the work of Schramm *et al*.[205b] where the Ir(I) diazo complex forms only the iridium hydride isomer, **5-13**, after addition of HCl (Scheme 5-10).

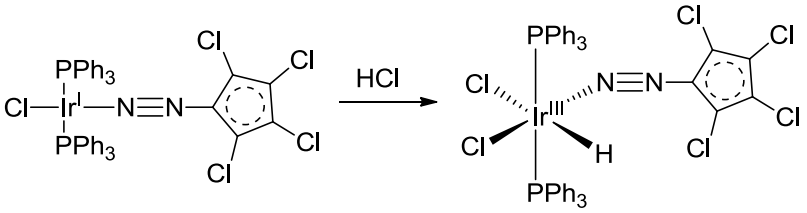

5-13

Scheme 5-10. Oxidative addition of HCl to form **5-13**.

The proposed molecular structure is based on the appearance of a single ^{31}P NMR signal coupled with the appearance of a Ir-H stretch at 2104 cm^{-1} which is confirmed through deuterium substitution studies in the IR spectra. It has been proposed that the ability of the dibenzoyldiazomethane ligand to form a bidentate coordination to the Ir center results in the protonated diazene, **5-12a**, to be the more stable isomer.

Using the same methodology, **5-7** is reacted with DMA.HCl (Scheme 5-11). The loss of the 1882 cm^{-1} band in IR is coupled with the appearance of a new band at 1625 cm^{-1}. There is also an instantaneous colour change from blackish-green to vermillion. In our case, the reaction requires two stoichiometric equivalent of HCl to allow for complete conversion as one equivalent of HCl results in only half of the starting complex **5-7** to react. This outcome indicates the initial intermediate that is formed from the first HCl addition is actually more reactive towards a second HCl addition. There is also no Ir-H stretch observed in the IR spectrum nor any Ir-H signal in the ^{1}H NMR. There are two singlets located at 13.34 and 8.36 ppm in the ^{1}H NMR which can be assigned to the protons on the nitrogen atoms. From the spectroscopic information, the structure of the isomer is assigned as complex **5-15a**. The ^{31}P NMR however show small amounts of other singlets which may correspond to the hydride isomer, **5-15b**. Therefore the room temperature solution NMR may however be at the fast exchange limit or the

equilibrium may lie towards the protonated diazene isomer **5-15a**. This result differs from the formation of **5-12a** as the second coordination of the diazeneketone saturates the coordination sphere of the metal center. Thus it can be suggested that the first addition of HCl is an oxidative one forming an Ir(III) center while the second addition of HCl is due to the coordination of the chloride anion as a ligand to satisfy the coordination requirements of Ir(III) center. This would further imply that the nitrogen coordinated to the perfluorobutylsulfonyl group is sufficiently electron-deficient to be a poor ligand for the Ir(III) center. However the above conjunctions are still insufficient to explain the observed phenomena as it does not explain the reactivity of the intermediate **5-14** towards the second HCl addition as compared to **5-13**.

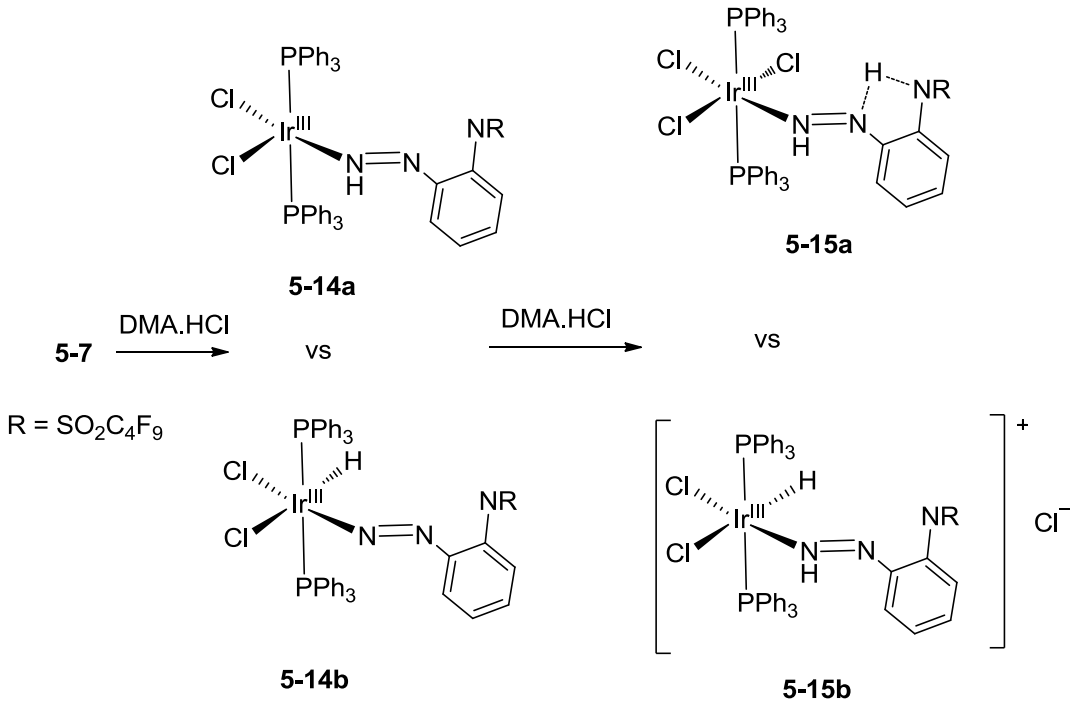

Scheme 5-11. Reaction of **5-7** with DMA.HCl.

The structure, **5-15a**, shown in Scheme 5-11 is observed in preliminary single crystal diffraction. However due to the poor quality of the crystal, the crystal did not diffract to high angles. This resulted in low data to parameter ratio (9:1) of the final solution contributing to unsuccessful anisotropic refinement of all the non-hydrogen atoms. There are also solvent disorders which complicate the final

refinement. However the location and assignment of all the non-hydrogen atoms of the complex is more certain with one of the protons on the diazene being located. The second proton is believed to be bound between the α-N and the nitrogen bonded to the sulfonyl group as there are also solvent molecules located in the region.

The similar formation of the unusual cis diazeneketone complex **5-12a** and **5-8** suggest that the less stable cis isomer can be stabilised by the bidentate coordination to the metal center. In the case of **5-8** it also implies a coordination induced oxidation of the Ir center. Together with the observed reactivity of **5-7**, the conversion of diazo to diazene ligands is not sufficient to induce an oxidation of the metal center.

5.5 Conclusions

The Dimroth/amidine rearrangement of benzotriazoles has been shown to exist in solution for **5-1** using VT ^{19}F NMR. There is some spectroscopic evidence that other benzotriazole derivatives exhibit such a phenomenon. By using a low valent organometallic complex, we have stabilised and trapped two forms of the coordination complexes of the benzotriazole derivatives. Complex **5-7** is a Ir(I) diazo complex while complex **5-8** is a Ir(III) diazene complex and they differ significantly in their reactivity. Ir complexes containing other benzotriazoles derivatives have been synthesized but were not isolated as a pure product. With the advent of copper catalyzed Huisgen [3+2] dipolar addition of alkynes to azides, triazoles are increasingly found in many applications. Benzotriazoles are also now widely used as auxiliaries in organic syntheses[210] and any reaction or methodology which leads to N-N activation of benzotriazole will allow for many new applications for this fundamental organic building block as well as for the triazole class as a whole. Diazo metal complexes are also often important intermediates in many transformations.[211] Our observation that a mononuclear Ir(I) complex is able to activate the most obdurate of triazoles suggests that this reaction may be quite general. Taming this reactivity remains an important problem to develop unclicking strategies and catalysts.

Chapter 6: Summary, Original contribution to Knowledge and Future Research

Summary and Original contribution to Knowledge

The biochemical reduction of nitrous oxide by N_2OR is poorly understood. Recent advances in unveiling the Cu_z cluster in N_2OR have provided more insight into the actual structural motif of N_2OR. With the newly discovered S(2) atom that make-up the Cu_4S_2 catalytic center of Cu_z (Figure 1-3), more accurate experimental studies of N_2OR can be carried out. Instead this has led to a debate on the true active form of N_2OR.

The first structurally characterised transition metal N_2O complex was reported in 2011, since than there have been no further reports using this vanadium N_2O complex. The recent report of nitrous oxide activated by carbenes is another example of nucleophilic addition to nitrous oxide. We hypothesized that late transition metal thiolates such as those in N_2OR would be able to add to nitrous oxide to give new addition complexes with SNNO or NN(S)O ligands.. With this concept as our hypothesis, this research embarked on synthesizing nitrous oxide precursors for coordination to transition metal complexes which may then allow us to study the oxygen analogs of the anticipated nitrous oxide addition complexes.

In Chapter 2, improvements in the synthetic procedures were made with regards to the N-nitroamides and N-nitrosocarbamate. In addition the new compounds, N-nitrosomethylcarbamate (2-6), as well as its potassium and silver salts were also synthesized. For the nitrogen acids as a whole the solid state molecular structures of the compounds **2-2** to **2-8** were also obtained. Similarly, crystals structures of selected potassium salts were also determined for comparison.

In Chapter 3, a new series of Ir(I) carbonyl complexes containing the nitrogen acids have been synthesized (**3-3** to **3-7**). For comparison studies, the new Ir(I) carbonyl dinitramide complex, **3-8**, and an unusual Ir(I) carbonyl complex silver bistriflimide adduct, **3-9**, have been synthesized. All the complexes have been

structurally characterised and their υ(CO) bands determined for comparison with Vaska's complex and other Ir(I) carbonyl complexes with electron-withdrawing groups. The preliminary synthesis of a Ir(N_2) nitrogen acid complex, **3-10**, has also been carried out.

The reaction of the neutral nitrogen acids with **3-2** have also been investigated which generated four new Ir(III) hydride complexes containing the N-nitroamide and N-nitrocarbamate ligands coordinated to the Ir(III) center. The N-nitro ligands are coordinated to the Ir(III) center uniquely through the nitrogen of the amide and the oxygen of the nitro group in a N,O bidentate mode. The ^{1}H NMR spectrum of **3-11** show an unusual broad signal for the Ir hydride resonance that is both field and solvent dependent alluding dynamic behavior in solution. This dynamic process may be a characteristic of the new Ir(III) nitrogen acid complexes. The reactivity studies of **3-11** with CO and P(CH_3)$_2$Ph result in the formation of isomer mixtures of the new addition products. The new Ir(III) nitrogen acid carbonyl complexes, **3-15**, were also metastable in solution, losing CO to regenerate **3-11**. For P(CH_3)$_2$Ph, nucleophilic substitution of the PPh_3 ligands occurred too to give isomers of **3-16**. Lastly methylation of **3-11** with methyl triflate results in the loss the N-nitroacetamide ligand to give the bis(acetonitrile) complex **3-17**.

In Chapter 4, new Re(I) dicarbonyl N-nitro nitrogen acid complexes (**4-8**, **4-9** and **4-12**) have been synthesized. All the complexes have been structurally characterised to have similar coordination modes to the Ir(III) complexes. New complexes **4-10** and **4-11** with the N-nitrosomethylcarbamate ligand in different conformations and coordination mode than the N-nitro nitrogen acid complexes have also been obtained. The crystal packing of **4-9** and **4-10** was determined in an unusual rhombohedral space group R-3, with large unit cell parameters that generate multiple solvent channels that can contain up to fourteen CH_2Cl_2 solvate molecules.

In Chapter 5, the first spectroscopic evidence for the Dimroth rearrangement equilibrium for benzotriazoles such as **5-1** has been shown. An extension of this phenomenon was exploited by the coordination of the ring-opened benzotriazole

5-1 and **5-2** to Ir center to give **5-7** and **5-8**. Complexes **5-7** and **5-8** contain benzotriazoles that have been 'trapped' in the ring-open forms. Complex **5-8** is relatively inert while **5-7** undergoes nucleophilic addition readily. Phosphine ligand substitution also occurs easily.

Future research

The coordination chemistry of the nitrogen acids can be further investigated with other transition metal complexes such as Os, Ru and the platinum group. Early transition metal chemistry may be interesting if successful as these transition metals tend to be oxophilic.

The successful synthesis of the Ir and Re nitrogen acids complexes provide a potential start point for research into nitrous oxide chemical transformations. In general, removal of the 'protecting' groups such as the acyl, ester or sulfonyl groups will generate the nitrous oxide addition complexes (Scheme 6-1) stabilised by transition metal coordination. These complexes may be monitored by spectroscopic means to better understand nitrous oxide chemistry.

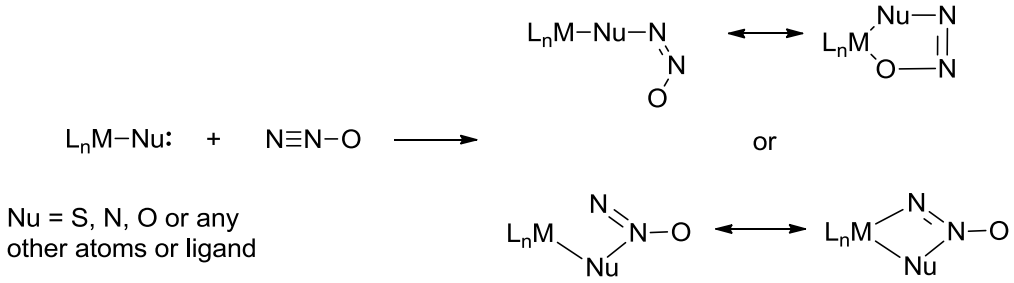

Scheme 6-1. Possible nitrous oxide addition complexes from N_2O and nucleophilic transition metal complexes.

The conversion of the Ir(I) carbonyl nitrogen acid complexes into the dinitrogen complexes may give rise to new stable Ir(I) N_2 complexes that may give more insight to dinitrogen chemistry.

The synthetically proven ability of transition metals to stabilised the ring open forms of benzotriazoles provide new avenue in the use of such complexes as possible diazo transfer reagents to generate new heterocycles from benzotriazoles. Other transition metal complexes such as the platinum group metals can also be investigated for coordination to the benzotriazole derivatives.

Appendix

Appendix A

The reported N-nitration of carboxamides to give N-nitroacetamides using NO_2BF_4[119] could not be repeated. Commercial NO_2BF_4 contains residual acid that decomposes the product. Synthesis of the nitronium salt involves using concentrated nitric acid, anhydrous HF and BF_3 gas that requires special apparatus and set-up. Various attempts at nitration of acetamide was carried out using conventional nitrating methods such as nitrate salts,[212] aroyl nitrates,[213] N-nitropyrazole[214] and trimethylsilyl nitrate with BF_3-etherate.[215] In most cases the nitration of acetamide was unsuccessful or acetic acid was isolated which results from the decomposition of either acetamide or N-nitroacetamide. The use of dinitrogen pentoxide may be possible but requires vacuum line techniques fitted with Teflon pumps. Most of the described nitration reactions are carried out on aromatic compounds which undergo nitration readily.[216] For nitration methods that were specific to amides such as a mixed media of ammonium nitrate/morpholinium nitrate and trifluoroacetic anhydride, it was only successful with secondary amides.[217] The use of silver nitrate with trifluoroacetic anhydride was unusual as a reddish-brown solution is generated most likely the presence of nitrogen oxides which tend to generate nitroso compounds.

As the amide nitrogen is a weak nucleophile, conventional nitration methods did not work. The unsuccessful nitration of amides to give N-nitroamides was approached by proposing an alternative method. 'Umpolung' nitrations have been reported[218] before where the substrate to be nitrated is reacted with nucleophiles which generates a 'masked' nitro group intermediate that could subsequently be oxidised to generate the nitro group (Scheme A-1).

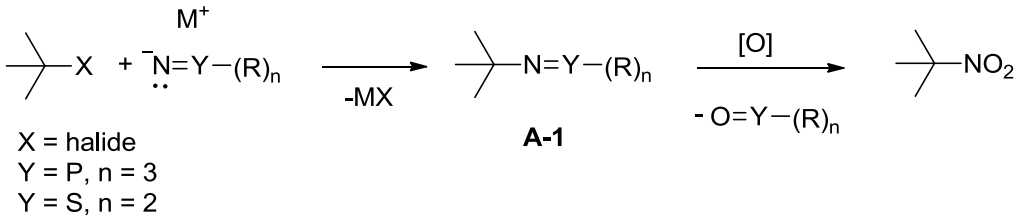

Scheme A-1. 'Umpolung' nitration method.

The 'masked' nitro group substrate **A-1** are usually ylides such as phosphinimine/phosphinimine salts or sulfilimines (Figure A-1).

phosphinimines sulfilimines

Figure A-1. Phosphinimines and sulfilimines.

The oxidation agents that have been successfully used to convert the phosphinimines to the corresponding nitro group include peracids and ozone.[219] For the sulfilimines, peracids such as MCPBA preferentially gives the nitro products while the use of peracid salts usually generate the sulfoximine products. This nitration methodology has only been applied for 'C-nitration' of poor nucleophilic substrates.

The Staudinger ligation reaction is used in synthetic biochemical transformation for the selective introduction of amide bonds within complex biological environments.[220] The reaction involves the reaction of an organic azide with arylphosphines to generate a phosphinimine through the loss of N_2 which is subsequently hydrolyzed to generate an amide bond and phosphine oxide (Scheme A-2). The mechanism and kinetics has been studied in detail.[221]

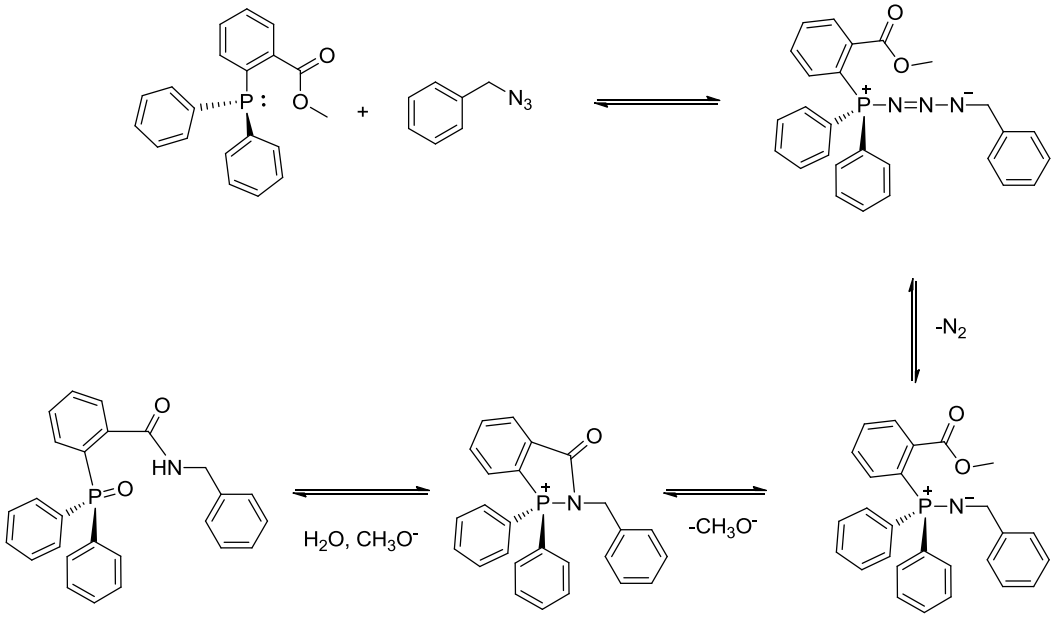

Scheme A-2. Mechanism of Staudinger ligation.

The phosphinimine that is generated is shown to be easily hydrolyzed by water to generate the phosphine oxide and amide bond. Since the phosphinimines could be easily generated, we decided to modify the final hydrolysis step to use an oxidising agent such as nitric acid or other nitrate salts to generate the N-nitroamide as a free acid or a salt (Scheme A-3).

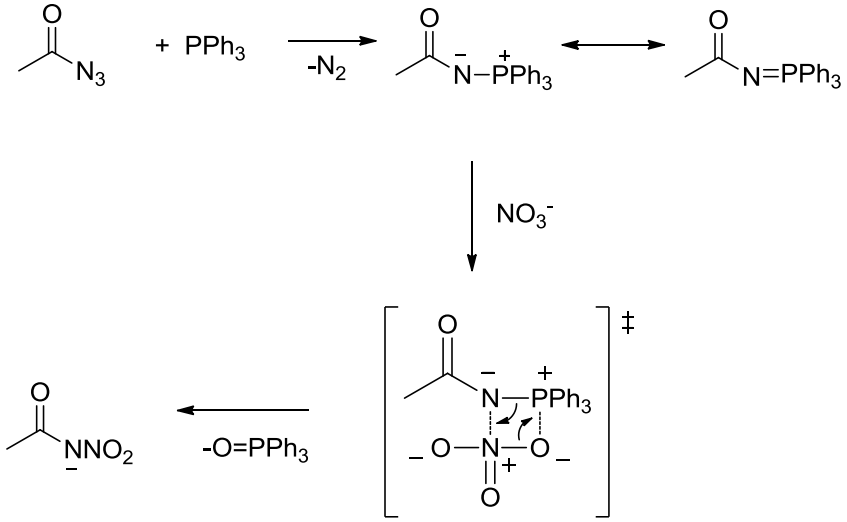

Scheme A-3. Proposed synthesis of N-nitroamides from phosphinimines and nitration.

Unfortunately the proposed synthetic method did not work as the hydrolysis of the phosphinimine by water to give triphenylphosphine oxide and acetamide was more rapid than the actual oxidation of the triphenylphosphinimine by the nitrate. The strongly oxidising concentrated nitric acid did not improve the outcome of the reaction as acidic conditions aid the hydrolysis of the tertiary phosphinimines.[222]

Appendix B

Table B-1. λ_{max}, abs and $\Delta\nu$ values of 3.2 mM **2-6** in CH_3OH and CD_3OD.

2-6 in CH_3OH			**2-6** in CD_3OD		
λ_{max} (nm)	ε (M^{-1} cm^{-1})	$\Delta\nu$ (cm^{-1})	λ_{max} (nm)	ε (M^{-1} cm^{-1})	$\Delta\nu$ (cm^{-1})
366	12.6	1348	366	13.8	1483
385	34.1	1036	387	38.4	902
401	61.6	956	401	67.0	956
417	88.5	1045	417	97.0	992
436	76.7		435	85.1	

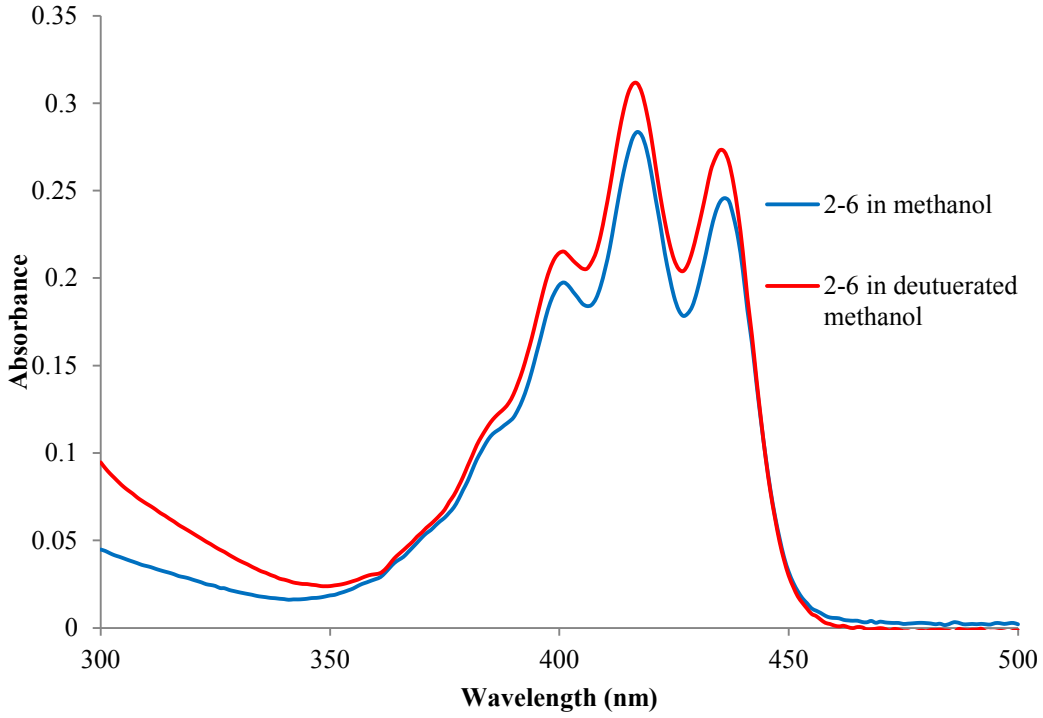

Figure B-1. UV-vis absorption spectrum of **2-6** in CH_3OH(blue) and CD_3OD(red).

Table B-2. λ_{max}, abs and $\Delta\nu$ values of 2.8 mM **2-7** in $CHCl_3$.

λ_{max} (nm)	ε (M^{-1} cm^{-1})	$\Delta\nu$ (cm^{-1})
366	13.8	1348
385	32.2	1036
401	63.5	957
417	91.1	1045
436	79.1	

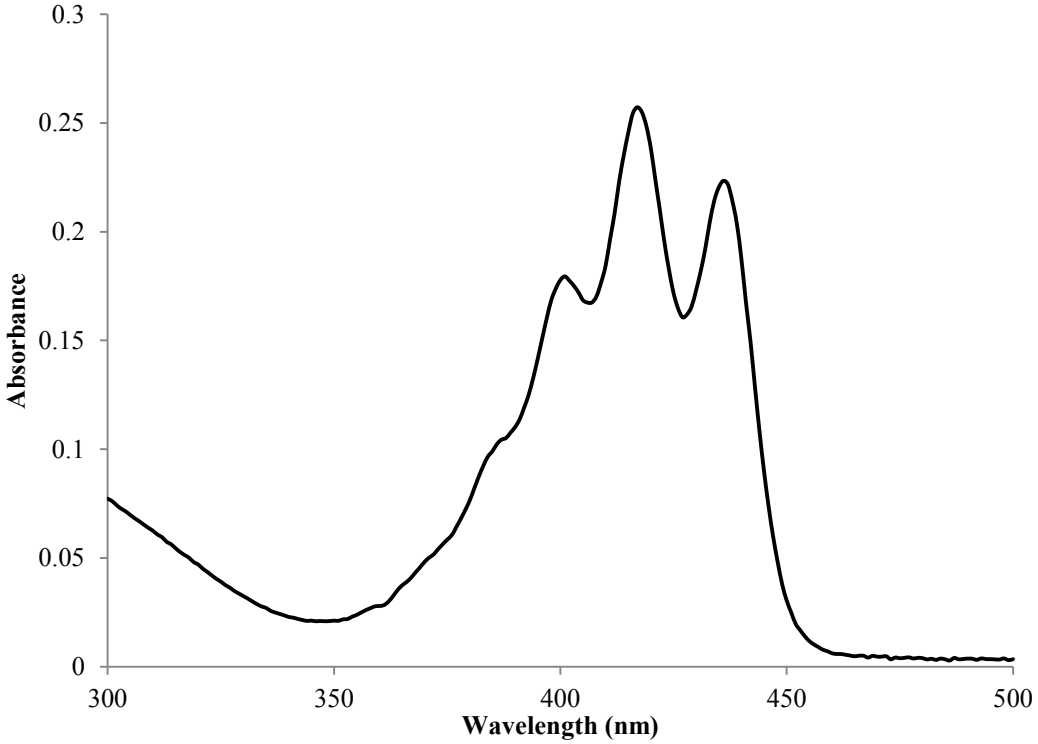

Figure B-2. UV-vis absorption spectrum of 2.8 mM **2-7** in CH_3OH.

Appendix C

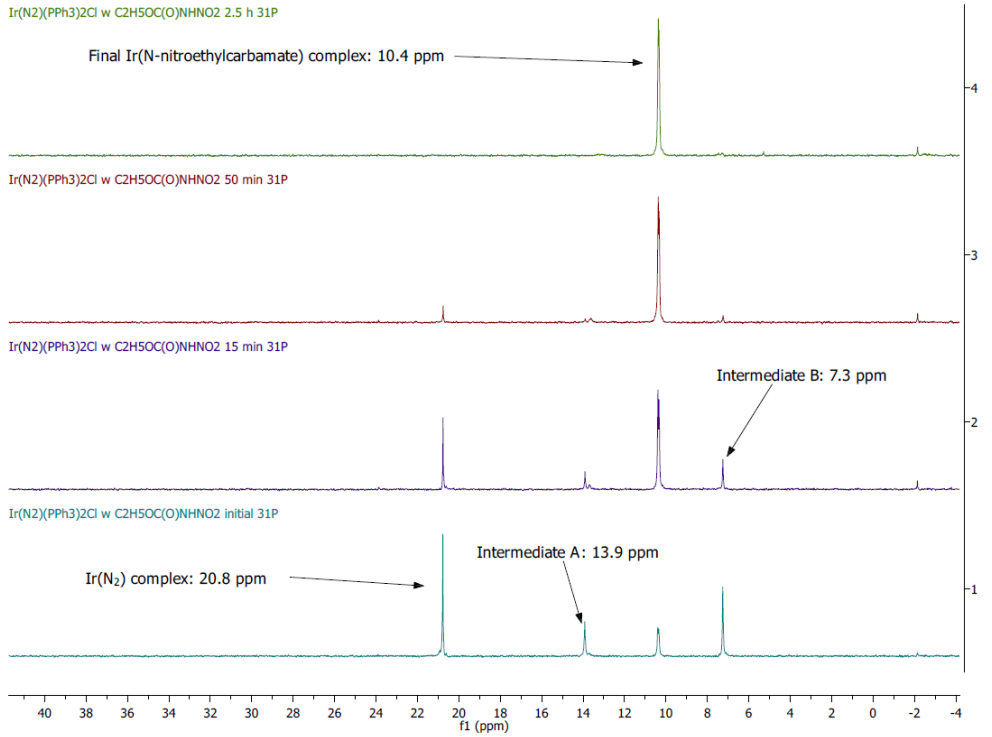

Figure C-1. ^{31}P NMR reaction monitoring of **3-2** with **2-5** to give **3-14**.

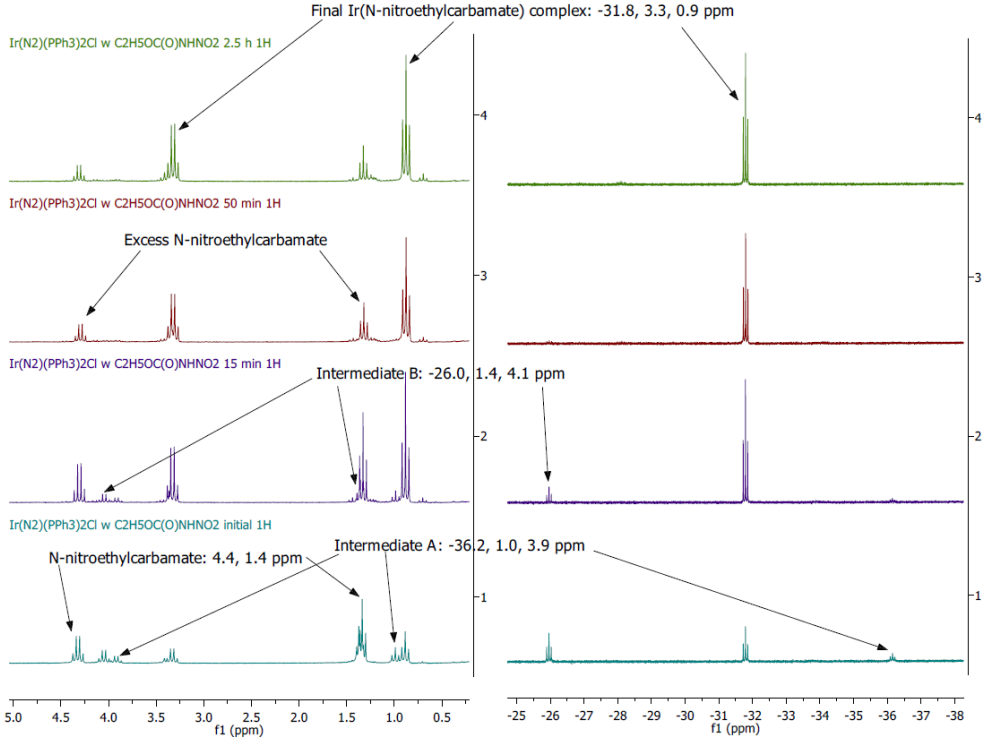

Figure C-2. ^{1}H NMR reaction monitoring of **3-2** with **2-5** to give **3-14**.

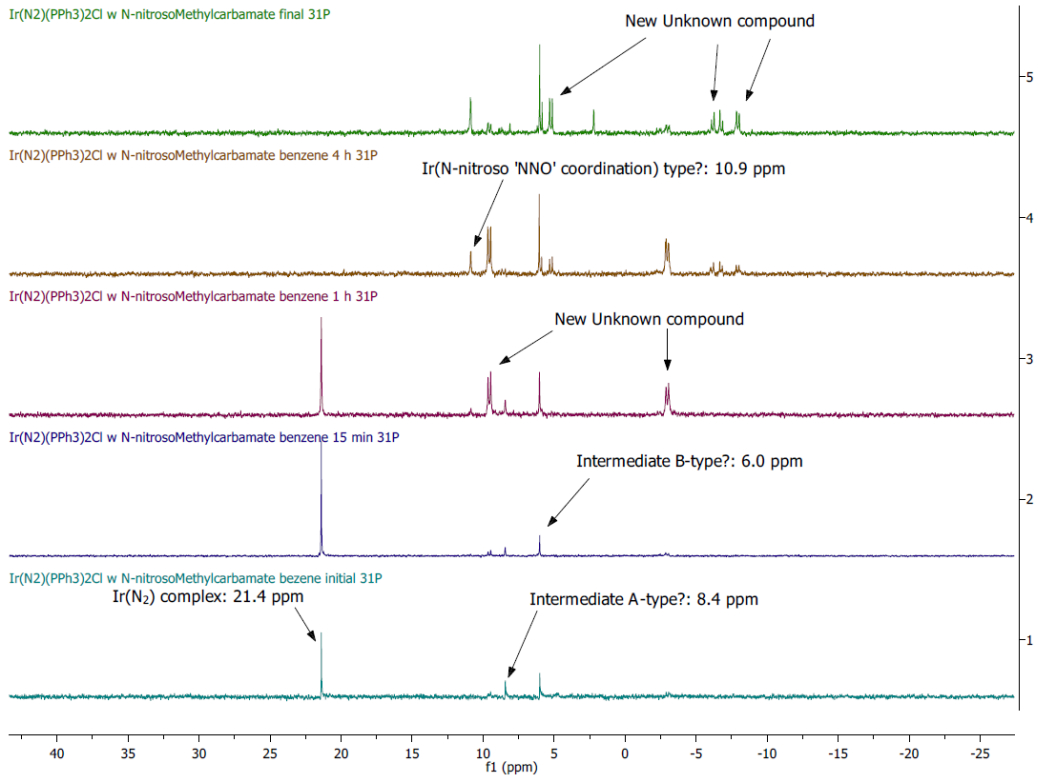

Figure C-3. ^{31}P NMR reaction monitoring of **3-2** with **2-6** in C_6D_6.

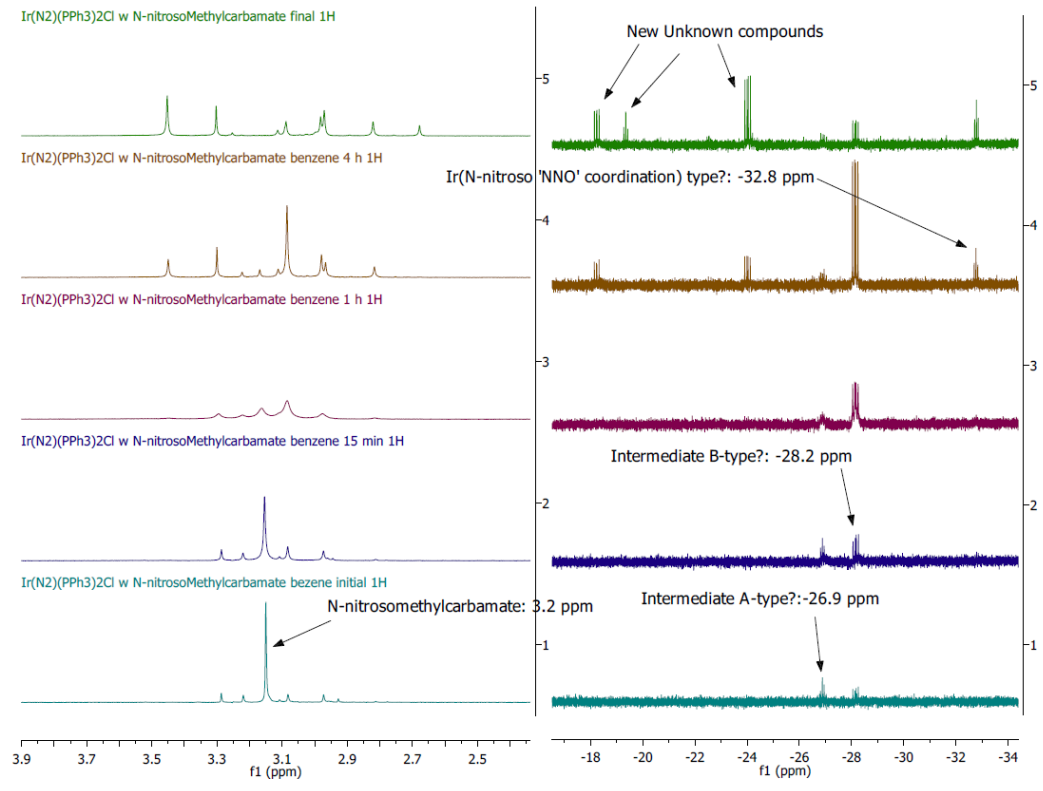

Figure C-4. ^{1}H NMR reaction monitoring of **3-2** with **2-6** in C_6D_6.

Table C-1: Crystallographic data for **3-17.**

Compound	**3-17**
empirical formula	$C_{20.5}H_{16.5}(IrClSN)_{0.5}(OF_{1.5})P$
T (K)	273(2)
fw (g mol^{-1})	490.17
cryst sys	Monoclinic
space group	$P2_1/m$
a (Å)	9.380(8)
b (Å)	23.239(19)
c (Å)	10.248(8)
α (deg)	90
β (deg)	95.498(12)
γ (deg)	90
V ($Å^3$)	2224(3)
Z	4
density (g cm^{-3})	1.464
abs coeff (mm^{-1})	3.230
No. of reflns collected	16465
No. of indep reflns	4256
Data/restraints/parameters	4256/709/353
Final R indices [$I > 2s(I)$] R1 wR2	0.0908 0.2146
R indices (all data) R1 wR2	0.1428 0.2425
Goodness-of-fit on F^2	1.062

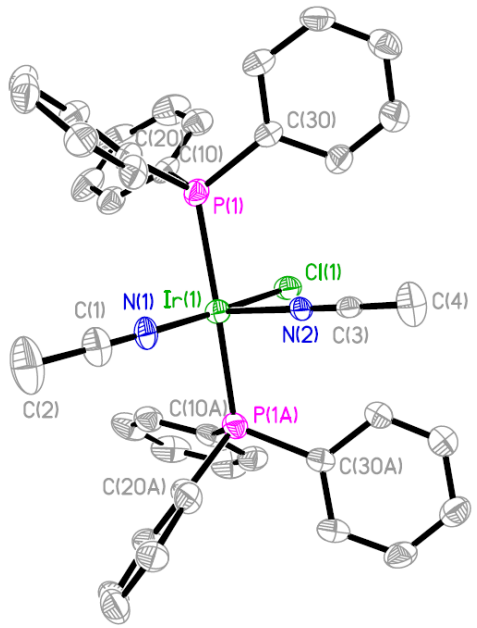

Figure C-5. Molecular structure of **3-17**. Hydrogen atoms and the triflate anion are omitted.

The atoms Ir(1), N(1), C(1), C(2), N(2), C(3), C(4), Cl(1) and the triflate anion are on the symmetry plane. The triflate anion is disordered between itself where the 'SO_3' fragment is disordered with the 'CF_3' fragment.

Due to the poor quality of the diffraction data, strong least squares thermal parameter restraints such as ISOR, SIMU and DELU have been applied to the whole structure. Least squares bond constraints such as DFIX is applied to the SO_3 fragment of the triflate anion and least square bond restraints SADI and SAME applied to the disordered triflate anion.

Appendix D

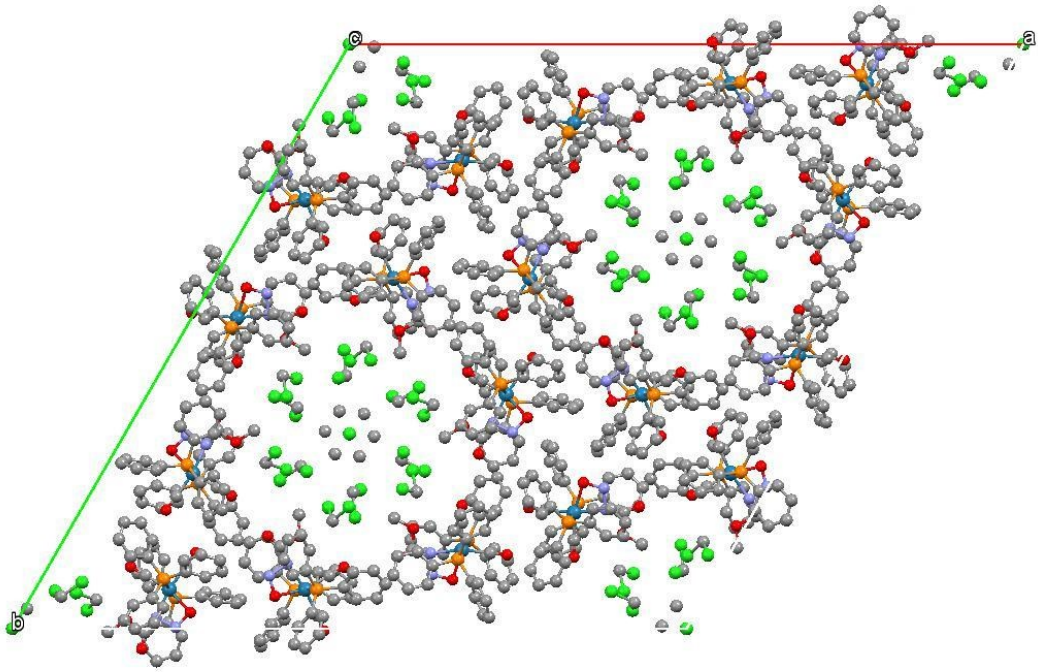

Figure D-1. Crystal packing of **4-10** in R-3 along the c-axis.

Table D-1: Crystallographic data for **4-9'** in alternative space group P-1.

Compound	**4-9'**
empirical formula	$C_{120}H_{99}Re_3P_6Cl_{14}N_6O_{18}.7CH_2Cl_2$
T (K)	100(2)
fw (g mol^{-1})	1083.98
cryst sys	triclinic
space group	P-1
a (Å)	11.9008(6)
b (Å)	26.5389(14)
c (Å)	26.5574(14)
α (deg)	117.7740(10)
β (deg)	98.6090(10)
γ (deg)	98.5690(10)
V ($Å^3$)	7104.7(6)
Z	6
density (g cm^{-3})	1.520
abs coeff (mm^{-1})	2.941
No. of reflns collected	69349
No. of indep reflns	25079
Data/restraints/parameters	25079/220/1567
Final R indices [$I > 2s(I)$] R1 wR2	0.0627 0.1826
R indices (all data) R1 wR2	0.879 0.2012
Goodness-of-fit on F^2	1.049

Appendix E

Table E-1: Chemical shift changes dependence on variable temperature ^{19}F NMR for **5-1**.

T, °C	^{19}F NMR peaks in DMF-d_7			
20	-81.05	-110.78	-121.17	-126.03
-10	-81.13	-111.41	-121.49	-126.39
-30	-81.15	-111.74	-121.65	-126.59
-40	-81.17	-111.37	-121.75	-126.72
		-111.43		
-57	-81.18	-114.67	-121.83	-126.84
Back to 20	-81.05	-110.78	-121.17	-126.03
^{19}F NMR peaks in CD_2Cl_2				
20	-81.002	-109.37	-120.96	-126.01
-60	-80.77	-110.35	-121.42	-126.64

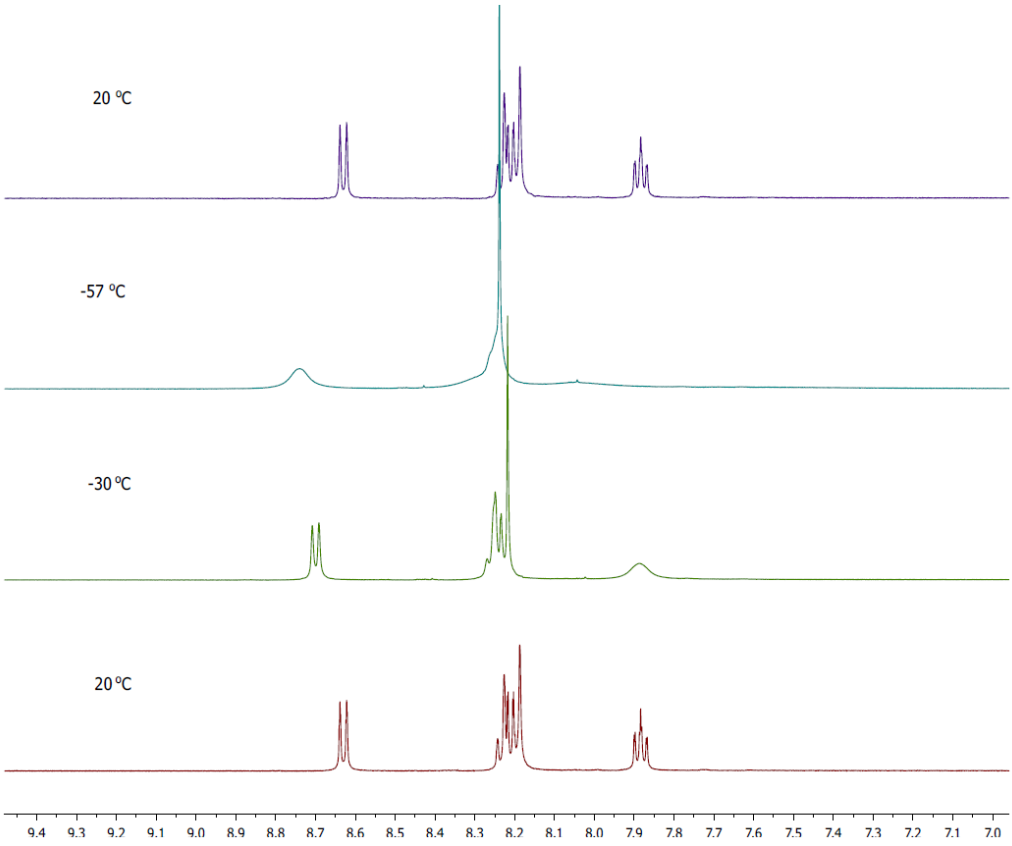

Figure E-1. Variable temperature ^1H NMR of **5-1** in d_6-DMF.

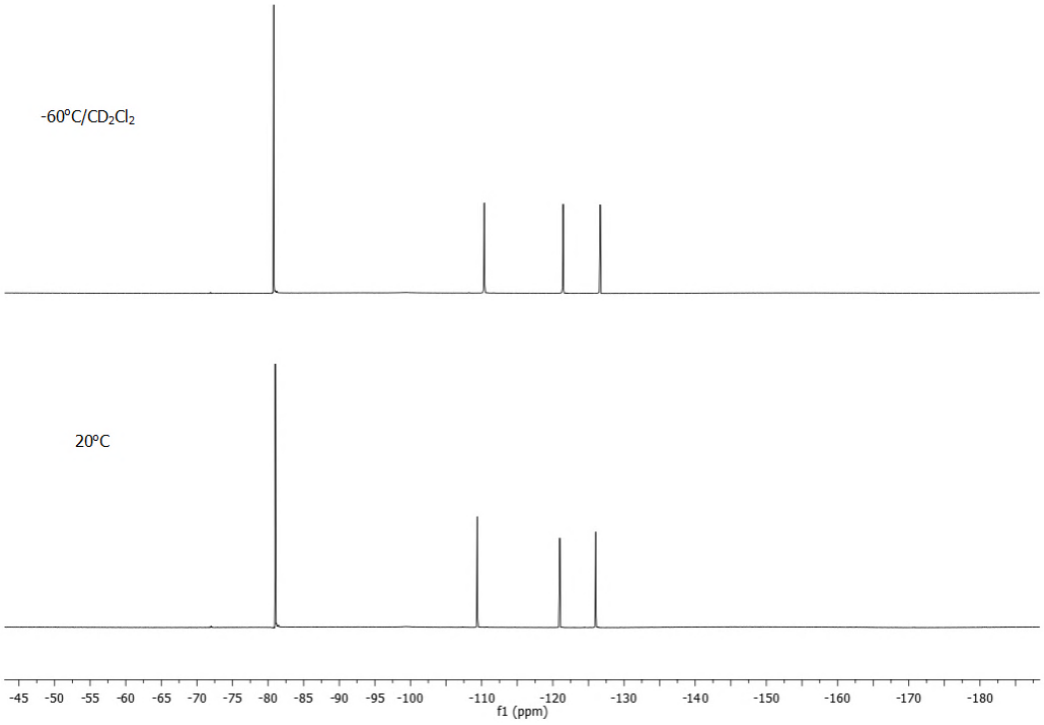

Figure E-2. Variable temperature ^{19}F NMR of **5-1** in CD_2Cl_2.

References

[1] a) B. C. Berks, S. J. Ferguson, J. W. B. Moir, D. J. Richardson, *Biochim. Biophys. Acta, Bioenerg.* **1995**, *1232*, 97-173; b) D. J. Richardson, N. J. Watmough, *Curr. Opin. Chem. Biol.* **1999**, *3*, 207-19.

[2] J. R. Jennings, Editor, *Catalytic Ammonia Synthesis. Fundamentals and Practice*, Plenum, **1991**.

[3] D. E. Canfield, A. N. Glazer, P. G. Falkowski, *Science* **2010**, *330*, 192-6.

[4] W. G. Zumft, *J. Mol. Microbiol. Biotechnol.* **2005**, *10*, 154-66.

[5] A. V. Leont'ev, O. g. A. Fomicheva, M. V. Proskurnina, N. S. Zefirov, *Russ. Chem. Rev.* **2001**, *70*, 91-104.

[6] W. L. Jolly, *The Inorganic Chemistry of Nitrogen*, W. A. Benjamin New York, **1964**.

[7] K. Jones in, J. C. Bailar, H. J. Emelous, R. Nyholm, A. F. Trottman-Dickenson, *Comprehensive Inorganic Chemistry, Vol. 4*, Pergamon, **1973**.

[8] a) A. R. Ravishankara, J. S. Daniel, R. W. Portmann, *Science* **2009**, *326*, 123-5; b) R. W. Portmann, J. S. Daniel, A. R. Ravishankara, *Philos. trans. R. Soc. B, Biol. sci.* **2012**, *367*, 1256-64.

[9] P. Forster, V. A. Ramaswamy, in *Climate Change 2007: The Physical Science Basis. Contribution of Working Group I to the Fourth Assessment Report of the Intergovernmental Panel on Climate Change*, **2007**, pp. 129-234.

[10] a) L. A. Codispoti, *Science* **2010**, *327*, 1339-40; b) A. Freing, D. W. R. Wallace, H. W. Bange, *Philos. trans. R. Soc. B, Biol. sci.* **2012**, *367*, 1245-55.

[11] K. A. Smith, A. R. Mosier, P. J. Crutzen, W. Winiwarter, *Philos. trans. R. Soc. B, Biol. sci.* **2012**, *367*, 1169-74.

[12] Y. Law, L. Ye, Y. Pan, Z. Yuan, *Philos. trans. R. Soc. B, Biol. sci.* **2012**, *367*, 1265-77.

[13] a) D. J. Wuebbles, *Science* **2009**, *326*, 56-7; b) U. Skiba, S. K. Jones, U. Dragosits, J. Drewer, D. Fowler, R. M. Rees, V. A. Pappa, L. Cardenas, D. Chadwick, S. Yamulki, A. J. Manning, *Philos. trans. R. Soc. B, Biol. sci.* **2012**, *367*, 1175-85.

[14] a) S. Spiro, *Philos. trans. R. Soc. B, Biol. sci.* **2012**, *367*, 1213-25; b) S. R. Pauleta, S. Dell'Acqua, I. Moura, *Coord. Chem. Rev.* **2013**, *257*, 332-49.

[15] W. G. Zumft, P. M. H. Kroneck, *FEMS Symp.* **1990**, *56*, 37-55.

[16] a) K. Brown, M. Tegoni, M. Prudencio, A. S. Pereira, S. Besson, J. J. Moura, I. Moura, C. Cambillau, *Nat Struct Mol Biol* **2000**, *7*, 191-5; b) T. Haltia, K. Brown, M. Tegoni, C. Cambillau, M. Saraste, K. Mattila, K. Djinovic-Carugo, *Biochem. J.* **2003**, *369*, 77-88.

[17] M. G. Savelieff, T. D. Wilson, Y. Elias, M. J. Nilges, D. K. Garner, Y. Lu, *Proc. Natl. Acad. Sci. U. S. A.* **2008**, *105*, 7919-24, s/1-s/12.

[18] K. Brown, K. Djinovic-Carugo, T. Haltia, I. Cabrito, M. Saraste, J. G. Moura, I. Moura, M. Tegoni, C. Cambillau, *J. Biol. Chem.* **2000**, *275*, 41133-6.

[19] K. Paraskevopoulos, S. V. Antonyuk, R. G. Sawers, R. R. Eady, S. S. Hasnain, *J. Mol. Biol.* **2006**, *362*, 55-65.

[20] A. Pomowski, W. G. Zumft, P. M. H. Kroneck, O. Einsle, *Nature (London, U. K.)* **2011**, *477*, 234-7.

[21] O. Einsle, F. A. Tezcan, S. L. A. Andrade, B. Schmid, M. Yoshida, J. B. Howard, D. C. Rees, *Science* **2002**, *297*, 1696-700.

[22] J. Yano, J. Kern, K. Sauer, M. J. Latimer, Y. Pushkar, J. Biesiadka, B. Loll, W. Saenger, J. Messinger, A. Zouni, V. K. Yachandra, *Science* **2006**, *314*, 821-5.

[23] A. Wuest, L. Schneider, A. Pomowski, W. G. Zumft, P. M. H. Kroneck, O. Einsle, *Biol. Chem.* **2012**, *393*, 1067-77.

[24] a) S. Ghosh, S. I. Gorelsky, P. Chen, I. Cabrito, Moura, I. MouraMoura, E. I. Solomon, *J. Am. Chem. Soc.* **2003**, *125*, 15708-9; b) P. Chen, S. I. Gorelsky, S. Ghosh, E. I. Solomon, *Angew. Chem. Int. Ed.* **2004**, *43*, 4132-40.

[25] T. Rasmussen, B. C. Berks, J. N. Butt, A. J. Thomson, *Biochem. J.* **2002**, *364*, 807-15.

[26] J. Riester, W. G. Zumft, P. M. H. Kroneck, *Eur. J. Biochem.* **1989**, *178*, 751-62.

[27] W. G. Zumft, P. M. H. Kroneck, in *Adv. Microb. Physiol., Vol. Volume 52* (Ed.: K. P. Robert), Academic Press, **2006**, pp. 107-227.

[28] S. Dell'Acqua, S. Pauleta, P. Paes de Sousa, E. Monzani, L. Casella, J. G. Moura, I. Moura, *J. Biol. Inorg. Chem.* **2010**, *15*, 967-76.

[29] S. Dell'Acqua, S. R. Pauleta, J. J. G. Moura, I. Moura, *Philos. trans. R. Soc. B, Biol. sci.* **2012**, *367*, 1204-12.

[30] P. Chen, S. DeBeer George, I. Cabrito, W. E. Antholine, J. J. G. Moura, I. Moura, B. Hedman, K. O. Hodgson, E. I. Solomon, *J. Am. Chem. Soc.* **2002**, *124*, 744-5.

[31] Y. Ilan, J. Rabani, *Int.J. Radiat. Phy. Chem.* **1976**, *8*, 609-11.

[32] a) S. Poh, R. Hernandez, M. Inagaki, P. G. Jessop, *Org. Lett.* **1999**, *1*, 583-6; b) A. V. Leont'ev, L. G. Tomilova, A. O. Fomicheva, M. V. Proskurina, N. S. Zefirov, *Russ. J. Gen. Chem.* **2001**, *71*, 648-9.

[33] a) G. I. Panov, G. A. Sheveleva, A. S. Kharitonov, V. N. Romannikov, L. A. Vostrikova, *Appl. Catal. A-General* **1992**, *82*, 31-6; b) M. S. Reisch, *Chem. Eng. News.* **1998**, *76*, 19-23; c) A. M. Thayer, *Chem. Eng. News.* **1998**, *76*, 21-3.

[34] F. Kapteijn, J. Rodriguez-Mirasol, J. A. Moulijn, *Appl. Catal. B-Environment* **1996**, *9*, 25-64.

[35] I. Bar-Nahum, A. K. Gupta, S. M. Huber, M. Z. Ertem, C. J. Cramer, W. B. Tolman, *J. Am. Chem. Soc.* **2009**, *131*, 2812-4.

[36] A. A. Diamantis, G. J. Sparrow, *J. Chem. Soc. D, Chem. Commun.* **1970**, 819-20.

[37] J. N. Armor, H. Taube, *J. Chem. Soc. D, Chem. Commun.* **1971**, 287-8.

[38] A. Diamantis, G. Sparrow, M. Snow, T. Norman, *Aust. J. Chem.* **1975**, *28*, 1231-44.

[39] a) F. Bottomley, J. R. Crawford, *J. Chem. Soc. D, Chem. Commun.* **1971**, 200-1; b) F. Bottomley, J. R. Crawford, *J. Am. Chem. Soc.* **1972**, *94*, 9092-5; c) F. Bottomley, J. N. Armor, in *Inorg. Synth., Vol. 16*, John Wiley & Sons, Inc., **1976**, pp. 75-7.

[40] a) J. N. Armor, H. Taube, *J. Am. Chem. Soc.* **1970**, *92*, 2560-2; b) A. A. Diamantis, G. J. Sparrow, *J. Colloid Interface Sci.* **1974**, *47*, 455-8; c) F. Bottomley, W. V. F. Brooks, *Inorg. Chem.* **1977**, *16*, 501-2; d) D. F. T. Tuan, R. Hoffmann, *Inorg. Chem.* **1985**, *24*, 871-6.

[41] F. Paulat, T. Kuschel, C. Näther, V. K. K. Praneeth, O. Sander, N. Lehnert, *Inorg. Chem.* **2004**, *43*, 6979-94.

[42] a) F. Bottomley, I. J. B. Lin, M. Mukaida, *J. Am. Chem. Soc.* **1980**, *102*, 5238-42; b) F. Bottomley, D. E. Paez, P. S. White, *J. Am. Chem. Soc.* **1982**, *104*, 5651-7; c) G. A. Vaughan, C. D. Sofield, G. L. Hillhouse, A. L. Rheingold, *J. Am. Chem. Soc.* **1989**, *111*, 5491-3; d) G. A. Vaughan, G. L. Hillhouse, A. L. Rheingold, *J. Am. Chem. Soc.* **1990**, *112*, 7994-8001; e) P. T. Matsunaga, G. L. Hillhouse, A. L. Rheingold, *J. Am. Chem. Soc.* **1993**, *115*, 2075-7; f) M. R. Smith, P. T. Matsunaga, R. A. Andersen, *J. Am. Chem. Soc.* **1993**, *115*, 7049-50; g) K. Koo, G. L. Hillhouse, A. L. Rheingold, *Organometallics* **1995**, *14*, 456-60; h) J. T. Groves, J. S. Roman, *J. Am. Chem. Soc.* **1995**, *117*, 5594-5; i) A. W. Kaplan, R. G. Bergman, *Organometallics* **1997**, *16*, 1106-8; j) W. H. Harman, C. J. Chang, *J. Am. Chem. Soc.* **2007**, *129*, 15128-9; k) N. D. Harrold, R. Waterman, G. L. Hillhouse, T. R. Cundari, *J. Am. Chem. Soc.* **2009**, *131*, 12872-3; l) A. G. Tskhovrebov, E. Solari, R. Scopelliti, K. Severin, *Organometallics* **2012**, *31*, 7235-40; m) E. R. Bartholomew, E. C. Volpe, P. T. Wolczanski, E. B. Lobkovsky, T. R. Cundari, *J. Am. Chem. Soc.* **2013**, *135*, 3511-27.

[43] a) C. E. Laplaza, A. L. Odom, W. M. Davis, C. C. Cummins, J. D. Protasiewicz, *J. Am. Chem. Soc.* **1995**, *117*, 4999-5000; b) A. R. Johnson, W. M. Davis, C. C. Cummins, S. Serron, S. P. Nolan, D. G. Musaev, K. Morokuma, *J. Am. Chem. Soc.* **1998**, *120*, 2071-85; c) J.-P. F. Cherry, A.

R. Johnson, L. M. Baraldo, Y.-C. Tsai, C. C. Cummins, S. V. Kryatov, E. V. Rybak-Akimova, K. B. Capps, C. D. Hoff, C. M. Haar, S. P. Nolan, *J. Am. Chem. Soc.* **2001**, *123*, 7271-86; d) J. P. Reeds, B. L. Yonke, P. Y. Zavalij, L. R. Sita, *J. Am. Chem. Soc.* **2011**, *133*, 18602-5.

[44] C. B. Pamplin, E. S. F. Ma, N. Safari, S. J. Rettig, B. R. James, *J. Am. Chem. Soc.* **2001**, *123*, 8596-7.

[45] a) A. Yamamoto, S. Kitazume, L. S. Pu, S. Ikeda, *J. Am. Chem. Soc.* **1971**, *93*, 371-80; b) J.-H. Lee, M. Pink, J. Tomaszewski, H. Fan, K. G. Caulton, *J. Am. Chem. Soc.* **2007**, *129*, 8706-7.

[46] a) K. Yamashita, K. Morokuma, *Chem. Phys. Lett.* **1986**, *131*, 237-42; b) H. Yu, G. Jia, Z. Lin, *Organometallics* **2009**, *28*, 1158-64; c) W. B. Tolman, *Angew. Chem. Int. Ed.* **2010**, *49*, 1018-24; d) J. G. Andino, K. G. Caulton, *J. Am. Chem. Soc.* **2011**, *133*, 12576-83.

[47] E. Otten, R. C. Neu, D. W. Stephan, *J. Am. Chem. Soc.* **2009**, *131*, 9918-9.

[48] a) R. C. Neu, E. Otten, D. W. Stephan, *Angew. Chem. Int. Ed.* **2009**, *48*, 9709-12; b) R. C. Neu, E. Otten, A. Lough, D. W. Stephan, *Chem. Sci.* **2011**, *2*, 170-6.

[49] N. A. Piro, M. F. Lichterman, W. H. Harman, C. J. Chang, *J. Am. Chem. Soc.* **2011**, *133*, 2108-11.

[50] A. G. Tskhovrebov, E. Solari, M. D. Wodrich, R. Scopelliti, K. Severin, *Angew. Chem. Int. Ed.* **2012**, *51*, 232-4.

[51] H. Zhou, W.-Z. Zhang, Y.-M. Wang, J.-P. Qu, X.-B. Lu, *Macromolecules* **2009**, *42*, 5419-21.

[52] A. G. Tskhovrebov, E. Solari, M. D. Wodrich, R. Scopelliti, K. Severin, *J. Am. Chem. Soc.* **2012**, *134*, 1471-3.

[53] C. Feldmann, M. Jansen, *Angew. Chem. Int. Ed.* **1996**, *35*, 1728-30.

[54] a) W. C. Trogler, *Coord. Chem. Rev.* **1999**, *187*, 303-27; b) J. A. Olabe, L. D. Slep, in *Comprehensive Coordination Chemistry II, Vol. 1*, Elsevier Ltd., **2004**, pp. 603-23.

[55] E. Divers, *Proc. R. Soc. Lond.* **1870**, *19*, 425-31.

[56] C. C. Addison, G. A. Gamlen, R. Thompson, *J. Chem. Soc.* **1952**, 338-45.

[57] C. N. Polydoropoulos, *Chim. Chronika* **1959**, *24*, 147-51.

[58] F. T. Bonner, M. N. Hughes, *Comments Inorg. Chem.* **1988**, *7*, 215-34.

[59] L. W. Jones, A. W. Scott, *J. Am. Chem. Soc.* **1924**, *46*, 2172-5.

[60] L. Kuhn, E. R. Lippincott, *J. Am. Chem. Soc.* **1956**, *78*, 1820-1.

[61] N. Arulsamy, D. S. Bohle, J. A. Imonigie, E. S. Sagan, *Inorg. Chem.* **1999**, *38*, 2716-25.

[62] a) F. T. Bonner, C. E. Donald, M. N. Hughes, *J. Chem. Soc., Dalton Trans.* **1989**, *0*, 527-32; b) M. N. Hughes, P. E. Wimbledon, G. Stedman, *J. Chem. Soc., Dalton Trans.* **1989**, *0*, 533-7; c) A. M. Al-Ajlouni, E. S. Gould, *J. Chem. Soc., Dalton Trans.* **2000**, *0*, 1239-42.

[63] J. Zevallos, A. Toro-Labbe, O. Mo, M. Yanez, *Struct. Chem.* **2005**, *16*, 295-303.

[64] a) R. J. Puddephatt, P. J. Thompson, *J. Chem. Soc., Dalton Trans.* **1976**, 2091-5; b) S. Bhaduri, B. F. G. Johnson, A. Pickard, P. R. Raithby, G. M. Sheldrick, C. I. Zuccaro, *J. Chem. Soc., Chem. Commun.* **1977**, *0*, 354-5; c) S. Bhaduri, B. F. G. Johnson, A. Khair, I. Ghatak, D. M. P. Mingos, *J. Chem. Soc., Dalton Trans.* **1980**, 1572-6; d) L. K. Bell, J. Mason, D. M. P. Mingos, D. G. Tew, *Inorg. Chem.* **1983**, *22*, 3497-502.

[65] C. Feldmann, M. Jansen, *Z. Anorg. Allg. Chem.* **1997**, *623*, 1803-9.

[66] a) N. Arulsamy, D. S. Bohle, J. A. Imonigie, S. Levine, *Angewandte Chemie International Edition* **2002**, *41*, 2371-3; b) N. Arulsamy, D. S. Bohle, J. A. Imonigie, R. C. Moore, *Polyhedron* **2007**, *26*, 4737-45.

[67] W. M. Latimer, H. W. Zimmermann, *J. Am. Chem. Soc.* **1939**, *61*, 1550-4.

[68] a) M. N. Hughes, G. Stedman, *J. Chem. Soc.* **1964**, *0*, 163-6; b) M. N. Hughes, *Quart. Rev. (London)* **1968**, *22*, 1-13.

[69] A. Angeli, *Gazz. Chim. Ital.* **1896**, *26*, 17-25.

[70] O. Piloty, *Chem. Ber.* **1896**, *29*, 1559-67.

[71] a) P. A. S. Smith, G. E. Hein, *J. Am. Chem. Soc.* **1960**, *82*, 5731-40; b) F. C. Kohout, F. W. Lampe, *J. Am. Chem. Soc.* **1965**, *87*, 5795-6.

[72] a) F. T. Bonner, Y. Ko, *Inorg. Chem.* **1992**, *31*, 2514-9; b) K. M. Miranda, *Coord.Chem. Rev.* **2005**, *249*, 433-55.

[73] A. Porcheddu, L. De Luca, G. Giacomelli, *Synlett* **2009**, 2149-53.

[74] a) M. N. Ackermann, R. E. Powell, *Inorg. Chem.* **1966**, *5*, 1334-7; b) K. Brink, W. Gombler, C. Bliefert, *Z. Anorg. Allg. Chem.* **1977**, *429*, 255-60.

[75] F. T. Bonner, B. Ravid, *Inorg. Chem.* **1975**, *14*, 558-63.

[76] R. Zamora, A. Grzesiok, H. Weber, M. Feelisch, *Biochem. J.* **1995**, *312*, 333-9.

[77] V. Shafirovich, S. V. Lymar, *Proc. Natl. Acad. Sci. U. S. A.* **2002**, *99*, 7340-5.

[78] a) K. R. Grundy, C. A. Reed, W. R. Roper, *J. Chem. Soc. D, Chem. Commun.* **1970**, 1501-2; b) R. D. Wilson, J. A. Ibers, *Inorg. Chem.* **1979**, *18*, 336-43; c) R. Melenkivitz, G. L. Hillhouse, *Chem. Commun.* **2002**, *0*, 660-1.

[79] S. Kura, S. Kuwata, T. Ikariya, *Angew. Chem. Int. Ed.* **2005**, *44*, 6406-9.

[80] D. Sellmann, T. Gottschalk-Gaudig, D. Häußinger, F. W. Heinemann, B. A. Hess, *Chem. Eur. J.* **2001**, *7*, 2099-103.

[81] J. S. Southern, G. L. Hillhouse, A. L. Rheingold, *J. Am. Chem. Soc.* **1997**, *119*, 12406-7.

[82] R. Melenkivitz, J. S. Southern, G. L. Hillhouse, T. E. Concolino, L. M. Liable-Sands, A. L. Rheingold, *J. Am. Chem. Soc.* **2002**, *124*, 12068-9.

[83] a) R. Lin, P. J. Farmer, *J. Am. Chem. Soc.* **2000**, *122*, 2393-4; b) F. Sulc, E. Fleischer, P. Farmer, D. Ma, G. La Mar, *J. Biol. Inorg. Chem.* **2003**, *8*, 348-52; c) C. E. Immoos, F. Sulc, P. J. Farmer, K. Czarnecki, D. F. Bocian, A. Levina, J. B. Aitken, R. S. Armstrong, P. A. Lay, *J. Am. Chem. Soc.* **2004**, *127*, 814-5; d) F. Sulc, C. E. Immoos, D. Pervitsky, P. J. Farmer, *J. Am. Chem. Soc.* **2004**, *126*, 1096-101; e) P. J. Farmer, F. Sulc, *J. Inorg. Biochem.* **2005**, *99*, 166-84; f) A. C. Montenegro, V. T. Amorebieta, L. D. Slep, D. F. Martín, F. Roncaroli, D. H. Murgida, S. E. Bari, J. A. Olabe, *Angew. Chem. Int. Ed.* **2009**, *48*, 4213-6; g) P. J. Farmer, M. R. Kumar, E. Almaraz, *Comments Inorg. Chem.* **2010**, *31*, 130-43.

[84] C. H. Switzer, T. W. Miller, P. J. Farmer, J. M. Fukuto, *J. Inorg. Biochem.* **2013**, *118*, 128-33.

[85] J. Thiele, A. Lachman, *Liebigs Ann.* **1895**, *288*, 267-311.

[86] C. A. Marlies, V. K. La Mer, J. Greenspan, W. A. Shine, L. F. Audrieth, in *Inorg. Synth., Vol. 1*, John Wiley & Sons, Inc., **1939**, pp. 68-74.

[87] A. A. Lobanova, S. G. Il'yasov, G. V. Sakovich, *Russ. Chem. Rev.* **2010**, *79*, 819-33.

[88] a) A. Hantzsch, *Liebigs Ann.* **1896**, *292*, 340-58; b) A. Hantzsch, *Chem. Ber.* **1933**, *66*, 1566-8.

[89] W. Traube, *Liebigs Ann.* **1898**, *300*, 81-128.

[90] K. W. F. Kohlrausch, H. Wittek, *Acta Phys. Austriaca* **1948**, *1*, 292-302.

[91] a) M. Davies, N. Jonathan, *Trans. Faraday Soc.* **1958**, *54*, 469-77; b) M. Nonella, R. P. Müller, J. Robert Huber, *J. Mol. Spectrosc.* **1985**, *112*, 142-52.

[92] a) C. A. Beevers, A. F. Trotman-Dickenson, *Acta Crystallogr.* **1957**, *10*, 34-6; b) A. Haussler, T. M. Klapotke, H. Piotrowski, *Z. Naturforsch., B: Chem. Sci.* **2002**, *57*, 151-6.

[93] a) K. Kaya, K. Kuwata, S. Nagakura, *Bull. Chem. Soc. Jpn.* **1964**, *37*, 1055-61; b) J. Stals, C. G. Barraclough, A. S. Buchanan, *Trans. Faraday Soc.* **1969**, *65*, 904-14.

[94] J. D. Ray, J. Richard A. Ogg, *J. Chem. Phys.* **1957**, *26*, 1452-4.

[95] J. K. Tyler, *J. Mol. Spectrosc.* **1963**, *11*, 39-46.

[96] J. P. Ritchie, *J. Am. Chem. Soc.* **1989**, *111*, 2517-20.

[97] J. N. Brønsted, *Recl. Trav. Chim. Pays-Bas Belg.* **1923**, *42*, 718-28.

[98] J. N. Bronsted, *Chem. Rev. (Washington, DC, U. S.)* **1928**, *5*, 231-338.

[99] a) J. N. Brønsted, K. Pedersen, *Z. physik. Chem.* **1924**, *108*, 185-235; b) J. N. Brønsted, K. Volqvartz, *Z. physik. Chem.* **1931**, *A155*, 211-24; c) J. N. Brønsted, J. E. Vance, *Z. physik. Chem.* **1933**, *A163*, 240-56; d) J. N. Brønsted, *Z. physik. Chem.* **1934**, *A169*, 52-74.

[100] C. H. Arrowsmith, A. Awwal, B. A. Euser, A. J. Kresge, P. P. T. Lau, D. P. Onwood, Y. C. Tang, E. C. Young, *J. Am. Chem. Soc.* **1991**, *113*, 172-9.

[101] C. H. Arrowsmith, A. J. Kresge, Y. C. Tang, *J. Am. Chem. Soc.* **1991**, *113*, 179-82.

[102] a) M. Eckert-Maksic, H. Maskill, I. Zrinski, *J. Chem. Soc., Perkin Trans. 2* **2001**, 2147-54; b) K. K. Kalnin'sh, *Russ. J. Appl. Chem.* **2007**, *80*, 934-40.

[103] R. A. Cox, *Can. J. Chem.* **1996**, *74*, 1779-83.

[104] P. Vast, *Bull. Soc. Chim. Fr.* **1970**, 2136-9.

[105] G. Sheldrick, *Acta Crystallogr.* **2008**, *A64*, 112-22.

[106] G. M. Sheldrick, University of Göttingen, Germany., **1996**.

[107] A. A. Lobanova, S. G. Il'yasov, N. I. Popov, R. R. Sataev, *Russ. J. Org. Chem.* **2002**, *38*, 1-6.

[108] P. G. Puranik, L. Sirdeshmukh, *Indian J. Pure Appl. Phys.* **1969**, *7*, 790-2.

[109] O. A. Luk'yanov, I. K. Kozlova, O. P. Shitov, Y. Y. Konnova, I. V. Kalinina, Y. A. Tartakovsky, *Russ. Chem. Bull.* **1996**, *45*, 863-7.

[110] G. Gattow, W. K. Knoth, *Z. Anorg. Allg. Chem.* **1983**, *499*, 194-204.

[111] V. Benin, P. Kaszynski, J. G. Radziszewski, *J. Am. Chem. Soc.* **2002**, *124*, 14115-26.

[112] B. R. Mathews, *J. Phys. Chem.* **1919**, *24*, 108-19.

[113] S. Tellier-Pollon, J. Heubel, *Rev. Chim. Miner.* **1967**, *4*, 413-23.

[114] M. N. Hughes, J. R. Lusty, H. L. Wallis, *J. Chem. Soc., Dalton Trans.* **1978**, *0*, 530-4.

[115] P. Vast, J. Heubel, *Compt. Rend.* **1965**, *260*, 5799-801.

[116] C. W. Sauer, R. P. Follett, *J. Am. Chem. Soc.* **1955**, *77*, 2560-1.

[117] a) P. Goede, N. Wingborg, H. Bergman, N. V. Latypov, *Propellants Explos. Pyrotech.* **2001**, *26*, 17-20; b) C. Ye, H. Gao, B. Twamley, J. n. M. Shreeve, *New J. Chem.* **2008**, *32*, 317-22.

[118] a) A. A. Lobanova, R. R. Sataev, N. I. Popov, S. G. Il'yasov, *Russ. J. Org. Chem.* **2000**, *36*, 164-7; b) A. I. Kazakov, V. V. Nedelko, A. V. Shastin, B. L. Korsounskii, *Int. Annu. Conf. ICT* **2007**, *38th*, 60/1-/11.

[119] S. A. Andreev, B. A. Lebedev, I. V. Tselinskii, *Zh. Org. Khim. (Eng. Trans.)* **1978**, *14*, 2513-16.

[120] a) O. A. Drozdova, A. A. Astrat'ev, L. L. Kuznetsov, V. F. Selivanov, *Zh. Org. Khim. (Eng. Trans.)* **1983**, *19*, 675-83; b) H. Egsgaard, L. Carlsen, T. Weiske, D. Sülzle, H. Schwarz, *Chem. Phys. Lett.* **1992**, *199*, 643-7.

[121] a) E. H. White, D. W. Grisley, Jr., *J. Am. Chem. Soc.* **1961**, *83*, 1191-6; b) E. H. White, R. J. Baumgarten, *J. Org. Chem.* **1964**, *29*, 3636-40; c) E. H. White, L. A. Dolak, *J. Am. Chem. Soc.* **1966**, *88*, 3790-5.

[122] a) S. A. Andreev, I. A. Sivaev, B. A. Lebedev, I. V. Tselinskii, B. V. Gidaspov, *Zh. Org. Khim. (Eng.Trans.)* **1977**, *13*, 1053-57; b) S. A. Andreev, L. A. Novik, B. A. Lebedev, I. V. Tselinskii, B. Gidaspov, *Zh. Org. Khim. (Eng. Trans.)* **1978**, *14*, 221-4; c) S. A. Andreev, B. A. Lebedev, G. I. Koldobskii, I. V. Tselinskii, B. V. Gidaspov, *Zh. Org. Khim. (Eng. Trans.)* **1978**, *14*, 907-9; d) S. A. Andreev, B. A. Lebedev, I. V. Tselinskii, *Zh. Org. Khim. (Eng. Trans.)* **1978**, *14*, 909-12; e) B. A. Lebedev, M. A. Ilyushin, S. A. Andreev, B. V. Gidaspov, *Zh. Org. Khim. (Eng. Trans.)* **1978**, *14*, 2055-7.

[123] R. Huisgen, C. Rüchardt, *Liebigs Ann.* **1956**, *601*, 21-39.

[124] E. H. White, C. A. Aufdermarsh, *J. Am. Chem. Soc.* **1961**, *83*, 1174-8.

[125] R. E. Olsen, D. W. Fish, E. E. Hamel, *Adv. Chem. Ser.* **1965**, *54*, 48-54.

[126] a) E. H. White, *J. Am. Chem. Soc.* **1955**, *77*, 6008-10; b) A. L. Fridman, F. M. Mukhametshin, S. S. Novikov, *Usp. Khim. (Eng. Trans.)* **1971**, *40*, 34-50; c) J. Lee, L. Chen, A. H. West, G. B. Richter-Addo, *Chem. Rev.* **2002**, *102*, 1019-66; d) M. A. Wilson, in *Comprehensive Organic Functional Group Transformations II* (Eds.: R. K. Editors-in-Chief: Alan, J. K. T. Richard), Elsevier, Oxford, **2005**, pp. 295-356.

[127] a) E. H. White, *J. Am. Chem. Soc.* **1955**, *77*, 6011-14; b) E. H. White, *J. Am. Chem. Soc.* **1955**, *77*, 6014-22.

[128] R. Robson, *Inorg. Chim. Acta* **1984**, *85*, 195-8.

[129] K. Minksztym, *Synthesis* **2007**, 1819-22.

[130] R. A. Cox, *J. Chem. Soc., Perkin Trans. 2* **1997**, 1743-50.

[131] O. A. Drozdova, A. A. Astrat'ev, L. L. Kuznetsov, V. F. Selivanov, *Zh. Org. Khim.* **1982**, *18*, 2335-40.

[132] E. H. White, M. C. Chen, L. A. Dolak, *J. Org. Chem.* **1966**, *31*, 3038-46.

[133] a) A. H. Lamberton, I. O. Sutherland, J. E. Thorpe, H. M. Yusuf, *J. Chem. Soc. (B)* **1968**, 6-8; b) P. Hampson, A. Mathias, *Chem. Comm.* **1968**, 825-6; c) A. R. Farminer, G. A. Webb, *Tetrahedron* **1975**, *31*, 1521-6.

[134] R. G. Coombes, in *Compr. Org. Chem., Vol. 2*, Pergamon, **1979**, pp. 305-81.

[135] a) G. J. Karabatsos, R. A. Taller, *J. Am. Chem. Soc.* **1964**, *86*, 4373-8; b) H. W. Brown, D. P. Hollis, *J. Mol. Spectrosc.* **1964**, *13*, 305-12; c) J. D. Cooney, S. K. Brownstein, J. W. ApSimon, *Can. J. Chem.* **1974**, *52*, 3028-36.

[136] D. L. Pavia, G. M. Lampman, G. S. Kriz, *Introduction to Spectroscopy: A Guide for Students of Organic Chemistry, 3rd Edition*, Harcourt College Publishers, **2001**.

[137] G. G. Suchkova, L. I. Maklakov, *Vib. Spectrosc.* **2009**, *51*, 333-9.

[138] R. L. Williams, R. J. Pace, G. J. Jeacocke, *Spectrochimica Acta* **1964**, *20*, 225-36.

[139] a) W. S. Layne, H. H. Jaffe, H. Zimmer, *J. Am. Chem. Soc.* **1963**, *85*, 435-8; b) D. R. Battiste, L. P. Davis, R. V. Nauman, *J. Am. Chem. Soc.* **1975**, *97*, 5071-8.

[140] R. N. Haszeldine, B. J. H. Mattinson, *J. Chem. Soc.* **1955**, 4172-85.

[141] H. McConnell, *J. Chem. Phys.* **1952**, *20*, 700-4.

[142] a) G. J. Brealey, M. Kasha, *J. Am. Chem. Soc.* **1955**, *77*, 4462-8; b) A. K. Chandra, S. Basu, *Trans. Faraday Soc.* **1960**, *56*, 632-7.

[143] N. D. Coggeshall, E. M. Lang, *J. Am. Chem. Soc.* **1948**, *70*, 3283-92.

[144] C. J. Michejda, N. E. Davidson, L. K. Keefer, *J. Chem. Soc., Chem Commun.* **1976**, 633-4.

[145] L. Vaska, *Acc. Chem. Res* **1968**, *1*, 335-44.

[146] J. Peone, L. Vaska, *Angew. Chem. Int. Ed.* **1971**, *10*, 511-2.

[147] a) P. B. Chock, J. Halpern, *J. Am. Chem. Soc.* **1966**, *88*, 3511-4; b) L. Vaska, *J. Am. Chem. Soc.* **1966**, *88*, 5325-7; c) L. Vaska, L. S. Chen, C. V. Senoff, *Science* **1971**, *174*, 587-9; d) H. Singer, G. Wilkinson, *J. Chem. Soc. A: Inorg, Phys, Theor.* **1968**, 2516-20.

[148] J. P. Collman, J. W. Kang, *J. Am. Chem. Soc.* **1966**, *88*, 3459-60.

[149] J. Chatt, D. P. Melville, R. L. Richards, *J. Chem. Soc. A: Inorg, Phys, Theor.* **1969**, 2841-4.

[150] a) A. Spek, *J. Appl. Cryst.* **2003**, *36*, 7-13; b) A. Spek, *Acta Crystallogr.* **2009**, *D65*, 148-55.

[151] a) K. Vrieze, J. P. Collman, C. T. Sears, M. Kubota, A. Davison, E. T. Shawl, in *Inorg. Synth., Vol. 11*, John Wiley & Sons, Inc., **1968**, pp. 101-4; b) J. P. Collman, C. T. Sears, M. Kubota, A. Davison, E. T. Shawl, J. R. Sowa, R. J. Angelici, in *Inorg. Synth., Vol. 28*, John Wiley & Sons, Inc., **1990**, pp. 92-4.

[152] R. J. S. J. C. Bottaro, P. E. Penwell, D. S. Ross, US Patent 5,254,324 ed. (Ed.: USPTO), US, **1993**, pp. 1-9.

[153] K. O. Christe, W. W. Wilson, M. A. Petrie, H. H. Michels, J. C. Bottaro, R. Gilardi, *Inorg. Chem.* **1996**, *35*, 5068-71.

[154] a) O. A. Luk'yanov, O. V. Anikin, V. P. Gorelik, V. A. Tartakovsky, *Russ Chem Bull* **1994**, *43*, 1457-61; b) H.-G. Ang, W. Fraenk, K. Karaghiosoff, T. M. Klapötke, P. Mayer, H. Nöth, J. Sprott, M. Warchhold, *Z. Anorg. Allg. Chem.* **2002**, *628*, 2894-900; c) T. M. Klapotke, B. Krumm, M. Scherr, *Dalton Trans.* **2008**, 5876-8.

[155] A. Vij, Y. Y. Zheng, R. L. Kirchmeier, J. n. M. Shreeve, *Inorg. Chem.* **1994**, *33*, 3281-8.

[156] D. B. Williams, M. E. Stoll, B. L. Scott, D. A. Costa, J. W. J. Oldham, *Chem. Commun.* **2005**, *0*, 1438-40.

[157] J. P. Collman, N. W. Hoffman, J. W. Hosking, G. W. Parshall, in *Inorg. Synth., Vol. 12*, John Wiley & Sons, Inc., **1970**, pp. 8-11.

[158] R. Arvai, F. Toulgoat, B. R. Langlois, J.-Y. Sanchez, M. Médebielle, *Tetrahedron* **2009**, *65*, 5361-8.

[159] a) D. J. Liston, C. A. Reed, C. W. Eigenbrot, W. R. Scheidt, *Inorg. Chem.* **1987**, *26*, 2739-40; b) Z. Xie, T. Jelinek, R. Bau, C. A. Reed, *J. Am. Chem. Soc.* **1994**, *116*, 1907-13.

[160] a) A. L. Balch, J. K. Nagle, M. M. Olmstead, P. E. Reedy, *J. Am. Chem. Soc.* **1987**, *109*, 4123-4; b) A. L. Balch, F. Neve, M. M. Olmstead, *J. Am. Chem. Soc.* **1991**, *113*, 2995-3001.

[161] a) L. Vaska, J. Peone, Jr., *J. Chem. Soc. D, Chem. Commun.* **1971**, 418-19; b) L. Vaska, J. Peone, Jr., *Inorg. Synth.* **1974**, *15*, 64-8; c) C. A. Read, W. R. Roper, *J. Chem. Soc., Dalton Trans.* **1973**, 1370-5.

[162] R. O. Harris, D. N. Cash, *Can. J. Chem.* **1971**, *49*, 867-73.

[163] J. Peone, Jr., B. R. Flynn, L. Vaska, *Inorg. Synth.* **1974**, *15*, 68-72.

[164] L. D. Brown, J. A. Ibers, A. R. Siedle, *Inorg. Chem.* **1978**, *17*, 3026-30.

[165] D. S. Bohle, B. J. Conklin, C.-H. Hung, *Inorg. Chem.* **1995**, *34*, 2569-81.

[166] J. P. Collman, M. Kubota, F. D. Vastine, J. Y. Sun, J. W. Kang, *J. Am. Chem. Soc.* **1968**, *90*, 5430-7.

[167] J. P. Collman, M. Kubota, J.-Y. Sun, F. Vastine, *J. Am. Chem. Soc.* **1967**, *89*, 169-70.

[168] A. J. Deeming, B. L. Shaw, *J. Chem. Soc. A: Inorg, Phys, Theor.* **1969**, 1802-4.

[169] a) S. F. Palopoli, S. J. Geib, A. L. Rheingold, T. B. Brill, *Inorg. Chem.* **1988**, *27*, 2963-71; b) S. N. Semenov, A. Y. Rogachev, S. V. Eliseeva, Y. A. Belousov, A. A. Drozdov, S. I. Troyanov, *Polyhedron* **2007**, *26*, 4899-907; c) G. Geisberger, T. M. Klapötke, J. Stierstorfer, *Eur. J. Inorg. Chem.* **2007**, *2007*, 4743-50; d) D. M. Liebig, J. H. Robertson, *J. Chem. Soc.* **1965**, 5801-9.

[170] a) G. Steinfeld, B. Kersting, *Z. Anorg. Allg. Chem.* **2009**, *635*, 260-4; b) D. M. Liebig, J. H. Robertson, M. R. Truter, *J. Chem. Soc. A: Inorg, Phys, Theor.* **1966**, 879-87.

[171] M. L. B. J. Tobe, *Inorganic reaction mechanisms*, Longman, Harlow, Essex, England; New York, **1999**.

[172] S. A. Smith, D. M. Blake, M. Kubota, *Inorg. Chem.* **1972**, *11*, 660-2.

[173] a) J. Ruiz, N. Cutillas, V. Rodriguez, J. Sampedro, G. Lopez, P. A. Chaloner, P. B. Hitchcock, *J. Chem. Soc., Dalton Trans.* **1999**, 2939-46; b) D. M. Tellers, J. C. M. Ritter, R. G. Bergman, *Inorg. Chem.* **1999**, *38*, 4810-8.

[174] D. M. Blake, M. Kubota, *J. Am. Chem. Soc.* **1970**, *92*, 2578-9.

[175] L. Vaska, *J. Am. Chem. Soc.* **1966**, *88*, 4100-1.

[176] G. La Monica, S. Cenini, E. Forni, M. Manassero, V. G. Albano, *J. Organomet. Chem.* **1976**, *112*, 297-308.

[177] a) D. R. Roberts, G. L. Geoffroy, M. G. Bradley, *J. Organomet. Chem.* **1980**, *198*, C75-C8; b) M. G. Bradley, D. A. Roberts, G. L. Geoffroy, *J. Am. Chem. Soc.* **1981**, *103*, 379-84.

[178] a) B. P. Sullivan, J. C. Brewer, H. B. Gray, D. Linebarrier, J. M. Mayer, in *Inorg. Synth., Vol. 29*, John Wiley & Sons, Inc., **1992**, pp. 146-50; b) G. A. Neyhart, K. Seward, B. P. Sullivan, in *Inorg. Synth., Vol. 31*, John Wiley & Sons, Inc., **1997**, pp. 262-7.

[179] G. M. Sheldrick, *University of Göttingen, Germany & Bruker AXS Inc, Madison (WI), USA* **2005**.

[180] G. W. Parshall, L. W. Shive, F. A. Cotton, in *Inorg. Synth., Vol. 17*, John Wiley & Sons, Inc., **1977**, pp. 110-2.

[181] X. L. Luo, H. Liu, R. H. Crabtree, *Inorg. Chem.* **1991**, *30*, 4740-2.

[182] K. L. Leighton, K. R. Grundy, K. N. Robertson, *J. Organomet. Chem.* **1989**, *371*, 321-8.

[183] A. P. Ginsberg, C. R. Sprinkle, J. F. Russell, F. N. Tebbe, E. L. Muetterties, in *Inorg. Synth., Vol. 13*, John Wiley & Sons, Inc., **1972**, pp. 219-25.

[184] P. Müller, I. Usón, V. Hensel, A. D. Schlüter, G. M. Sheldrick, *Helv. Chim. Acta.* **2001**, *84*, 778-85.

[185] a) M. Ruck, *Z. Kristallogr.* **2000**, *215*, 148; b) J. W. Steed, *CrystEngComm* **2003**, *5*, 169-79; c) Y. V. Nelyubina, I. L. Dalinger, K. A. Lyssenko, *Angew. Chem. Int. Ed.* **2011**, *50*, 2892-4.

[186] M. A. Hitchman, G. L. Rowbottom, *Coord. Chem. Rev.* **1982**, *42*, 55-132.

[187] a) R. Huisgen, *Proc. Chem. Soc.* **1961**, 357; b) R. Huisgen, *Pure App. Chem.* **1989**, *61*, 613-28.

[188] H. C. Kolb, M. G. Finn, K. B. Sharpless, *Angew. Chem. Int. Ed.* **2001**, *40*, 2004-21.

[189] M. G. Finn, V. V. Fokin, *Chem. Soc. Rev.* **2010**, *39*, 1231-2.

[190] J. N. Brantley, K. M. Wiggins, C. W. Bielawski, *Science* **2011**, *333*, 1606-9.

[191] Y. Lin, Q. Wang, *Angew. Chem. Int. Ed.* **2012**, *51*, 2006-7.

[192] X. Àlvarez Micó, T. Ziegler, L. R. Subramanian, *Angew. Chem. Int. Ed.* **2004**, *43*, 1400-3.

[193] A. R. Katritzky, L. Khelashvili, K. N. B. Le, P. P. Mohapatra, P. J. Steel, *J. Org. Chem.* **2007**, *72*, 5805-8.

[194] M. Uhde, T. Ziegler, *Synth. Commun.* **2010**, *40*, 3046-57.

[195] T. V. Hughes, S. D. Hammond, M. P. Cava, *J. Org. Chem.* **1998**, *63*, 401-2.

[196] M. Cowie, S. J. Loeb, I. R. McKeer, *Organometallics* **1986**, *5*, 854-60.

[197] a) M. E. Hermes, F. D. Marsh, *J. Am. Chem. Soc.* **1967**, *89*, 4760-4; b) G. Himbert, M. Regitz, *Liebigs Ann.* **1973**, *1973*, 1505-29.

[198] A. R. Katritzky, F. B. Ji, W. Q. Fan, J. K. Gallos, J. V. Greenhill, R. W. King, P. J. Steel, *J. Org. Chem.* **1992**, *57*, 190-5.

[199] a) C. L. Habraken, C. Erkelens, J. R. Mellema, P. Cohen-Fernandes, *J. Org. Chem.* **1984**, *49*, 2197-200; b) A. R. Katritzky, R. Akue-Gedu, A. V. Vakulenko, *ARKIVOC,* **2007**, *3*, 5-12; c) M. Uhde, M. U. Anwar, T. Ziegler, *Synth. Commun.* **2008**, *38*, 881-8; d) M. Colonna, M. Poloni, *Gazz. Chim. Ital.* **1988**, *118*, 673-4.

[200] H. Zollinger, in *Diazo Chemistry II*, Wiley-VCH Verlag GmbH & Co. KGaA, **2004**, pp. 421-54.

[201] P. Sartori, N. Ignat'ev, S. Datsenko, *J. Fluorine Chem.* **1995**, *75*, 157-61.

[202] M. Regitz, H. Scherer, *Chem. Ber.* **1969**, *102*, 417-22.

[203] G. Himbert, M. Regitz, *Chem. Ber.* **1972**, *105*, 2975-84.

[204] a) K. D. Schramm, J. A. Ibers, *J. Am. Chem. Soc.* **1978**, *100*, 2932-3; b) J. A. Ibers, T. R. Gaffney, K. D. Schramm, *Coord. Chem.* **1981**, *21*, 141-9.

[205] a) B. L. Haymore, J. A. Ibers, *J. Am. Chem. Soc.* **1973**, *95*, 3052-4; b) K. D. Schramm, J. A. Ibers, *Inorg. Chem.* **1980**, *19*, 2435-40; c) K. D. Schramm, J. A. Ibers, *Inorg. Chem.* **1980**, *19*, 1231-6.

[206] a) A. Nakamura, T. Yoshida, M. Cowie, S. Otsuka, J. A. Ibers, *J. Am. Chem. Soc.* **1977**, *99*, 2108-17; b) K. D. Schramm, J. A. Ibers, *Inorg. Chem.* **1980**, *19*, 2441-8; c) J. R. Dilworth, I. A. Latham, G. J. Leigh, G. Huttner, I. Jibril, *J. Chem. Soc., Chem Commun.* **1983**, 1368-70; d) I. A. Latham, G. J. Leigh, G. Huttner, I. Jibril, *J. Chem. Soc., Dalton Trans.* **1986**, 377-83.

[207] a) D. Sutton, *Chem. Rev.* **1993**, *93*, 995-1022; b) Y. Mizobe, Y. Ishii, M. Hidai, *Coord. Chem. Rev.* **1995**, *139*, 281-311.

[208] a) A. P. Gaughan, Jr., B. L. Haymore, J. A. Ibers, W. H. Myers, T. E. Nappier, Jr., D. W. Meek, *J. Am. Chem. Soc.* **1973**, *95*, 6859-61; b) B. L. Haymore, J. A. Ibers, *J. Am. Chem. Soc.* **1975**, *97*, 5369-79; c) M. Cowie, B. L. Haymore, J. A. Ibers, *Inorg. Chem.* **1975**, *14*, 2617-23; d) S. Krogsrud, J. A. Ibers, *Inorg. Chem.* **1975**, *14*, 2298-300; e) M. Cowie, B. L. Haymore, J. A. Ibers, *J. Am. Chem. Soc.* **1976**, *98*, 7608-17.

[209] K. H. Pannell, A. J. Mayr, D. VanDerveer, *J. Am. Chem. Soc.* **1983**, *105*, 6186-8.

[210] A. R. Katritzky, X. Lan, J. Z. Yang, O. V. Denisko, *Chem. Rev.* **1998**, *98*, 409-548.

[211] M. Dartiguenave, M. Joëlle Menu, E. Deydier, D. Yves, H. Siebald, *Coord. Chem. Rev.* **1998**, *178–180, Part 1*, 623-63.

[212] J. B. Menke, *Recl. Trav. Chim. Pays-Bas Belg.* **1925**, *44*, 141-9.

[213] M. E. Kurz, L. T. A. Yang, E. P. Zahora, R. C. Adams, *J. Org. Chem.* **1973**, *38*, 2271-7.

[214] G. A. Olah, S. C. Narang, A. P. Fung, *J. Org. Chem.* **1981**, *46*, 2706-9.

[215] M. Kimura, K. Kajita, N. Onoda, S. Morosawa, *J. Org. Chem.* **1990**, *55*, 4887-92.

[216] a) G. A. Olah, A. P. Fung, S. C. Narang, J. A. Olah, *J. Org. Chem.* **1981**, *46*, 3533-7; b) G. A. Olah, S. C. Narang, J. A. Olah, K. Lammertsma, *Proc. Natl. Acad. Sci. U. S. A.* **1982**, *79*, 4487-94.

[217] a) S. C. Suri, R. D. Chapman, *Synthesis* **1988**, 743-5; b) P. Romea, M. Aragones, J. Garcia, J. Vilarrasa, *J. Org. Chem.* **1991**, *56*, 7038-42.

[218] R. W. Millar, R. P. Claridge, J. P. B. Sandall, C. Thompson, *ARKIVOC (Gainesville, FL, U. S.)* **2002**, 19-36.

[219] E. J. Corey, B. Samuelsson, F. A. Luzzio, *J. Am. Chem. Soc.* **1984**, *106*, 3682-3.

[220] E. Saxon, C. R. Bertozzi, *Science* **2000**, *287*, 2007-10.

[221] F. L. Lin, H. M. Hoyt, H. van Halbeek, R. G. Bergman, C. R. Bertozzi, *J. Am. Chem. Soc.* **2005**, *127*, 2686-95.

[222] G. Singh, H. Zimmer, *Organomet. Chem. Rev.* **1967**, *2*, 279-348.